Université de Montréal

Étude structurale, biomécanique et génétique des interactions cellulaires avec une surface de titane modifiée à l'échelle nanométrique

Par

Dainelys Guadarrama Bello

Département de Stomatologie

Faculté de Médecine

Thèse présentée en vue de l'obtention du grade de *Philosophiæ Doctor* (Ph.D.)

en Sciences Biomédicales, option Médecine expérimentale

Avril, 2022

Cette thèse intitulée

Étude structurale, biomécanique et génétique des interactions cellulaires avec une surface de titane modifiée à l'échelle nanométrique

Présentée par

Dainelys Guadarrama Bello

A été évalué(e) par un jury composé des personnes suivantes

Stéphane Roy
Président-rapporteur

Antonio Nanci
Directeur de recherche

Antonella Badia
Codirectrice

Davide Brambilla
Membre du jury

Diego Mantovani
Examinateur externe

Résumé

Le titane (Ti) est largement utilisé en orthopédie et médecine dentaire. Ce matériau présente d´excellentes propriétés mécaniques, est biocompatible et résiste à la corrosion. L'interaction entre les cellules et la surface d'un implant joue un rôle décisif dans l'ostéointégration. Malgré la grande variété d'études que nous trouvons dans la littérature, le comportement des cellules en contact avec des matériaux implantables comme le Ti n'est toujours pas élucidé à toutes les échelles topographiques. Notre laboratoire a développé une méthode de modification physico-chimique de la surface de métaux à intérêt médical. Cette méthode génère des surfaces nanoporeuses qui favorisent la différenciation de cellules souches, affectent le comportement cellulaire de façon différentielle, promeuvent la formation osseuse *in vitro* et *in vivo*, et qui ont une capacité antibactérienne.

Afin de mieux comprendre comment cette surface influence le comportement cellulaire, nous avons étudié leur influence sur la formation et la maturation des adhésions focales (FAs, de l'anglais) et la formation des filopodes. De plus, nous avons examiné comment les caractéristiques physico-chimiques de la surface obtenue guident l'expression génique des protéines associées aux FAs et aux filopodes en utilisant différentes lignées cellulaires. Finalement, afin de mieux comprendre la biomécanique de la cellule, la force d'adhésion à la surface des filopodes a été déterminée à l'aide de la microscopie à force atomique (AFM).

Des disques de Ti commercialement pur (Cp-Ti) ont été polis a fini miroir (Ti-Control), une partie des disques a été traité avec un mélange d'acide sulfurique et de peroxyde d'hydrogène pour créer une surface nanostructurée poreuse (Ti-Nano). L'influence de la nanoporosité, de la cristallinité et la mouillabilité de cette surface sur des cellules pre-ostéoblastiques de souris (MC3T3) et des bactéries a été évalué par la microscopie électronique à balayage (MEB) et par immunofluorescence (IF). Nous avons ensuite utilisé une lignée cellulaire épithéliale (CHO-K1) qui exprime la paxilline (une protéine des FAs) de type sauvage ou la paxilline avec des mutations. De plus, la force d'interaction des filopodes avec la surface a été quantifié en mesurant la force latérale nécessaire pour les déplacer avec une pointe d'AFM. Finalement, la centrifugation a été utilisée pour étudier les changements fonctionnels des cellules MC3T3.

L'analyse du comportement des cellules MC3T3 sur des surfaces amorphes et cristallines n'a pas montré de différence par rapport au nombre des cellules ou la quantité des FAs. La cristallinité de la couche superficielle n'avait également aucune incidence sur l'adhésion bactérienne. Les deux lignées cellulaires utilisées ont montré une présence abondante de filopodes avec des nanoprotrusions latérales en réponse à la nanoporosité. La taille et la forme des cellules CHO-K1 ont été grandement affectées par la topographie. L'expression génique des protéines associées aux différents marqueurs des FAs et aux protrusions a été aussi significativement augmentée sur la surface nanoporeuse, quel que soit le type de cellule. Les filopodes sur Ti-Nano ont montré une plus grande résistance au détachement latéral, ce qui indique qu'ils adhèrent à la surface avec plus de force. Également, l'analyse par MEB a révélé une restructuration de la membrane cellulaire accompagnée d'un changement de la forme cellulaire après centrifugation. Parce que les mitochondries fournissent de l'énergie pour les processus cellulaires, l'organisation du réseau mitochondrial a été influencée aussi par la topographie de surface et la centrifugation. Bien qu'il ne puisse pas être exclu que la cristallinité et la mouillabilité de la surface contribuent dans une certaine mesure à déterminer le comportement des cellules, nos résultats suggèrent que les caractéristiques physiques des surfaces représentent le principal déterminant. Nous avons démontré aussi, pour la première fois, que la topographie de surface peut modifier l'interaction adhésive d'une structure subcellulaire qui est fondamentale dans la détection des caractéristiques physico-chimiques des surfaces. En conclusion, nos résultats montrent que la topographie de surface peut modifier des propriétés fondamentales dans les cellules. Dans leur ensemble, ils soulèvent la possibilité que les surfaces nanostructurées puissent être utilisées non seulement pour guider/accélérer l'intégration de biomatériaux dans des conditions normales, mais également dans des situations où l'activité cellulaire est compromise ou également pour les prothèses soumises à des charges externes, telles que les implants orthopédiques et dentaires.

Mots-clés : nanotopographie, filopodes, adhésions focales, expression des gènes, force d'adhésion, AFM, centrifugation.

Abstract

Titanium (Ti) is widely used in orthopedics and dentistry. This material has excellent mechanical properties, is biocompatible and corrosion resistant. The interaction between the cells and the surface of an implant plays a key role in osseointegration. Despite the wide variety of studies found in the literature, the behavior of cells in contact with implantable materials such as Ti is not yet fully elucidated at all topographic scales. Our laboratory has developed a method for the physicochemical modification of the surface of medically relevant metals. This method generates nanoporous surfaces that promote stem cell differentiation, differentially affect cellular behavior, promote bone formation *in vitro* and *in vivo* and have antibacterial capacity.

To better understand how this surface influences cell behavior, we studied their influence on the formation and maturation of focal adhesions (FAs) and filopodia formation. Furthermore, we examined how the physicochemical characteristics of the resulting surface guide the gene expression of proteins associated with FAs and filopodia using different cell lines. Finally, to better understand the biomechanics of the cell, the adhesion strength of filopodia to the surface was determined using atomic force microscopy (AFM).

Commercially pure Ti discs (Cp-Ti) were polished to a mirror finish (Ti-Control), some of the polished discs were treated with a mixture of sulfuric acid and hydrogen peroxide to create a nanostructured surface (Ti-Nano). The influence of nanoporosity, crystallinity and wettability of this surface on mouse pre-osteoblastic cells (MC3T3) and bacteria was evaluated by scanning electron microscopy (SEM) and immunofluorescence. Then, to evaluate the response to nanotopography, we used an epithelial cell line (CHO-K1) that expresses wild type paxillin (a protein of FAs) or paxillin with mutations. In addition, the interaction forces of the filopodia with the surface were quantified by measuring the lateral force required to displace these structures from the surface with an AFM tip. Finally, centrifugation was used to study functional changes in MC3T3 cells.

Analysis of the behavior of MC3T3 cells on amorphous and crystalline surfaces showed no difference in cell number or the number of focal adhesions. The crystallinity of the surface layers also had no effect on bacterial adhesion. Both cell lines used showed abundant presence of filopodia

with lateral nanoprotrusions in response to nanoporosity. The size and shape of CHO-K1 cells was greatly affected by the topography. Gene expression of proteins associated with different focal adhesion markers and protrusions was also significantly increased on the nanoporous surface, regardless of cell type. Filopodia on the Ti-Nano showed greater resistance to lateral detachment force, indicating that they adhere to the surface with greater strength. Also, SEM analysis revealed a restructuring of the cell membrane accompanied by a corresponding change in cell shape after centrifugation. Because mitochondria provide energy for cell processes, the organization of the mitochondrial network was also influenced by surface topography and centrifugation. Although it cannot be excluded that surface crystallinity and wettability contribute to some extent to determining cell behavior, our results suggest that the physical characteristics of the surfaces represent the main determinant. We have also shown for the first time that surface topography can modify the adhesive interaction of a subcellular structure that is fundamental in the detection of the physicochemical characteristics of surfaces. In conclusion, our results show that surface topography can modify fundamental properties in cells. Together, they raise the possibility that nanostructured surfaces can be used not only to guide/accelerate the integration of biomaterials under normal conditions, but also in situations where cellular activity is compromised or also for prostheses under external loads, such as orthopedic and dental implants.

Table des matières

Liste des tableaux

Liste des figures

13

Liste des sigles et abréviations

α-MEM : *Alpha Minimum Essential Medium*

ACTN1 : Alpha-actinin

AFM : Microscopie à force atomique

ATCC : *American Type Culture Collection*

BMP : Protéines morphogénétiques osseuses

bp : *Primer lengh*

BSP : Sialoprotéine osseuse

CA : Angle de contact

Cdc42 : *Cell division control protein 42 homolog*

CHO-K1 : *Stable Chinese hamster ovary*

Cp-Ti : Titane commercialement pur

CSM : Cellules souches mésenchymateuses

DAPI : 4',6-diamidino-2-phénylindole

DMEM : *Dulbecco's Modified Eagle Medium*

EGFP : *Enhanced Green Fluorescent Protein*

FAK : *Focal adhesion kinase*

FAs : Adhésions focales

FE-SEM : *Field-Emission Scanning Electron Microscopy*

FGF : Facteur de croissance fibroblastique

FTIR : Spectroscopie infrarouge à transformée de Fourier

GAPDH : Glyceraldehyde 3-phosphate dehydrogenase

GIT1 : *G-protein-Coupled Receptor Kinase-Interacting Protein 1*

HA : Hydroxyapatite

HIM : *Helium ion electron microscopy*

HR-FESEM : Microscopie électronique à balayage à haute résolution

IF : Immunofluorescence

ITGα1 : Integrin α1

ITGβ1 : Integrin β1

M : Molaire

MEC : Matrice extracellulaire

MC3T3-E1 : Cellules ostéogéniques de souris

MS : Protéines mécanosensibles

NWs : *Nanowires*

OPG : Ostéoprotégérine

PB : Tampon de phosphate

PLP : Periodate-Lysine-Paraformaldehyde

Pxn : Paxillin

Ra : *Arithmetic mean*

Rac1 : *Ras-related C3 botulinum toxin substrate 1*

RGD : Tripeptide Arg-Gly-Asp

RNA : Acide ribonucléique

ROCK : *Rho associated coiled-coil containing protein Kinase*

RhoA : *Ras homolog family member A*

RT : Température ambiante

RT-qPCR : *Quantitative Real-Time PCR*

S273 : Serine 273

SCFS : Spectroscopie de force unicellulaire

Rq : Root-mean-square

RT-PCR : Réaction en chaîne par polymérase en temps réel

SD : Écart type

SE : Énergie de surface

SEM : Microscopie électronique à balayage

SS : Acier inoxydable

Ti : Titane

Tln : Talin

UV : Rayonnement ultraviolet

Vcl : Vinculin

WT : *Wild-Type*

Y31 : Tyrosine 31

À ma famille

Remerciements

Je remercie chaleureusement toutes les personnes qui m'ont aidé pendant l'élaboration de ma thèse et notamment mon directeur de recherche, le professeur Antonio Nanci, pour son intérêt et son soutien, sa grande disponibilité et ses nombreux conseils durant cette période. Il m'encouragé toujours à donner mon maximum pour produire des résultats de haute qualité. Je voudrais remercier aussi ma codirectrice de recherche, la professeure Antonella Badia, pour son aide dans le projet.

Je tiens aussi à remercier à mes amis et collègues du groupe, avec qui j'ai partagé des moments inoubliables tout au long de mes études. Katia, Aurélien, Sandra, Charline, Renan, Ana, Doaa, Daylin, Serine, un gros merci pour avoir été présente dans les différentes étapes de la réalisation de ce projet.

Un grand merci à toute ma famille, qui m'a fortement encouragé tout le long de mes études, spécialement mon mari Adrian pour son soutien au fils des ans et à mon petit Josué pour faire mes journées plus amusantes.

Je voudrais remercier les membres de mon jury, Dr. Stéphane Roy, Dr Davide Brambilla et Dr Diego Mantovani d'avoir gentiment accepté d'évaluer ma thèse.

Finalement, je voudrais remercier le Réseau de Recherche en Santé Buccodentaire et Osseuse (RSBO), la Faculté de Médecine et Médecine dentaire, la faculté des études supérieures et postdoctorales de l'Université de Montréal, ainsi qu'aux Fonds de recherche du Québec pour leur contribution financière.

Chapitre 1 – Introduction

Les biomatériaux sont des matériaux d'origine naturelle ou synthétique conçus pour interagir avec des systèmes biologiques à des fins médicales afin de traiter, augmenter ou remplacer un tissu, un organe ou une fonction du corps (1, 2). Sa finalité est de maintenir ou améliorer la qualité de vie de l'individu (2). Malgré de nombreuses avancées notables ces dernières années, les biomatériaux conventionnels continuent de poser de multiples défis, parmi lesquels, l'infection, la réaction inflammatoire et l'incompatibilité. De nombreux matériaux tels les métaux, les céramiques, les polymères et les verres ont été étudiés en tant que biomatériaux (3). Parmi ceux-ci, les biomatériaux métalliques sont largement utilisés dans les remplacements articulaires, les implants dentaires, les fixations orthopédiques et les stents (4).

Les arthroplasties de la hanche et du genou figurent parmi les interventions les plus courantes au monde. Plus de 138 000 interventions incluant les chirurgies de reprise sont pratiquées chaque année au Canada (5). Le nombre de patients subissant une chirurgie d'implant dentaire est encore plus élevé (6). L'utilisation du Ti pour ces implants osseux a des résultats prévisibles à long terme et des taux de réussite élevés (7, 8). Cependant, leurs performances diminuent considérablement chez les patients médicalement compromis (*i.e.* patients dont l'état de santé est altéré, tels que les patients atteints d'anomalies du métabolisme osseux, de diabète, de xérostomie, de dysplasies ectodermiques, de maladies systémiques telles que les cardiopathies ischémiques, les cardiopathies congénitales et les patients immunodéprimés) (9-11). Il est bien établi que ces troubles ou conditions influencent l'ostéointégration, entre eux, les facteurs systémiques sont considérés comme jouant un rôle essentiel. Ces anomalies, entraînent une altération du processus de minéralisation réduisant la solidité osseuse et affectent négativement l'ostéointégration (12). Les facteurs spécifiques du patient ne sont souvent pas contrôlables.

Comme les implants osseux resteront une modalité de traitement courante pour les années à venir, mieux comprendre et contrôler les événements biologiques à l'interface os-implant pour assurer une ostéointégration plus rapide et plus stable est très importante. Certains critères sont cruciaux pour la réussite des implants tel que les propriétés mécaniques appropriées pour supporter les forces qu'ils subissent, leur résistance à la corrosion pendant la durée d'implantation, et l'absence de cytotoxicité, de mutagénicité, d'immunogénicité et de cancérogénicité (1). À ce titre,

la capacité du Ti à s'ostéointégrer, ses propriétés non corrosives et sa biocompatibilité en font un matériau populaire pour les implants dans de nombreux types de chirurgies et pour la quasi-totalité des parties du corps.

Étant donné que les cellules se développent naturellement sur des matrices extracellulaires (MEC) nanostructurées, les caractéristiques topographiques à l'échelle nanométrique des biomatériaux jouent un rôle central lors des interactions cellule-surface. Les implants de Ti commercialisés actuellement ont une topographie très variable, allant de l'échelle micrométrique à l'échelle nanométrique. L'obtention des surfaces nanostructurées est un défi pour la science de matériaux. De la même façon, il est très difficile de trouver la meilleure topographie pour favoriser l'adhésion des cellules ostéoblastiques. C'est pour cela que les études sur les interactions cellule-matériau ont un grand intérêt dans le domaine biomédical. Actuellement, la recherche scientifique est dirigée vers la modification des surfaces pour induire non seulement l'attachement cellulaire initial, mais aussi de permettre aux cellules de mieux proliférer. Une compréhension poussée de l'interaction de la cellule avec la surface des implants est nécessaire pour mieux contrôler le processus d'ostéointégration, ce qui permettra d'adapter intentionnellement les surfaces de l'implant en fonction des patients.

1.1 L'os

La matrice osseuse est composée d'une phase minérale, l'hydroxyapatite (HA) ($Ca_{10} (PO_4)_6 (OH)_2$), étant le composant majoritaire (~64 % en masse), une phase organique (~22 % en masse) (~90 % de collagène de type I, ~5 % de protéines non collagéniques, ~2 % de lipides) et de l'eau (~14 % en masse) (13-17). Les molécules de collagène s'entrelacent pour former des brins de tropocollagène qui s'alignent pour former des régions qui se chevauchent et qui sont périodiquement séparées par de petits intervalles. Ces espaces entre les extrémités des sous-unités du tropocollagène servent probablement de sites de nucléation pour le dépôt de cristaux longs, durs et fins du composant minéral, comme la HA et d'autres phosphates. De nombreux brins minéralisés se combinent pour former une fibrille, élément constitutif d'architectures de niveau supérieur telles que les fibres et les lamelles cylindriques qui forment les structures ostéoniques dans l'os compact. Au centre de chaque ostéon court un canal de Havers, chargé d'alimenter le tissu en sang. Au niveau macroscopique, l'os est composé de deux types de tissus osseux : l'os cortical et l'os trabéculaire. Cette organisation hiérarchique rend l'os à la fois solide et léger. À l'échelle microscopique, la

structure est différente, l'os cortical est composé d'ostéons ou de systèmes haversiens, tandis que l'os trabéculaire ou spongieux est caractérisé par un lacis de trabécules ou de spicules de tissu osseux (6, 18). L'os cortical et l'os trabéculaire sont généralement constitués de lamelles, qui sont principalement composées de faisceaux de fibrilles ou de fibres de collagène minéralisées, d'un diamètre qui varie dans l'échelle micrométrique (Figure 1) (18).
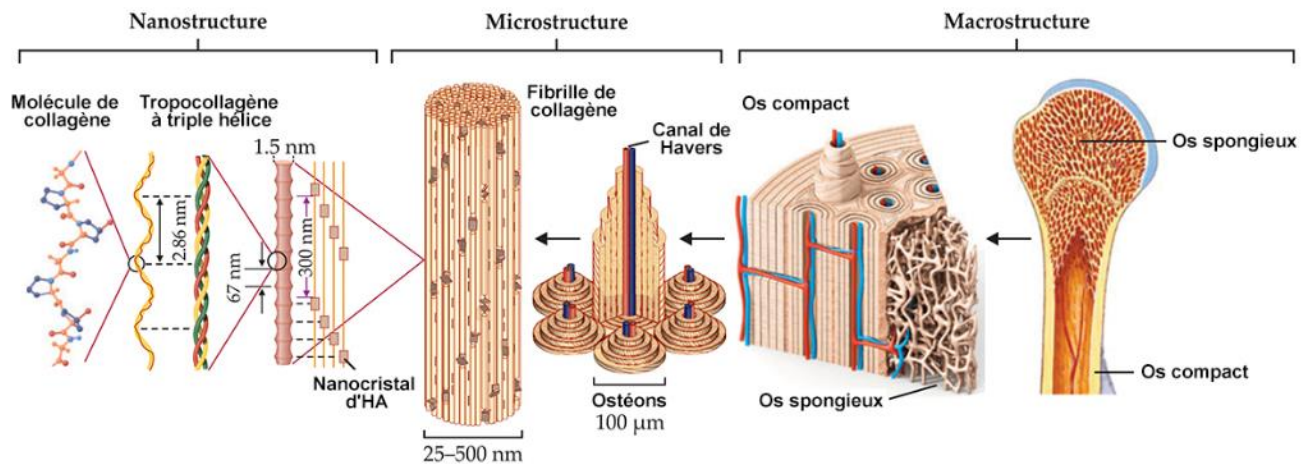
Figure 1. – Organisation structurelle hiérarchique de l'os. Adapté de (6) conformément à la licence Creative Commons Attribution (CC BY) (https://creativecommons.org/licenses/by/4.0/).

Le tissu osseux est un système dynamique qui est en constant renouvellement et constitué de multiples cellules, l'origine de ces cellules sont des cellules mésenchymateuses pluripotentes indifférenciées (19). Il est connu que ces cellules peuvent donner naissance à cinq types de cellules différents selon la cascade d'activation de différents gènes qui est activée (fibroblastes, ostéoblastes, chondroblastes, adipocytes et myoblastes) (19, 20). Les ostéoclastes sont des cellules de résorption osseuse et fonctionnent conjointement avec les ostéoblastes. Elles sont les cellules chargées de maintenir un équilibre entre la dégradation du « vieil os » et la synthèse du « nouvel os ». Dans ce processus de résorption et formation successives de tissus osseux, les ostéoclastes et ostéoblastes sont étroitement associés, c'est ce qui permet d'adapter la masse osseuse à la charge mécanique, une condition préalable pour que les implants métalliques ostéo-intégrés puissent supporter une charge fonctionnelle à long terme (13).

1.2 Biomatériaux à base de Ti

L'utilisation du Ti et de ses alliages en tant que biomatériaux résulte de leur faible module d'élasticité, de leur biocompatibilité supérieure et de leur meilleure résistance à la corrosion par rapport aux aciers inoxydables et les alliages de cobalt-chrome (21). Ensemble, ils constituent l'une des grandes familles de métaux utilisés dans le domaine biomédical choisis pour la fabrication d'implants dentaires, orthopédiques et cardiovasculaires (Figure 2) (22).
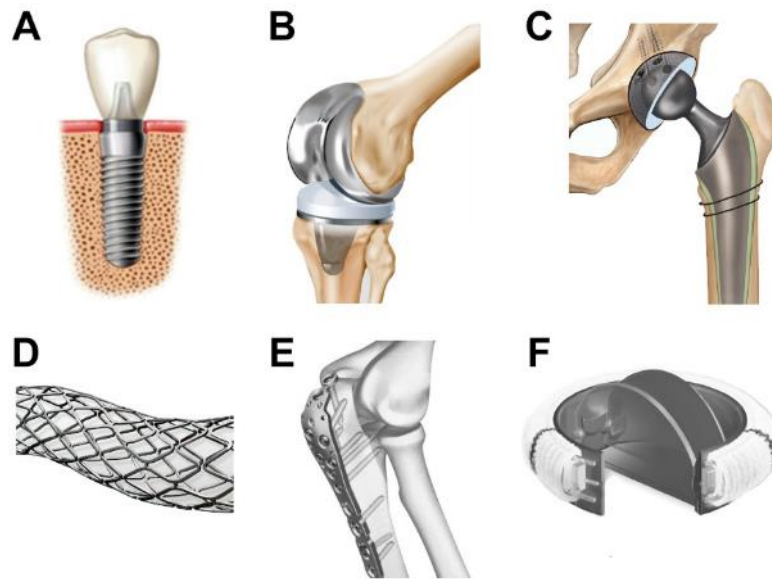
Figure 2. –   Certaines des applications du Ti. (A) Implant dentaire, (B) Prothèse totale du genou (C) Prothèse totale de la hanche, (D) Stent coronaire, (E) plaque osseuse et (F) Prothèse valvulaire aortique.

Le Ti est classé selon sa composition chimique, ses propriétés physiques et mécaniques en plusieurs grades. Les grades de 1 à 4 sont considérés comme un Ti commercialement pur (Ti c.p.). Le Ti c.p. est celui dont les propriétés mécaniques sont les plus proches de l'os, avec des valeurs qui lui permettent de résister aux contraintes auxquelles l'implant sera soumis (23).

Il est bien connu qu'une mince couche d'oxyde (TiO_2) de quelques nanomètres se forme spontanément lors de l'exposition du Ti à l'air, l'humidité ou les fluides physiologiques (21). Le TiO_2 peut se trouver en phase amorphe ou sous trois formes cristallines principales : anatase (tétragonal), rutile (tétragonal) et brookite (rhomboédrique) sur la surface d'un implant, avec des rapports très différents (24). Le traitement de surface influence considérablement la composition

et la structure cristalline de la surface (25). La stabilité chimique et la structure de cette couche d'oxyde de Ti sont responsables de l'excellente inertie chimique, la résistance à la corrosion, la capacité de repassivation et même la biocompatibilité du Ti et des autres alliages de Ti (26).

La biocompatibilité est définie comme "la capacité d'un matériau à fonctionner avec une réponse hôte appropriée dans une application spécifique" (27, 28). Cette propriété n'est pas suffisante par elle-même pour assurer le succès d'un implant, puisque le Ti n'est pas bioactif (*i.e.* capacité des matériaux à développer une liaison directe, adhérente et forte à l'interface avec les tissus hôtes), une propriété influençant grandement le succès d'un implant en contact avec l'os (29). C'est pourquoi il y a tant d'intérêt à modifier la surface pour la rendre bioactive pour des applications où la ostéointégration est souhaitée.

Actuellement les matériaux métalliques en implantologie et prothèse sont largement utilisés dans le monde entier. Les implants dentaires représentent une option de traitement fiable dans la réhabilitation orale des patients partiellement ou totalement édentés afin de sécuriser différents types de prothèses (30). Les implants dentaires sont devenus une procédure standard pour le remplacement des dents, offrant de nombreux avantages mais aussi des défis. Aujourd'hui, il existe environ 1300 systèmes d'implants différents, variant en forme, dimension, volume et matériau de surface, conception de filetage, connexion implant-pilier, topographie de surface, chimie de surface, mouillabilité et modification de surface. Les formes courantes d'implants sont cylindriques ou coniques (31). Également, le Ti est utilisé pour le remplacement prothétique du genou, une technique chirurgicale aussi courante que l'arthroplastie totale de hanche.

1.3 Ostéointégration

1.3.1 Interface os-implant

L'utilisation clinique réussie des implants endo-osseux entraîne le besoin d'améliorations continues dans la conception des implants et l'optimisation des réponses de cicatrisation biologique après la pose de l'implant. L'ostéointégration est le domaine le plus étudié en implantologie (32).

Les premières observations de l'ostéointégration ont été faites dans les années 1950 lors de l'étude de la circulation dans la moelle osseuse utilisant un implant en Ti avec un canal central (33). Le concept initial d'ostéointégration a été défini comme une connexion structurelle et

fonctionnelle directe entre l'os vivant et la surface d'un implant (34). Cependant, au fil des années, cette définition a évolué et de nos jours, un implant est considéré comme ostéo-intégré lorsqu'il n'y a pas de mouvement relatif progressif entre l'implant et l'os avec lequel il est en contact direct (35). Depuis l'introduction du concept d'ostéointégration, les caractéristiques de l'interface entre l'os et l'implant, et les moyens possibles de l'améliorer, ont suscité un intérêt particulier dans la recherche sur les implants dentaires et orthopédiques (25). La biocompatibilité des implants et l'application réussie de ces dispositifs médicaux dépendent largement des événements biologiques qui se produisent au niveau des surfaces (36).

L'ostéointégration comprend une cascade de mécanismes physiologiques complexes similaires à la cicatrisation directe des fractures. Le forage d'une cavité d'implant conduit à des phases distinctes de cicatrisation (31). L'ostéointégration est une procédure continue représentant le processus de formation et d'adaptation à la fonction et à la réparation, qui a lieu en raison de l'activité ostéoblastique et ostéoclastique de l'os, également connu sous le nom de couplage (32). Les ostéoblastes sont d'origine mésenchymateuse et se différencient sous l'influence de facteurs de croissance locaux tels que le facteur de croissance fibroblastique (FGF), les protéines morphogénétiques osseuses (BMP) et les protéines Wnt, et nécessitent également la transcription des facteurs de transcription de la famille RUNX (Runx2) et osterix (Osx) (37). Les ostéoblastes régissent également l'activité des ostéoclastes en sécrétant l'ostéoprotégérine (OPG), un inhibiteur naturel du RANK, qui inhibe la résorption osseuse ostéoclastique.

Il est essentiel pour l'efficacité des implants orthopédiques ou dentaires d'établir une interface mécaniquement solide entre la surface du matériau et le tissu osseux sans interface de tissu fibreux (Figure 3) (38, 39). Comprendre le comportement des cellules à l'interface matériau-tissu de l'hôte est une condition préalable fondamentale pour concevoir des biomatériaux capables de diriger des événements cellulaires vers un résultat biologique souhaité. Quel que soit leur environnement, les cellules vont répondre de manière inhérente aux signaux et stimuli chimiques et physiques (40, 41).
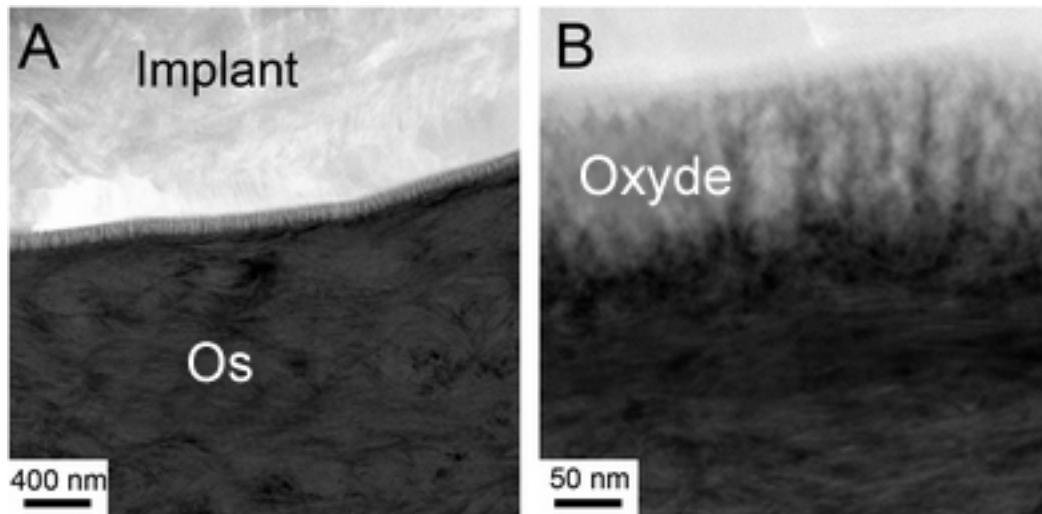
Figure 3. –   Interface os-implant à (A) faible et (B) fort grossissement entre un vise de Ti modifié au laser et le tibia proximal d'une lapine. Un contact intime entre l'os et la couche d'oxyde de Ti interfaciale nanostructurée suggère une ostéointégration. Adapté de (42) avec la permission de Royal Society of Chemistry.

De nombreux efforts de recherche ont été dirigés vers l'amélioration de l'interface os/implant, dans le but d'accélérer la cicatrisation osseuse et d'améliorer l'ancrage osseux à l'implant (25). L'os ne s'attache pas aux biomatériaux d'une façon traditionnelle, l'attachement ne se produit pas par une liaison du type covalent ou ionique (6). Quand un biomatériau est implanté dans le corps, il induit un réponse appelée réaction à corps étranger (Figure 4)(43).
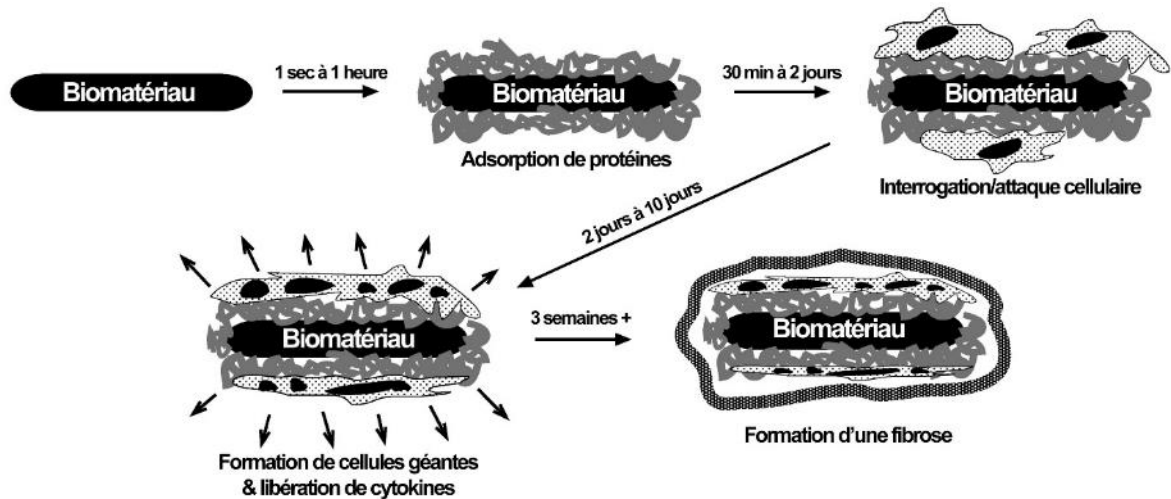
Figure 4. –   Réaction à un matériau synthétique implanté (Réaction à corps étranger). Adapté de (43) avec la permission d'Annual Review of Biomedical Engineering.

Immédiatement après l'implantation, de quelques secondes à quelques minutes, les protéines s'adsorbent à la surface du matériau (44). Les processus d'adsorption-désorption sont contrôlés par l'effet Vroman (45) qui relie les propriétés de surface du matériau (énergie et charge de surface) à la couche de protéines adsorbées (concentration, conformation et taille). Les protéines les plus concentrées et les plus petites ont tendance à s'adsorber d'abord à la surface, puis à être déplacées par des protéines plus grosses et interagissant plus fortement qui peuvent arriver à la surface à un moment ultérieur. La couche de protéines adsorbées sera un mélange de différentes protéines dans différents états de conformation, dont la composition dépend largement des propriétés de surface de l'implant (Figure 5)(44, 46).
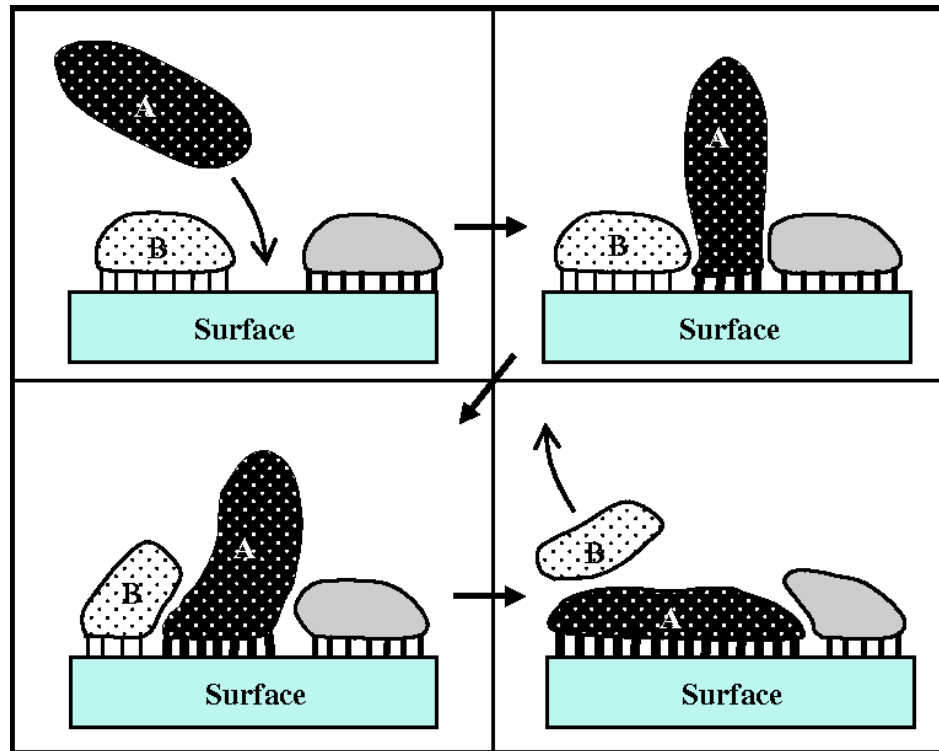
Figure 5. –   Illustration de l'effet Vroman représentant une réaction d'échange entre deux protéines, A et B. La protéine "B", qui est initialement adsorbée à la surface, est déplacée de la surface par la protéine "A". Adapté de (44) avec la permission de Springer Nature.

Les résultats des rapports sur l'adsorption de protéines aux surfaces nanostructurées sont assez contradictoires: certains auteurs ne signalent aucune influence de la morphologie de surface à l'échelle nanométrique (47), tandis que d'autres études ont présenté des données indiquant une augmentation de la quantité de protéines adsorbées pour une rugosité de surface à l'échelle nanométrique (48). En effet, l'adsorption de protéines à la surface de l'implant dépend de la densité de charge à la surface, qui est fortement influencée par la rugosité à l'échelle nanométrique (49). Les surfaces des implants, comme le TiO_2 ainsi que les membranes cellulaires, ont une charge négative (50, 51); il est donc nécessaire de disposer d'un médiateur pour contrôler la force répulsive qui les sépare. Les protéines sont alors souvent utilisées comme ces médiateurs, permettant de combler les interactions électrostatiques répulsives entre les surfaces (50). Les propriétés de surface, y compris la mouillabilité et la charge, influencent l'adsorption des protéines qui facilitent l'adhésion des cellules à l'implant (52). En effet, il a été montré que certaines cellules préfèrent s'attacher sur des surfaces hydrophiles, alors que d'autres préfèrent les surfaces hydrophobes (49). Il a été signalé que les surfaces de biomatériaux moyennement hydrophiles présentent une

31

croissance cellulaire et une biocompatibilité améliorée. Néanmoins, l'adhésion cellulaire peut diminuer lorsque le matériau devient trop hydrophile, ainsi les surfaces doivent généralement conserver une hydrophilie modérée (angle de contact de 40 à 60 °) (53); la charge négative sur les surfaces améliore la prolifération tandis que la charge positive augmente l'étalement et la différenciation (52). Après l'étalement des protéines, un certain nombre de cellules, telles que les monocytes, les leucocytes, vont s'adhérer à la surface du biomatériau et cela peut conduire à augmentation de l'expression des cytokines et à des processus pro-inflammatoires ultérieurs (54). Ce processus donne normalement comme résultat l'intégration de l'implant dans le tissu hôte. Cependant, dans des conditions défavorables, les cellules fibroblastiques qui synthétisent le collagène sont recrutées pour former une capsule de tissu conjonctif autour de l'implant, ce qui entraîne généralement son rejet (54).

L'efficacité ultime de l'ostéointégration dépend entre autres, de la topographie de surface d'un implant. Pour l'intégration réussite de l'implant les propriétés de la surface sont cruciales dans l'adhésion et la différenciation des ostéoblastes pendant la phase initiale de l'ostéointégration ainsi que pour le remodelage osseux à long terme (1). Dans des études précédentes (55) avec une surface de Ti modifié à l'échelle nanotopographique, nous avons démontré que les propriétés physico-chimiques sont détectées par des macrophages U937. Collectivement, la morphologie amiboïde, l'activité de phagocytose et le profil de cytokines obtenus suggèrent que la surface générée tend vers un faible profil inflammatoire qui pourrait faciliter l'osteointégration.

1.4 Infection microbienne

L'introduction d'un implant dans l'organisme est toujours associée à un risque d'infection microbienne, un problème majeur en orthopédie qui peut conduire à l'échec de l'implant et une reprise chirurgicale (56, 57). La capacité des bactéries à adhérer, à survivre et à former ensuite des biofilms sur des surfaces des implants est la principale cause d'infection après une intervention chirurgicale (57). Les sources de bactéries infectieuses plus fréquentes incluent l'environnement de la salle d'opération, l'équipement chirurgical, les bactéries résidentes sur la peau du patient et les bactéries déjà présentes dans le corps du patient. Les espèces *Staphylococcus aureus* et *Staphylococcus* epidermidis sont les principaux agents responsables des infections liées aux implants en orthopédie.

D'autre part, l'une des principales raisons de l'échec des implants dentaires, est la péri-implantite, un processus inflammatoire qui affecte les tissus autour des implants qui résulte en une perte d'os de soutien. La principale cause de la péri-implantite est la prolifération de bactéries de la plaque dentaire dans les tissus de soutien des implants (58). Le biofilm oral implique plus de 700 espèces bactériennes différentes en interaction. Les phases initiales de la formation du biofilm sur les dents et sur les implants peuvent être considérées comme identiques (59). La complexité bactérienne de la plaque dentaire est divisée en deux groupes concernant leur effect dans la formation du biofilm : les colonisateurs primaires et tardifs (60). Le contrôle du biofilm est l'une des principales conditions préalables au maintien de la santé du tissu péri-implantaire et du tissu parodontal (59).

1.5 Topographie et méthodes de modification de la surface du Ti

La surface des matériaux joue un rôle extrêmement important dans la réponse de l'environnement biologique aux dispositifs médicaux artificiels. La modification de la surface doit tenir compte les propriétés des matériaux à modifier, les caractéristiques de surface requises pour l'application finale, la stabilité des modifications ainsi que les aspects pratiques de la technique à utiliser (61).

En plus de la topographie et la rugosité, l'hydrophilie des implants est un autre aspect essentiel qui affecte l'ostéointégration. Des surfaces hydrophiles sont nécessaires pour que les protéines puissent conserver leur conformation et leur fonction, alors que les surfaces d'implants hydrophobes provoquent des changements dans la conformation des protéines (1).

Sur la base des recherches fondamentales qui ont démontré l'importance de contrôler les propriétés des surfaces des implants, un grand nombre de techniques et de méthodologies de modification de surface ont été développées. Grâce à ces techniques, il est possible d'obtenir de manière fiable des nanopores, des nanorainures, des nanopuits, des nanopiliers, des nanotubes et des nanofibres, ainsi que des surfaces avec des nanocaractéristiques superposées sur des surfaces microrugueuses (structures hiérarchiques) (62, 63) .

De façon générale, les propriétés de surface des métaux implantables peuvent être modifiées à différentes échelles par diverses techniques. Dans le cas des implants en Ti, la couche d'oxyde nanométrique formée spontanément, se contamine rapidement par les hydrocarbures

présents dans l'environnement et, est non uniforme et plutôt mal définie (64). Cette surface « native » n'est pas appropriée pour les applications biomédicales et certains traitements de surface doivent être effectués pour promouvoir la biocompatibilité et ajouter de la bioactivité au Ti (65).

Parmi les méthodes utilisées spécifiquement pour modifier la surface de Ti, il existe différentes techniques qui sont classées par rapport au type de procédé sur lequel elles reposent. Nous retrouvons des approches physiques et chimiques qui sont définies selon le mécanisme de formation de la couche modifiée à la surface du métal (21, 25). Certaines technologies peuvent impliquer de multiples processus physiques et chimiques. Ainsi, il est impossible de séparer strictement les méthodes physiques et chimiques (66).

Il existe de nombreuses techniques de dépôt des céramiques bioactives sur des implants métalliques. Les techniques les plus fréquemment appliquées sont : le revêtement sol-gel (solution-gélification), la pulvérisation au plasma, le dépôt biomimétique et le dépôt électrochimique (67). La synthèse d'hydroxyapatite voie sol-gel implique plusieurs étapes : (1) la préparation du sol à l'aide des précurseurs appropriés tels que les alcoxydes métalliques ou les sels métalliques, (2) la gélification où une polymérisation adéquate a lieu pour former une réticulation des molécules, et (3) le séchage pour éliminer l'excès du solvant (68).

Avec ces techniques, il est possible de recouvrir la surface des implants avec des céramiques bioactives comme l'hydroxyapatite, dans certains cas, d'une façon très rapide et avec un bon contrôle de l'épaisseur de la couche bioactive (Figure 6). Par contre, Il faut noter qu'avec l'application des méthodes telles que le revêtement sol-gel et la pulvérisation plasma il n'y a pas d'interaction chimique entre le revêtement et la surface du Ti, ce qui fait que la résistance mécanique du revêtement soit généralement faible et des échecs d'implants aient été signalés (Figure 6)(67, 69).
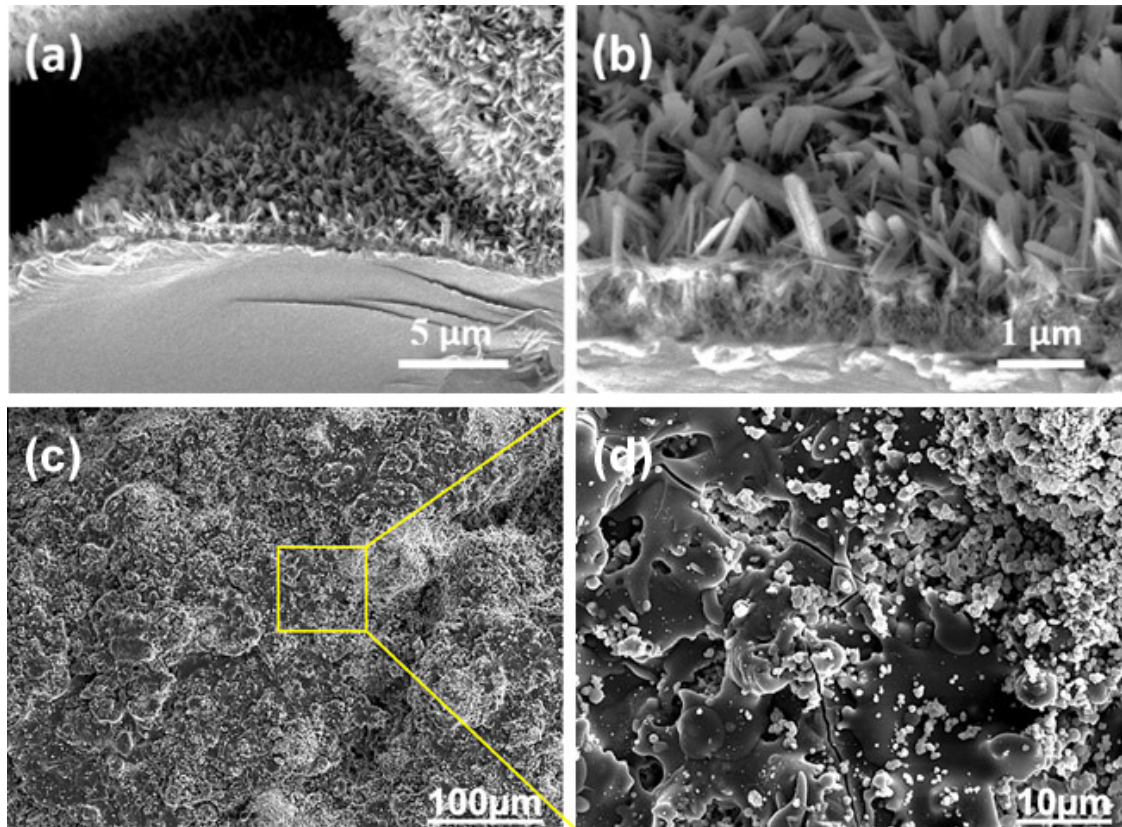
Figure 6. –   Surface de Ti recouverte d'HA en utilisant la méthode du dépôt par pulvérisation au plasma. Micrographies MEB de la section transversale de la couche d'HA à (A) faible grossissement et à (B) plus forte grossissement. Adapté de (70) conformément à la licence Creative Commons Attribution (CC BY) (https://creativecommons.org/licenses/by/4.0/). Micrographies MEB de la surface du dépôt d'HA à (C) faible et (D) plus forte grossissement. Adapté de (71) avec la permission d'Elsevier.

Le traitement par sablage est une autre méthode physique pour modifier la rugosité des implants de Ti. Dans cette technique, une surface macro-rugueuse est obtenue par sablage à gros grains avec des particules d'oxyde d'aluminium à haute pression. Un processus ultérieur de gravure avec des mélanges d'acides tels que le HCl/H_2SO_4 à haute température est souvent utilisé pour transformer la rugosité de la surface de l'échelle macro à une microscopique. Ce traitement génère une plus grande surface active avec une meilleure adhésion cellulaire (Figure 7) (72).
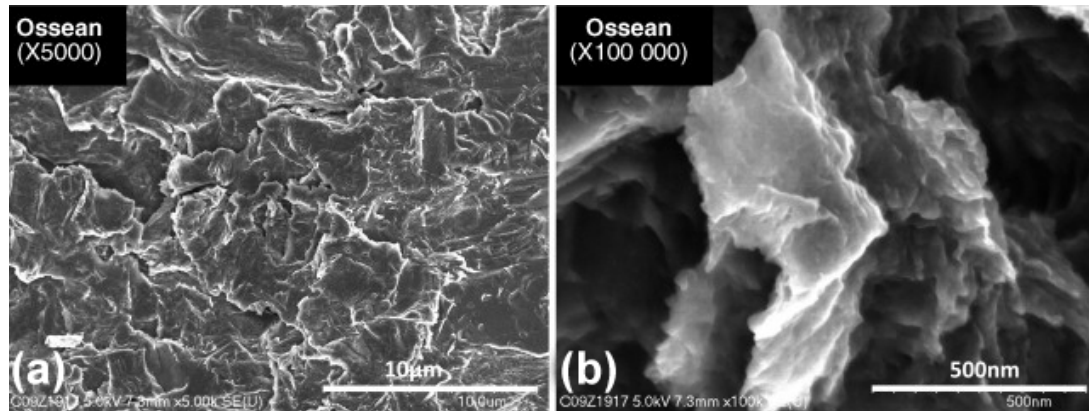
Figure 7. –   (A) Principales caractéristiques de la surface microrugueuse d'un implant dentaire commercial (Ossean), obtenue par sablage et gravure à l'acide. (B) À fort grossissement peut être observé une nanorugosité dense. Adapté de (25) avec la permission d'Elsevier.

Les technologies laser modernes deviennent également des méthodes de plus en plus utilisées pour modifier divers matériaux. Le traitement de surface par irradiation laser génère à la surface des couches dont l'épaisseur varie du micromètre à la dizaine de micromètres. Leur composition et leur microstructure vont dépendre des conditions d'irradiation, de la nature et de la composition de l'atmosphère et des propriétés thermiques et physiques du matériau. Souvent, ses traitements conduisent à un amélioration de propriétés mécaniques et anticorrosives (73).

Dans les méthodes chimiques, nous pouvons différencier deux voies. Le premier est l'attaque chimique du substrat lui-même, tandis que le second consiste en le dépôt de produits issus de certaines réactions chimiques. Ces traitements reposent sur des réactions chimiques qui se produisent à l'interface du matériau. Les traitements les plus utilisés au sein de ce groupe sont classés selon le composé impliqué dans la réaction (peroxyde d'hydrogène, solutions alcalines ou solutions acides). La gravure à l'acide est souvent effectuée à l'aide d'acide fluorhydrique, nitrique ou sulfurique et de leurs combinaisons. La topographie de la surface, la mouillabilité, la micro et nanorugosité, ainsi que l'épaisseur de la couche d'oxyde, peuvent être contrôlées avec précision en ajustant la durée d'exposition, la température et la composition des solutions de gravure (74, 75). Les surfaces générées sur des matériaux comme le Ti (Figure 8), les alliages Ti6Al4V et CrCoMo, et le tantale (Ta) montrent un réseau de nanopuits d'un diamètre entre 20 et 100 nm (75, 76).
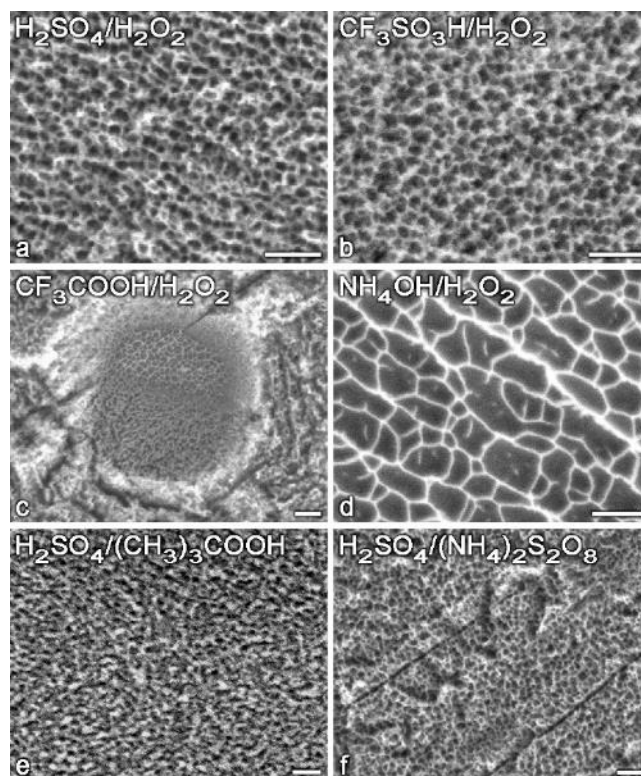
Figure 8. –   Morphologies obtenues sur le Ti à partir des différents traitements de gravure à l'acide. Adapté de (75) avec la permission de American Chemical Society.

De nombreux procédés d'ingénierie peuvent combiner les modifications chimiques et physiques de la surface. Par exemple, l'anodisation électrochimique, est un des moyens les plus courants et plus souples de modifier les surfaces métalliques à l'échelle nanométrique (74). L'oxydation anodique a été utilisée avec succès pour transformer des surfaces lisses de Ti en structures nanotubulaires de diamètres inférieurs à 100 nm (Figure 9) (74).
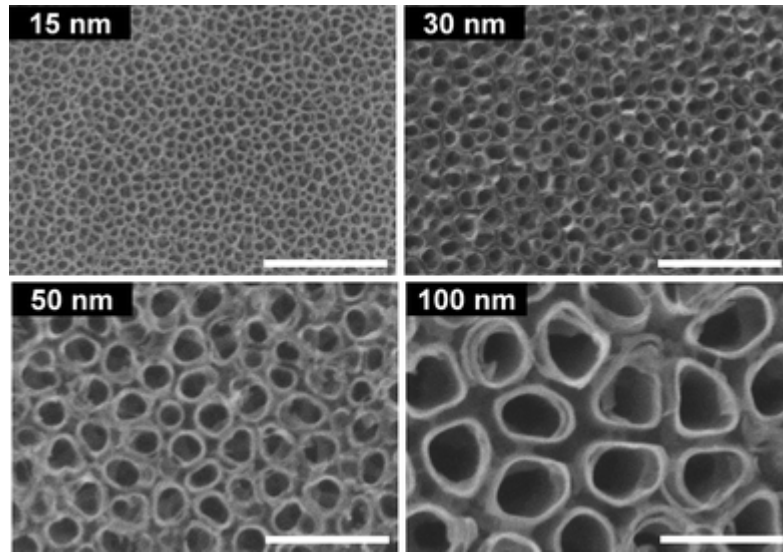
Figure 9. –   Images MEB de nanotubes de TiO$_2$ orientés verticalement de différents diamètres. Échelle : 200 nm. Adapté de (74) avec la permission de Royal Society of Chemistry.

Étant donné que les interactions biologiques se produisent au niveau moléculaire, il est important de caractériser les propriétés de la surface jusqu'à l'échelle nanométrique (65). En particulier, la nanotopographie peut modifier la couche de protéine adsorbée sur le substrat et le comportement des cellules incluant l'adhésion, la morphologie, le cytosquelette et l'expression génique (77).

Les techniques de modification de surface appropriées conservent non seulement les excellents attributs de masse du Ti et de ses alliages, tels qu'un module d'élasticité relativement faible, une bonne résistance à la fatigue, une formabilité et une usinabilité, mais améliorent également les propriétés de surface spécifiques requises par différentes applications cliniques.

1.6 Réponses cellulaires à la nanotopographie

Il est bien établi que les changements dans les caractéristiques topographiques des surfaces peuvent influencer de manière significative le comportement des cellules en modifiant les réponses mécanosensibles (78). Globalement, la façon dont les cellules interagissent avec une surface présentant une topographie à l'échelle nanométrique est la même qu'aux autres échelles. Lorsqu'un nanomatériau se trouve exposé à un milieu biologique son comportement dépend de différents

facteurs et non uniquement de ses caractéristiques intrinsèques. L'interface d'une cellule avec une surface est constituée de points d'attachements (Figure10) (79).
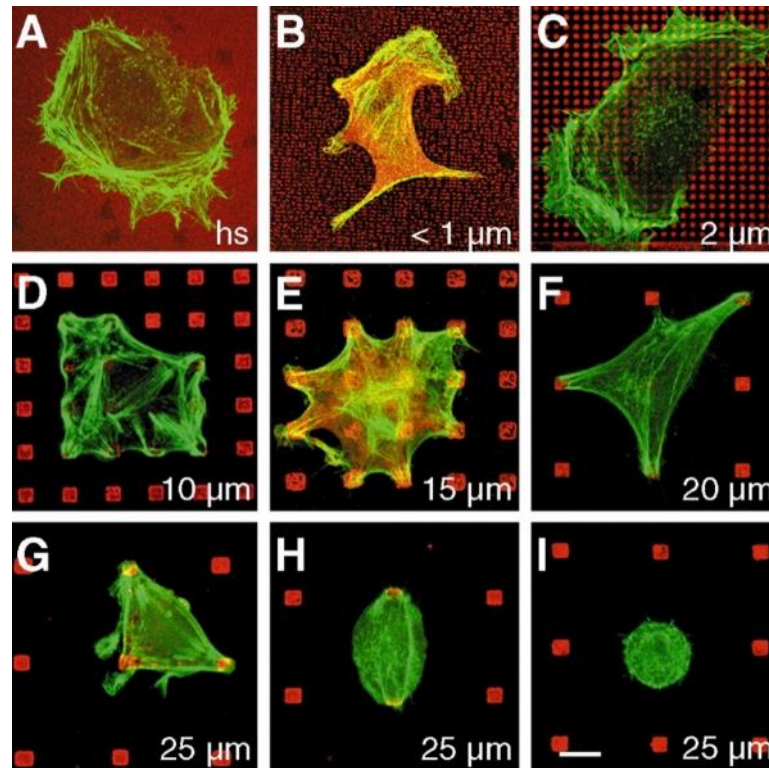
Figure 10. – Étalement cellulaire selon la géométrie du substrat. La distance entre les piliers est décrite sur chaque image. Échelle : 10 µm. Adapté de (80) avec la permission de Company of Biologists LTD.

Les cellules détectent et répondent aux signaux mécaniques des substrats biologiques ou artificiels environnants à travers des lamellipodes et des filopodes (78, 81), ces structures qui se trouvent à la périphérie des cellules sont des protrusions de membrane plasmique riches en actine avec une architecture et une organisation géométrique interne distinctes (82, 83). Dans les cas des filopodes, ils contiennent des filaments d'actine qui s'organisent en longs faisceaux hautement organisés unidirectionnels et parallèlement (83). Lors de l'adhésion à un substrat, les filopodes sondent l'environnement autour de la cellule et leurs extrémités servent de points d'ancrage pour le mouvement (79). Durant la migration cellulaire, les filopodes peuvent exercer des forces sur le substrat et agir comme précurseur des FAs (84). Ils définissent la position des sites de FAs, des filaments d'actine, de la génération de force cellulaire et la formation de nouveaux filopodes (85).

Le taux d'assemblage et de réticulation des filaments d'actine régulera leur initiation et leur allongement (Figure 11) (82, 86).
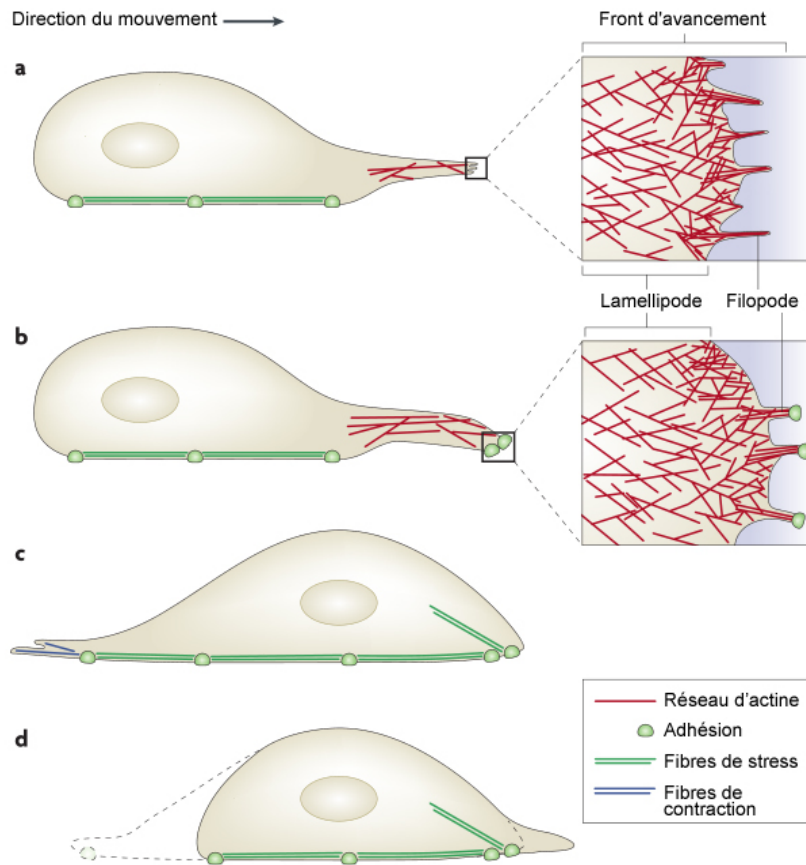
Figure 11. –   Schéma des filopodes et lamellipodes développés par la cellule pendant le sondage de l'environnement superficiel. Adapté de (82) avec la permission de Springer Nature.

L'adhésion cellulaire à la MEC est un processus sophistiqué qui implique une reconnaissance spécifique par des récepteurs transmembranaires des intégrines, une machinerie moléculaire contractile et adhésive qui effectue une détection chimique, physique et topographique (87). Plus précisément, les intégrines sont des récepteurs transmembranaires hétérodimériques existant dans au moins 24 combinaisons uniques de sous-unités α (18 types) et de sous-unités β (8 types) interagissant de manière non covalente, contenant des complexes d'adhésion et se liant à des ligands de la MEC, tels que le peptide RGD (78, 88). Les intégrines s'associent à d'autres protéines cytoplasmiques, qui constituent un lien structurel entre les récepteurs membranaires et le cytosquelette d'actine et qui peuvent jouer le rôle de molécules de signalisation (87) . Cette association permet la formation des FAs (Figure 12), qui fournissent non seulement un lien

mécanique entre la MEC et le cytosquelette, mais qui agissent également en tant que mécanosenseurs responsables des voies de signalisation régulant le phénotype cellulaire (87, 89).
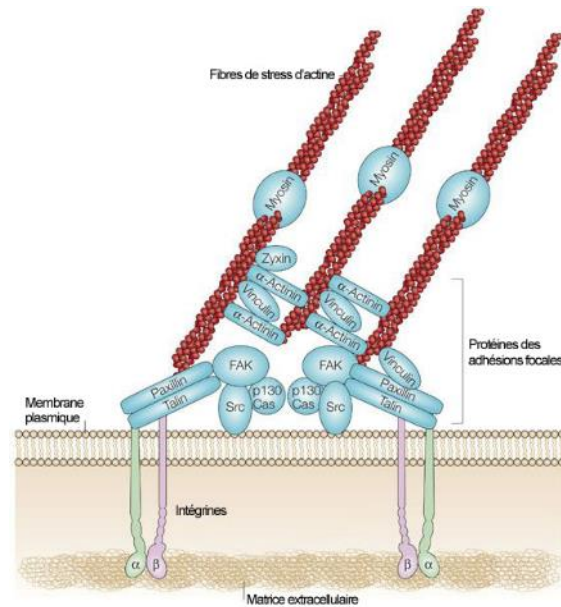
Figure 12. –   Architecture moléculaire des FAs. Adapté de (89) avec la permission de Springer Nature.

La distance requise pour que les hétérodimères d'intégrine se regroupent et forment des FAs est un paramètre important contrôlant les premières étapes de leur développement (87). Diverses études topographiques ont démontré la présence d'une distance maximale entre les sites de liaison (50-70 nm) qui permet le regroupement des intégrines. Au-delà de cette distance, les cellules ne développent pas de FAs résultant en une signalisation par intégrine restreinte empêchant alors l'étalement cellulaire (87, 90). D'autres études ont montré que la hauteur d'un motif est également importante, 15 nm favorisant l'étalement cellulaire, la formation de FAs matures, la formation de cytosquelettes hautement organisés et la différentiation ostéogénique des cellules souches (91). Zouani *et al.* (62), quant à eux, ont observé qu'une plus grande profondeur nanotopographique (100 nm) favorisait la différenciation ostéogénique des cellules souches mésenchymateuses (CSM). Les CSM sont des cellules multipotentes d'origine mésodermique (92). Ces cellules peuvent être isolées à partir des différents tissus adultes, y compris la moelle osseuse et le tissu adipeux. Les CSM sont capables de s'auto-renouveler, mais aussi de se différencier en plusieurs lignées cellulaires, par exemple les adipocytes, les chondrocytes, les ostéoblastes, ainsi que les myoblastes et les cellules neuronales (93). Ces caractéristiques font des CSM une source

de cellules inestimables pour diverses applications biomédicales el biologiques (62). La différenciation des CSM est régulée par des facteurs physiques et chimiques à partir de leur environnement extracellulaire complexe (94, 95). Plusieurs études ont démontré qu'une modulation de la topographie du microenvironnement au niveau subcellulaire et cellulaire peux contrôler la forme et le devenir des cellules souches (96-98) . La différenciation des ostéoblastes est généralement associée à une déformation ou une tension cellulaire élevée. Diverses surfaces ont été utilisés pour obtenir ces conditions, notamment les gels rigides, les surfaces convexes ou les nanopores désordonnés. Au contraire, avec des conditions de basse tension, les cellules souches demeurent indifférenciées, par exemple, sur des surfaces avec des nanopores ordonnés (96). Les topographies anisotropes telles que les nano- ou les micro-rainures favorisent l'allongement et la différenciation cellulaire en myoblastes ou en neurones (Figure 13). Ces résultats montrent que les changements dans la morphologie des cellules en réponse à la nanotopographie modifient la tension du cytosquelette et l'organisation nucléaire interphasique, influençant ainsi directement le profil d'expression des gènes (99, 100).
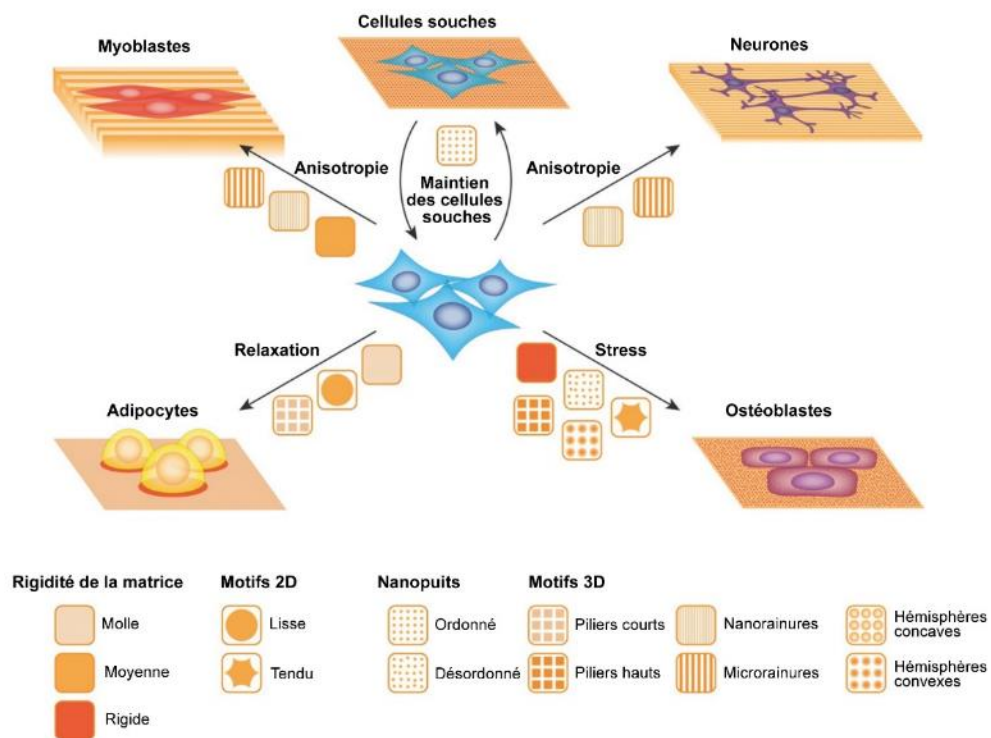
Figure 13. –   La rigidité et la topographie des substrats influencent le destin des cellules souches.

Adapté de (96) avec la permission de CCL Copyright Clearance Center's RightsLink®

La formation des adhésions cellulaires et la réorganisation des filaments d'actine, influencées par la topographie ou non, sont des processus régulés par des GTPases de la famille Rho (101, 102). La formation des FAs et la polymérisation de l'actine à la périphérie des cellules sont régulées par Rac, alors que l'activation de RhoA et de la kinase associée à Rho (ROCK) est liée aux fibres de stress d'actine et au développement de contacts focaux en FAs. La formation de fibres de stress médiées par RhoA est associée à la localisation de taline et de vinculine sur des FAs (103, 104). Sur certaines surfaces nanotopographiques, les intégrines pourraient suivre un recrutement latéral libre et une liaison avec les protéines de la MEC, et ainsi se regrouper et former des FAs matures et stables (Figure 13) (62). L'activation de la voie RhoA/ROCK augmente la tension du cytosquelette par la formation de fibres de stress et de grandes FAs. Ce mécanisme s'appuie sur des études moléculaires montrant qu'une activité plus élevée de RhoA est associée à une tension cellulaire accrue, à un étalement et à une réorganisation du cytosquelette qui stimulent la différenciation ostéogénique des CSM. Le concept général acquis à partir de ces études indique que les CSM se différencient le long d'une lignée ostéogénique lorsque la voie RhoA/ROCK est activée, ce qui conduit à la propagation cellulaire, alors que l'adipogenèse (formation d'adipocyte) est dominée lorsque la voie RhoA/ROCK est inhibée et que la propagation cellulaire est restreinte (99, 105).
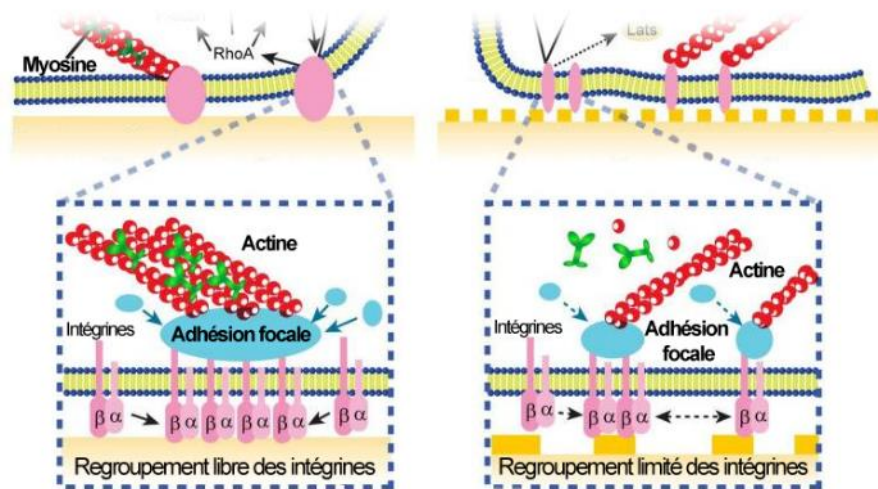
Figure 14. – Recrutement (A) libre et (B) limité des intégrines et formation des FAs. Adapté de (62) avec la permission d'Elsevier.

La composition des FAs varie donc constamment en fonction des signaux externes et des réponses cellulaires (89). De plus en plus de preuves indiquent que les FAs et leurs dynamiques jouent un rôle essentiel dans la détection des propriétés physiques à l'échelle nanométrique du microenvironnement (87). Les adhésions qui se forment peuvent prendre la forme de points ou de plaques focales d'adhésion et varient en termes de composition moléculaire, de maturation, de propriétés mécaniques et de durée d'existence (106-108).

1.7 Phosphorylation de la paxilline

La phosphorylation des protéines joue un rôle important dans la régulation de la formation et du renouvellement des FAs (109, 110). Différents composants des FAs, tels que la kinase d'adhésion focale (FAK), la paxilline et la p130Cas, entre autres, sont phosphorylés en réponse à l'adhésion cellule-MEC médiée par les intégrines (111, 112). Par exemple, le complexe FAK-Src intervient dans la phosphorylation de deux molécules très connues, la paxilline et la p130Cas. Ces deux protéines peuvent recruter d'autres molécules pour former des FAs et pour réguler l'organisation du cytosquelette d'actine (109).

La paxilline, un composant principal des FAs, est une protéine adaptatrice, multifonctionnelle et multidomaine qui joue un rôle important au niveau des FAs en recrutant des molécules structurelles et de signalisation lorsqu'elle est phosphorylée sur des résidus tyrosine et serine spécifiques (113). Les voies de signalisation activées, conduisent à la réorganisation du cytosquelette d'actine et à l'assemblage/désassemblage des FAs nécessaires à l'attachement, à l'étalement et à la migration des cellules. La paxilline contient cinq motifs répétitifs LD riches en leucine situés à l'extrémité N-terminale (LD1 à LD5) et quatre domaines LIM enrichis en cystéine-histidine à l'extrémité C-terminale. Les domaines LD fournissent des sites d'accueil pour les protéines associées aux FAs, notamment les tyrosine kinases de la famille Src, la FAK, la vinculine et la taline, entre autres. Spécifiquement, le domaine LD4, où se trouve le résidus phosphorylable S273, est considéré comme un site de liaison clé pour un certain nombre de molécules de signalisation (114, 115). La délétion du domaine LD4 entraîne une migration perturbée et dans une diminution du nombre de protrusions (116). Différentes études ont identifié la phosphorylation de la paxilline à S273 comme un régulateur critique de l'activation de Rac, de l'adhésion cellulaire et de la formation des filopodes (116). Ce type de mutation est avantageuse car elle permet d'évaluer la contribution de groupes fonctionnels spécifiques dans la réponse aux caractéristiques de surface.

1.8 Propriétés antibactériennes des surfaces

De nombreuses techniques de modification de surface telles que l'application de revêtements sur la surface de l'implant contenant des antibiotiques ou d'autres substances bactéricides comme l'argent, le cuivre ou le zinc, sont souvent utilisées pour rendre les surfaces antibactériennes (117, 118). Les études récentes se concentrent à empêcher la fixation initiale des bactéries sur une surface pour prévenir les infections. Il a été démontré que la topographie des surfaces a un impact significatif sur l'attachement des bactéries et la formation ultérieure de biofilms (Figure 14). Cependant, les mécanismes antibactériens et l'efficacité des paramètres de surface ne sont pas bien compris en raison de la compréhension limitée des interactions entre les bactéries et la nanotopographie. Récemment, différents points de vue et explications ont été proposés pour comprendre le mécanisme des lésions membranaires (57). Il est crucial de déterminer les mécanismes sous-jacents qui entraînent la mort des cellules bactériennes sur les nanotopographies synthétiques, car cela permettra de concevoir de manière rationnelle des surfaces d'implants médicaux résistant à la formation de biofilms (119).
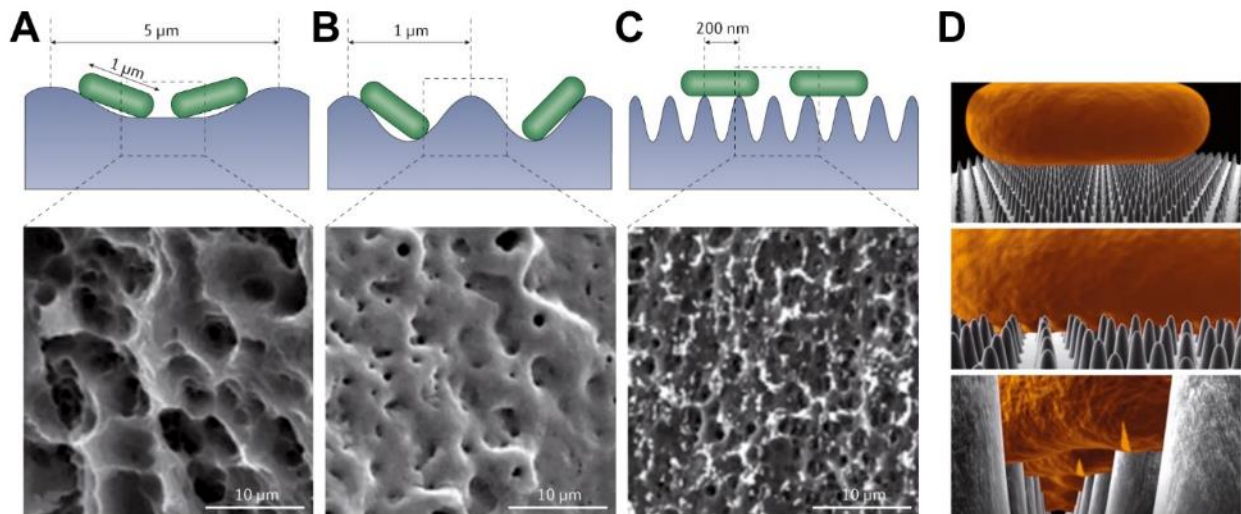
Figure 15. – Fixation différentielle des bactéries sur des surfaces micro-nanostructurées. (A) double gravure à l'acide, (B) anodisation et incorporation électrochimique de Ca/P et (C) gravure acide et dépôt de Ca/P. (D) la membrane s'adsorbe sur les protrusions et se produit un étirement important de la région de la membrane cellulaire suspendue entre chaque nanopilier qui conduise à une éventuelle lyse cellulaire. Adapté de (120) avec la permission de Springer Nature.

1.9 Mesures de forces d'adhésion

De plus en plus de preuves indiquent que les FAs et leur dynamique jouent un rôle essentiel dans la détection des propriétés physiques à l'échelle nanométrique du microenvironnement (87). La mécanotransduction, c'est-à-dire les mécanismes par lesquels les cellules détectent, intègrent, transmettent et transduisent des stimuli mécaniques en une réponse biochimique, c'est un moyen par lequel les changements conformationnels et/ou biochimiques induits par la force dans les environnements cellulaires entraînent l'activation et l'amplification des cascades de signalisation intracellulaires. Ces cascades sont connues pour influer le développement, la différenciation, la migration, la prolifération et la progression des cellules (121-123). En outre, la mécanotransduction par des FAs est une caractéristique majeure de la détection de l'environnement cellulaire, conduisant à des modifications en aval des fonctions cellulaires dépendantes des FAs, y compris l'expression des gènes (124). L'analyse des réponses cellulaires aux signaux physiques suggère que lorsque les cellules adhèrent à une surface, elles détectent leur environnement en le sondant mécaniquement (Figure 15 A et B) (123).
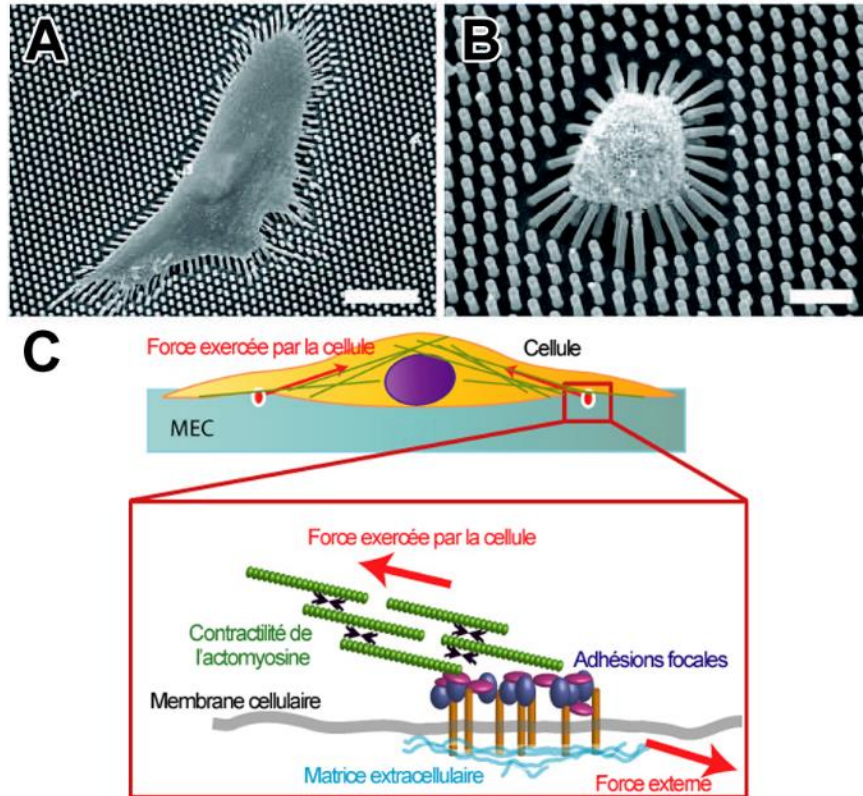
Figure 16. – Micrographies obtenues par MEB pour des cellules MSC humains sur des matrices des poly(diméthylsiloxane) avec des micropiliers de différentes hauteurs (A) L = 6,10 µm et (B) 12,9 µm. Adapté de (41) avec la permission de Royal Society of Chemistry. (C) Forces générées par des cellules adhérentes sur un substrat déformable (flèches rouges). Les forces exercées par les cellules sont générées vers l'intérieur ainsi que les forces exercées par le substrat (force externe) sont opposés. Ces forces sont générées par les FAs et la contractilité acto-myosine. Adapté de (123) avec la permission d'IOP Publishing.

La régulation de la biomécanique cellulaire fonctionne à l'échelle nanométrique puisque les cellules interagissent avec les MEC constituées des éléments à l'échelle nanométrique (79, 125). Par conséquent, une meilleure compréhension de la relation biomécanique entre les filopodes et les caractéristiques de surface à l'échelle nanométrique est très pertinente pour améliorer les surfaces des implants. Il est connu que l'adhésion cellulaire est étroitement liée au cytosquelette d'actine, dont l'organisation est cruciale pour déterminer les propriétés structurelles et mécaniques des cellules (126). Les cellules adhérées à la surface exercent des forces contractiles, également appelées forces de traction, sur le substrat en utilisant leur cytosquelette d'actine-myosine pour se

propulser (Figure 15 C). Les FAs et la génération de tension intracellulaire sont évidemment liées, mais elles se produisent par différentes voies qui se croisent et s'influencent mutuellement (127). Les principaux acteurs de ces voies sont les GTPases de la famille Rho, telles que RhoA, Rac1 et Cdc42 qui agissent en tant que récepteurs de la mécanotransduction et jouent des rôles distincts dans la régulation de la réorganisation du cytosquelette d'actine (Figure 16) (128). Une propagation cellulaire correcte est considérée comme une exigence générale pour une activité RhoA/ROCK élevée et pour la formation de fibres de stress, tandis que les cellules de formes arrondies et petites sont généralement associées à une activité RhoA/ROCK faible (97).
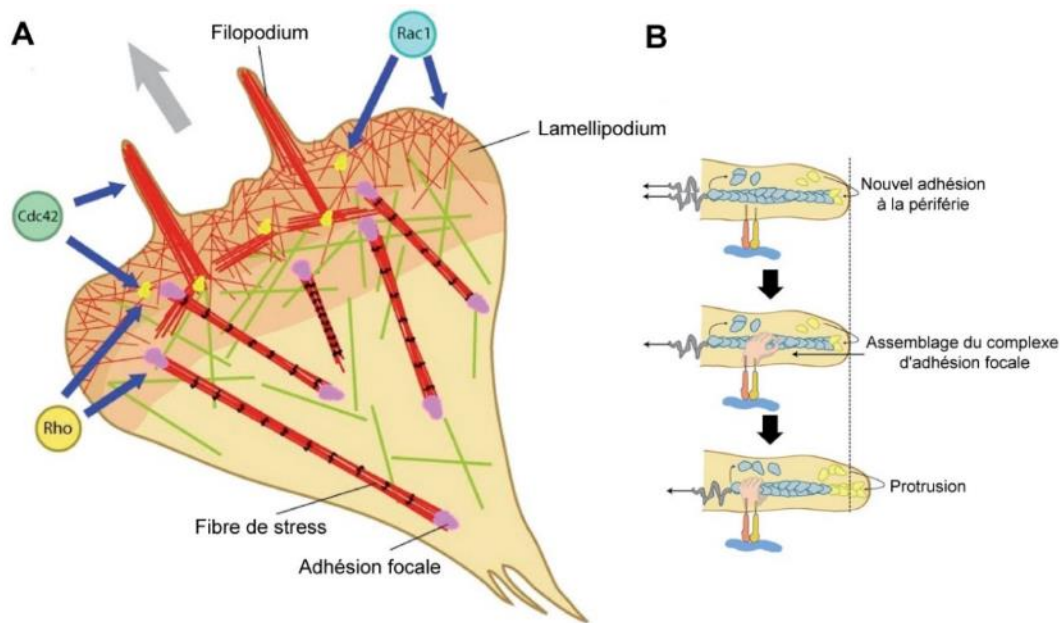
Figure 17. –   Organisation des différentes structures du cytosquelette d'actine au sein d'une cellule adhérente et rôle des structures adhésives dans l'organisation de l'actine. (A) Distribution des FAs focales et matures et des structures d'actine à l'intérieur de la cellule. Rôle des différentes GTPases de la famille Rho (Cdc42, Rho, Rac1) dans des régions spécifiques d'une cellule en mouvement. (B) L'adhésion entre les intégrines ancrées à la membrane et le substrat extracellulaire provoque le regroupement des composants des FAs (représenté par une main). Adapté de (123) avec la permission d'IOP Publishing.

Le nombre de protéines trouvées lors des adhésions ponctuelles est élevé et beaucoup d'entre elles sont des protéines mécanosensibles (MS) (122). La protéine MS la plus importante est la FAK, essentielle pour les adhésions dynamiques (assemblage/désassemblage) (129). La FAK, codée par le gène de la protéine tyrosine kinase (PTK) 2 (PTK2), est une PTK intracellulaire

non-réceptrice activée par autophosphorylation de l'acide aminée Tyr397 (130). Cette phosphorylation induit plusieurs cascades de signalisation en initiant le recrutement de multiples protéines de structure et de signalisation, notamment la vinculine, la paxilline, la taline, la p130Cas et la famille Src kinases (131). La formation d'une complexe Src kinase-FAK est nécessaire pour maintenir l'activation de Rac1 et Cdc42. Ces dernières régulent la nucléation, favorisant ainsi la formation de filopodes et de lamellipodes et la propagation cellulaire qui à son tour, favorise l'agrégation des protéines d'échafaudage et l'élargissement des FAs naissantes; ce processus étant régulé positivement par la disponibilité de molécules d'adhésion dans la matrice. L'augmentation de force qui en résulte à l'interface cellule matrice déclenche l'activation de RhoA et Rac1 (122, 132). RhoA favorise l'interaction de la myosine II avec les filaments d'actine et la contraction de l'acto-myosine, ce qui finalement permet la formation de fibres de stress composées de filaments d'actine orientés longitudinalement. La tension intracellulaire générée par la myosine II induit des changements conformationnels dans diverses protéines d'adhésion, ce qui entraîne une mécanotransduction et une régulation améliorée de plusieurs voies de signalisation (122). L'inhibition des voies menant à l'activation de la myosine II entraîne le désassemblage des regroupements des FAs (133), ce qui indique que les forces de traction contribuent à la stabilité des FAs (134). Une propagation cellulaire correcte est considérée comme une exigence générale pour une activité RhoA/ROCK élevée et pour la formation de fibres de stress, tandis que les cellules de formes arrondies et petites sont généralement associées à une activité RhoA/ROCK faible (97). Les surfaces nanostructurées peuvent aussi moduler les réponses ostéoinductives initiales des cellules pour augmenter l'expression des gènes spécifiques à l'os. Différentes études ont montré une augmentation du niveau d'expression pour Runx2 et Osx en réponse aux surfaces nanostructurées (135). D'autres (136, 137) ont observé une expression précoce et accrue de l'ostéopontine (OPN) et de la sialoprotéine osseuse (BSP) dans des cellules ostéogéniques cultivées sur des surfaces de Ti à l'échelle nanométrique par rapport au Ti poli.

Différentes approches ont été utilisées pour estimer la force d'adhésion cellulaire et quantifier les propriétés mécaniques des cellules (138). Les méthodes les plus simples sont basées sur un flux de cisaillement hydrodynamique pour détacher les cellules de la surface, celle-ci incluent la centrifugation, l'essai de lavage simple, la technique du disque rotatif et les chambres à flux radial (126). Toutes ces techniques appliquent une contrainte de cisaillement bien contrôlée aux cellules adhérentes et elles sont basées sur une population des cellules ou la force d'adhésion

es calculée par le taux de débit appliqué (126). Dans le cas des techniques utilisés pour mesurer la force d'adhésion pour un cellule individuelle, nous pouvons retrouver la microscopie à force atomique (AFM), la spectroscopie de force unicellulaire (SCFS) basée sur l'AFM, l'aspiration par micropipette, pinces magnétiques et cytométrie par torsion parmi les principales (139).

1.9.1 Centrifugation

Dans un essai de détachement cellulaire par centrifugation un substrat recouvert de cellules est placé au fond d'une plaque de culture contenant du milieu. Ensuite, la plaque est centrifugée pendant un certain temps et/ou à diverses vitesses pour ensuite quantifier par microscopie optique le nombre des cellules qui y restent collées (Figure 17) (126, 140).
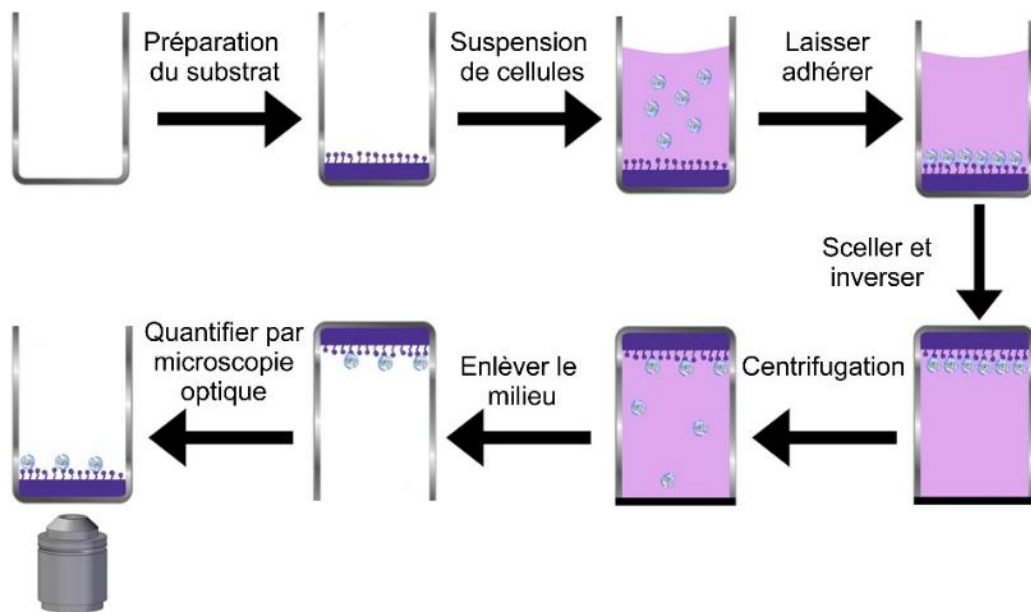
Figure 18. – Scheme qui représente un essai de détachement cellulaire par centrifugation. Adapté de (126) avec la permission d'Elsevier.

1.9.2 Microscopie à force atomique

La microscopie à force atomique est basée sur l'interaction d'une pointe très fine attachée au levier avec la surface du matériau à analyser. Au même temps que la pointe explore la surface, un laser focalise sur le levier et réfléchi sur des photodiodes, enregistre la variation d'hauteur de la pointe. L'intensité (réponse) des interactions entre la pointe et la surface permet d'obtenir de

l'information sur la topographie, ainsi que différentes propriétés de surface. Grâce aux caractéristiques de la pointe, il est possible d'obtenir une haute résolution à l'échelle nanométrique (d'environ 0.1 nm) (141).

Dans des mesures de la biomécanique cellulaire, la pointe est utilisée pour sonder la cellule, et la déformation relative de la cellule qui peut ensuite être utilisée pour estimer la force appliquée et la rigidité de la cellule (142).

1.9.3 Spectroscopie de force unicellulaire

La SCFS basée sur l'AFM est une méthode ultrasensible pour quantifier les forces d'adhésion cellulaire de cellules individuelles dans des conditions physiologiques. Cette technique consiste à utiliser une pointe d'AFM avec une cellule immobilisée comme sonde de mesure. Une cellule vivante est d'abord attachée à un levier sans pointe. Pour faciliter l'immobilisation des cellules, les leviers peuvent être recouverts de différentes protéines de la matrice extracellulaire, telles que la fibronectine ou la laminine, ce qui permet une fixation cellulaire douce via des protéines de surface cellulaire glycosylées. Cette pointe fonctionnalisée est ensuite approchée sur une cellule attachée à une surface et le contact cellule-cellule est maintenu sous une force de contact constante pendant un temps prédéfini. La force d'adhésion cellulaire peut être mesurée à partir du degré de déformation du levier pendant la rétraction de la cellule (Figure 18) (139, 143). Une stratégie similaire consiste à amener un cantilever recouvert de protéines sur une cellule fermement attachée au substrat, puis à rétracter le cantilever.
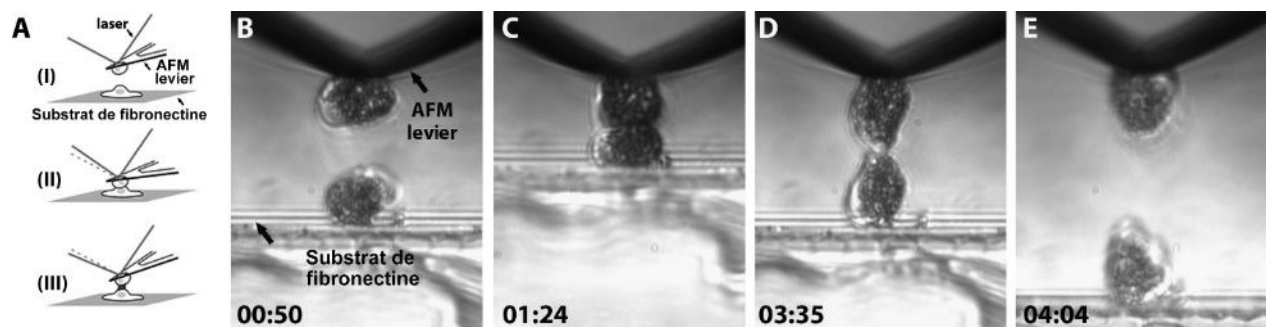
Figure 19. – Spectroscopie de force unicellulaire basée sur l'AFM. (A) Représentation schématique d'une expérience. Adapté de (139) avec la permission d'Elsevier.

1.9.4 Aspiration par micropipette

La technique d'aspiration par micropipette ou microaspiration permet de quantifier la force d'adhésion d'une cellule à partir de la force d'aspiration requise pour détacher la cellule de la surface. La micropipette est positionnée perpendiculairement à la surface d'une cellule adhérente et une pression d'aspiration à taux constant est appliquée. Les cellules et la position de la micropipette sont sélectionnées à l'aide d'un microscope à champ clair (Figure 19) (144).
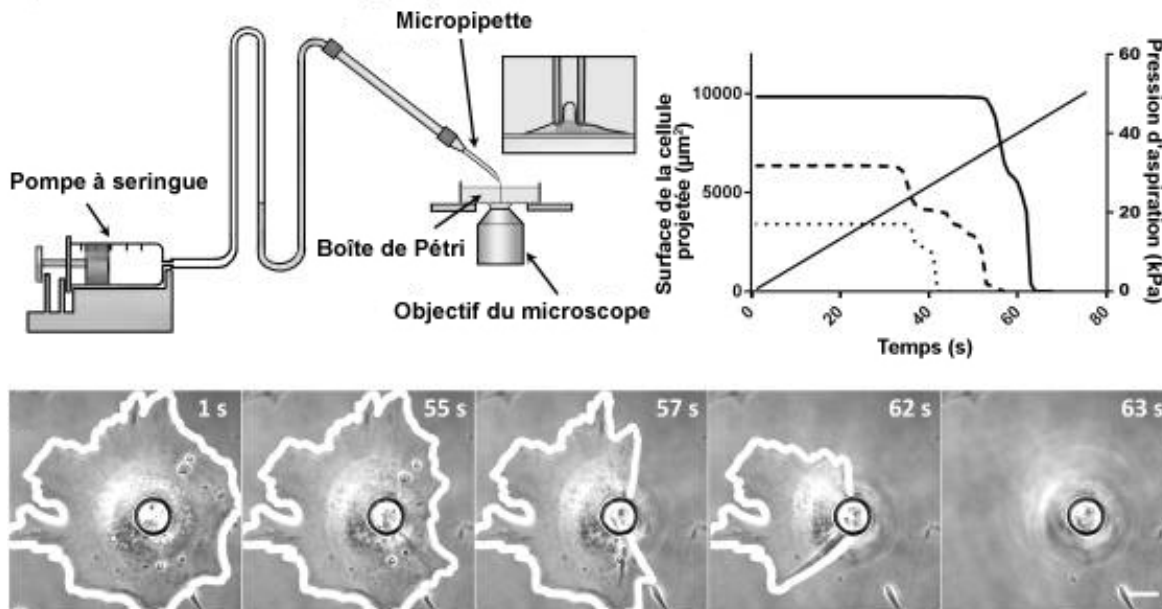
Figure 20. –   Montage expérimental pour la technique d'aspiration. La micropipette est positionnée perpendiculairement à la surface des cellules cultivées au fond d'une boîte de Pétri. La pompe à seringue crée une augmentation constante de la pression d'aspiration. Graphique de la surface de cellule projetée en fonction du temps pour trois cellules différentes. Time-lapse d'une cellule tout au long d'un test de détachement. Échelle 10 μm. Adapté de (144) avec la permission d'Elsevier.

Figure 21. –

1.10 Autres techniques de caractérisation utilisées

1.10.1 Microscopie électronique à balayage

La MEB est une technique de microscopie électronique capable de produire des images en haute résolution de la surface d'un échantillon à partir des interactions électrons-matière (145).
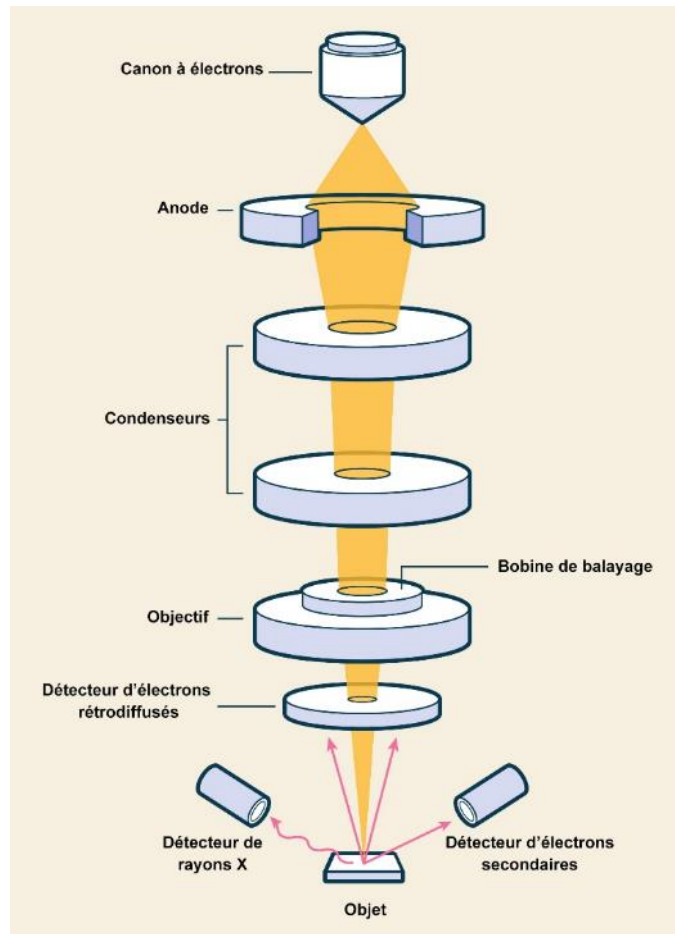
Figure 22. – Schéma du microscope électronique à balayage

La capacité à distinguer des détails fins avec un microscope optique est limité par la longueur d'onde de la lumière et des lentilles de verre utilisées. Les microscopes électroniques utilisent plutôt des électrons dont la longueur d'onde beaucoup plus faible. Le faisceau d'électrons passe à travers d'une colonne à haut vide et est concentré par une série de lentilles électromagnétiques. Dans le MEB, ce faisceau balaye la surface de l'échantillon et l'interaction entre la sonde électronique et l'échantillon génère divers signaux, dont les électrons secondaires de basse énergie. Ces électrons sont accélérés vers un détecteur qui va amplifier le signal (Figure 20) (145). À chaque point d'impact correspond un numérique qui est interprété comme intensité de la couleur du blanc au noir afin de former l'image finale. Ainsi, les régions qui génèrent la plus grande quantité d'électrons secondaires auront une couleur plus claire et celles avec moins d'électrons secondaires seront plus foncées (145).

La qualité des échantillons influence grandement la qualité d'image qui va être obtenue. L'échantillon doit idéalement conduire l'électricité afin de pouvoir évacuer les électrons. Les échantillons biologiques nécessitent donc une préparation spécifique qui vise à les déshydrater, entre autres étapes pour finalement les rendre conductif avec un dépôt métallique de quelques nanomètres habituellement du carbone ou de l'or (146). Des nouvelles générations de microscopes utilisent un nouveau canon à émission de champ froid optimisé pour l'imagerie à haute résolution qui permet imager des échantillons biologiques à faible voltage sans avoir besoin du faire un dépôt métallique (147).

1.10.2 Diffraction des rayons-X

La diffraction des rayons-X (DRX) est un phénomène physique qui se produit lors de l'interaction d'un faisceau de rayons X d'une longueur d'onde particulière, avec la matière cristalline. Cette technique est basée sur la dispersion cohérente du faisceau lumineux par l'objet, qui provoque une interférence constructive des ondes, qui se dispersent vers certaines directions spécifiques dans l'espace (148).

Le phénomène de diffraction peut être décrite par la loi de Bragg (Eq. 1), qui prédit la direction dans laquelle se produit une interférence constructive (pics de diffraction) entre des faisceaux de rayons X diffusés de façon cohérente par un cristal selon:

$$2d \sin\Theta = n \lambda \qquad \text{Eq. 1}$$

Où *d* est la distance entre deux plans cristallographiques (Figure 21), l'angle Θ est le demi-angle de déviation, *n* est l'ordre de réflexion et λ est la longueur d'onde des rayons X.
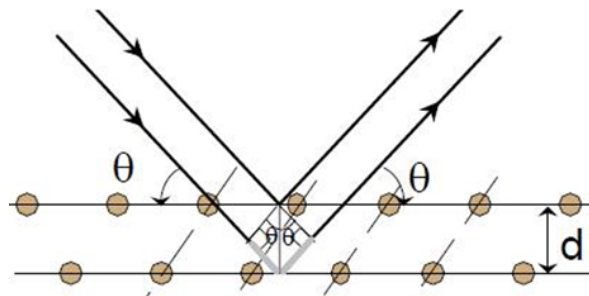
Figure 23. –   Deux plans atomiques représentés en condition de diffraction.

Par la mesure des angles et de l'intensité des rayons réfractés, il est possible d'obtenir une image tridimensionnelle de la densité électronique dans le cristal. À partir de cette densité on peut déterminer la position moyenne des atomes, ions ou molécules qui forment le cristal. Ces données permettent d'obtenir le diagramme de diffraction (diffractogramme).

La technique de DRX sert à identifier les différentes phases cristallographiques du dioxyde de titane (149).
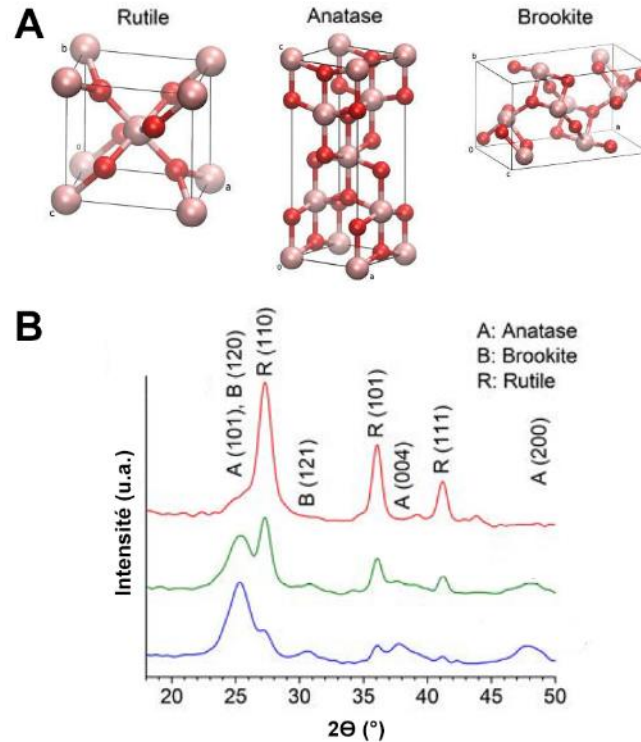
Figure 24. – (A) Structure cristalline des trois polymorphes du TiO_2. Adapté de (149) avec la permission de creative commons CC. (B) diffractogramme montrant ses pics caractéristiques. Adapté de (150) avec la permission d'Elsevier.

Le rutile et l'anatase ont une cellule unitaire tétragonale (mais avec une disposition des atomes différente) tandis que la brookite a une cellule orthorhombique (Figure 22 A). Grâce à ces différences, les trois polymorphes donnent des pics caractéristiques à des endroits différents du diffractogramme (Figure 22 B).

1.10.3 Immunofluorescence

L'immunofluorescence (IF) est une technique immunochimique qui permet la détection et la localisation d'antigènes dans différents types de tissus et diverses préparations cellulaires. Cette large capacité est obtenue grâce à des anticorps spécifiques révélés par des fluorophores. Deux méthodes sont disponibles, en fonction de l'expérience ou des anticorps spécifiques utilisés : directe (primaire) ou indirecte (secondaire) (151). La fixation est une étape préliminaire essentielle dans la coloration pour l'IF afin de préserver la morphologie tout en maintenant l'antigénicité. Cette étape sert à préserver et immobiliser les antigènes cibles en maintenant l'architecture cellulaire. Une étape de perméabilisation postérieur, avec des détergents non ioniques, permet aux anticorps un accès maximal à tous les composants cellulaires ciblés (151, 152). Les fixateurs chimiques comprennent des réactifs de réticulation et des solvants organiques. Des exemples courants incluent le formaldéhyde et le glutaraldéhyde. Les solvants organiques (le méthanol et l'acétone) éliminent les lipides et déshydratent les cellules, dénaturant et précipitant les composants cellulaires. De plus, en perméabilisant les membranes cellulaires, les solvants organiques éliminent le besoin de traitements détergents.

Après la fixation et la récupération de l'antigène, l'une des deux méthodes IF peut être utilisée : IF directe (primaire) ou IF indirecte (secondaire). Dans la méthode directe, le marqueur fluorophore est conjugué directement à l'anticorps primaire qui réagira avec la cible. La méthode indirecte implique un processus d'incubation en deux étapes : 1) un anticorps primaire se lie à la cible, 2) un anticorps secondaire marqué par un fluorophore reconnaît et se lie à l'anticorps primaire.

1.11 Hypothèses et objectifs de recherche

Ce travail vise à contribuer à la compréhension des phénomènes qui contrôlent et régulent le comportement cellulaire en contact avec une surface modifiée à l'échelle nanométrique, plus spécifiquement à l'adhésion cellulaire. Nous pensons que la force d'attachement des FAs, des filopodes et de leurs extensions engendrent une cascade de signalisation biomécanique qui module le comportement cellulaire. La variation des caractéristiques physiques de la surface des implants à l'échelle nanométrique (rugosité et nanoporosité) permet d'obtenir des résultats sans nécessairement avoir besoin d'utiliser des molécules bioactives telles que des protéines et des facteurs de croissance et ceci sans risque d'effet secondaire.

Dans nos travaux nous avons utilisé une surface nanoporeuse de Ti, produite par oxydation chimique, qui a un effet bénéfique sur le comportement de cellules ostéogéniques et simultanément a une capacité antibactérienne. Cette connaissance est nécessaire pour mieux contrôler l'intégration d'un matériau dans le corps, particulièrement le processus d'ostéointégration, ce qui permettra d'adapter intentionnellement les surfaces des implants en fonction des patients. Dans cette optique, nous allons spécifiquement :

1. Évaluer l'effet de la cristallinité de la surface sur le comportement des cellules ostéoblastiques MC3T3 et des bactéries.
2. Tester le rôle de la paxilline dans la réponse cellulaire à la nanotopographie en exploitant une ligné cellulaire qui exprime la protéine paxilline avec des mutations qui affectent la phosphorylation.
3. Déterminer la contribution biomécanique des filopodes et de leurs nanoprotrusions[1] à l'interaction adhésive des cellules avec le Ti.

1.12 Structure de la Thèse

Le chapitre 1 présente le contexte et la problématique de l'étude. Cette section démarre avec une description de l'os, des biomatériaux et des applications osseuses des biomatériaux. Ensuite, des aspects tels que l'osteo-intégration, la topographie et les modifications de surfaces des biomatériaux en titane sont discutés. Les interactions des cellules avec la surface, y compris les bactéries, sont aussi abordées. Finalement, les techniques utilisées pour les mesures de forces d'adhésion, les objectifs de recherche et d'autres techniques de caractérisation ont été abordées. Cette première section est suivie des chapitres suivants :

Chapitre 2
- Premier article qui présente les aspects physico-chimiques de la nanotopographie d'une surface de titane créé par une traitement chimique, ainsi que les effets de la topographie, la cristallinité et de l'hydrophilie sur des cellules et des bactéries.

Chapitre 3
- Deuxième article qui aborde les résultats obtenus sur le comportement cellulaire en utilisant un modèle de mutation génétique en interaction avec la nanotopographie de surface.

Chapitre 4
- Troisième article qui montre une analyse sur la contribution biomécanique des filopodes et de leurs nanoprotrusions à l'interaction adhésive des cellules avec des surfaces nanostructurées.

Chapitre 5
- Aborde une discussion générale intégrée des résultats obtenus dans les 3 articles que composent la Thèse.

Chapitre 6
- Montre les conclusions générales de cette thèse, permettant de faire un bilan global sur les objectifs principaux proposés.

Chapitre 7
- Présente les perspectives de ce travail.

Annexe
- Article qui présente l'obtention d'une couche mince mésoporeuse d'oxyde cristallin à la surface de l'acier inoxydable, qui présente simultanément un impact sélectif sur l'activité cellulaire et les propriétés antibactériennes.

1.12.1 Situation des articles à la date du dépôt et contribution des auteurs

Chapitre 2 – Surface nanoporosity has a greater influence on osteogenic and bacterial cell adhesion than crystallinity and wettability. Alejandra Rodriquez-Contreras[1], **Dainelys Guadarrama Bello**[1], Antonio Nanci. *Applied Surface Science* **2018**, *445*, 255–261. [1]Contribution égale.

Pour ce manuscrit, Alejandra Rodriquez-Contreras et moi-même avons contribué de manière égale. Nous avons fait la préparation des surfaces des disques de Ti (polis et nanotexturisées). La caractérisation des surfaces par Diffraction de Rayons X et l'angle de contact a été effectué ailleurs (McGill Institute for Advanced Materials). La culture cellulaire et des bactéries a été effectué par Alejandra Rodriguez-Contreras. J'ai pour ma part préparé les échantillons pour immunofluorescence et pour MEB. L'acquisition des images et le traitement des données a été fait entre nous deux. L'analyse de l'ensemble des données été effectuée par les trois auteurs. L'écriture des premières versions du manuscrit a été faite par Alejandra Rodriguez-Contreras et moi-même. Antonio Nanci a été le superviseur de l'ensemble du projet et a participé dans l'écriture et la révision afin de soumettre la version finale du manuscrit. Les réponses aux arbitres ont été développés par les trois auteurs.

Chapitre 3 – Nanoporosity stimulates cell spreading and focal adhesion formation in cells with mutated paxillin. **Dainelys Guadarrama Bello**, Aurélien Fouillen, Antonella Badia, and Antonio Nanci. *ACS Appl. Mater. Interfaces* **2020** (12), *13*, 14924–14932.

Pour ce manuscrit, j'ai préparé les surfaces des disques de Ti (polis et nanotexturisées). J'ai effectué la caractérisation des surfaces par MEB at AFM. La culture cellulaire a été effectuée par moi-même ainsi que la préparation des échantillons pour immunofluorescence et la MEB. J'ai collecté l'ARN et la technique de RT-PCR a été réalisée par Aurélien Fouillen. L'acquisition des images, le traitement et l'analyse de l'ensemble des données et l'analyse statistique ont été effectués par moi. L'écriture de la première version du manuscrit a été faite par moi-même. Antonella Badia a participé à la révision du manuscrit. Antonio Nanci a été le superviseur de l'ensemble du projet et a participé dans l'écriture et la révision afin de soumettre la version finale du manuscrit. Les réponses aux arbitres ont été développés par Antonio Nanci et moi-même.

Chapitre 4 – Adhesion response of filopodia to an AFM lateral detachment force and functional changes after centrifugation of cells grown on nanoporous titanium. **Dainelys Guadarrama Bello**, Patricia Moraille, Serine Boughari, Antonella Badia, Antonio Nanci. *Materials Today Bio* **2022**, *14*, 100250.

Pour ce manuscrit, les surfaces des disques de Ti (polies et nanotexturisées) ont été préparées par Serine Boughari et moi. J'ai effectué la caractérisation des surfaces par MEB. La culture cellulaire pour les études d'AFM ainsi que les mesures des forces par AFM ont été réalisées par moi avec l'aide et la supervision de Patricia Moraille dans le cas des mesures. Serine Boughari a participé à l'expérience de centrifugation, l'acquisition des images pour les FAs et l'expression des mitochondries en immunofluorescence sous ma supervision. L'ensemble du traitement, de l'analyse des données et de l'analyse statistique ont été effectuées par moi. L'écriture du manuscrit a été faite para moi-même. Antonella Badia a participé à la supervision des expériences par AFM et la révision de la version initiale du manuscrit. Patricia Moraille a participé à la révision du manuscrit initial. Antonio Nanci a été le superviseur de l'ensemble du projet et a participé à l'écriture de la première version du manuscrit et la révision afin de soumettre la version finale. Les réponses aux arbitres ont été développés par Antonio Nanci et moi-même.

---

[1] nanoprotrusions : extensions latérales de taille nanométrique émis par les filopodes en réponse à la nanotopographie.

Chapitre 2 – Surface nanoporosity has a greater influence on osteogenic and bacterial cell adhesion than crystallinity and wettability

Alejandra Rodriguez-Contreras [a,1], Dainelys Guadarrama Bello [a,1], Antonio Nanci [a,b*]

[a]Laboratory for the Study of Calcified Tissues and Biomaterials, Department of Stomatology, Université de Montréal, Montréal, Québec, Canada

[b]Department of Biochemistry and Molecular Medicine, Faculty of Medicine, Université de Montréal, Montréal, Québec, Canada

[1]Contributed equally.

Corresponding Author

Antonio Nanci

Faculté de Médecine Dentaire

Université de Montréal

C.P. 6128, succ. Centre-ville

Montréal (Québec) H3C 3J7

E-mail: antonio.nanci@umontreal.ca

Phone: 514 343-5846

Fax: 514 343-2233

Abstract

There has been much emphasis on the influence of crystallinity and wettability for modulating cell activity, particularly for bone biomaterials. In this context, we have generated titanium oxide layers with similar mesoporous topography and surface roughness but with amorphous or crystalline oxide layers and differential wettability. We then investigated their influence on the behavior of MC3T3 osteoblastic and bacterial cells. There was no difference in cell adhesion, spreading and growth on amorphous and crystalline surfaces. The number of focal adhesions was similar, however, cells on the amorphous surface exhibited a higher frequency of mature adhesions. The crystallinity of the surface layers also had no bearing on bacterial adhesion. While it cannot be excluded that surface crystallinity, roughness and wettability contribute to some degree to determining cell behavior, our data suggest that physical characteristics of surfaces represent the major determinant.

Keywords: Titanium, Crystallinity, Nanotopography, Wettability, Osteogenic cells, Bacteria

2.1 Introduction

When the surface of Titanium (Ti) and its alloys is exposed to oxygen, it instantaneously forms a thin (5 nm), protective oxide layer (1–3). This thin natural, forming oxide surface layer is generally amorphous (4), and transforms Ti into a biologically inert metal (5). To improve the biological performance of Ti-based materials for bone applications, several investigations have focused on modifying their surface properties such as topography, chemical composition, and surface energy (6,7). Most of these efforts have resulted in crystalline surface oxides that can exhibit different crystal lattices, including anatase, rutile and brookite (5). In general, it was concluded that the anatase form of the oxide layer shows higher hydrophilicity that positively affects cell behavior (8–13).

Our group has introduced a simple oxidative method using mixtures of H_2SO_4 and H_2O_2 to create an intricate network of nanometric pores on surfaces of Ti-based metals (14–16), a process we have recently termed as nanocavitation (17). This mesoporous surface has been shown to selectively influence the growth and activity of various cells *in vitro*, including stem cells (18,19), and to promote osteogenic activity *in vitro* (20), and *in vivo* (21). More recently, we further demonstrated that the mixture can also be used as an atypical anodization electrolyte to similarly nanocavitate stainless steel (SS) in order to improve cellular activity and achieve antibacterial properties (17). The oxide layer that nanocavitation generates on Ti-based surfaces is amorphous whereas it is crystalline on SS. The similar cellular results obtained with Ti and SS, however, raise questions about the role of crystallinity. In fact, a recent study comparing the efficacy of evaporated TiO_2 coatings concluded that amorphous films are better than crystalline ones at stimulating osteogenic activity *in vitro*, and related this to dissimilarities in surface properties such as polarity (22).

It is still not resolved whether crystallinity of titania layers has a determinant influence on biological events (23). Surface chemistry and topography modulate the wettability of titanium surfaces. As regards, wettability, values ranging widely from superhydrophobic to superhydrophilic have been reported for commercial implants (24). A better understanding and control of these parameters should permit the rational design of implants to improve the success rates of dental and orthopedic bone implants.

Our objective was to compare a same mesoporous surface with crystalline and amorphous oxide layers. Crystalline surfaces are normally achieved by annealing at high temperatures (25). We have found that such a treatment, however, alters the nanoscale surface details (26). To avoid this complication, we have developed a non-thermal approach to transform the amorphous surface into a crystalline one so we could directly compare their influence. The use of a same material with different crystallinity to eliminates experimental inconsistencies and variations related to comparing different materials. Our results reveal that mesoporosity supersedes any influence that the crystallinity of the surface may have on the growth of MC3T3 osteogenic and on bacterial cell adhesion.

2.2 Material and methods

2.2.1 Nanocavitation of Ti discs

Commercially pure grade 2 Ti discs (cpTi) with a diameter of 12 mmand a height of 2 mmwere polished to a mirror finish (control). For nanocavitation, cpTi samples were cleaned with 100% ethanol (Fisher Scientific, Fair Lawn, NJ) in an ultrasonic bath and dried in air. Then, they were treated with a 50:50 mixture of 96% sulfuric acid (J.T. Baker, Phillipsburg, NJ) and 30% aqueous hydrogen peroxide (Fisher). The components were combined on ice to control the exothermic reaction, and the cooling bath was removed when the temperature of the oxidizing composition stabilize to 22 °C. The discs were introduced to the mixture (10 mL/disc) and kept for 1.5 h under constant agitation (14,27). Afterwards, discs were rinsed with distilled water five times to remove any trace of the acidic mixture, sonicated for 15 min in distilled water and airdried. Some samples were used immediately, while others were kept for 0 (freshly-prepared), 1, 2 and 4 months inside a desiccator (Dry-Keeper desiccator, Samplatec Corp., Japon) at 22 degrees prior to use. Preliminary analyses revealed the change in atomic state takes place by the 4th month. Thus, from here on all analyses will relate to 4-month-old samples.

2.2.2 Surface characterization

2.2.2.1 X-ray photoelectron spectroscopy (XRD)

The surface crystallinity of control, freshly-prepared and 4- month-old nanocavitated Ti was analyzed by XRD using a Bruker D8 Discovery X-ray Diffractometer equipped with a Vantec

2000 Area Detector and copper X-ray source (Cu Kα radiation, k = 0.15 405 nm). Grazing-incidence XRD with x/2h mode was used to investigate the ultra-thin oxide layer on Ti discs. The incident beam angle (x) was chosen to be 3° in accordance with Bouroushian and Kosanovic studies (28), with an analysis range was 11–60°. The step size and set time were 0.005 and 300 s, respectively. The main peaks (2θ) appearing in Ti surface patterns analyzed in this study and the ones in the bibliography (29–32) were compared. Crystallinity was unequivocally observed after 4-months under ambient conditions, and further characterization as well as cell analysis, were carried out on only control, freshly-prepared and 4-month-old samples.

2.2.2.2 Contact angle

To assess surface wettability of the samples, water contact angles were measured with dH_2O at room temperature with a Ramé-Hart NRL-100 goniometer. Water drops (10 µl) were placed on the control, and freshly-prepared and 4-month-old nanocavitated Ti discs and contact angles were measured 10 s after application. The average contact angle was obtained from 5 measurements performed on different samples from each substrate.

2.2.2.3 Scanning electron microscopy (SEM)

The topography of Ti surfaces and the morphology of cells were examined using a JEOL JSM-7400F (JEOL Ltd., Tokyo, Japan) or a Zeiss Gemini SEM 500 instrument (Zeiss GmbH, Oberkochen, Germany) field emission scanning electron microscope (FE-SEM) operating at 1.5–2 kV and 20 kV, respectively, without any coating. Pore diameter was measured on FE-SEM images using Photoshop (Adobe Systems, San Jose, CA, USA).

2.2.2.4 Atomic force microscopy (AFM)

The surface topography and roughness (root-mean-square (Rq), arithmetic mean (Ra) and average distance between the highest peak and lowest valley (Rz)) were analyzed by AFM. Images were acquired in air at 21 °C using tapping mode on a JSPM-5200 scanning probe microscope (JEOL Ltd.) performed at a scan rate of 2 Hz using NSC14 cantilevers (MikroMash, Sofia, Bulgaria) with a nominal spring constant of ~ 5.7 N/m and tip radius <10 nm.

2.2.3 Cellular assays

Mouse calvaria-derived osteoblasts (MC3T3, ATCC® CRL-2593TM American Type Cultural Collection) were cultured on the various Ti surfaces in Falcon 12-well plates (Becton-Dickinson, Lincoln Park, NJ) for 6 h, 1, and 3 days at a cellular density of 10,000 cells/well. Ti samples were previously washed with 100% ethanol and left under UV overnight. Osteoblasts were grown in alpha minimum essential medium with Earle's salts, L-glutamine, ribonucleosides, and deoxyribonucleosides (α-MEM, Invitrogen, Burlington, Ontario, Canada), supplemented with 10% fetal bovine serum (Invitrogen) and incubated at 37 °C in a humidified atmosphere with 5% CO_2.

2.2.4 Cell preparation for FE-SEM

For morphological studies, cells on Ti discs were fixed with 2.5% glutaraldehyde for 1 h at 4 °C, washed 3 times (5 min each) with 0.1 M phosphate buffer (PB, pH 7.2–7.4), post-fixed with a 1% aqueous osmium solution (1h at 4 °C), and washed 3 times (5 min) with PB. The cells were then dehydrated by exposure to a graded sequence of aqueous ethanol (30–100%) and finally dried in a critical point drier (Leica Microsystems Inc., Buffalo Grove, IL, USA). Characterization of the cell morphology on the polished and chemically-treated surfaces was carried out by FE-SEM as above.

2.2.5 Immunofluorescence microscopy

Cells were fixed for 30 min at 4 °C using periodate-lysine-paraformaldehyde (PLP) solution in PB. The cells were then permeabilized by exposure to a 0.5% solution of Triton X-100 in PB (10 min), followed by blocking with 5% skimmed milk in PB (1 h). The first antibody, anti-vinculin (1:200; Monoclonal Anti-Vinculin Clone hVIN-1, Sigma), was used simultaneously with rhodamine-phalloidin (red fluorescence for actin labeling) (1:150, Thermo Fisher). The secondary antibody used was Alexa Fluor 488 (green fluorescence for vinculin labeling) (1:400, Thermo Fisher Scientific, Waltham, MA, USA). Antibodies were diluted in a 0.5% solution of skimmed milk in PB and the samples were incubated in a dark humidified environment for 2 h at 22 °C. Between each incubation step, the samples were washed with PB (3 times for 5 min). The incubated disc surfaces were mounted with a glass coverslip using a medium containing 40,6-diamidino-2-phenylindole (DAPI) to make nuclei blue-fluorescent (Molecular Probes, Thermo Fisher Scientific). Samples were then examined under a Zeiss Axio Imager upright fluorescence microscope (Zeiss GmbH). For quantitative cell counting, 60 microscope fields under the 10X

objective were selected at random from the untreated and treated surfaces. To estimate the size of the focal adhesions (FA), the captured immunofluorescence images under 40X objective were separated into single-channel grayscale images using the ImageJ split-channel command. To quantify the adhesion length, images taken from the 6 and 24 h cultures were used to measure the length of each individual vinculin point. FAs with length >5 mm were considered as mature (33). These were classified in ranges and expressed as a percentage of the total measurements.

2.2.6 Bacterial assays

Escherichia coli was used to evaluate the antibacterial properties of Ti surfaces with different crystalline structure. The inoculum was prepared by adjusting bacterial suspension to an OD600 of 0.2 (108 CFU/mL) with lysogeny broth. A standard volume of this solution (2 mL) was placed onto sterilized Ti samples, which were then incubated at 37 °C for 2 h. The samples were then washed with PB, fixed with a 2.5% solution of glutaraldehyde in PB for 30 min, washed 3 times with PB, post-fixed in a 1% aqueous osmium solution for 30 min, dehydrated in graded aqueous ethanol (30–100%), and dried in a critical point drier (Leica Microsystems Inc.).

2.2.7 Statistical analyses

Biological results were expressed as a mean value of standard deviation (SD) for each sample. The t-test was used with a 95% confidence interval to evaluate statistical differences of parametric data in means between two groups.

2.3 Results and discussion

A key tenet of medical device design relies on the ability of biological systems to respond to physicochemical features, a process that has led to the development of the next generation of biomaterials for a wide variety of clinical applications. In this study, we aimed at elucidating the contribution of topography by itself, as well as clarifying the benefit of crystallinity and wettability of the surface oxide layer on adhesion and proliferation of osteogenic and bacterial cells adhesion on mesoporous Ti surfaces. The finding that simple storage at dry conditions and room temperature can transform an amorphous Ti oxide layer into a crystalline one without changing the surface topography made it possible to achieve direct comparisons to address our questions.

2.3.1 Surfaces characterization

The surface structure of both freshly treated and 4 months-old Ti samples was characterized by FE-SEM and AFM. We confirmed that in both cases the surfaces exhibit a similar network of nanoscale cavities with an average diameter of 19.6 ± 9.3 nm and 20.0 ± 5.7 nm, respectively (Fig. 1a). (Fig. 1a, b). AFM further showed that the surfaces roughness was not affected over time (Fig. 1b, c). Furthermore, in both cases, the surfaces were similar to what was previously reported (14,34).
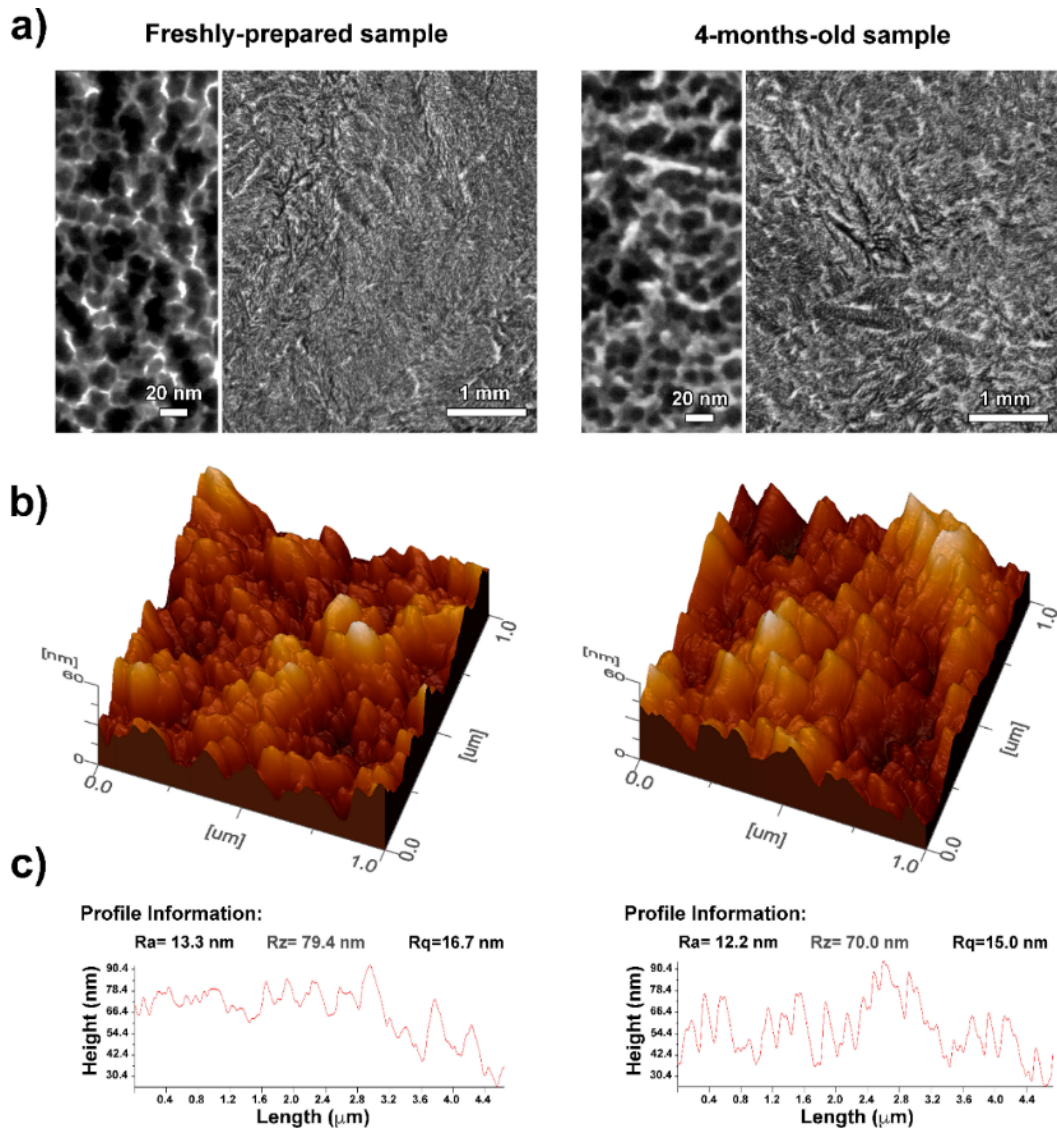
Figure 25. – Fig. 1. Comparative FE-SEM (a) and AFM (b, c) images of freshly-prepared and 4-month-old nanocavitated surfaces.

XRD analysis was performed to determine the crystallinity of the Ti oxide layers. The freshly-prepared and 4-month-old samples showed different XRD patterns (Fig. 2a). Control, freshly-prepared and 4 month-old samples showed peaks around 36.4°, 38.9° and 41.3° degrees, which correspond to the position of a-Ti peaks (35) (Fig. 2c). The presence of these multiple peaks is due to the fact that X-Rays pass through the thin amorphous surface oxide layer (~5 nm for polished Ti and ~30 nm for nanocavitated Ti) into the bulk material (35). Definitive crystalline peaks were only seen as of 4-months. The spectra showed peaks for α-Ti as well as the main peak at 2h at 25.2° and a subtler one at 26.4°, which correspond to the anatase and rutile phase, respectively. The higher anatase peak of the X-ray pattern compared to the rutile peak indicates that the anatase phase predominates. This coincides with the FTIR results (Fig. 2b). Anatase and rutile peaks are difficult to distinguish, however, the relative amounts of anatase compared to rutile can be seen through the shift in the TiO_2 peak. The FTIR analyses also show differences in the crystalline structure of the samples. Spectra of the control and of the freshly-prepared sample do not show any sign of crystallinity (Fig. 2c), thus, confirming their amorphous nature. For 4-months-old samples, FTIR analyses showed the presence of both anatase and rutile crystalline phases (870 cm^{-1} and 830 cm^{-1}, respectively) (36).

Water contact angle results revealed a change in the wettability of the nanocavitated surfaces. Freshly-prepared samples were significantly hydrophilic, with values lower than 90° (37) compared with the 4-months-old ones ($p < 0.05$) (Fig. 2d). Water contact angles of the polished Ti surfaces were found to be similar to what is reported in the literature (38). Hydrophobicity can be modulated by the topography of the surface (22,38,39). Thus, the lower value obtained for the freshly nanocavitated amorphous surfaces agree with previously reported results, their hydrophilic nature basically due to the increase of hydroxyl groups incorporated during the etching process (35). The sample stored for 4 months showed an increase of the water contact angle, revealing a change in wettability of the surface. This hydrophobicity agrees with studies reporting that deposited crystalline anatase thin films show higher contact angles than amorphous and rutile thin films (40).
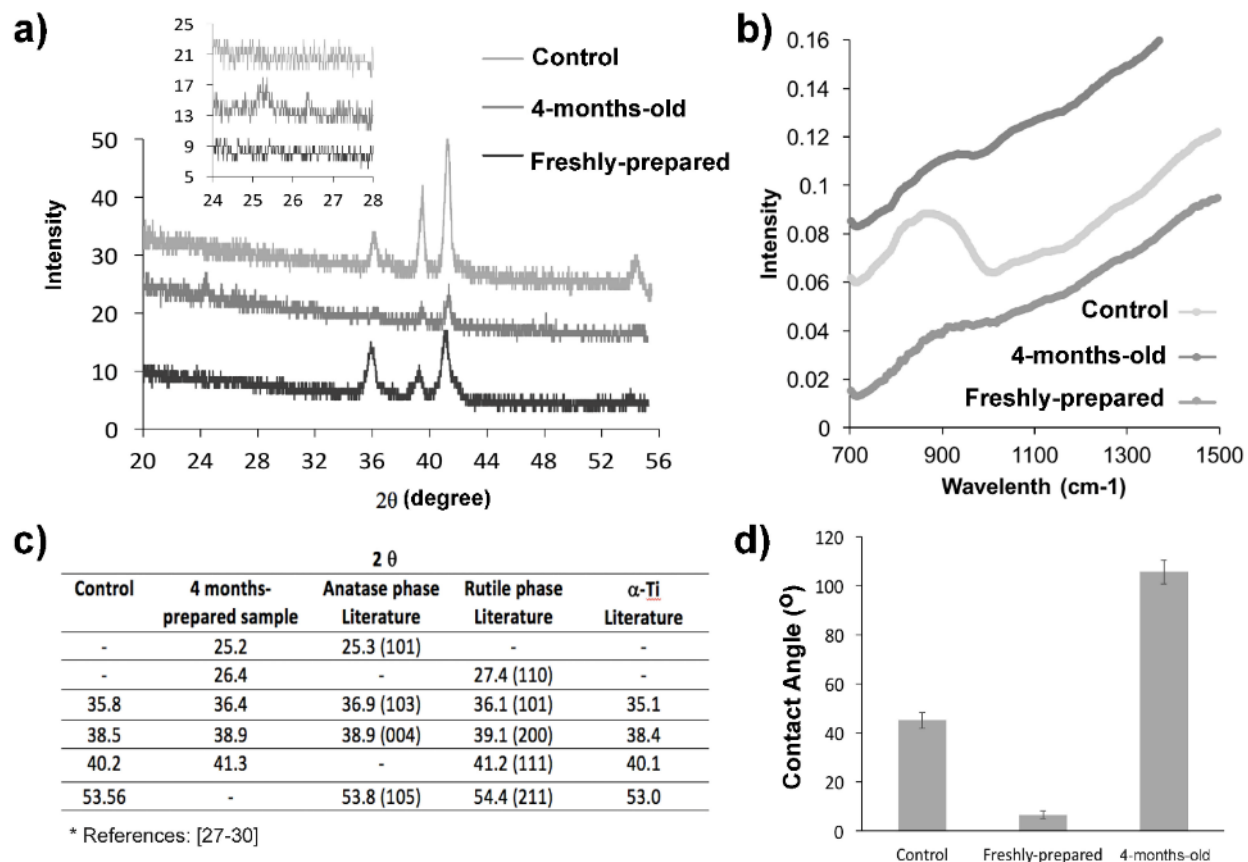
Figure 26. – Fig. 2. XRD patterns (a) and FTIR spectra (b) of Ti surfaces polished (control), freshly prepared and 4-month-old samples (4 months). Comparison of the main peaks (2h) appearing in Ti surface patterns analyzed in this study and the ones in the bibliography (29–32) (c). Water contact angles of the different Ti surfaces (d).

While surface topography and roughness are similar (see above) XRD, FTIR and water contact angle analyses demonstrate that both freshly-prepared and 4-months-old samples show different crystalline phases. The freshly-prepared Ti surface is amorphous and hydrophilic, consistent with what has been reported for samples analyzed soon after their preparation (27,35). In contrast, the 4- months-old is crystalline and hydrophobic (Fig. 2), consistent with the chemical properties of anatase and rutile (29–32).

2.3.2 Cell behavior

Osteoblastic cells spread out more on both nanocavitated Ti samples than on control, extended more filopodia with unique nanoscale lateral membrane protrusions and showed several vinculin immunoreactive plaques associated with actin filaments (Fig. 3a–c), as previously published (15,19,27). Overall cell morphology was similar on freshly-prepared (amorphous) and 4-month-old (crystalline) surfaces.
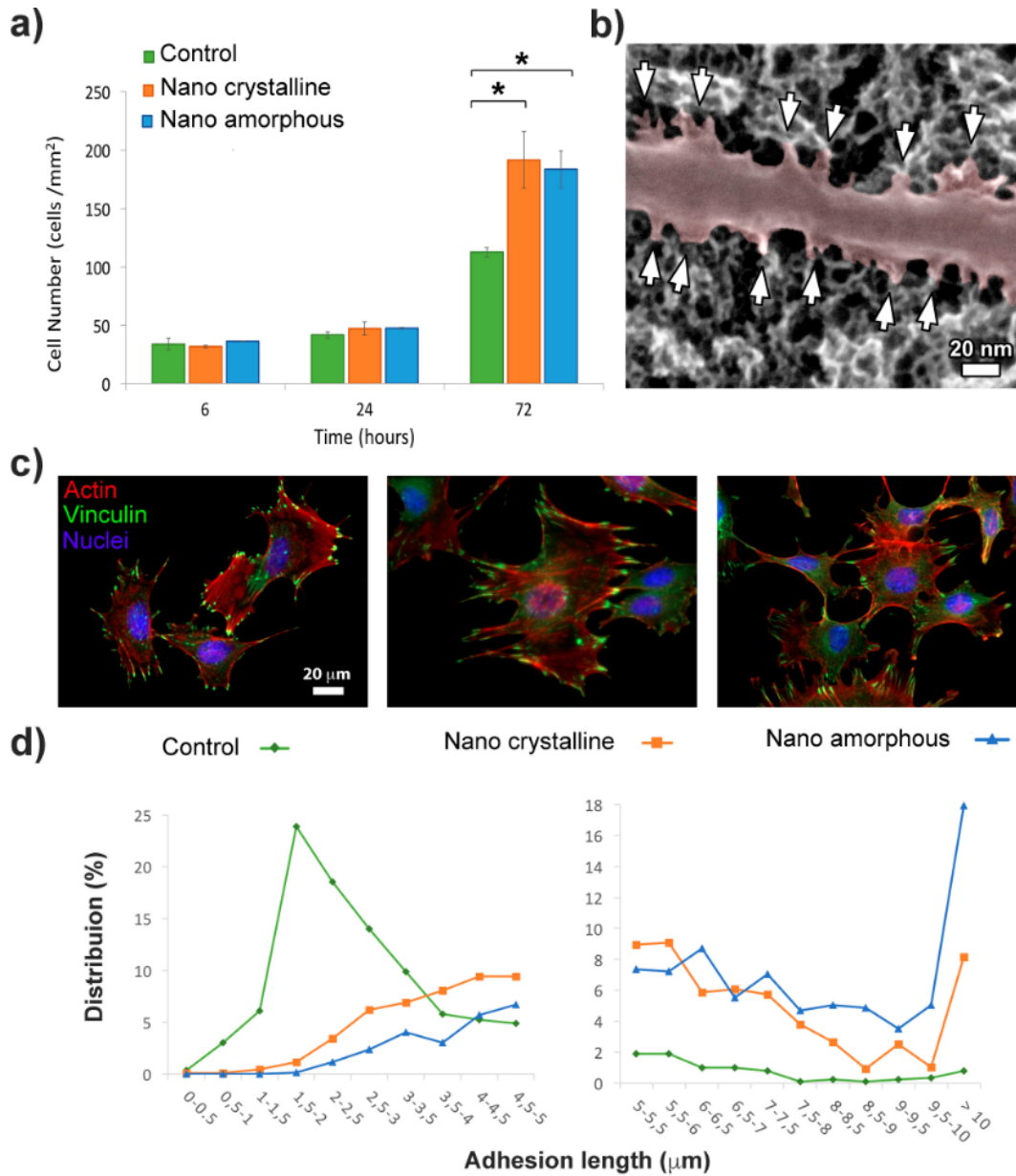
Figure 27. – Fig.3. Osteogenic cell attachment, growth, and spreading: (a) Number of cells at 6, 24, and 72 h of incubation on untreated (control), Nano crystalline (4 months-old samples) and

Nano amorphous (freshly-prepared samples) Ti surfaces. Values showing significant differences ($p < 0.05$) are indicated with an asterisk. (b) FE-SEM image lateral membrane protrusions (white arrows) emerging from a filopodium of an osteogenic cell growing on Ti surface with crystalline nanotopography. (c) Fluorescence micrographs showing vinculin (green) and actin (red) distribution in cells after 24 h of culture. Nuclei are stained in blue. (d) Quantitative analysis of FA lengths after 6 h of culture (For 24 h of culture see Supplementary material Fig. 1S). (For interpretation of the references to colour in this figure legend, the reader is referred to the web version of this article.)

However, there were no significant differences in cell number between the amorphous and crystalline surfaces (Fig. 3a). The higher cell number observed on both nanocavitated surfaces correlates with a significant increase in the quantity and size of the FAs, as well as their degree of maturity (Fig. 3c and d) with respect to the polished surface. Notably, the amorphous nanotopography showed more mature FA (Fig. 3d). This indicates that topographical features of the surface can trigger the cellular mechanisms that regulate the formation and maturation of the FAs, regardless of the crystallinity of the oxide layer and its surface wettability. These results contrast with some reports, which claim that the chemistry of the substrate affects the cell density (10–12,41). Concerning the crystalline structure of surfaces, Oh *et al*. (41) concluded that amorphous TiO2 nanotubes caused a slight reduction in cell proliferation compared to ones with an anatase phase. However, it was assumed that this difference is attributed to the presence of fluorine on the amorphous surface derived from the anodization process. He *et al.* (11) reported that the anatase phase of titania with nanoscale topography yields the best biological effects for cell adhesion, spreading, proliferation and differentiation, mainly due to surface wettability. Consistent with this conclusion, it was found that portions of cells migrate inside crystalline nanotubes due to their higher hydrophilicity (10). On the other hand, Silva- Bermudez (22) found that amorphous TiO2-coated surfaces showed an increase in the level of proteins related to the mineralization of bone as compared to crystalline films. While we did not specifically analyze protein expression, since cell number was not affected, our results would suggest no difference in overall performance of the osteogenic cells, an effect that could be attributed specifically to the nature of the nanocavitated surface. The created mesoporous network represents a nanoconfined environment (34,35,42) that could directly influence various processes such a protein trapping,

packing and orientation, as discussed for integrins (34). Concerning the wettability of biomaterial surfaces, it is known that hydrophilicity is an important physicochemical property that can regulate protein adsorption and cell behavior. Most studies indicate that cells tend to attach better onto hydrophilic surfaces rather than hydrophobic ones (43). Nevertheless, it has also been reported that cells adhere and proliferate at the highest rate when cultured on a substrate with hydrophobic surfaces or a contact angle of around 70 degrees (44). In our work, different surface wettability degrees showed similar cellular reactions. This overall limited influence on cell activity is further emphasized by our results with SS where the hydrophilicity of the surface did not change dramatically with the nanocavitation process, there was an enhancement on cell behavior.

Despite the fact that cell number - here specifically for MC3T3 osteogenic cells - is similar amorphous and crystalline surfaces, it is important to highlight that the maturation of FA is greater on the amorphous nanotopography. Some studies suggest that hydrophilic surfaces may influence osteoblast behavior by changing protein absorption that directly induces differentiation through the assembly of focal adhesions and subsequent activation of intracellular signaling cascade (45). Structurally, mature FA link the actin rich cytoskeleton of cells with the extracellular matrix through integrins to mediate cell adhesion, migration, mechanosensing and signaling events (46,47). It could thus be assumed that amorphous mesoporous Ti surfaces have more influence on the regulation of integrins in osteoblastic cells. However, how this translates into the longer-term osteogenic capacity of the cell remains to be determined.

2.3.3 Bacterial attachment

Nanocavitated amorphous Ti surfaces have proven to be antimicrobial (42). In this work, we have used the same nanocavitated material with different crystallinity in order to evaluate whether the surface phase composition has any effect on bacterial cell attachment. The results show that very few E. coli attached to the nanotextured Ti surface compared to the control sample (Fig. 4). However, no differences were observed between the crystalline and amorphous surfaces. Only a few works have dealt with the influence of the atomic arrangement or crystallinity of titania on this aspect. For instance, Del Curto *et al*. (48) reported that titania anatase layers significantly reduced bacterial cell attachment. However, Almaguer - Flores *et al*. (49) concluded that bacterial cell adhesion was slightly lower on the amorphous phase compared to their crystalline counterpart. Thus, as for eukaryotic cells, there is still debate on which factor is more relevant for bacterial

attachment, topography or crystallinity. As for the MC3T3 cells, our results indicate that the antibacterial properties that the nanotopography confers to Ti are not affected by the surface phase composition. Therefore, this would indicate that the mechanism by which bacteria interact with a surface is in first instance biophysical.
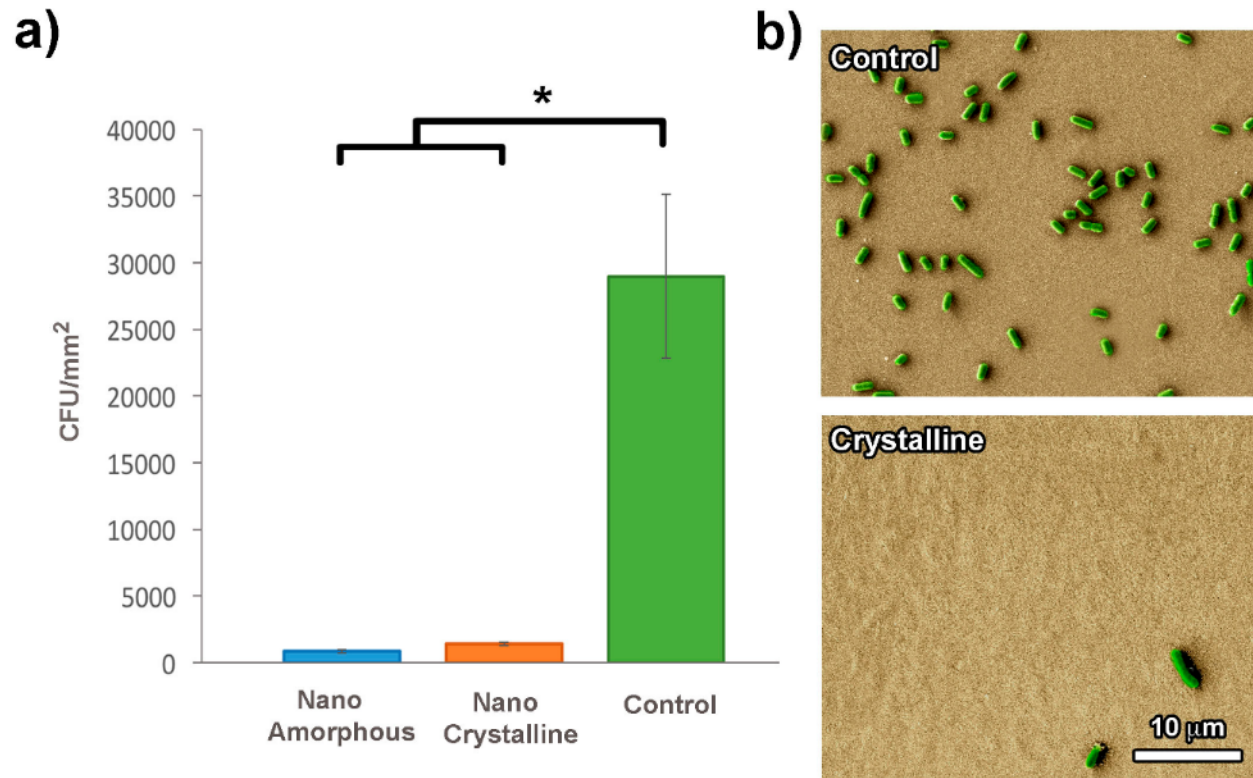
Figure 28. –   Fig. 4. Bacterial attachment: (a) E. coli number on Ti surfaces with different crystalline structures. Values showing significant differences ($p < 0.05$) are indicated with an asterisk. (b) FE-SEM images of E. coli on polished and nanocavitated with crystalline oxide layer.

2.4 Conclusions

It is still not resolved whether crystallinity of titania layers has a determinant influence on biological events. Similarly, there are no reported works with a clear conclusion about the impact of wettability of nanotextured surfaces, and how these changes with the atomic arrangement of the surface. This study provides evidence that physical aspects of nanotopography of titania surfaces predominate on the effect of crystallinity and hydrophilicity. While the nanocavitated surface influences the formation and maturation of FA and elicits the outgrowth of filopodia, regardless

the of crystallinity or its surface wettability, the amorphous surface exhibited a higher frequency of mature adhesions on nanotextured titania. In addition, the antibacterial properties that nanotopography confers to Ti are maintained with both crystalline phases. Thus, similarly to cell behavior, there is no predominant influence of the crystallinity on bacterial cell adhesion. While additional studies will be needed to establish the universality of our findings, the information provided by our analyses offers a route for the rational design of implant surfaces to control cell behavior and to inhibit bacterial cell adhesion. It also indicates that, while there may be an evolution of the surface state during standard storage of treated titania surfaces, this is not expected to significantly alter their performance, an important consideration for manufacturing of medical devices. While our work is highly pertinent to bone biomaterials, it has a broader impact essentially everywhere in the body where titania are used, and for certain industrial usages as well.

Acknowledgments

Supplementary material
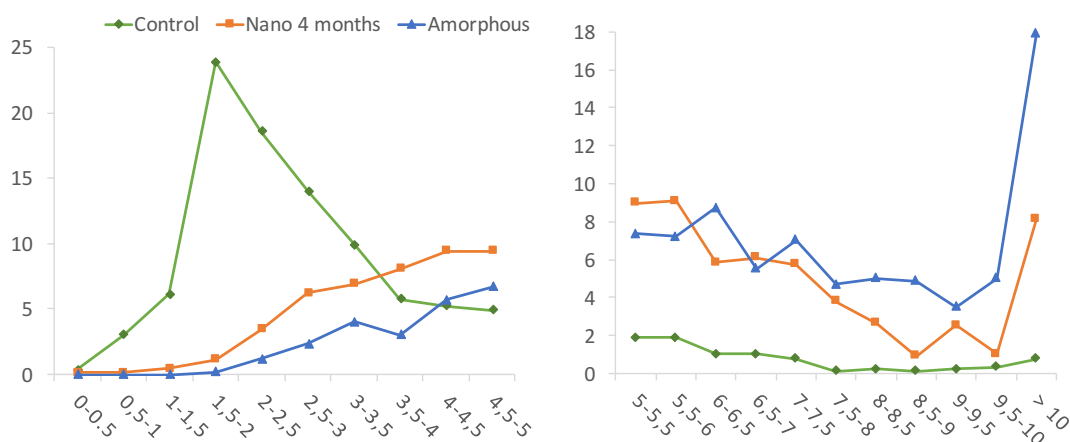
Figure 29. –   Fig. 1S. Quantitative analysis of FA lengths after 24h of culture.

References

1. M. Long, H.J. Rack, Titanium alloys in total joint replacement a materials science perspective, Biomaterials 19 (1998) 1621–1639.

2. E. Eisenbarth, D. Velten, K. Schenk-Meuser, P. Linez, V. Biehl, H. Duschner, J.Breme, H. Hildebrand, Interactions between cells and titanium surfaces, Biomol. Eng. 19 (2002) 243–249.

3. F. Variola, A. Nanci, Titania Thin Films in Biocompatible Matals and Medical Implants, in: Oxide Ultrathin Films, Wiley-VCH Verlag GmbH & Co. KGaA, 2011, pp. 309–328.

4. M. Textor, C. Sittig, V. Frauchiger, S. Tosatti, D.M. Brunette, Properties and Biological Significance of Natural Oxide Films on Titanium and Its Alloys, in: D. M. Brunette, P. Tengvall, M. Textor, P. Thomsen (Eds.), Titanium in Medicine: Material Science, Surface Science, Engineering, Biological Responses and Medical Applications, Springer, Berlin Heidelberg, 2001, pp. 171–230.

5. X. Liu, P.K. Chu, C. Ding, Surface modification of titanium, titanium alloys, and related materials for biomedical applications, Mater. Sci. Eng.: R: Rep. 47 (2004) 49–121.

6. Anodization: A Promising Nano-Modification Technique of Titanium-based Implants for Orthopedic Applications, in: M.J. Jackson, W. Ahmed (Eds.) Surface Engineered Surgical Tools and Medical Devices, Springer US, Boston, MA, 2007, pp. 21–47.

7. R.S. Williamson, J. Disegi, J.A. Griggs, M.D. Roach, Nanopore formation on the surface oxide of commercially pure titanium grade 4 using a pulsed anodization method in sulfuric acid, J. Mater. Sci. – Mater. Med. 24 (2013) 2327–2335.

8. S.G. Steinemann, Titanium — the material of choice?, Periodontology 2000 (17) (1998) 7–21.

9. S.-H. Oh, R.R. Finõnes, C. Daraio, L.-H. Chen, S. Jin, Growth of nano-scale hydroxyapatite using chemically treated titanium oxide nanotubes, Biomaterials 26 (2005) 4938–4943.

10. T. Shokuhfar, A. Hamlekhan, J.-Y. Chang, C.K. Choi, C. Sukotjo, C. Friedrich, Biophysical evaluation of cells on nanotubular surfaces: the effects of atomic ordering and chemistry, Int. J. Nanomed. 9 (2014) 3737–3748.

11. J. He, W. Zhou, X. Zhou, X. Zhong, X. Zhang, P. Wan, B. Zhu, W. Chen, The anatase phase of nanotopography titania plays an important role on osteoblast cell morphology and proliferation, J. Mater. Sci. – Mater. Med. 19 (2008) 3465– 3472.

12. W.Q. Yu, Y.L. Zhang, X.Q. Jiang, F.Q. Zhang, *In vitro* behavior of MC3T3-E1 preosteoblast with different annealing temperature titania nanotubes, Oral Dis. 16 (2010) 624–630.

13. K. Kim, B.-A. Lee, X.-H. Piao, H.-J. Chung, Y.-J. Kim, Surface characteristics and bioactivity of an anodized titanium surface, J. Periodont. Implant Sci. 43 (2013) 198–205.

14. A. Nanci, J.D. Wuest, L. Peru, P. Brunet, V. Sharma, S. Zalzal, M.D. McKee, Chemical modification of titanium surfaces for covalent attachment of biological molecules, J. Biomed. Mater. Res. 40 (1998) 324.

15. P. Tambasco de Oliveira, A. Nanci, Nanotexturing of titanium-based surfaces upregulates expression of bone sialoprotein and osteopontin by cultured osteogenic cells, Biomaterials 25 (2004) 403–413.

16. F. Variola, J.-H. Yi, L. Richert, J.D. Wuest, F. Rosei, A. Nanci, Tailoring the surface properties of Ti6Al4V by controlled chemical oxidation, Biomaterials 29 (2008) 1285–1298.

17. A. Rodriguez-Contreras, D. Guadarrama Bello, S. Flynn, F. Variola, J.D. Wuest, A. Nanci, Chemical nanocavitation of surfaces to enhance the utility of stainless steel as a medical material, Colloids Surf., B 161 (2018) 677–687.

18. P.T. de Oliveira, S.F. Zalzal, M.M. Beloti, A.L. Rosa, A. Nanci, Enhancement of *in vitro* osteogenesis on titanium by chemically produced nanotopography, J. Biomed. Mater. Res. Part A 80A (2007) 554–564.

19. L. Richert, F. Vetrone, J.-H. Yi, S.F. Zalzal, J.D. Wuest, F. Rosei, A. Nanci, Surface nanopatterning to control cell growth, Adv. Mater. 20 (2008) 1488–1492.

20. F. Vetrone, F. Variola, P. Tambasco de Oliveira, S.F. Zalzal, J.-H. Yi, J. Sam, K.F. Bombonato-Prado, A. Sarkissian, D.F. Perepichka, J.D. Wuest, F. Rosei, A. Nanci, Nanoscale oxidative patterning of metallic surfaces to modulate cell activity and fate, Nano Lett. 9 (2009) 659–665.

21. R.M. Wazen, S. Kuroda, C. Nishio, K. Sellin, J.B. Brunski, A. Nanci, Gene expression profiling and histomorphometric analyses of the early bone healing response around nanotextured implants, Nanomedicine (London, England) 8 (2013) 1385–1395.

22. P. Silva-Bermudez, A. Almaguer-Flores, V.I. Garcia, R. Olivares-Navarrete, S.E. Rodil, Enhancing the osteoblastic differentiation through nanoscale surface modifications, J. Biomed. Mater. Res. Part A 105 (2017) 498–509.

23. J. Barthes, S. Ciftci, F. Ponzio, H. Knopf-Marques, L. Pelyhe, A. Gudima, I. Kientzl, E. Bognár, M. Weszl, J. Kzhyshkowska, N.E. Vrana, Review: the potential impact of surface crystalline states of titanium for biomedical applications, Crit. Rev. Biotechnol. (2017) 1–15.

24. R.A. Gittens, L. Scheideler, F. Rupp, S.L. Hyzy, J. Geis-Gerstorfer, Z. Schwartz, B. D. Boyan, A review on the wettability of dental implant surfaces II: biological and clinical aspects, Acta Biomater. 10 (2014) 2907–2918.

25. L. Yang, M. Zhang, S. Shi, J. Lv, X. Song, G. He, Z. Sun, Effect of annealing temperature on wettability of TiO(2) nanotube array films, Nanoscale Res. Lett. 9 (2014), 621 621.

26. F. Variola, Surface modifications of biocompatible metals to improve biological response, Institut National de la Recherche Scientifique - Énergie, Matériaux et Télècommunications, 2010.

27. G.B. Dainelys, F. Aurélien, B. Antonella, N. Antonio, A nanoporous titanium surface promotes the maturation of focal adhesions and the formation of filopodia with distinctive nanoscale protrusions by osteogenic cells, Acta Biomater. (2017).

28. M. Bouroushian, T. Kosanovic, Characterization of thin films by low incidence X-ray diffraction, Cryst. Struct. Theory Appl. 1 (2012) 35–39.

29. T. Busani, R.A.B. Devine, Dielectric and infrared properties of TiO_2 films containing anatase and rutile, Semicond. Sci. Technol. 20 (2005) 870.

30. R. Abazari, A.R. Mahjoub, S. Sanati, A facile and efficient preparation of anatase titania nanoparticles in micelle nanoreactors: morphology, structure, and their high photocatalytic activity under UV light illumination, RSC Adv. 4 (2014) 56406–56414.

31. Y. Kim, H.M. Hwang, L. Wang, I. Kim, Y. Yoon, H. Lee, Solar-light photocatalytic disinfection using crystalline/amorphous low energy bandgap reduced TiO_2, Sci. Rep. 6 (2016) 25212.

32. M. Jafari, M. Vaezzadeh, S. Noroozizadeh, Thermal stability of a phase of titanium by using X-ray diffraction, Metall. Mater. Trans. A 41 (2010) 3287–3290.

33. J.W. Cassidy, J.N. Roberts, C.-A. Smith, M. Robertson, K. White, M.J. Biggs, R.O.C. Oreffo, M.J. Dalby, Osteogenic lineage restriction by osteoprogenitors cultured on nanometric grooved surfaces: The role of focal adhesion maturation, Acta Biomater. 10 (2014) 651–660.

34. D. Guadarrama Bello, A. Fouillen, A. Badia, A. Nanci, A nanoporous titanium surface promotes the maturation of focal adhesions and formation of filopodia with distinctive nanoscale protrusions by osteogenic cells, Acta Biomater. 60 (2017) 339–349.

35. J.-H. Yi, C. Bernard, F. Variola, S.F. Zalzal, J.D. Wuest, F. Rosei, A. Nanci, Characterization of a bioactive nanotextured surface created by controlled chemical oxidation of titanium, Surf. Sci. 600 (2006) 4613–4621.

36. M.D. Hamilton, Anatase phase, hydrophilicity, and thickness of thermally oxidized TiO_2 layer on titanium-V alloy, J. Undergrad. Res. 6 (2013) 16–19.

37. F. Rupp, R.A. Gittens, L. Scheideler, A. Marmur, B.D. Boyan, Z. Schwartz, J. Geis-Gerstorfer, A review on the wettability of dental implant surfaces: theoretical and experimental aspects, Acta Biomater. 10 (2014) 2894–2906.

38. D. Khang, J. Lu, C. Yao, K.M. Haberstroh, T.J. Webster, The role of nanometer and sub-micron surface features on vascular and bone cell adhesion on titanium, Biomaterials 29 (2008) 970–983.

39. J. Li, W. Qin, K. Zhang, F. Wu, P. Yang, Z. He, A. Zhao, N. Huang, Controlling mesenchymal stem cells differentiate into contractile smooth muscle cells on a TiO_2 micro/nano interface: Towards benign pericytes environment for endothelialization, Colloids Surf., B 145 (2016) 410–419.

40. L. Lv, K. Li, Y. Xie, Y. Cao, X. Zheng, Enhanced osteogenic activity of anatase TiO_2 film: surface hydroxyl groups induce conformational changes in fibronectin, Mater. Sci. Eng., C 78 (2017) 96–104.

41. S. Oh, C. Daraio, L.-H. Chen, T.R. Pisanic, R.R. Fiñones, S. Jin, Significantly accelerated osteoblast cell growth on aligned TiO2 nanotubes, J. Biomed. Mater. Res. Part A 78A (2006) 97–103.

42. F. Variola, S.F. Zalzal, A. Leduc, J. Barbeau, A. Nanci, Oxidative nanopatterning of titanium generates mesoporous surfaces with antimicrobial properties, Int. J. Nanomed. 9 (2014) 2319–2325.

43. Y. Arima, H. Iwata, Effect of wettability and surface functional groups on protein adsorption and cell adhesion using well-defined mixed self-assembled monolayers, Biomaterials 28 (2007) 3074–3082.

44. W. Jianhua, I. Toshio, O. Naoto, I. Takayasu, M. Takashi, L. Baolin, Y. Masao, Influence of surface wettability on competitive protein adsorption and initial attachment of osteoblasts, Biomed. Mater. 4 (2009) 045002.

45. G. Zhao, A.L. Raines, M. Wieland, Z. Schwartz, B.D. Boyan, Requirement for both micron- and submicron scale structure for synergistic responses of osteoblasts to substrate surface energy and topography, Biomaterials 28 (2007) 2821–2829.

46. B. Geiger, J.P. Spatz, A.D. Bershadsky, Environmental sensing through focal adhesions, Nat. Rev. Mol. Cell Biol. 10 (2009) 21–33.

47. L.B. Case, M.A. Baird, G. Shtengel, S.L. Campbell, H.F. Hess, M.W. Davidson, C.M. Waterman, Molecular mechanism of vinculin activation and nano-scale spatial organization in focal adhesions, Nat. Cell Biol. 17 (2015) 880–892.

48. B. Del Curto, M.F. Brunella, C. Giordano, M.P. Pedeferri, V. Valtulina, L. Visai, A. Cigada, Decreased bacterial adhesion to surface-treated titanium, Int. J. Artif. Organs 28 (2005).

49. A. Almaguer-Flores, P. Silva-Bermudez, R. Galicia, S.E. Rodil, Bacterial adhesion on amorphous and crystalline metal oxide coatings, Mater. Sci. Eng., C 57 (2015) 88–99.

50.

Chapitre 3 – Nanoporosity Stimulates Cell Spreading and Focal Adhesion Formation in Cells with Mutated Paxillin

Dainelys Guadarrama Bello, Aurélien Fouillen, Antonella Badia, and Antonio Nanci*

[a]Laboratory for the Study of Calcified Tissues and Biomaterials, Department of Stomatology, Faculty of Dentistry, Université de Montréal, Montréal, Québec H3C3J7, Canada

[b]Department of Chemistry, Faculty of Arts and Sciences, Université de Montréal, Montréal, Québec H3C3J7, Canada

[c]Department of Biochemistry and Molecular Medicine, Faculty of Medicine, Université de Montréal, Québec H3C3J7, Canada

Corresponding Author

Antonio Nanci

Faculté de Médecine Dentaire

Université de Montréal

C.P. 6128, succ. Centre-ville

Montréal (Québec) H3C 3J7

E-mail: antonio.nanci@umontreal.ca

Phone: 514 343-5846

Fax: 514 343-2233

Abstract

We have evaluated the response to nanotopography of CHO-K1 cells that express wild-type paxillin or paxillin with mutations at serine 273 that inhibit phosphorylation. Cells were grown on nanoporous and polished titanium surfaces. With all cell types, immunofluorescence showed that adhesion and spreading were minimally affected on the treated surface and that the actin filaments were more abundant and well-aligned. Scanning electron microscopy revealed changes in cell shape and abundant filopodia with lateral nanoprotrusions in response to nanoporosity. Gene expression of proteins associated with cellular adhesion and protrusions was significantly increased on the nanoporous surface regardless of the cell type. In particular, ACTN1, Rac1, Cdc42, and ITGα1 were upregulated in S273 cells with alanine substitutions, whereas FAK, Pxn, and Src were downregulated, leading to improved focal adhesion formation. These findings suggest that the surface nanoporosity can "compensate for" the genetic mutations that affect the biomechanical relationship of cells to surfaces.

KEYWORDS: titanium, nanoporosity, focal adhesion, paxillin mutation, gene expression

3.1 Introduction

The surface topography of biomaterials has been shown to provide cues to cells that induce a large number of cellular responses, including cell shape, adhesion, and gene regulation (1). Because cells naturally grow on nanostructured extracellular matrices, biomaterials with nanoscale topographies are the focus of continuous investigation (2−5). Different surface fabrication and treatment procedures have been successfully developed to generate nanotopographical surfaces for cell interaction research. It is now possible to reliably obtain nanogrooves, nanopits, nanopillars, nanotubes, and nanofibers, including nanofeatures superimposed on microrough surfaces (3,6,7). However, each of these surfaces has distinctive physicochemical characteristics that make it difficult to predict cellular outcomes based only on topography. As such, any relevant nanostructure topography must be evaluated for its capacity to modulate cell activity. In this study, we have evaluated a nanoporous surface which shows the ability to promote selectively cell activity *in vitro* (8) and osteogenesis *in vivo* (9) and identified certain components of the cell signaling using a genetic mutation model with specific emphasis on cell attachment.

Cell adhesion implicates focal adhesion (FA) formation, a multiprotein structure that mediates signaling events related to cell biomechanics. Protein phosphorylation plays important roles in the regulation of FA formation and turnover (10,11). Different components of FAs, such as focal adhesion kinase (FAK), paxillin, and p130Cas, among others, are phosphorylated in response to integrin-mediated cell-extracellular matrix adhesion (12,13). FAs are regulated by a set of molecules comprising integrin-binding proteins, adaptors, and scaffolding proteins, such as paxillin. The latter is a multifunctional and multidomain adapter protein that plays a key role by recruiting numerous FA structural proteins and molecules associated with signaling pathways (14−16). Paxillin phosphorylation has been associated with the coordinate formation of FAs and stress fibers (16). As well as being a target for tyrosine kinases, paxillin is heavily phosphorylated on serine residues during cell adhesion.16 Brown *et al* (14). demonstrated that mutations of phosphorylatable residues of paxillin affect its overall localization to FAs that have reached a steady state. For example, paxillin phosphorylation on tyrosine 31 (Y31), Y119, or serine 273 (S273) results in robust protrusion and assembly of adhesions in the protrusions, whereas unphosphorylated paxillin suppresses protrusion and produces stable adhesions (17). Paxillin also coordinates the activation of the proteins Cdc42, Rac1, and RhoA GTPases associated with various pathways (15). These pathways ultimately lead to the reorganization of the actin cytoskeleton and

the assembly/disassembly of FAs required for cell attachment, spreading, and migration. In this context, the LD4 domain of paxillin is considered as a key binding site for a number of signaling molecules, including FAK and the G-protein-coupled receptor kinase-interacting protein 1 (GIT1) (18,19). Deletion of the LD4 domain results in a perturbed migration and the diminution of the number of protrusions.20 This domain contains the phosphorylatable residues S273. The S273D paxillin mutant is a phosphomimetic mutant where the serine has been changed for an aspartic acid, which is chemically similar to phopho-serine and the protein can be phosphorylated. Moreover, in the S273A paxillin mutant, the serine residue is substituted with alanine, which has a similar R group but cannot be phosphorylated because of the absence of a hydroxyl group necessary for phosphorylation (20).

An oxidative chemical treatment of titanium, recently defined as nanocavitation (21), has been used to create a unique nanoporous surface network that has a major impact on the formation of FAs, thereby affecting cell adhesion and the resulting signaling cascades (22). The phosphorylation status of paxillin has been implicated in the regulation of adhesion formation, disassembly, and signaling (23). The phosphorylation of serine residues in particular has been associated with the regulation of paxillin localization at FAs (15). CHO-K1 cells that express wild-type paxillin or paxillin with point mutations at position S273 that affect phosphorylation (20) were grown for the first time on a nanocavitated titanium surface (22,24). Although paxillin deletion has been used to test cell response (25), to the best of our knowledge, site-directed mutagenesis has never been used on any nanotopography. Such mutation is advantageous because it allows evaluation of the contribution of specific functional groups in the response to surface features. The formation of FAs and filopodia, as well as the expression of multiple genes that are usually tested in relation to cell − surface interaction, were examined. Our results show that nanotopography can counteract mutations that affect the formation of FAs.

3.2 Materials and methods

3.2.1 Surface Modification

Commercially pure grade II titanium discs (12 mm diameter) were chemically oxidized to produce a nanoscale topography (Ti-Nano). The samples were first polished (Ti-Control), sonicated in distilled water, subsequently cleaned in 70% ethanol, and dried in air. To nanocavitate the surfaces, some polished discs were immersed in a solution of equal volumes of concentrated H_2SO_4 and 30% H_2O_2 at room temperature (RT), as previously described (24). The procedure is detailed elsewhere (22). Before seeding the cells, the Ti-Control and Ti-Nano discs were sterilized using 70% ethanol and UV light.

3.2.2 Surface Characterization

The Ti-Control and Ti-Nano surfaces were analyzed using a JEOL JSM-7400F (JEOL Ltd., Tokyo, Japan) field-emission scanning electron microscope (FE-SEM) operated at 1.5 kV. A complete characterization of the surfaces was already reported (22). Additionally, the surface topography was analyzed by atomic force microscopy (AFM) using an ICON scanning probe microscope (Bruker Nano Surfaces, Santa Barbara, CA). The microscope was operated in air using the PeakForce QNM mode and a microlever probe (type-MLCT, Bruker AFM Probes Americas) with nominal tip radius of 20 nm and spring constant of 0.6 N/m.

3.2.3 Cell Culture

Stable Chinese hamster ovary paxillin wild-type (WT) enhanced green fluorescent protein (EGFP) cells (CHO-K1), paxillin S273A, and paxillin S273D EGFP mutants (courtesy of C. Brown) were cultured in low-glucose Dulbecco's modified eagle medium (DMEM) supplemented with nonessential amino acids, Pen-Strep, HEPES, Geneticin G418, and 10% fetal bovine serum at 37 °C in a humidified atmosphere with 5% CO_2. Cells were plated on Ti-Control and Ti-Nano discs placed in 12-well plates at a cell density of 10 000 cells/well and grown for 6 or 24 h.

3.2.4 Cell Spreading and Cell/Titanium Interface

FE-SEM was used to observe the morphology and the area of cells grown on control and treated surfaces. After incubation, discs were washed three times in 0.1 M sodium phosphate buffer (PB), pH 7.3, to remove nonadherent cells and fixed for 1 h at 4 °C using 2.5% (v/v) glutaraldehyde

solution in PB. After fixation, cells were washed with PB and incubated for 1 h in 1% aqueous osmium tetroxide at 4 °C, followed by dehydration with graded ethanol. Cells were then dried in a Leica EM CPD 300 Critical Point Dryer (Leica Microsystems Inc., Ontario, Canada). Quantification of the cell area was performed for at least 30 cells per condition across two independent experiments. A Regulus 8230 ultrahigh-resolution FE-SEM (Hitachi, Ltd., Japan) operated at 0.1 kV was used for higher resolution images of the filopodia and the nanoscale lateral protrusions they emit on the nanostructured surface.[22] To further investigate the relationship between S273A mutated cells and Ti-Control and Ti-Nano surfaces, ion milling was performed using an Ethos NX5000 Focused Ion Beam (FIB) system (Hitachi Ltd., Chiyoda, Japan) to obtain cross-section images of the cell-surface interface. The samples were sputter-coated with Pt prior to observation to alleviate charging.

3.2.5 Immunofluorescence Visualization of FAs

To visualize paxillin expression, we washed normal and mutated cells incubated for 24 h on Ti-Control and Ti-Nano with PB and subsequently fixed with 4% (w/v) paraformaldehyde solution in PB at 4 °C for 30 min. After fixation, cells were washed in PB and permeabilized with 0.5% (v/v) Triton X-100 in PB for 10 min. Nonspecific binding sites were blocked with 5% (w/v) skimmed milk in PB for 1 h followed by fluorescent staining of the actin filaments with rhodamine-phalloidin (1:150, Life Technologies) at RT for 30 min. The samples were washed in PB and the titanium discs were mounted face-up on glass slides. Cell nuclei were stained and mounted with mountain medium containing DAPI (Prolong antifade 4′,6-diamidino-2-phenyl-indole, dihydrochloride, Molecular Probes, Invitrogen). Coverslips were finally used to cover the discs. After immunostaining, samples were examined using a Zeiss Axio Imager M2 Optical Microscope (Carl Zeiss, Jena, Germany). GFP-Paxillin expression was quantified using ImageJ processing software (NIH Image). Fluorescent images of the cells stained with DAPI were used to estimate the number of cells on each surface after 24 h. A minimum of 2000 cells were counted for each disc.

3.2.6 Gene Expression

After 24 h of incubation, quantitative real-time PCR (RT-qPCR) was carried out to evaluate the gene expression levels of paxillin (Pxn), vinculin (Vcl), talin (Tln), focal adhesion kinase (FAK), α-actinin (ACTN1), Cdc42, Rac1, Myosin II, Src, p130Cas, Zyxin, integrin α1 (ITGα1), and integrin β1 (ITGβ1) in CHO-K1, S273A, and S273D mutant cells grown on the Ti-Control and Ti-Nano surfaces. The total RNA was extracted using Trizol reagent (Invitrogen, Life Technologies), according to the manufacturer's instructions. The oligonucleotide primers utilized are listed in Table 1.

gene	gene primer sequence[a] (5′-3′)	product length (bp)
Pxn	F: ATGGGGGTCCTGGGAAGAAT	222
	R: CCATCACAGGGGGCCTCTAC	
Vcl	F: GCCTCCCTCGAAAGAAGCAA	125
	R: GGCAATCTCAAACCCCGAA	
Tln	F: CTGGCTCAAGCCACCTCAGA	133
	R: CCTCCACCATCTTGGCAGTG	
FAK	F: CCGGCACAATGTCTTCAAGC	164
	R: GCCTCAGCCACTGGGAATCT	
Cdc42	F: CGCAGGTGTGTGCTGCTATG	181
	R: TACCAACGGGCCTTGTCTCA	
Rac1	F: GCAGCAGCACAGCCTCCTTA	241
	R: CCAGCACACCCACGACTAGG	
α-actinin	F: TCTTGACTCGGGATGCCAAA	115
	R: GCGCGGAAATCATCTGTGTC	
Myosin II	F: CCAAGGCCAACAGTGAGGTG	290
	R: CTGCTTCCACTCTGCCAGGA	
ITGα1	F: TCCCGCGAAGTTGGCTTTAT	125
	R: CGCTTTTCACATCCCAGACG	
ITGβ1	F: GGTCAACAGCGCATTTCTGG	133
	R: CAGCATCCGTGGAAAACACC	
Src	F: CCTGGTTGGGGAGAATCTGG	129
	R: AGAGCAGCTTCGGGAGCAGT	
P130Cas	F: GAACGAAGCCCCCAACAAAG	280
	R: GGCAGGCCTTTCTCCACACT	
Zyxin	F: CCAAGCCTCACCTCTGCTCA	100

	R: AGCGCACCTGGTTTTGGTTT	
GAPDH	F: CCATCACTGCCACCCAGAAG	210
	R: CCAGGCGACATGTCAGATCC	

a$5'$-$3'$; F, forward; R, reverse.

Tableau 1. –   Table 1: Primer Sequences and Product Size (bp) for Real-Time PCR Reactions.

The extracted RNA was reverse transcribed using the QuantiNova SYBR Green RT-PCR kit (Qiagen) following these conditions: 50 °C for 10 min, followed by 95 °C for 2 min, then 60 cycles of 95 °C for 5 s and 65 °C for 10 s using the LightCycler 96 PCR system (Roche). The gene expression was calculated by the comparative $2^{-\Delta\Delta CT}$ method (26), normalized to GAPDH, and expressed relative to Ti-Control discs.

3.2.7 Statistical Analysis

Data was analyzed using Student's t test with a 95% confidence interval ($p < 0.05$) and Origin Pro 9.2 software (OriginLab Corporation) to determine the statistically significant differences between the means of different groups. Data normality was verified using a Shapiro-Wilk test. All results are presented as the mean value ± standard deviation (SD) of two independent experiments run in triplicate for each condition and interval of time studied.

3.3 Results

3.3.1 Characterization of the Titanium Surfaces

Figure 1 illustrates the topographies of the control and treated titanium surfaces used in this study. The Ti-Control showed no distinctive topographical features (Figure 1A) while nanocavitation with H_2SO_4/H_2O_2 (22,24) creates a network of nanopores that are homogeneously distributed across the surface (Figure 1B). The pore size diameter of 20 ± 5 nm. As previously reported (22), roughness measurements of the Ti-Control revealed average roughness (Ra) values of 0.50 ± 0.03 nm compared to 9.2 ± 0.7 nm for Ti-Nano. AFM profiling revealed nanopore depths ranging from 5 to 25 nm (Figure 1 C, D).
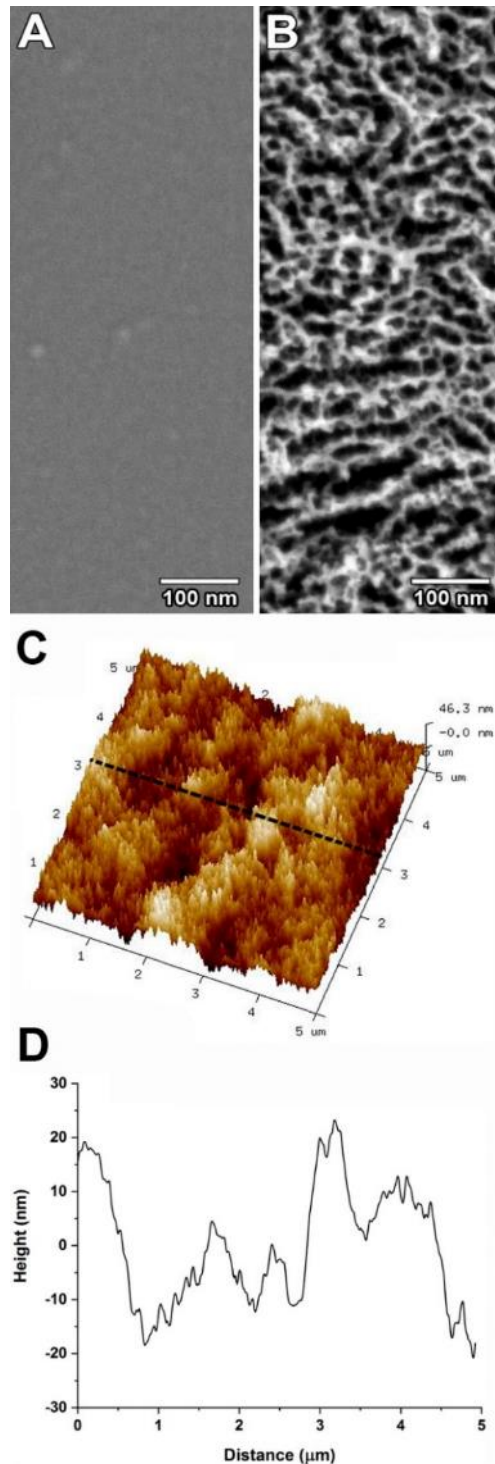
Figure 30. –   Figure 1. Scanning electron microscopy imaging of the topography of (A) polished and (B) nanocavitated titanium surfaces. (C) AFM 3D topography of Ti-Nano and (D) the corresponding line section.

3.3.2 Cell Proliferation

To evaluate how the surface topography modulates cell proliferation, we determined the number of wild type and mutated cells at 24 h of culture by fluorescence microscopy using the DAPI staining to visualize nuclei. There are generally more S273A-paxillin mutant cells on both surfaces compared to CHO-K1. While counts of the CHO-K1 and S273A cells are higher on the nanoporous surface, the differences between surfaces are not statistically significant (95% confidence interval) (Figure 2). CHO-K1 and S273D cells yield similar results on both surfaces (see Figure S1A).
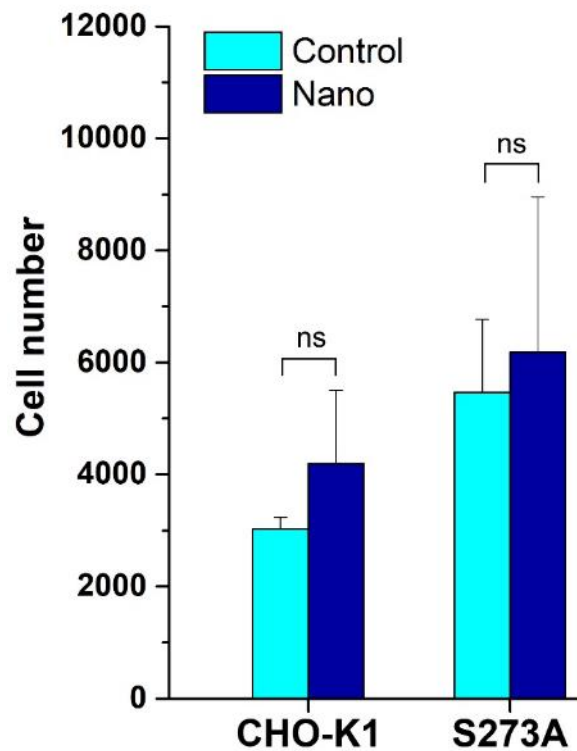
Figure 31. – Figure 2. Cell count by immunofluorescence microscopy after 24 h of culture. Error bars represent the standard deviation and ns indicates no significant statistical difference (95% confidence).

3.3.3 Cell Morphology

Figure 3 illustrates representative SEM micrographs of the cell morphology on control and treated discs after 24 h of culture. There are structural differences as a function of the topography. Cells on Ti-Control spread less and show a rounded morphology with few and short protrusions (Figure 3A, B). On the other hand, on Ti-Nano, CHO-K1, S273A (Figure 3E, F) and S273D cells (see Figure S1C, F) all appear to spread more on the surface (more evident on CHO-K1 cells) and present multiple protrusions. Cross-sectional analyses of S273A cells on Ti-Control and Ti- Nano (Figure 3C, G) show that contacts on Ti-Nano appear more numerous and their membrane intimately adapts to the surface topography.
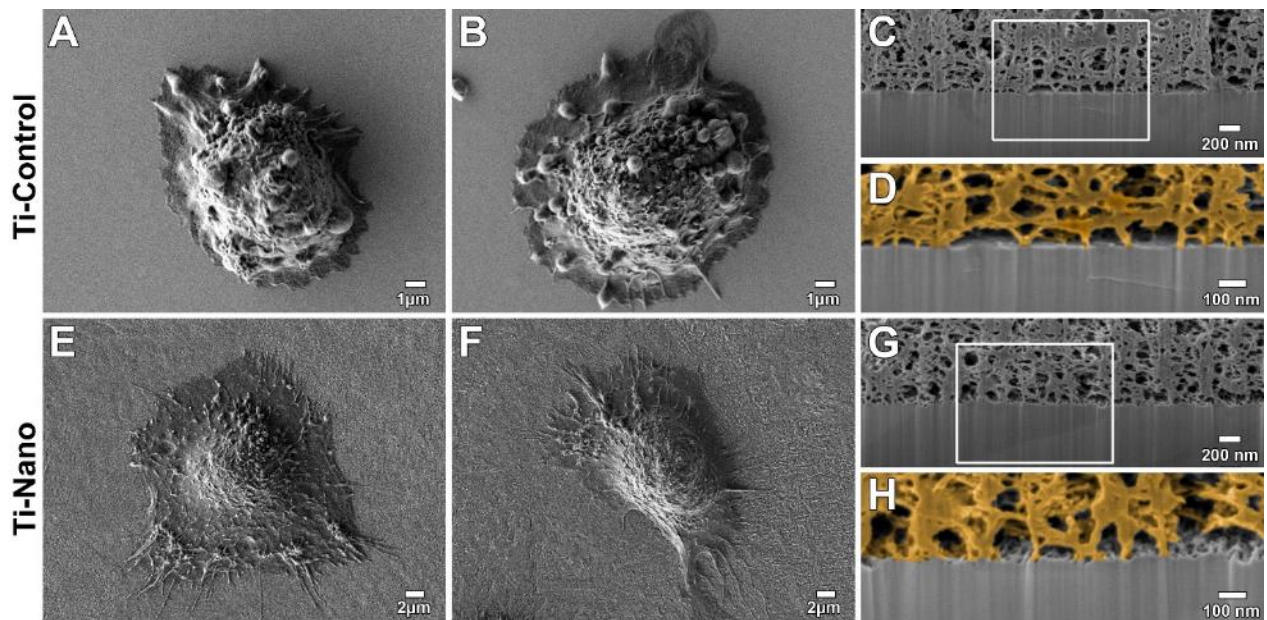
Figure 32. – Figure 3. SEM images of (A, E) CHO-K1 and (B, F) S273A cells cultured for 6 h. Cells on the (A, B) Ti-Control appear rounded, whereas on (E, F) Ti-Nano, they are more spread out and show multiple filopodial extensions. (C, G) Cross-sectional views of S273A cells grown on Ti-Control and Ti-Nano. (D, H) Colored high-resolution images of boxed areas.

At 6 h of culture, cellular areas are not statistically different between the control and treated surfaces. However, after 24 h of culture, cells from all three lines show different behaviors on the two surfaces. In all cases, there is an approximately 2-fold increase in cell area on Ti-Nano as compared to Ti-Control surfaces (Figure 4 and Figure S1D).
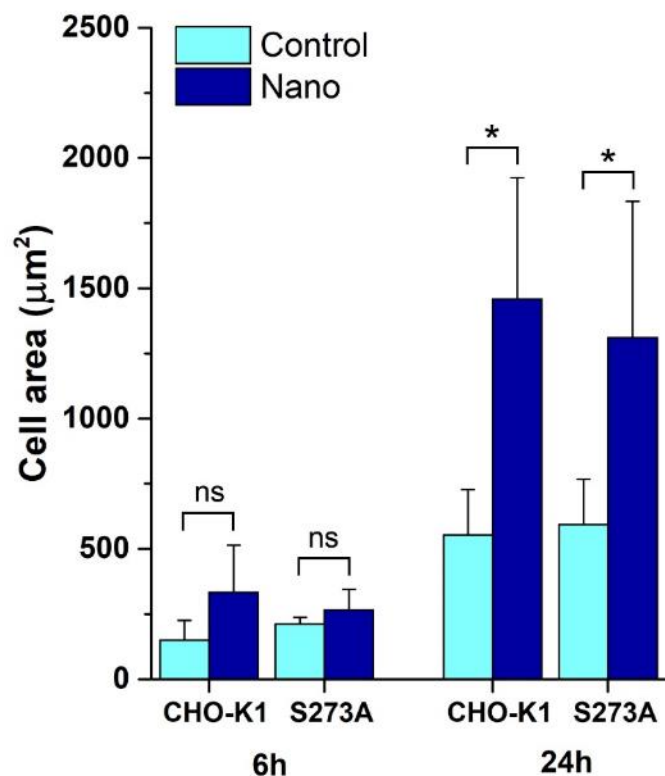
Figure 33. –   Figure 4. Quantification of cell area. At 6 h of culture, there is no statistical difference in cell area, whereas at 24 h, the cell area is several fold larger on Ti-Nano. Error bars represent the standard deviation, * indicates statistically significant differences and ns indicates no significant difference.

Figure 5 shows high-magnification SEM images of filopodia emitted by cells after 24 h of culture. There is no difference in the appearance of the filopodia on each surface but there are marked differences between Ti-Control and Ti-Nano. Filopodia on Ti-Nano appear flattened and exhibit abundant lateral nanoscale protrusions. Those on the Ti-Control are generally more rounded and show few or no lateral protrusions (see Figure S1E, F for the S273D cells).
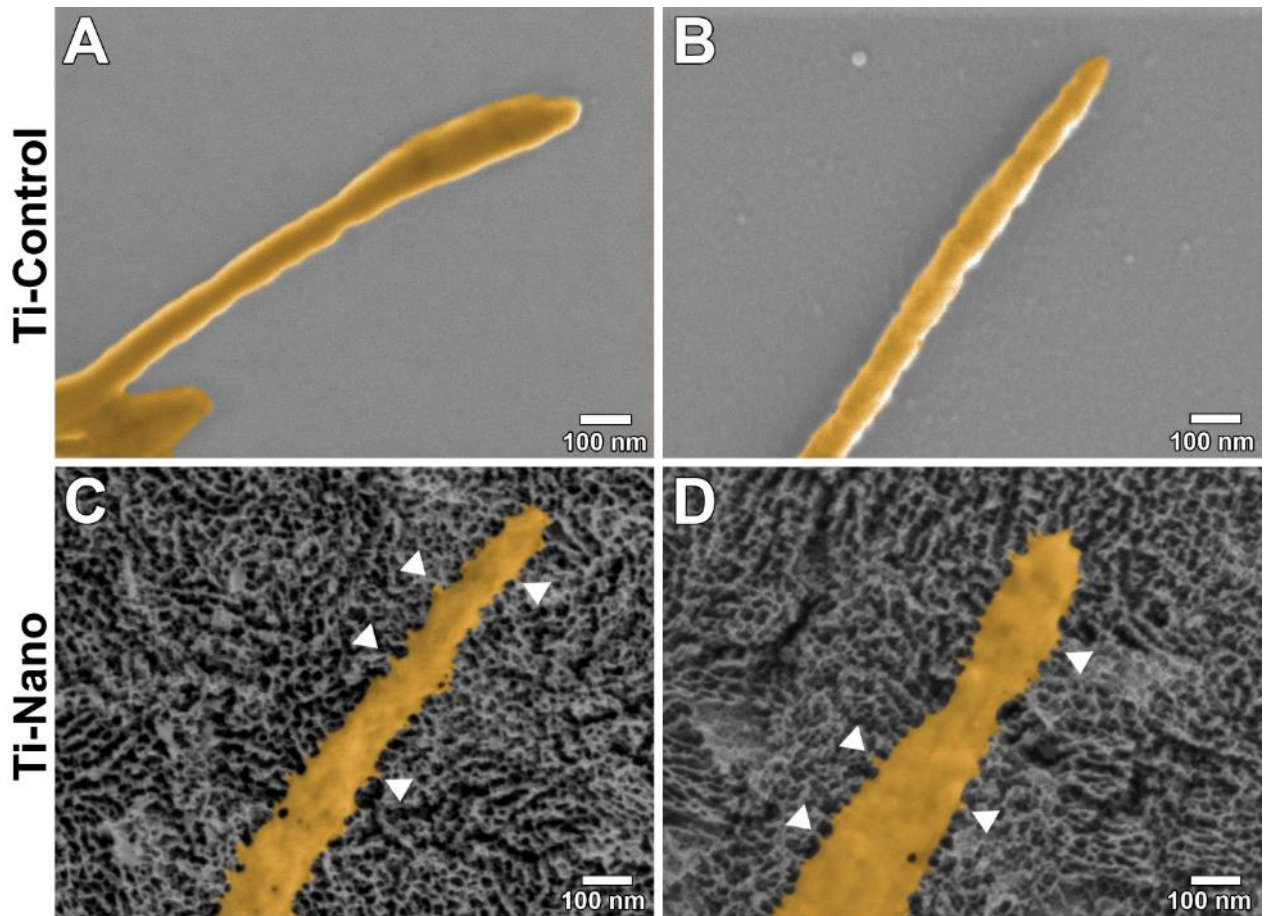
Figure 34. – Figure 5. Colored high-resolution scanning electron microscopy images of (A, C) CHO-K1 and (B, D) S273A grown for 24 h showing (C, D) the presence of nanoscale lateral protrusions (arrows) emanating from a filopodium on Ti-Nano.

3.3.4 Fluorescence Microscopy

Because nanotopography induces major changes in cell spreading and adhesion, we have examined actin and FA distribution. The fluorescence micrographs (Figure 6) illustrate staining for actin filaments. In general, in all three cell types grown on the Ti-Control surface, a diffuse perinuclear labeling for actin with only few bundles present can be observed (Figure 6A, B). On Ti-Nano, actin filaments are more abundant and well-aligned (Figure 6C) in CHO-K1. S273A cells on Ti-Nano show the presence of aligned filaments but they are not as abundant as in the CHOK1 cells (Figure 6D) and S273D cells (see Figure S2A, B).
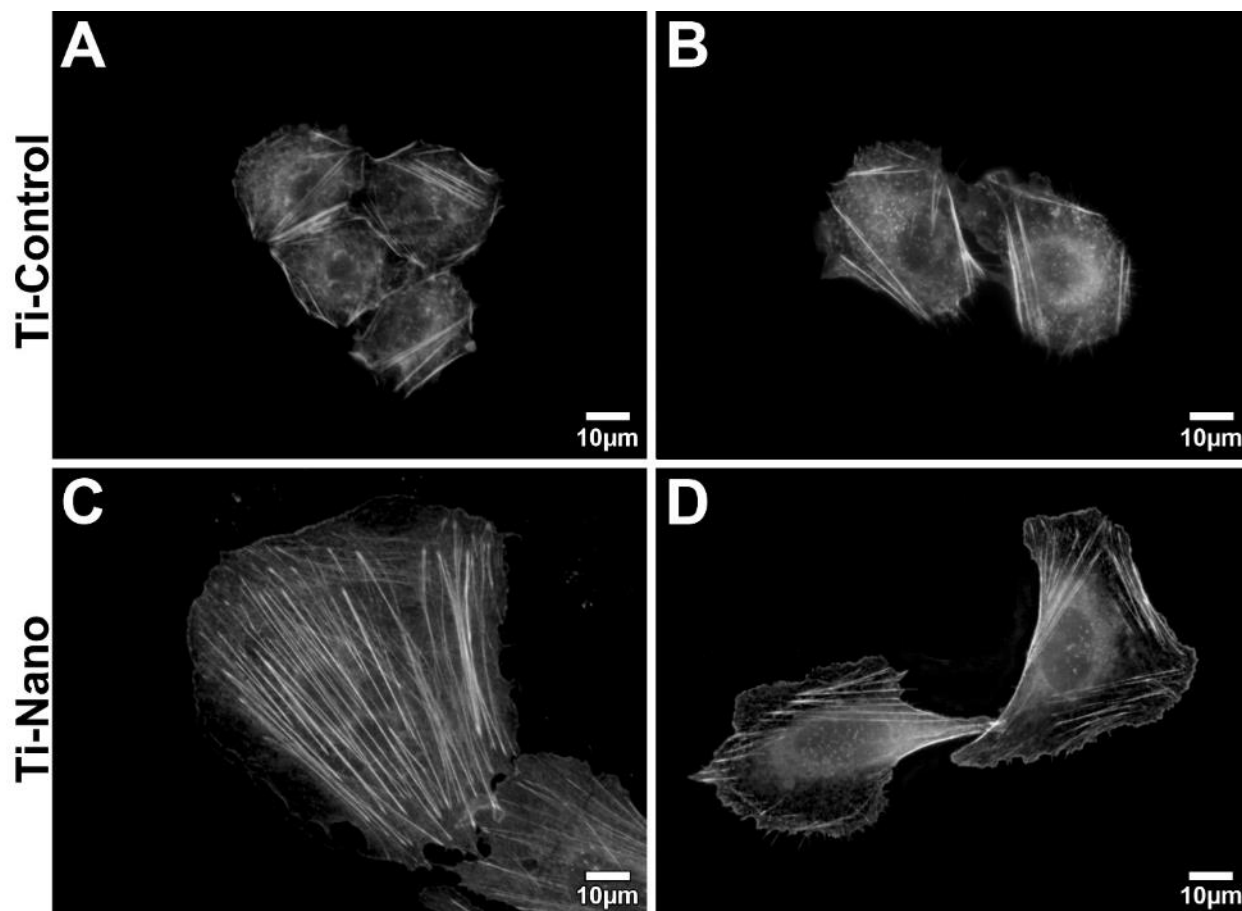
Figure 35. – Figure 6. Actin fluorescent labeling of (A, C) CHO-K1 and (B, D) S273A cells cultured for 24 h on Ti-Control and Ti-Nano surfaces.

In this study, we also investigated the influence of nanotopography on the number of FAs labeled with EGFPpaxillin (Figure 7A−D). The number of FAs is higher on the nanoporous surfaces for CHO-K1 and S273A cells, but statistically significant differences between the surfaces are only found for S273A (Figure 7E). The number of FAs for S273D cells is similar to that of the CHO-K1 cells (see Figure S2C, D). Quantification of the FA length shows differences in the size distribution between surfaces. CHO-K1 cells tend to form larger FAs on Ti-Nano when compared to both mutant cells (Figure 7F, G; Figure S2F).
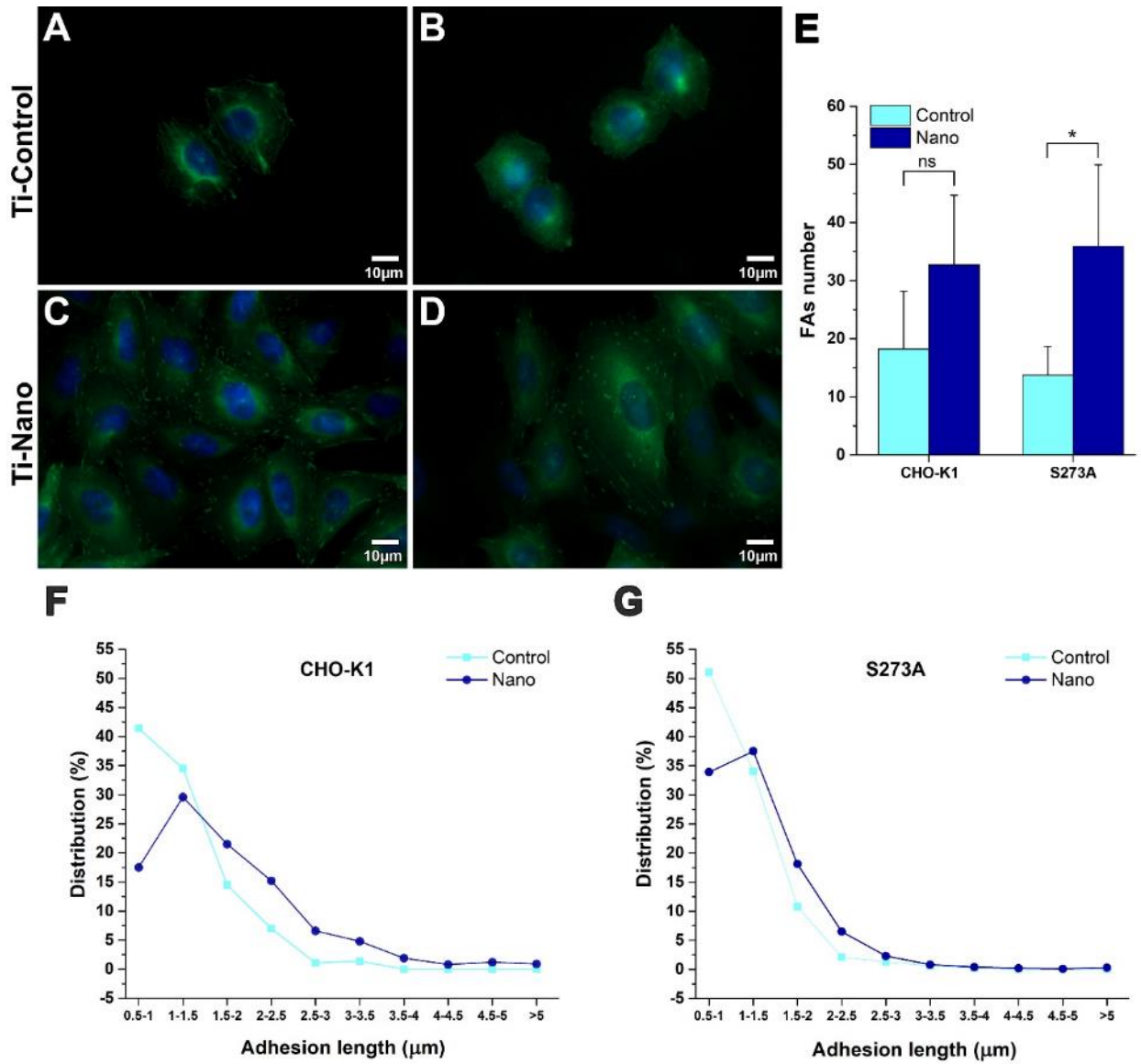
Figure 36. – Figure 7. Fluorescence micrographs of (A, C) CHO-K1 and (B, D) S273A cells cultured for 24 h. (E) Number and (F, G) length distribution of focal adhesions formed by CHO-K1 and S273A cultured for 24 h on Ti-Control and Ti-Nano surfaces. Error bars represent the standard deviation, * indicates statistically significant differences and ns indicate no significant difference.

3.3.5 Gene Expression

We used RT-qPCR to determine the influence of the nanostructured surface on the expression of multiple genes associated with cell adhesion and protrusion. After 24 h of culture, the Ti-Nano surface induces upregulation in the expression of a majority of the genes evaluated, as compared with Ti-Control (Figure 8A, B). Of these, α-actinin, Rac1, Cdc42, and ITGα1 are 9- to 21-fold upregulated in S273A-paxillin mutation cells (Figure 8B). Talin is the only gene downregulated in CHO-K1, whereas for the S273Apaxillin mutation cells, FAK, Pxn, and Src are downregulated (Figure 8B). Differently from CHO-K1 and S273A cells, Pxn are 7-fold and Myosin 27-fold upregulated by S273D cells on Ti-Nano (Figure S2G). Similar to the CHO-K1 cells, talin is also downregulated on Ti-Nano for S273D cells (Figure S2G).
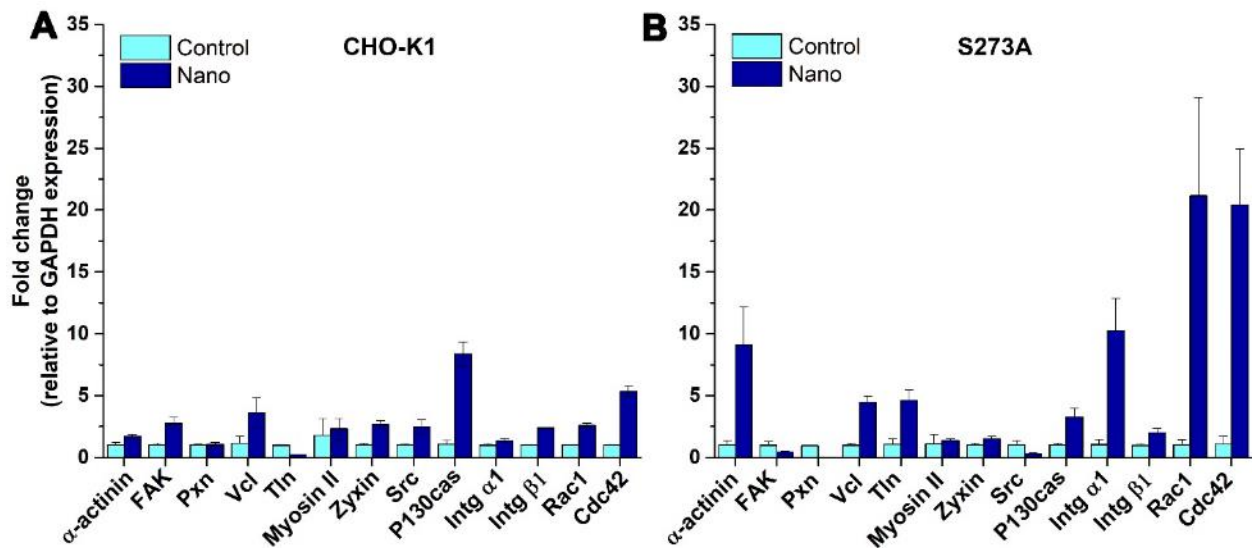
Figure 37. – Figure 8. Comparative gene expression profile of focal adhesion markers, integrins, and Rho family GTPases by (A) CHO-K1 and (B) S273A cells cultured on Ti-Control and Ti-Nano surfaces.

3.4 Discussion

The mechanism by which proteins assemble to form the highly complex structure of FAs that link the cytoskeleton with natural and engineered substrates and mediate the cellular effects of the topography has not yet been defined. There is no linear succession of events in the FA assembly and its multiple components appear almost simultaneously (27). The assembly and function of FAs

are affected by small differences in the binding of integrins to extracellular ligands and/or cytoplasmic adapter proteins (27). Members of the paxillin molecular adaptors family interact with integrins to regulate the dynamics of adhesion sites. Different strategies have been exploited to investigate the role of paxillin in this process (28). So far, few studies have taken advantage of site-directed mutagenesis, to explore the influence of nanoscale surface modifications on FA formation. Because the localization and function of paxillin as an adaptor molecule are regulated by phosphorylation (29), we have exploited CHO-K1 cell lines that express paxillin with point mutations at position S273 to interfere with this posttranslational modification (20). The fact that there are multiple phosphorylation domains situated both at the Cterminal (14,18) or N-terminal half of the paxillin molecule (18,29) complicates such studies, however, mutation in S273 have been shown to have a major impact on cell behavior (20,30). This work contributes to this challenging endeavor and further shows that nanotopography can palliate for phosphorylationrelated changes in FA.

The data presented here and our previous results (22), demonstrate that the physicochemical nature of the Ti-Nano surface positively affects cell behavior irrespective of cell type and regardless of the presence or absence of paxillin mutations. Taken together, our results suggest that the increase in the number of FAs, as well as the abundance of filopodia with lateral nanoprotrusions contribute to increasing cell adhesion, and thereby alter the nanoscale biomechanical relationships that regulate cell behavior and ultimately the body's response to implants. It has been shown that changes in surface topography induce changes in the morphology of the cell (31). Cells cultured on smooth controls show a rounded morphology with fewer FAs. Even in the case of S273A mutation, which has a major impact on paxillin phosphorylation, nanoporosity achieves reorganization of the cytoskeleton resulting in a concurrent increase in cell area, cell spreading, FA number, and size. The actin−myosin-based cytoskeleton is a dynamic system essential for contraction (32). Actin filament orientation and the regulation of myosin activity are influenced by the spatial organization and pattern of the substrate (33−35). Certain topographies have been shown to inhibit the formation of stress fibers (36,37). In this study, cells cultured on the nanoporous surface exhibit longer parallel actin filaments (more evident with CHO-K1 and S273D cells) and upregulation of myosin II. Such an arrangement is consistent with the ability of the actin network to sustain contractile forces (38).

This is accompanied by a concurrent increase in FA structuring. These findings indicate that the nanocavitated surface is independently able to sustain biomechanical adaptations. The nanocavitated surface may improve the availability of binding sites for proteins (39), including the adhesion ones and thereby engender above cellular outcomes. Paxillin S273A may be unable to bind Src, FAK or structural proteins, such as vinculin (40,41). Stabilization of integrin clusters by the binding of paxillin seems sufficient to compensate for the reduction in FAs on the Ti-Control surface induced by this mutation. A precise regulation of the polymerization, convergence, and cross-linking of actin filaments are determining factors for the initiation and elongation of filopodia (42). Cells normally spread on a surface via lamellipodia and filopodia, the latter serve as sensors for detecting topography features (43). In previous studies, we demonstrated that osteogenic cells developed more filopodia with distinctive lateral nanoprotrusions on nanoporous surfaces (21,22). A similar outcome is observed here with all three cell lines used, irrespective of the presence or absence of mutations, indicating that this is an intrinsic characteristic of the surface. The surface nanoporosity created by oxidative chemical etching can elicit, depending on the cell state, a difference of signaling molecules to regulate FA dynamics, cytoskeletal organization, and filopodia formation. Such a capacity, together with the improvement of osteogenesis at the surface of titanium implants *in vivo* (9) and its antimicrobial capacity (44), falls within the realm of smart surface properties with tunable biological effects (45).

The LD motif, where the mutations used in this study are localized, has been implicated in numerous interactions with adhesion components or regulators, such as FAK, Src, p130Cas, talin, and vinculin (40). Different studies have identified the phosphorylation of paxillin at S273 as a critical regulator of Rac activation, cell adhesion, and protrusion (20). Additionally, FAK has been involved as an indirect actor in various Rac1 activation mechanisms, with subsequent positive effects on cell spreading (46). The extensive list of genes analyzed from the three cell lines studied reveals major changes in S273A and S273D cells cultured on Ti-Nano. In the case of S273A cells, there is a downregulation of key genes such as FAK, Pxn, and Src that are typically implicated in FA formation and the upregulation of Rac1 and Cdc42. This suggests that nanoporosity regulates FA formation through an alternative pathway that bridges integrin clustering with activation of members of the Rho GTPases family. Alternatively, as we have observed *in vivo*, nanoporosity activates a number of unclassified genes (unpublished data).

Because these genes, whose function remains to be elucidated, are consistently upregulated they may hold answers to how nanoporosity regulates cell function in general, including adhesion. Rac1 and Cdc42 may also be implicated in the increased filopodial response observed. Rac1 plays an essential role in promoting the formation of nascent focal complexes and is activated by the adhesion of integrins to the extracellular matrix (11,47). and biomaterials. The upregulation of this gene on Ti-Nano corroborates our hypothesis that the nanostructured surface induces clustering of integrin that leads to FA assembly (22). This takes place even in the absence of paxillin phosphorylation that leads to the activation of signaling pathways associated with Rac. Also, the association of the adapter protein p130Cas, with focal contacts, occurs following integrin clustering (48). This could also explain the upregulation of p130Cas we have observed with all three cell lines on Ti-Nano.

3.5 Conclusions

This work exploits a genetic mutation model to demonstrate that nanoporosity, created by the chemical oxidative nanocavitation of titanium surfaces, stimulates cell spreading, formation of FA and filopodia with nanoprotrusions. This stimulation is confirmed by the upregulation of a subset of genes associated with protrusions, FA markers, and integrins. The gene analysis suggests that this takes place through alternative pathways to those typically involved in these events, that can only be elicited by the nanoporous surface itself and that relate to the specific physicochemical properties of the surface. Altogether, our results raise the possibility that nanostructured surfaces can be used not only to guide/accelerate the integration of biomaterials under normal conditions but also in situations where the cellular activity is compromised. This represents a yet undescribed functionality for the nanoporous surface.

Supporting Information
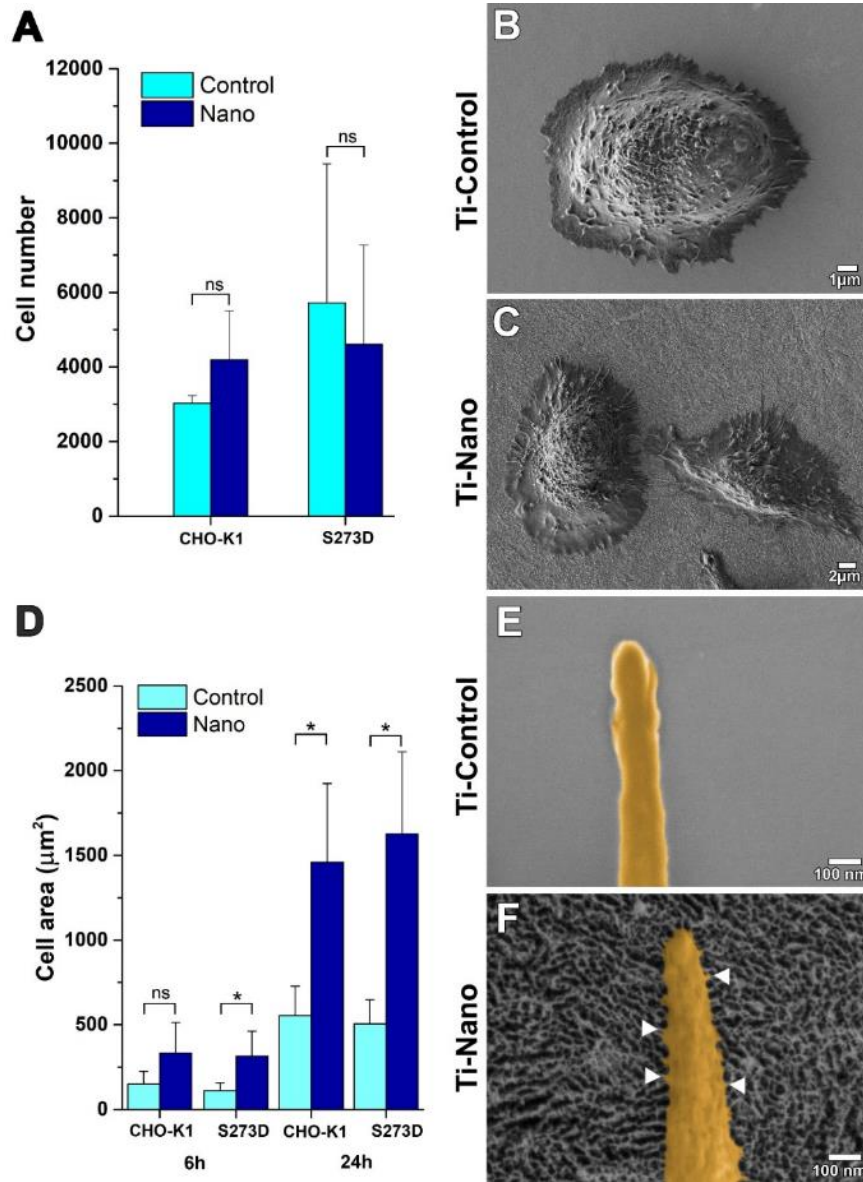
Figure 38. – Figure S1. (A) Cell count by immunofluorescence microscopy after 24 h of culture. (B,C) Scanning electron microscopy images of S273D cells cultured for 6 h on (B) Ti-Control and (C) Ti-Nano. (D) Quantification of the cell area. Colored high-resolution scanning electron microscopy images of S273D grown for 24 h on (E) Ti-Control and (F) Ti-Nano showing the presence of nanoscale lateral protrusions (arrows) emanating from a filopodium. (B) Scale bar = 1 μm, (C) scale bar = 2 μm, and (E,F) scale bar = 100 nm. Error bars represent the standard deviation, * indicates statistically significant differences and ns indicate no significant difference.
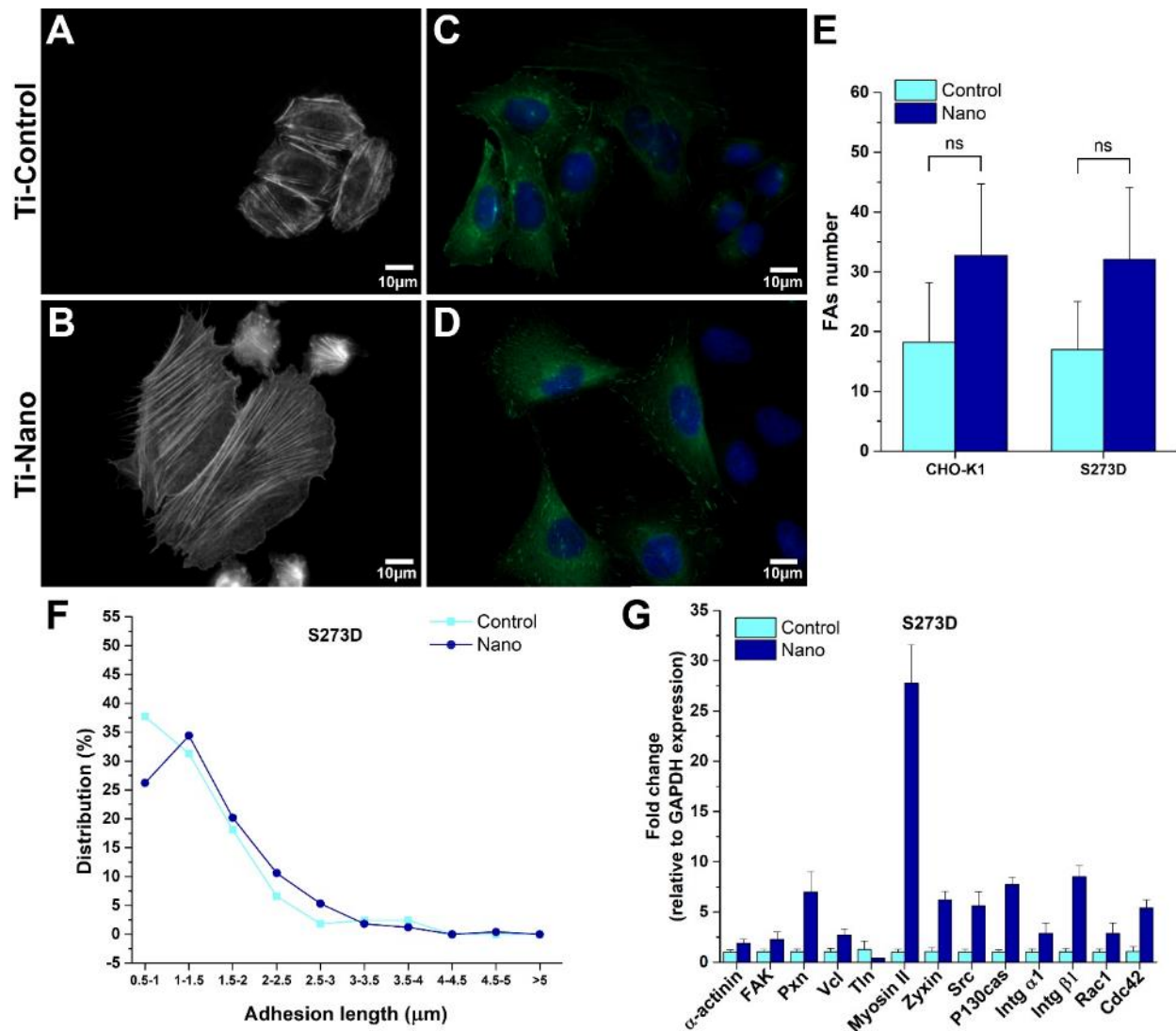
Figure 39. – Figure S2. (A,B) Actin labeling and (C,D) fluorescence micrographs of S273D cells cultured for 24 h on Ti-Control and Ti-Nano surfaces. (E) Number of focal adhesions formed by CHO-K1 and S273D cells. (F) Length distribution of focal adhesions formed by S273D cultured for 24 h on the Ti-Control and Ti-Nano surfaces. (G) Comparative gene expression profile of focal adhesion markers, integrins, and Rho family GTPases by S273D cells cultured on the Ti-Control and Ti-Nano surfaces. Error bars represent the standard deviation, * indicates statistically significant differences and ns indicate no significant difference.

Author Contributions

The manuscript was written through contributions of all authors. All authors have given approval to the final version of the manuscript.

Funding

Acknowledgments

References

1. Kuhn, L. T. Biomaterials. In Introduction to Biomedical Engineering, second ed.; Enderle, J. D.; Blanchard, S. M.; Bronzino, J. D., Eds.; Academic Press: Boston, 2005; pp 255−312.

2. Yim, E. K. F.; Darling, E. M.; Kulangara, K.; Guilak, F.; Leong, K. W. Nanotopography-Induced Changes in Focal Adhesions, Cytoskeletal Organization, and Mechanical Properties of Human Mesenchymal Stem Cells. Biomaterials 2010, 31, 1299−1306.

3. Chen, W.; Shao, Y.; Li, X.; Zhao, G.; Fu, J. Nanotopographical Surfaces for Stem Cell Fate Control: Engineering Mechanobiology from the Bottom. Nano Today 2014, 9, 759−784.

4. Dalby, M. J.; Gadegaard, N.; Oreffo, R. O. C. Harnessing Nanotopography and Integrin-Matrix Interactions to Influence Stem Cell Fate. Nat. Mater. 2014, 13, 558−569.

5. Rosa, A. L.; Kato, R. B.; Castro Raucci, L. M. S.; Teixeira, L. N.; de Oliveira, F. S.; Bellesini, L. S.; de Oliveira, P. T.; Hassan, M. Q.; Beloti, M. M. Nanotopography Drives Stem Cell Fate Toward Osteoblast Differentiation Through α1β1 Integrin Signaling Pathway. J. Cell. Biochem. 2014, 115, 540−548.

6. Gittens, R. A.; Olivares-Navarrete, R.; Schwartz, Z.; Boyan, B. D. Implant Osseointegration and the Role of Microroughness and Nanostructures: Lessons for Spine Implants. Acta Biomater. 2014, 10, 3363−3371.

7. Gittens, R. A.; McLachlan, T.; Olivares-Navarrete, R.; Cai, Y.; Berner, S.; Tannenbaum, R.; Schwartz, Z.; Sandhage, K. H.; Boyan, B. D. The Effects of Combined Micron-/Submicron-Scale Surface Roughness and Nanoscale Features on Cell Proliferation and Differentiation. Biomaterials 2011, 32, 3395−3403.

8. de Oliveira, P. T.; Zalzal, S. F.; Beloti, M. M.; Rosa, A. L.; Nanci, A. Enhancement of *In Vitro* Osteogenesis on Titanium by Chemically Produced Nanotopography. J. Biomed. Mater. Res., Part A 2007, 80A, 554−564.

9. Tavares, M. G.; Tambasco de Oliveira, P.; Nanci, A.; Hawthorne, A. C.; Rosa, A. L.; Xavier, S. P. Treatment of a Commercial, Machined Surface Titanium Implant With $H_2SO_4/H2O_2$ Enhances Contact Osteogenesis. Clin. Oral Implants Res. 2007, 18, 452−458.

10. Webb, D. J.; Donais, K.; Whitmore, L. A.; Thomas, S. M.; Turner, C. E.; Parsons, J. T.; Horwitz, A. F. FAK-Src Signalling Through Paxillin, ERK and MLCK Regulates Adhesion Disassembly. Nat. Cell Biol. 2004, 6, 154−161.

11. Wu, C. Focal Adhesion: a Focal Point in Current Cell Biology and Molecular Medicine. Cell Adh. Migr. 2007, 1, 13−18.

12. Zouq, N. K.; Keeble, J. A.; Lindsay, J.; Valentijn, A. J.; Zhang, L.; Mills, D.; Turner, C. E.; Streuli, C. H.; Gilmore, A. P. FAK Engages Multiple Pathways to Maintain Survival of Fibroblasts and Epithelia: Differential Roles for Paxillin and p130Cas. J. Cell Sci. 2009, 122, 357−367.

13. Janoštiak, R.; Pataki, A. C.; Brábek, J.; Rösel, D. Mechanosensors in Integrin Signaling: the Emerging Role of p130Cas. Eur. J. Cell Biol. 2014, 93, 445−454.

14. Brown, M. C.; Perrotta, J. A.; Turner, C. E. Serine and Threonine Phosphorylation of the Paxillin LIM Domains Regulates Paxillin Focal Adhesion Localization and Cell Adhesion to Fibronectin. Mol. Biol. Cell 1998, 9, 1803−1816.

15. López-Colomé, A. M.; Lee-Rivera, I.; Benavides-Hidalgo, R.; López, E. Paxillin: a Crossroad in Pathological Cell Migration. J. Hematol. Oncol. 2017, 10, 50.

16. Turner, C. E. Paxillin and Focal Adhesion Signalling. Nat. Cell Biol. 2000, 2, E231−E236.

17. Choi, C. K.; Zareno, J.; Digman, M. A.; Gratton, E.; Horwitz, A. R. Cross-Correlated Fluctuation Analysis Reveals Phosphorylation-Regulated Paxillin-FAK Complexes in Nascent Adhesions. Biophys. J. 2011, 100, 583−592.

18. Brown, M. C.; Curtis, M. S.; Turner, C. E. Paxillin LD Motifs May Define a New Family of Protein Recognition Domains. Nat. Struct. Mol. Biol. 1998, 5, 677−678.

19. Brown, M. C.; Perrotta, J. A.; Turner, C. E. Identification of LIM3 as the Principal Determinant of Paxillin Focal Adhesion Localization and Characterization of a Novel Motif on Paxillin Directing Vinculin and Focal Adhesion Kinase Binding. J. Cell Biol. 1996, 135, 1109−1123.

20. Nayal, A.; Webb, D. J.; Brown, C. M.; Schaefer, E. M.; Vicente-Manzanares, M.; Horwitz, A. R. Paxillin Phosphorylation at Ser273 Localizes a GIT1-PIX-PAK Complex and Regulates Adhesion and Protrusion Dynamics. J. Cell Biol. 2006, 173, 587−589.

21. Rodriguez-Contreras, A.; Guadarrama Bello, D.; Flynn, S.; Variola, F.; Wuest, J. D.; Nanci, A. Chemical Nanocavitation of Surfaces to Enhance the Utility of Stainless Steel as a Medical Material. Colloids Surf., B 2018, 161, 677−687.

22. Guadarrama Bello, D.; Fouillen, A.; Badia, A.; Nanci, A. A Nanoporous Titanium Surface Promotes the Maturation of Focal Adhesions and Formation of Filopodia with Distinctive Nanoscale Protrusions by Osteogenic Cells. Acta Biomater. 2017, 60, 339−349.

23. Quizi, J. L.; Baron, K.; Al-Zahrani, K. N.; O'Reilly, P.; Sriram, R. K.; Conway, J.; Laurin, A. A.; Sabourin, L. A. SLK-Mediated Phosphorylation of Paxillin is Required for Focal Adhesion Turnover and Cell Migration. Oncogene 2013, 32, 4656−4663.

24. Yi, J.-H.; Bernard, C.; Variola, F.; Zalzal, S. F.; Wuest, J. D.; Rosei, F.; Nanci, A. Characterization of a Bioactive Nanotextured Surface Created by Controlled Chemical Oxidation of Titanium. Surf. Sci. 2006, 600, 4613−4621.

25. Sero, J. E.; Thodeti, C. K.; Mammoto, A.; Bakal, C.; Thomas, S.; Ingber, D. E. Paxillin Mediates Sensing of Physical Cues and Regulates Directional Cell Motility by Controlling Lamellipodia Positioning. PLoS One 2011, 6 (12), No. e28303.

26. Livak, K. J.; Schmittgen, T. D. Analysis of Relative Gene Expression Data Using Real-Time Quantitative PCR and the $2^{-\Delta\Delta CT}$ Method. Methods 2001, 25, 402−408.

27. Wehrle-Haller, B. Structure and Function of Focal Adhesions. Curr. Opin. Cell Biol. 2012, 24, 116−124.

28. Zaidel-Bar, R.; Milo, R.; Kam, Z.; Geiger, B. A Paxillin Tyrosine Phosphorylation Switch Regulates the Assembly and Form of Cell-Matrix Adhesions. J. Cell Sci. 2006, 120, 137−148.

29. Webb, D. J.; Schroeder, M. J.; Brame, C. J.; Whitmore, L.; Shabanowitz, J.; Hunt, D. F.; Horwitz, A. R. Paxillin Phosphorylation Sites Mapped by Mass Spectrometry. J. Cell Sci. 2005, 118, 4925−4929.

30. Rajah, A.; Boudreau, C. G.; Ilie, A.; Wee, T.-L.; Tang, K.; Borisov, A. Z.; Orlowski, J.; Brown, C. M. Paxillin S273 Phosphorylation Regulates Adhesion Dynamics and Cell Migration through a Common Protein Complex with PAK1 and βPIX. Sci. Rep. 2019, 9, 1−20.

31. Anselme, K.; Davidson, P.; Popa, A. M.; Giazzon, M.; Liley, M.; Ploux, L. The Interaction of Cells and Bacteria with Surfaces Structured at the Nanometre Scale. Acta Biomater. 2010, 6, 3824−3846.

32. Chen, G.; Hou, Z.; Gulbranson, D. R.; Thomson, J. A. Actin-Myosin Contractility is Responsible for the Reduced Viability of Dissociated Human Embryonic Stem Cells. Cell Stem Cell 2010, 7, 240−248.

33. Reymann, A.-C.; Martiel, J.-L.; Cambier, T.; Blanchoin, L.; Boujemaa-Paterski, R.; Théry, M. Nucleation Geometry Governs Ordered Actin Networks Structures. Nat. Mater. 2010, 9, 827−832.

34. Reymann, A.-C.; Boujemaa-Paterski, R.; Martiel, J.-L.; Guérin, C.; Cao, W.; Chin, H. F.; De La Cruz, E. M.; Théry, M.; Blanchoin, L. Actin Network Architecture Can Determine Myosin Motor Activity. Science 2012, 336 (6086), 1310−1314.

35. Di Cio, S.; Gautrot, J. E. Cell Sensing of Physical Properties at the Nanoscale: Mechanisms and Control of Cell Adhesion and Phenotype. Acta Biomater. 2016, 30, 26−48.

36. Giannini, M.; Primerano, C.; Berger, L.; Giannaccini, M.; Wang, Z.; Landi, E.; Cuschieri, A.; Dente, L.; Signore, G.; Raffa, V. Nano-topography: Quicksand for Cell Cycle Progression? Nanomedicine 2018, 14, 2656−2665.

37. Orita, T.; Tomita, M.; Kato, K. Regulation of Cellular Responses to Macroporous Inorganic Films Prepared by the Inverse-Opal Method. Colloids Surf., B 2011, 84, 187−197.

38. Kang, B.; Jo, S.; Baek, J.; Nakamura, F.; Hwang, W.; Lee, H. Role of Mechanical Flow for Actin Network Organization. Acta Biomater. 2019, 90, 217−224.

39. Nanci, A.; Wuest, J. D.; Peru, L.; Brunet, P.; Sharma, V.; Zalzal, S.; McKee, M. D. Chemical Modification of Titanium Surfaces for Covalent Attachment of Biological Molecules. J. Biomed. Mater. Res. 1998, 40, 324−335.

40. Petropoulos, C.; Oddou, C.; Emadali, A.; Hiriart-Bryant, E.; Boyault, C.; Faurobert, E.; Vande Pol, S.; Kim-Kaneyama, J.-r.; Kraut, A.; Coute, Y.; Block, M.; Albiges-Rizo, C.; Destaing, O. Roles of Paxillin Family Members in Adhesion and ECM Degradation Coupling at Invadosomes. J. Cell Biol. 2016, 213 (5), 585−599.

41. Deakin, N. O.; Turner, C. E. Paxillin comes of age. J. Cell Sci. 2008, 121, 2435−2444.

42. Mattila, P. K.; Lappalainen, P. Filopodia: Molecular Architecture and Cellular Functions. Nat. Rev. Mol. Cell Biol. 2008, 9, 446−454.

43. Tian, A.; Wu, A.; Zhang, H.; Xing, D.; Yang, H.; Qiu, B.; Xue, X.; Zhang, D.; Xu, Q.; Xiaofei, Q.; Dong, C. Nanoscale TiO_2 Nanotubes Govern the Biological Behavior of Human Glioma and Osteosarcoma Cells. Int. J. Nanomed. 2015, 10, 2423−2439.

44. Variola, F.; Francis-Zalzal, S.; Leduc, A.; Barbeau, J.; Nanci, A. Oxidative Nanopatterning of Titanium Generates Mesoporous Surfaces with Antimicrobial Properties. Int. J. Nanomed. 2014, 9, 2319−2325.

45. Ma, Y.; Tian, X.; Liu, L.; Pan, J.; Pan, G. Dynamic Synthetic Biointerfaces: From Reversible Chemical Interactions to Tunable Biological Effects. Acc. Chem. Res. 2019, 52, 1611−1622.

46. Chang, F.; Lemmon, C. A.; Park, D.; Romer, L. H. FAK Potentiates Rac1 Activation and Localization to Matrix Adhesion Sites: a Role for BetaPIX. Mol. Biol. Cell 2007, 18, 253−264.

47. Geiger, B.; Bershadsky, A. Assembly and Mechanosensory Function of Focal Contacts. Curr. Opin. Cell Biol. 2001, 13, 584−592.

48. Mitra, S. K.; Hanson, D. A.; Schlaepfer, D. D. Focal Adhesion Kinase: in Command and Control of Cell Motility. Nat. Rev. Mol. Cell Biol. 2005, 6, 56−68.

Chapitre 4 – Adhesion response of filopodia to an AFM lateral detachment force and functional changes after centrifugation of cells grown on nanoporous titanium

Dainelys Guadarrama Bello[a], Patricia Moraille[b], Serine Boughari[a], Antonella Badia[b], Antonio Nanci [a,c*]

[a]Laboratory for the Study of Calcified Tissues and Biomaterials, Department of Stomatology, Faculty of Dental Medicine, Université de Montréal, Montréal, Québec H3C3J7, Canada

[b]Department of Chemistry, Faculty of Arts and Sciences, Université de Montréal, C.P 6128 succursale Centre-Ville, Montréal, Québec H3C3J7, Canada

[c]Department of Biochemistry and Molecular Medicine, Faculty of Medicine, Université de Montréal, Montréal, Québec H3C3J7, Canada

Corresponding Author
Antonio Nanci
Faculté de Médecine Dentaire
Université de Montréal
C.P. 6128, succ. Centre-ville
Montréal (Québec) H3C 3J7
E-mail: antonio.nanci@umontreal.ca
Phone: 514 343-5846
Fax: 514 343-2233

Abstract

Cells sense and respond to mechanical cues from the surrounding substrate through filopodia. Regulation of cellular biomechanics operates at the nanoscale. Therefore, a better understanding of the relationship between filopodia and nanoscale surface features is highly relevant for the rational design of implant surfaces. The objective of this work was to determine the biomechanical contribution of filopodia and their nanoprotrusions to the adhesive interaction of cells with nanostructured surfaces. We have also analyzed the functional changes of entire cells subjected to an external force. MC3T3-E1 osteogenic cells were cultured on polished (Ti-Control) and nanotextured titanium discs (Ti-Nano). An AFM approach was used to measure the lateral detachment force of filopodia. Filopodia on Ti-Nano exhibited higher resistance to a lateral detachment force, which indicates that they adhere to the surface with more strength. SEM analysis revealed a restructuration of the cell membrane in response to centrifugation, being more evident on Ti-Nano. Fluorescence labeling also highlighted a difference in the mitochondrial footprint, a cellular compartment that provides energy for cellular processes. Together, these results show for the first time that surface topography can change the adhesive interaction of a subcellular structure that is fundamental in sensing physico-chemical surfaces features.

Keywords: titanium; nanotopography; filopodia; mechanotransduction; AFM; centrifugation.

4.1 Introduction

The different mechanical forces that the human body experiences promote tissue growth and remodeling (1). These forces are ultimately translated by cells that interact mechanically with their local environment and represent the basic structural and functional unit of the organism (2,3). Although the structural and molecular aspects of cells are known, their response to mechanical loads and how they convert mechanical signals into biological responses are still not completely defined (4,5).

Cells sense and respond to mechanical cues from the surrounding biological or artificial substrates through lamellipodia and filopodia (6), both actin-rich plasma-membrane protrusions found at the leading edge of cells (7). During cell migration, filopodia can exert forces on the substrate and act as precursor of focal adhesions (FAs) (8). This structure is present in almost every moving cell type and its function goes far beyond just probing the surrounding environment. Filopodia define the position of cellular adhesion sites, actin bundles, cell force generation and the formation of new filopodia (9). The rate of actin filament assembly, and cross-linking will regulate their initiation and elongation (7,10). Distinct steps have been described in their formation which includes, among others, force dependent adhesion, traction, and retraction. A fundamental aspect of this cell behavior is adhesion, an activity that involves integrin receptor-ligand binding and clustering to form FA complexes (11). These mechanically link the actin-rich cytoskeleton of cells with the extracellular matrix (ECM) (12). The cytoskeletal networks of actin, intermediate filaments, and other proteins associated with them determine in large part the mechanical stiffness of cells (13). Integrins, a family of membrane proteins, act as receptors for cell adhesion molecules via the tripeptide Arg-Gly-Asp (RGD) motif to mediate mechanotransduction to the cytoskeleton (14). This process transduces mechanical signals from the microenvironment into biological responses (14–16). The fundamental cell signaling pathways activated regulate diverse cellular activities such as polarization, migration, proliferation, and differentiation (6,17). These events are influenced by the strength of cell adhesion and are essential for understanding the functioning of cells in the body. They are also critical for the rational design of biomaterials, especially those that are continuously exposed to forces, such as implant loading (18) and blood flow (14,19).

The regulation of cellular biomechanics operates at the nanoscale since cells interact with ECMs comprise of nanoscale constituents such as hydroxyapatite crystals, collagen fibrils, or

proteoglycans (20,21). This also applies to nanostructured medically relevant materials and for this reason, there has been a focus on nanotopography as a tool to improve cell adhesion and activity (14,22). Therefore, a better understanding of the biomechanical relationship between filopodia and nanoscale surface features is highly relevant for improving implant surfaces.

Real-time force measurements are complex to determine. Different approaches have been used to estimate the cell adhesion strength and quantify the mechanical properties of cells (17). These include the use of techniques like atomic force microscopy (AFM), optical stretching magnetic twisting cytometry, micropipette aspiration and acoustic radiation-induced deformation, as well as shear forces to detach the cells (e.g. spinning disks, centrifugation, and flow chambers) (23). Albuschies and Vogel (24), using flexible silicon nanowires (NWs), indirectly estimated the traction force exerted by filopodia from de deflection of the NWs by scanning electron microscopy (SEM) after fixation of the cells. The dynamic behavior of the F-actin present in filopodia has also been investigated on traction and retraction force exerted by live cells, using optical trap and simultaneous optical tweezers and confocal laser-scanning measurements (8,25). AFM is a unique, high-resolution tool that has been extensively used to study cellular adhesion forces from the single-molecule level to the entire cell (26). An approach commonly reported in literature is a cantilever tip with an immobilized cell as a measuring probe (13,26). This technique, known as AFM-based single-cell force spectroscopy (SCFS), is an ultrasensitive method for quantifying cell adhesion forces of single cells. Cellular adhesion force can be measured from the degree of cantilever deflection during cell retraction (26,27). A similar strategy involves bringing a protein-coated cantilever onto a cell firmly attached to the substrate and then retracting the cantilever (13). However, these AFM approaches measure the adhesion force exerted by the entire cell and give no information about the contribution of specific subcellular structures to the force.

In previous studies, we have demonstrated that a nanoporous surface induces the formation of more filopodia with abundant nanoscale lateral protrusions that contour the walls of the nanopores (12). It has been suggested, but not demonstrated, that these distinctive filopodia together with the formation of larger FAs contribute to the overall adhesion strength of the cell. Filopodia traction and retraction have been studied (8,25), but their adhesion, that represents a major component of the filopodia mechanical sensing function has not. In this study, we have determined the biomechanical contribution of filopodia and nanoprotrusions to the adhesive

interaction of cells with the surface. These events occur at the subcellular level and measuring forces at the nanoscale is particularly challenging. In fact, to our knowledge, direct measurement of the adhesion force of filopodia in response of a nanotopography, has never been reported. We have adapted an AFM approach used to measure the lateral detachment force of bacteria (23,28) to compare the adhesion forces exerted by filopodia on polished control and nanostructured titanium surfaces. A polished surface was selected to eliminate any topographical features which could confound the contribution of the nanotopography by creating multilevel topography. In order to evaluate the impact of the surface on the adhesion force of the entire cell, we have also analyzed the structural and functional changes exhibited by cells when subjected to an external centrifugal shearing force that does not inherently cause cell damage. Mitochondria are an essential component of all cells in the body that provide energy to perform biochemical reactions and different cellular processes (29). Because extracellular mechanical factors and the cytoskeleton have an impact on mitochondrial activity, we have also compared the mitochondrial footprint before and after centrifugation (30). The measurements carried out on fixed cells demonstrate that filopodia and their associated nanoprotrusions induced by the topography exhibit higher resistance to a lateral detachment force, indicating that they adhere to the surface with more strength. Centrifugation results demonstrate an increase in the number of filopodia associated with membrane changes in response to the nanotopography. We also found that the nanoporous surface plays an essential role in regulating mitochondrial networks. Altogether, our combined approach highlighted the profound impact of the nanoporous surface on the adhesion strength of filopodia, and on mitochondrial functionality.

4.2 Materials and Methods

4.2.1 Surface modification

Commercially pure grade II titanium discs (12 mm diameter x 2 mm thickness) (Firmetal Co., Ltd., Shanghai, China) were first polished in three stages as previously described (12) using silicon carbide abrasive paper followed by a Texmet carpet with MetaDi fluid, and 9 mm diamond suspension. Finally, a MicroFloc carpet with distilled water and MasterMet SiO2 solution was used. The polished discs were rinsed with distilled water in an ultrasonic bath and subsequently cleaned in 70% ethanol and dried with air. Oxidative chemical treatment was used to generate a nanoscale surface topography (Ti-Nano). The polished discs were immersed in a solution of equal

volumes of concentrated H2SO4 (98% mass fraction) and 30% H_2O_2 at room temperature (RT) for 1.5 h as detailed elsewhere (12, 31). Polished surfaces were used as controls (Ti-Control).

4.2.2 Surface characterization

The Ti-Control and Ti-Nano surfaces were imaged using an ultrahigh-resolution scanning electron microscope (SEM) Regulus 8220 (Hitachi, Ltd., Tokyo, Japan) operated at 1kV. Images were obtained in deceleration mode with a combination of signal from secondary and backscattered electrons without coating the sample. The working distance was around 1.5-3 mm. The average pore diameter was measured using ImageJ (http://imagej.nih.gov/ij/features.html).

4.2.3 Cell culture

The Ti-Control and Ti-Nano discs were sterilized using 70% ethanol and UV light for 2 h before seeding the cells. MC3T3-E1 (mouse calvaria-derived osteogenic) cells from American Type Culture Collection (ATCC) were cultured in Alpha Minimum Essential Medium with Earle's salts, L-glutamine, ribonucleosides, and deoxyribonucleosides (α-MEM) supplemented with 10% fetal bovine serum at 37 °C in a humidified atmosphere with 5% CO_2. A cell density of 10,000 was plated on Ti-Control and Ti-Nano discs placed in 12-well plates. The cells were grown for 24 h.

4.2.4 AFM Imaging

Images of attached cells were obtained by AFM using a Dimension Icon NSV scanning probe microscope (Bruker Nano Surfaces, Santa Barbara, California, USA) operated in contact mode in 0.1 M sodium phosphate buffer (PB), pH 7.3PB after fixation for 1 h at 4 °C in 2.5% glutaraldehyde. A silicon nitride tip and cantilever (ScanAsyst Fluid probe, Bruker AFM probes, Camarillo, California, USA) with a low spring and high sensitivity (nominal spring constant = 0.7 N/m) was used. The ScanAsyst Fluid is a probe that has a dull tip ideal for force measurements and imaging extremely delicate samples in fluids. The silicon nitride cantilever has a triangular geometry and a back side coating of reflective gold. The tip is connected to the base of the cantilever by an irregular quadrilateral pyramid. The tip radius has a nominal value of 20 nm with a maximum of 60 nm with a height that varies between 2.5-8 μm with front, back and side angles from 15 to 25° (According to manufacturer). To select the appropriate filopodia, cells were imaged at a scan size of 40 μm2 and a scan rate of 1Hz with 128 pixels by line resolution and low set point.

Only those filopodia with a length of at least 5 µm, a diameter between 400-800 nm, and a height of 100 nm or more were selected, eliminating width and height as possible variables in the respective force measurements. These dimensions were abundant and readily apparent and therefore we opted to select this. A more refine search using the contact mode was eliminated because the damage it can cause and the time it requires. The tip's scan direction relative to the filopodia was 90° ± 5°. Selected filopodia were distanced from other structures (e.g., other filopodia or cell bodies) by a minimum of 5 µm to avoid direct contact with other obstacles during measurements. In order to achieve reliable force measurements, all measurements were performed on filopodia displaying similar size as well as overall orientation.

4.2.5. Lateral detachment force quantification. Force calculation

During the force measurement, the AFM tip (Fig. 1A, B) was scanned across the filopodium at a speed of 1 Hz with successive increases of the deflection setpoint with the slow scan axis disabled, therefore ensuring the incremental force was consistently applied along the same scan line until the filopodium detached (Fig. 1C). This force can be calculated using Hooke's Law. However, according to Deupree and Schoenfisch (28), when the probe interacts with a large feature, in this case, a filopodium, the interaction between the tip and the feature will occur on the side of the probe. The equation to describe this interaction and calculate the force is as follows (Eq. 1):

$$F_{lat} = kSV_{total}\sin(\theta + \Phi)\cos\theta \qquad \text{Eq. 1}$$

where the F_{lat} is the lateral detachment force (nN), k and S are the spring constant (nN/nm) and sensitivity (nm/V) of the applied cantilever, respectively. For each specific AFM probe used, k was determined by performing a thermal tune in air and Lorentzian fitting and S by acquiring a force-distance curve against a clean sapphire substrate. θ and Φ angles are parameters of the probe geometry and cantilever orientation. Vtotal is the total vertical deflection of the laser beam detected by the position-sensitive detector and is directly correlated to the total compression of the cantilever. Three independent experiments (different culture and substrate preparation) were conducted. A total of 9 individual filopodium from 3 different replicas were analyzed for each condition.
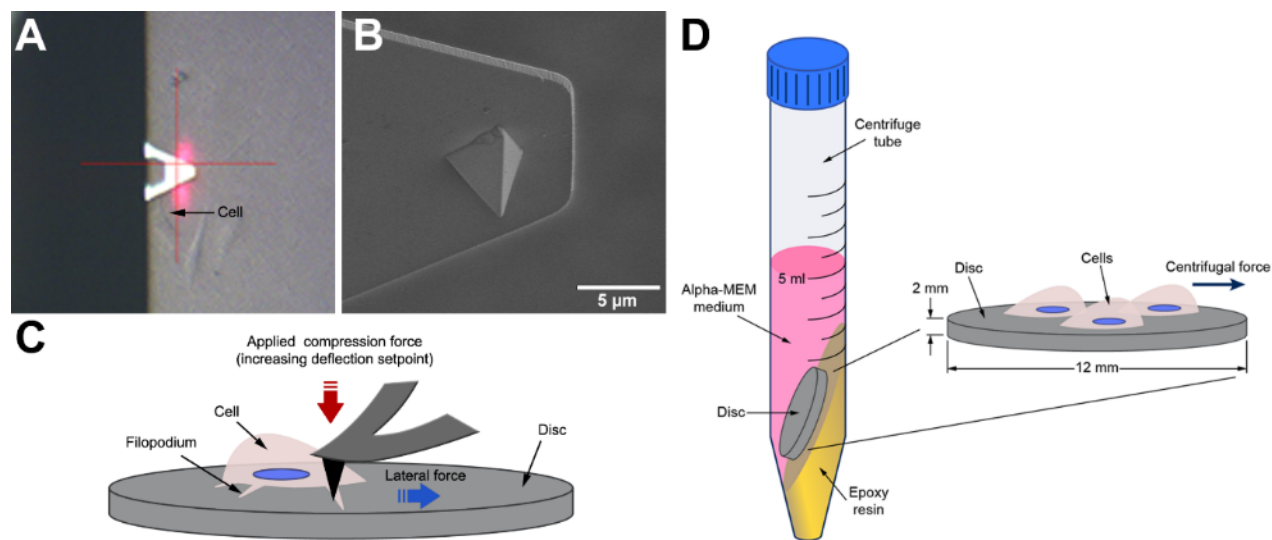
Figure 40. – Fig. 1. (A) Image from the optical camera showing the top view of the AFM cantilever scanning a cell. (B) SEM micrograph of the lateral view of the pyramidal silicon nitride tip. (C) Schematic representation of the lateral view showing the direction of the compression and lateral forces applied to move the cell. (D) Schematic representation of the disc arrangement for the centrifugation assay.

4.2.6 Centrifugation assay. Functional changes on cells

We used a modified centrifugation cell adhesion assay that applies controlled force to the adherent cells in the same direction as the force quantification approach described previously. After 24 h of culture, cells cultured on Ti-Control and Ti-Nano discs on the 12-well plates were placed directly into 15 mL tubes with 5 mL of α-MEM medium supplemented with 10% fetal bovine serum at 37 °C as represented in Fig. 1D. The discs were placed in a tilt position (15°) to ensure that adherent cells only received a shear centrifugal force. A resin was polymerized at the bottom of each tube with the desired angle, the minimum inclination that was able to keep the disc at the right position through the experiment. Then, the tubes were placed into a centrifuge (Centrifuge Allegra™ X-22R, Ontario, Canada), and cells were centrifuged for 30 min at a speed of 1900 g.

4.2.7 Morphology, cell number and FAs

Following centrifugation, cells were fixed for 30 min at 4°C using periodate-lysine-paraformaldehyde in PB. Discs without centrifuging were used as control. Then, cells were washed

in PB and permeabilized with 0.5% Triton X-100 in PB for 10 min. 5% skim milk in PB was used to block nonspecific binding sites for 1 h. Cells were incubated for 2 h with the specific primary antibody (1:200; Monoclonal Anti-Vinculin Clone hVIN-1 Sigma, MO, USA) and Rhodamine-phalloidin (1:150, Life Technologies) diluted in blocking solution. Alexa Fluor 488 (green fluorescence) conjugated goat anti-mouse was used as a secondary antibody (1:500, Life technologies). All steps of the incubations were performed in a humidified environment at RT protected from light. Between each incubation step, the samples were washed three times (5 min each) in PB. Glass slides were used to mount the discs face up, and cell nuclei were stained and mounted with mountain medium containing DAPI (Prolong antifade 4′,6-diamidino-2-phenyl-indole, dihydrochloride, Molecular Probes, Invitrogen) covered with round-glass coverslips. The samples were analyzed with a Zeiss Axio Imager M2 Optical Microscope (Carl Zeiss, Jena, Germany). A 63x objective was used to acquire high-magnification immunofluorescence images to study the cytoskeleton distribution, area, and FA formation on the cells. For each substrate, more than 30 individual cells from three different replicates were evaluated.

To obtain high-resolution images of the entire disc, images were captured with a large field of view using a 10x objective, and the surface was subdivided into multiple smaller images to capture tiles. Four discs for each condition (16 images of the whole disc) were used to count the total number of cells. In parallel, control and centrifuged cells were fixed for 1 h at 4 °C in 2.5% glutaraldehyde and subsequently rinsed three times with PB, followed by incubation for 1 h in 1% osmium tetroxide at 4 °C. Cells were dehydrated through a graded series of ethanol (30%, 50%, 70%, 90%, 95%, and two times 100%) followed by drying in a Leica EM CPD300 Critical Point Dryer (Leica Microsystems Inc., Ontario, Canada). An SEM Regulus 8220 operated at 1 kV was used to observe the morphology of cells grown on control and treated surfaces.

4.2.8 Mitochondrial morphology

To label mitochondria, cells cultured on Ti-Control and Ti-Nano for 24 h before and after centrifugation were incubated with MitoTracker® probes (200 nM) for 45 min at 37 °C in a humidified atmosphere with 5% CO_2. Then, cells were washed with α-MEM without FBS followed by fixation for 15 min at 37 °C using 4% paraformaldehyde in PB. The samples were washed three times (5 min each) in PB. Glass slides were used to mount the discs face up, and cell nuclei were stained and mounted with mounting medium containing DAPI (Prolong antifade 4′,6-diamidino-

2-phenyl-indole, dihydrochloride, Molecular Probes, Invitrogen) covered with round-glass coverslips. Images were acquired using a 63x objective with a Zeiss Axio Imager M2 Optical Microscope. More than 10 cells from three different replicates were analyzed by each condition.

4.2.9 Image analysis

Image J ((http://imagej.nih.gov/ij/features.html)) was used to estimate the number of the FAs, the area, the number of cells, and the mitochondrial morphology. Images were processed as described in Bello *et al* (12). Images from mitochondrial assays were treated following these steps: (as described by A.J. Valente *et al* (32)): unsharp mask, CLAHE, and median. Then, images were binarized and skeletonized to analyze the skeleton as described in Fig. 1S (supplemental materials). Mitochondrial network features as branches, footprint, junctions and rods (individuals) were analysed. All graphs were constructed with Origin Pro 9.2 software (OriginLab Corporation).

4.2.10 Statistical analysis

The Origin Pro 9.2 software was used to determine the statistically significant differences between the means of different groups using a Student's t-test analysis of mean values. Values of $p < 0.05$ were considered statistically different, while the values above were not different. Data normality was verified using a Shapiro-Wilk test and the Grubbs test was conducted to verify the existence of outliers. All results are presented as the mean value ± standard deviation (SD).

4.3 Results

4.3.1 Characterization of surface topography

Fig. 2 illustrates the surface topographies of the polished titanium discs before (Ti-Control) and after (Ti-Nano) oxidative chemical treatment. The Ti-Control showed a smooth surface without topographical features (Fig. 2A). A three-dimensional network of nanopores is observed on the treated surface (Fig. 2B). The mean diameter of the generated nanopores of 19 ± 5 nm (Fig. 2C) is consistent with previous reports (12, 31).
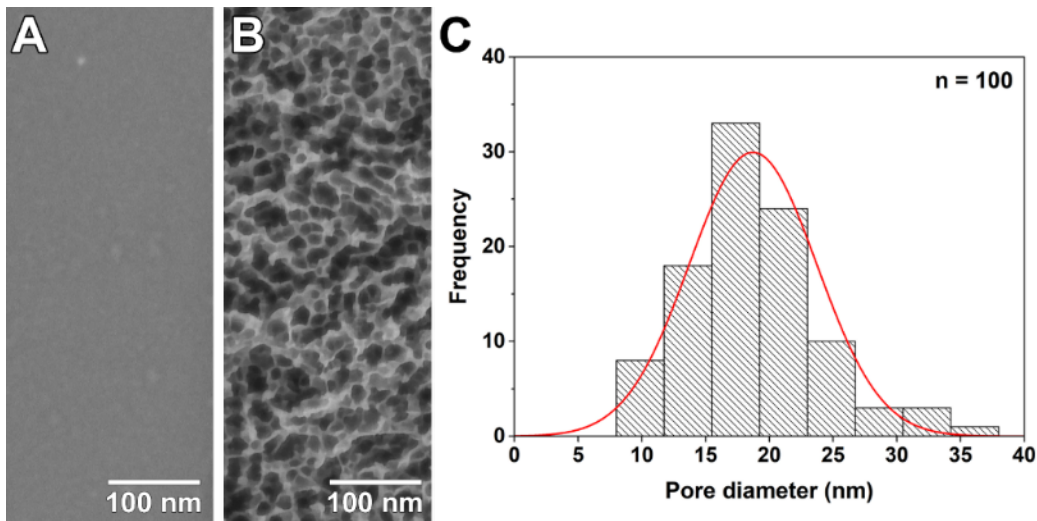
Figure 41. – Fig. 2. Scanning electron micrographs of the (A) smooth polished Ti surface and (B) nanoporous topography created by the oxidative chemical treatment. (C) Size distribution of the nanopores (n=100).

4.3.2 Adhesion force quantification

We measured the cell-substrate adhesion force of MC3T3 cells cultured on Ti-Control and Ti-Nano by contact mode AFM. This method was used to quantify the adhesion strength of filopodia after 24 h of culture on the 2 different substrate surfaces.

The measurements showed that filopodia adhered to the Ti-Nano with more strength than Ti-Control (Fig. 3). Filopodia displaced more readily and using lower cantilever deflection on Ti-Control (Fig. 3A and B), whereas on Ti-Nano (Fig. 3C and D), displacement of the filopodia required significantly higher deflection of the cantilever, in some cases, resulting in tearing of the filopodia. The lateral force increased from 43 ± 21 nN to 228 ± 27 nN following oxidative nanopatterning on Ti-Nano (Fig. 3E).
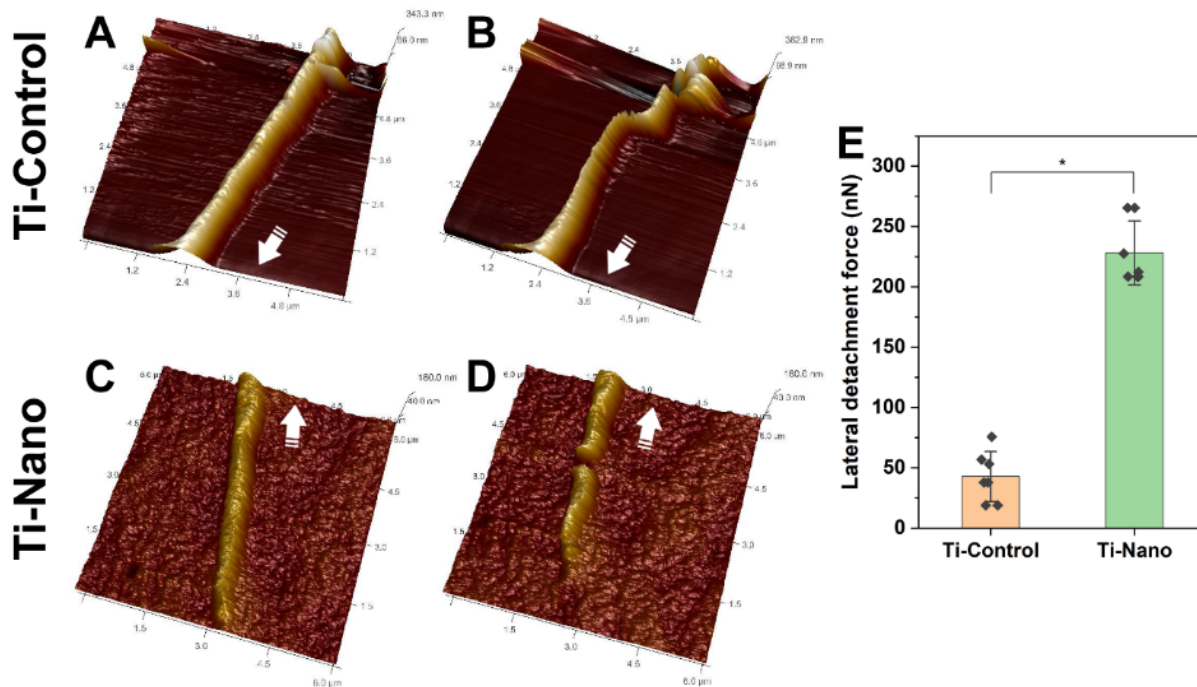
Figure 42. – Fig. 3. AFM images of filopodia on (A) Ti-Control and (C) Ti-Nano showing the probed regions (A, C) before and (B, D) after increasing the deflection setpoint of the cantilever. In all AFM images arrows represent the direction of the cell body. (E) Quantitative analysis of the lateral force required to detach or break the filopodium on both surfaces obtained after calculation. Dots represent individual data points. Error bars represent the standard deviations, * indicates statistically significant differences ($p < 0.05$).

4.3.3 Centrifugation

Centrifugation was employed to investigate the functional changes experienced by cells according to the characteristics of the substrate surface.

4.3.3.1 Counting and visualizing cells before and after centrifugation

The number of adherent cells before and after 30 min of centrifugation was measured (Fig. 4). A representative immunofluorescence image used to quantify cells is shown in Fig. 4A, B. Quantitative analysis indicated that centrifugation does not drastically reduce the cell number on Ti-Control and Ti-Nano (Fig. 4E). Most cells remain attached to the surface under the applied centrifugal force.
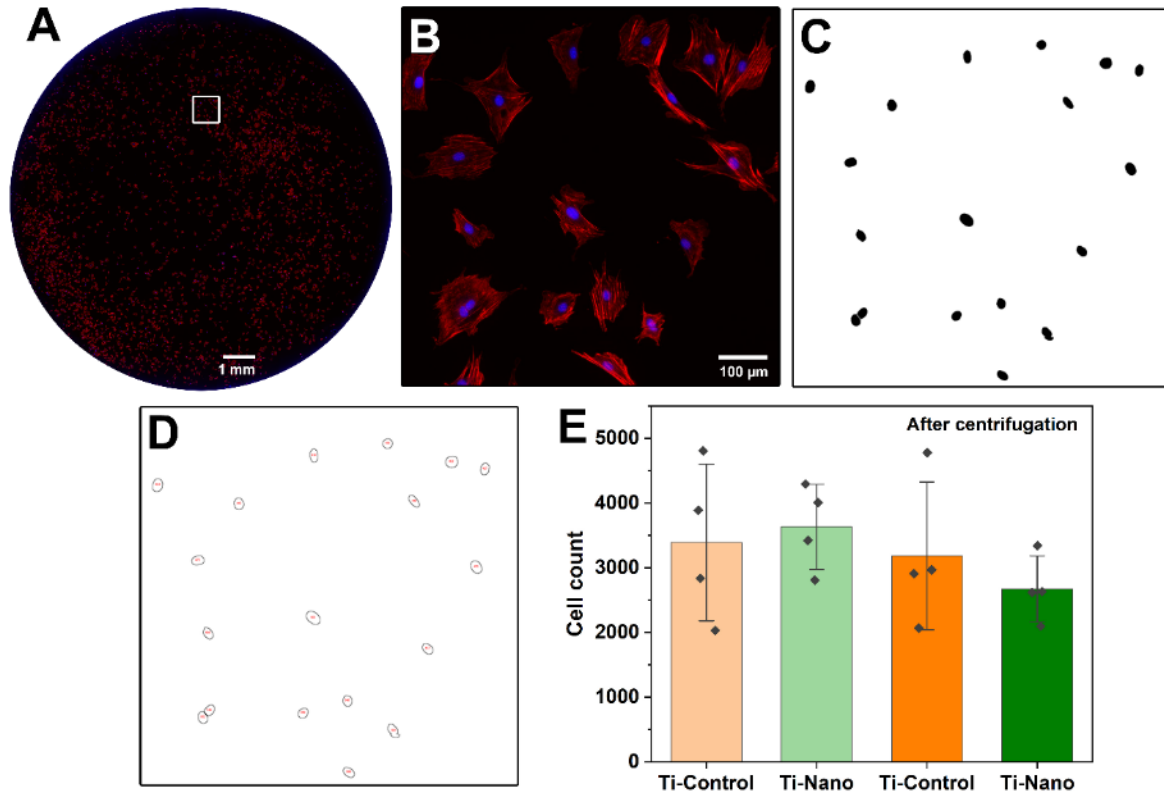
Figure 43. – Fig. 4. (A) Count from fluorescence microscopy images of cells stained with DAPI (blue) for nuclei and rhodamine/phalloidin (red) for actin. (B) Enlargement of the area outlined by the white square in a. (C) Nuclei maps generated using Image J to automatically calculate (D) the cell number. (E) Number of cells on the polished (Ti-Control) and nanoporous (Ti-Nano) surfaces before and after centrifugation. Dots represent individual data points. Error bars represent the standard deviation. The results show no statistical differences.

To further understand the effect of centrifugation on cells cultured on both surfaces, we analyzed the cell area (Fig. 5). The cell area is not affected by centrifugation (Fig. 5E). We can observe normal variation concerning cell growth. However, some cells showed regions of peripheral membrane folding, suggesting that adhesions or the cytoskeleton were affected by centrifugation (Fig. 5B, D, white ovals).
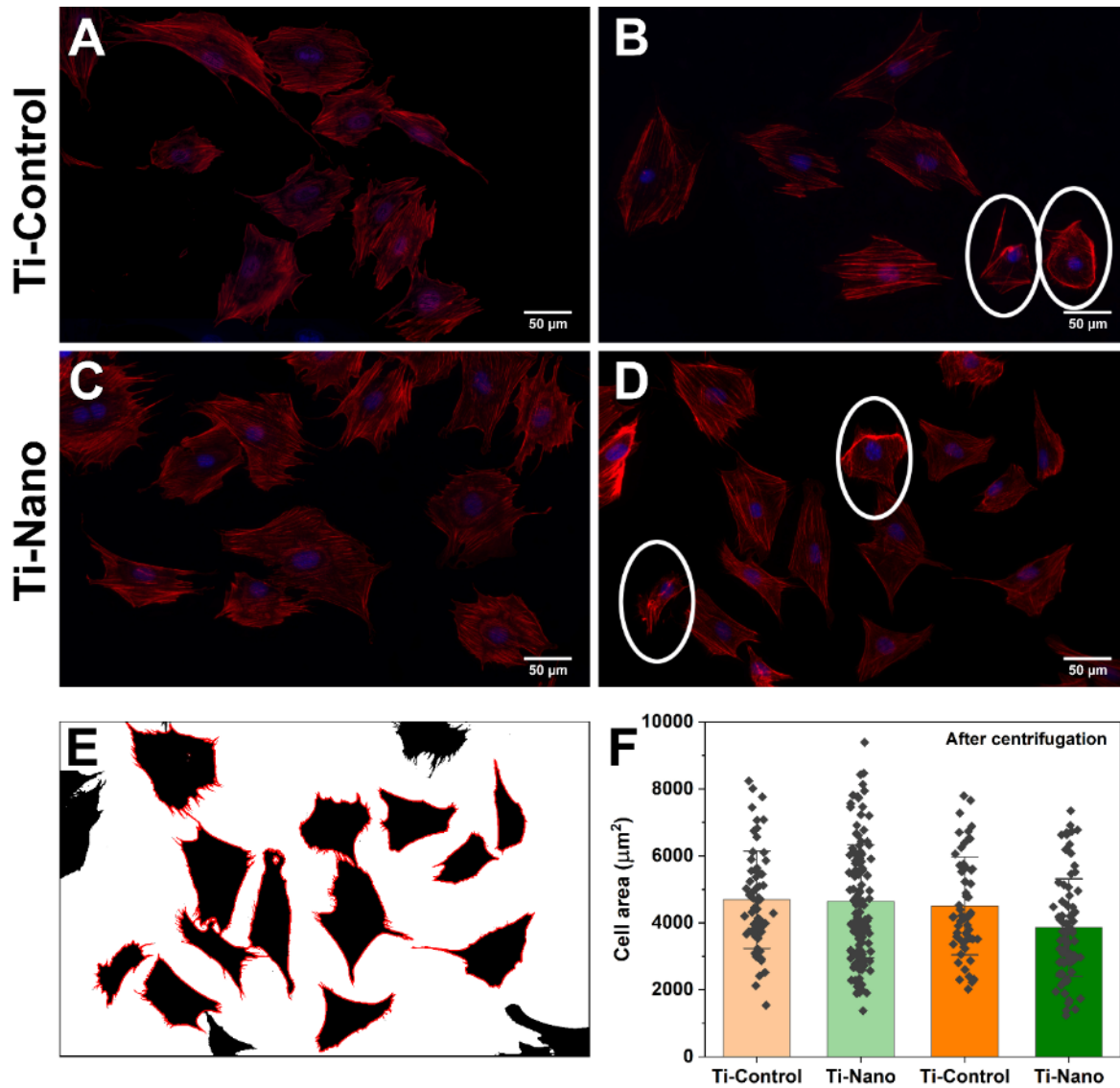
Figure 44. –   Fig. 5. Fluorescence microscopy images of cells stained with DAPI (blue) for nuclei and rhodamine/phalloidin (red) for actin attached on Ti-Control and Ti-Nano (A, C) before and (B, D) after centrifugation. (E) Cells map generated using Image J to automatically calculate the cell area, incomplete cells were excluded from data. Some cells showed regions of peripheral membrane folding (white ovals). (F) The cell areas on Ti-Control and Ti-Nano surfaces before and after centrifugation show no statistical differences under all conditions. Dots represent individual data points. Error bars represent the standard deviations.

SEM analysis revealed a restructuration of the cell membrane accompanied by a corresponding change in cell shape after centrifugation (Fig. 6). On some cells, the filopodia concentrated on one aspect of the cells (Fig. 6B, F (arrowheads)), and they were more abundant on the Ti-Nano. On this surface, cells also showed the presence of abundant cell membrane veils, poor in cytoskeleton elements, in response to the centrifugation (Fig. 6G). High magnification images allow us to see that the cell is still developing nanoprotrusions emerging from filopodia in response to the nanotopography (Fig. 6H (arrows)).
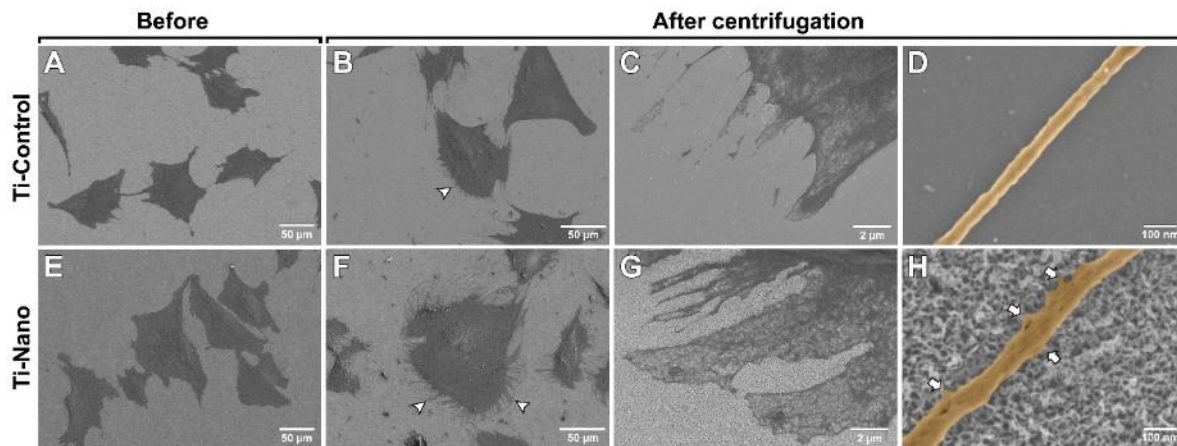
Figure 45. – Fig. 6. Representative SEM images of cells attached on (A-D) Ti-Control and (E-H) Ti-Nano (A, E) before and (B, C, D, F, G, H) after centrifugation. The distribution of filopodia is represented with arrowheads. High-resolution images of filopodium on (D) Ti-Control and (F) Ti-Nano after centrifugation. (H) Nanoscale protrusions emanating from a filopodium attached to the Ti-Nano surface (arrows).

4.3.3.2 Changes in the mitochondrial dynamics in cells after centrifugation

Surface topography and centrifugation influence the mitochondrial network organization (Fig. 7A-D). The surface of the mitochondria increased. This increase is only statistically significant on Ti-Nano (Fig. 7E). The number of junctions was not affected (Fig. 1S, Supplemental materials).
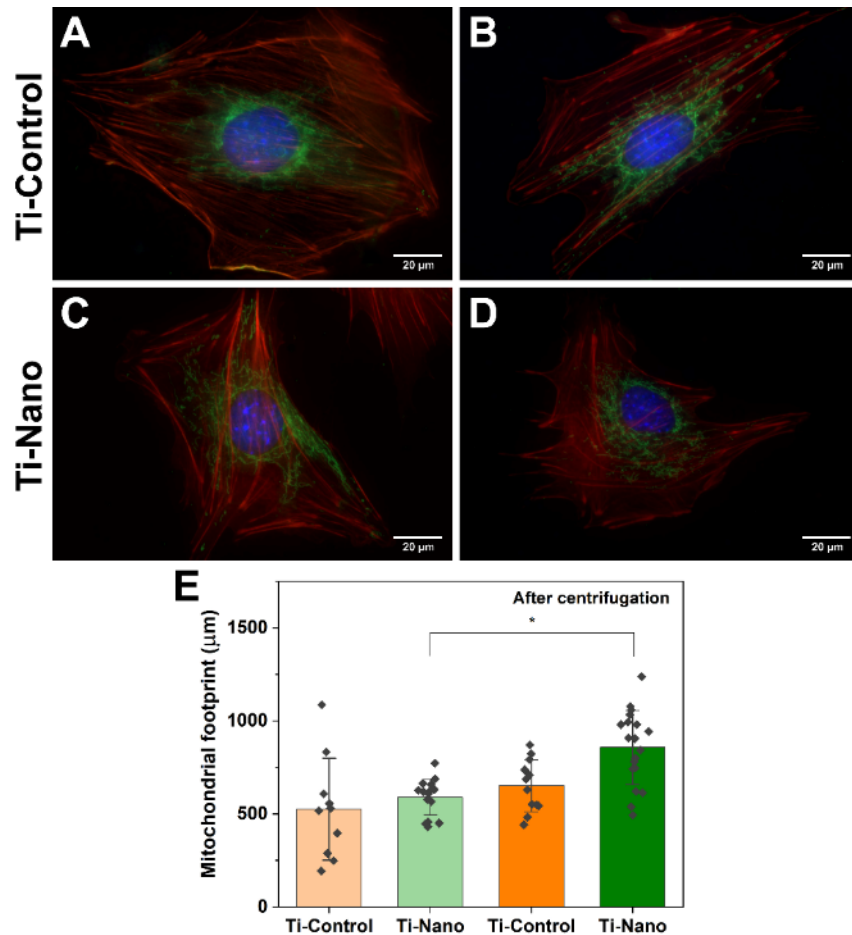
Figure 46. –   Fig. 7. Representative fluorescence micrographs of cells stained with DAPI (blue) for nuclei, rhodamine/phalloidin (red) for actin, and MitoTracker Green (green) for mitochondrial network attached on Ti-Control and Ti-Nano (A, C) before and (B, D) after centrifugation. (E) The surface occupied by the mitochondria. Dots represent individual data points. Error bars represent the standard deviations, * indicates statistically significant differences ($p < 0.05$).

4.3.3.3 FAs and cytoskeleton organization

To analyze cell adhesion and morphology before (Fig. 8A, C) and after (Fig. 8B, D) centrifugation, cells were stained with Rhodamine-phalloidin to visualize the cytoskeletal organization and anti-vinculin for FA number. There was a tendency for FAs to increase after centrifugation (Fig. 8E), and the images from Ti-Nano suggested a higher concentration of FAs under the region of the nucleus and its immediate surroundings (Fig. 8D).
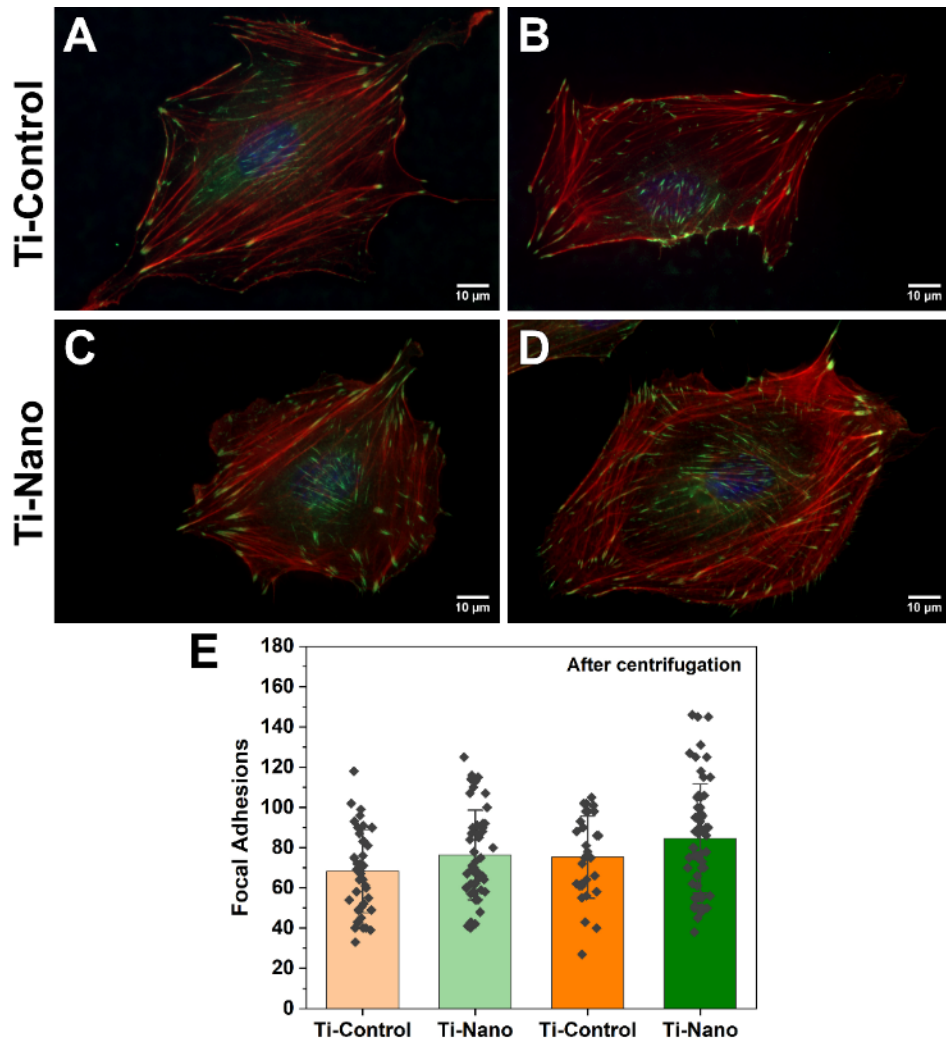
Figure 47. –   Fig. 8. Immunofluorescence images of cells stained with DAPI (blue) for nuclei, rhodamine/phalloidin (red) for actin, and Anti-vinculin (green) for FAs attached on Ti-Control and Ti-Nano, (A, C) before and (B, D) after centrifugation. (E) Number of FAs. Dots represent individual data points. Error bars represent the standard deviations. The results show no statistical differences.

4.4 Discussion

While various studies have investigated the effects of the substrate surface topography on the adhesion of entire cell (33, 34), very few have focused on the role played by filopodia. Here we show that filopodia extended by osteoblastic cells perceive and respond to the underlying nanoporous titanium surface created by oxidative nanopatterning to locally develop stronger

biomechanical relationship with the substrate. The fact that five-fold more force is required to displace/break filopodia on the Ti-Nano surface compared to the Ti-Control indicates a significant higher adhesion. Since lateral nanoprotrusions are only found on Ti-Nano, the observed adhesion differential must partly result from their development. Essentially, these very thin membrane extensions allow filopodia to establish more adhesive interactions with the surface. The more frequently observed filopodia breaks on the Ti-Nano, in comparison with the Ti-Control, may reflect an overall differential in stiffness resulting from the more intimate interaction with the surface and/or the distribution of cytoskeletal elements in them that are independent of the cell fixation used. As we have discussed previously (12), the intimate association of filopodia and their nanoprotrusions with the surface suggests that the mechanism may involve changes in integrin conformation and clustering that alter the dynamic organization of signaling proteins in FAs. Using the same experimental conditions, it was shown an increase in the FA area using vinculin staining and the upregulation of the expression of various integrins responsible for the cell-substrate interaction. The higher adhesion force shown here can be correlated with the above molecular findings, demonstrating that filopodia play a critical role in surface topography sensing.

In this work, we complemented the biomechanical AFM analysis with cytochemical and morphological analysis of entire cells following exposure to an external centrifugal shearing force (23). García *et al* (35), used a centrifugation assay to evaluate the influence of multiple biomaterial surface treatments and protein coatings on adhesion of entire cells. They established a correlation between the adhesive properties of cells and different substrate surfaces. Similarly, a centrifugation assay was used to examine the cell adhesion responses to different ligand densities and demonstrated that ligand clustering increased cell adhesion (36). Neither of these examples analyzed the role of filopodia and their nanoprotrusions. Unlike these above studies, our results revealed no dramatic effect on cell number and area on both the control and nanostructured surfaces. These findings are not surprising because both the duration and the centrifugal force applied were selected to avoid significant cellular damage, and results could change by increasing the time and/or force of centrifugation. However, our study put in evidence that nanoporosity induces pertinent functional changes during as little as 30 minutes of centrifugation. There was, in general, more filopodia which assumed an overall spiraling orientation with respect to the cell surface on the Ti-Nano. One striking particularity is that membrane reorganization resulted in their preferential concentration on one aspect of the cell. This suggests that cells respond to both the

strength and orientation of the force applied, which was not the case on Ti-Control. Another distinctive observation is that filopodia on Ti-Nano maintain nanoprotrusions while they are exposed to force. This reaffirms their importance for the adhesive strength of filopodia and may be very relevant for maintaining cell adhesion under more stringent centrifugal conditions.

The highly dynamic mitochondria provide energy to cellular processes (29), and has the ability to fuse and divide and link to the actin network that responds to mechanical forces (30). Mitochondrial content and their morphology are difficult to quantify due to the degree of branching and their heterogeneity in length (37). We observed that the mitochondrial footprint of cells on the Ti-Nano surface was more extensive than that of cells on Ti-Control. However, the number of junctions where branches originate does not appear to be affected by the centrifugation on both surfaces (Fig. 1S, Supplemental materials). Consequently, the size of branches and rods must increase, suggesting a concurrent increase in mitochondria fusion that favors activity across the entire tubular network (38). This suggests that nanotopography would

undoubtedly influence mitochondrial function by having an impact on branching.

FAs link the actin-rich cytoskeleton of cells through integrins with the ECM to mediate major cellular events such as mechanosensing and signaling (39, 40), but the mechanism by which mechanical stimuli influence FA development remains unclear. As illustrated by the vinculin labeling, there is tendency for to increase in the number of FAs after centrifugation that is more prominent on Ti-Nano. They also appear to concentrate in the membrane under and surrounding the nucleus, an intriguing observation that may relate to the distribution of forces along the cell on Ti-Nano. These observations provide a functional confirmation that the physico-chemical changes induced by oxidative nanopatterning influence the behavior of by FAs and their response to external mechanical stress.

Filopodia are essential membrane protrusions that facilitate cellular sensing and interaction with the environment (25). Our study offers a new approach for the direct measurement of the filopodium adhesion force and represent a significant advance in nanoscale cell mechanobiology. Because filopodia are important mediators of mechanotransduction and they are affected by surface topography (41), it is important to understand how they respond to forces. There is a paucity of studies that measure forces at the subcellular level and the few available use diverse methodologies making difficult to directly compare our results with that of others.

Some studies had dealt with the adhesion force of entire cells (42, 43) or with the traction and retraction forces of filopodia (24, 25). However, it has so far not been possible to reliably measure the force with which filopodia adhere to a substrate, essentially for methodological reasons. The differential adhesion force that we have observed between the smooth and nano surfaces reflects different filopodial dynamics on these two surfaces. It also cannot be excluded that this differential adhesion would have an impact on traction and retraction functions of filopodia. In fact, when filopodial adhesion fails, retraction takes place (9). Therefore, understanding how topography creates different adhesive strengths is important because it can be exploited for the rational design of biomaterial surfaces that will achieve selective adhesive relationship for optimal cellular responses.

There is still no perfect method for measuring the strength of cell adhesion in terms of sensitivity and reproducibility. In fact, all studies have strengths and limitations, and the important consideration is to keep them in mind when interpreting the results. In our study, measuring the force of filopodia after chemical fixation, certainly needs consideration. However, since both surfaces were tested under the same conditions, the difference in lateral detachment force is meaningful. In fact, fixation immobilized in time and space pre-existent adhesive interactions of filopodia on both surfaces. Chemical fixation has also been used in the study of Jörg Albuschies & Viola Vogel (24) to immobilize cells during filopodia traction measurements that resulted in very relevant results. Clearly, the next step will be measuring adhesion forces on live cells, but this will present a challenge because filopodia are dynamic structures that could respond and change during the process of lateral force measurement.

4.5 Conclusions

To our knowledge, this is the first *in vitro* study that has directly examined the adhesive interaction between a subcellular structure and a surface. We have applied a quantitative AFM method to compare the adhesion strength of filopodia on smooth and nanoporous titanium surfaces. The formation of filopodia with nanoprotrusions increases and these adhere with more strength on the nanoporous topography. Therefore, these must make an important contribution to the overall adhesion strength of the cell. We have also distinctly analyzed the structural and functional changes of cells when subjected to an external centrifugal force. The observed changes in the filopodia

number and distribution, in the overall size of the mitochondrial network footprint, and the distribution of FAs indicate that cells grown on nanoporous titanium also respond differently to an external force. Together, these results show that surface topography can change the adhesive properties of a subcellular component that is fundamental in sensing physico-chemical surfaces features, and this change affects the cell response to an external force. These findings are particularly relevant for prosthetic devices that are subject to external loads, such as orthopedic and dental implants.

Supplementary Materials
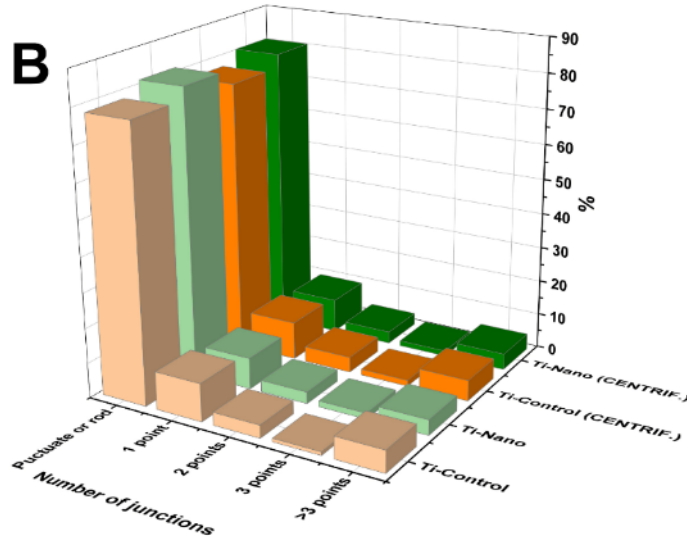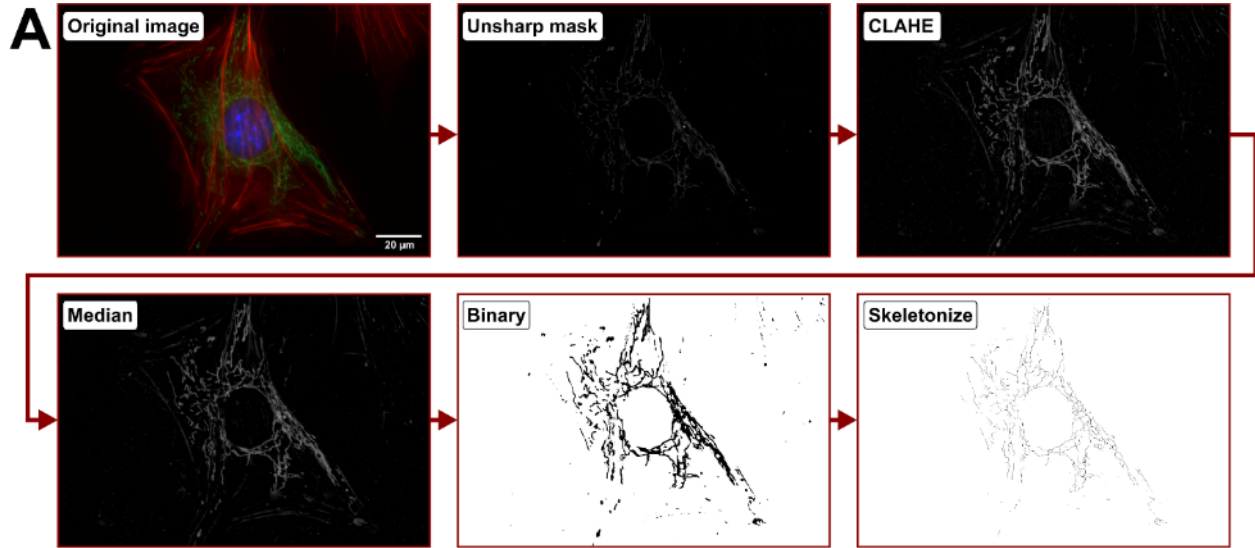
Figure 48. – **Figure 1S.** (a) Representative fluorescence micrograph of cells stained with DAPI (blue) for nuclei, rhodamine/phalloidin (red) for actin, and MitoTracker Green (green) for the mitochondrial network followed by the generated images after Image J processing using: unsharp mask, CLAHE, median, binary and skeletonize tools. (b) Number of junctions quantified for each surface before and after the centrifugation. The number of junctions expressed as a percentage was not significantly affected by surface or centrifugation. However, the mitochondrial footprint on Ti-Nano was altered after centrifugation (see Figure 7).

Author Contributions:

Dainelys Guadarrama Bello: Conceptualization, Methodology, Investigation, Writing- Original draft preparation, Visualization. Patricia Moraille: Supervision, Writing- Reviewing and Editing. Serine Boughari: Investigation, Writing- Reviewing. Antonella Badia: Supervision, Writing- Reviewing and Editing. Antonio Nanci: Conceptualization, Methodology, Validation, Supervision, Writing- Reviewing and Editing, Funding acquisition.

Funding:

Acknowledgments:

References

1. S. P. Banavar, E. K. Carn, P. Rowghanian, G. Stooke-Vaughan, S. Kim, and O. Campàs, Mechanical control of tissue shape and morphogenetic flows during vertebrate body axis elongation, Scientific Reports 11 (2021) 8591.

2. N. Nijenhuis, X. Zhao, A. Carisey, C. Ballestrem, and B. Derby, Combining AFM and acoustic probes to reveal changes in the elastic stiffness tensor of living cells, Biophysical journal 107 (2014) 1502-1512.

3. H. Huang et al., Recent Advances on the Model, Measurement Technique, and Application of Single Cell Mechanics, International journal of molecular sciences 21 (2020) 6248.

4. K. Y. Volokh, Challenge of biomechanics, Mol Cell Biomech 10 (2013) 107-35.

5. J. H. C. Wang and B. P. Thampatty, An Introductory Review of Cell Mechanobiology, Biomechanics and Modeling in Mechanobiology 5 (2006) 1-16.

6. X. Wang and T. Ha, Defining Single Molecular Forces Required to Activate Integrin and Notch Signaling, Science 340 (2013) 991.

7. P. K. Mattila and P. Lappalainen, Filopodia: molecular architecture and cellular functions, Nature Reviews Molecular Cell Biology 9 (2008) 446-454.

8. T. Bornschlögl, S. Romero, L. Vestergaard Christian, J.-F. Joanny, T. Van Nhieu Guy, and P. Bassereau, Filopodial retraction force is generated by cortical actin dynamics and controlled by reversible tethering at the tip, Proceedings of the National Academy of Sciences 110 (2013) 18928-18933.

9. B. Hoffmann and C. Schäfer, Filopodial focal complexes direct adhesion and force generation towards filopodia outgrowth, Cell adhesion & migration 4 (2010) 190-193.

10. C. Yang and T. Svitkina, Filopodia initiation, Cell Adhesion & Migration 5 (2011) 402-408.

11. N. D. Gallant, K. E. Michael, and A. J. García, Cell adhesion strengthening: contributions of adhesive area, integrin binding, and focal adhesion assembly, Molecular biology of the cell 16 (2005) 4329-4340.

12. D. Guadarrama Bello, A. Fouillen, A. Badia, and A. Nanci, A nanoporous titanium surface promotes the maturation of focal adhesions and formation of filopodia with distinctive nanoscale protrusions by osteogenic cells, Acta Biomater. 60 (2017) 339-349.

13. A. Sancho, I. Vandersmissen, S. Craps, A. Luttun, and J. Groll, A new strategy to measure intercellular adhesion forces in mature cell-cell contacts, Scientific Reports 7 (2017) 46152.

14. A. A. Khalili and R. M. Ahmad, A Review of Cell Adhesion Studies for Biomedical and Biological Applications, International Journal of Molecular Sciences 16 (2015).

15. B. Özkale, M. S. Sakar, and D. J. Mooney, Active biomaterials for mechanobiology, Biomaterials 267 (2021) 120497.

16. S. Dobner, O. C. Amadi, and R. T. Lee, "Chapter 14 - Cardiovascular Mechanotransduction," in Muscle, J. A. Hill and E. N. Olson, Eds. Boston/Waltham: Academic Press, 2012, pp. 173-186.

17. D. W. Zhou and A. J. García, Measurement systems for cell adhesive forces, Journal of biomechanical engineering 137 (2015) 020908-020908.

18. E. L. B. R. de Barros, K. J. Ponce, A. P. Dias, D. Guadarrama Bello, J. B. Brunski, and A. Nanci, Influence of Nanotopography on Early Bone Healing during Controlled Implant Loading, Nanomaterials (Basel) 10 (2020).

19. V. K. Gupta, I. A. Sraj, K. Konstantopoulos, and C. D. Eggleton, Multi-scale simulation of L-selectin-PSGL-1-dependent homotypic leukocyte binding and rupture, Biomech Model Mechanobiol 9 (2010) 613-27.

20. K. Anselme, P. Davidson, A. M. Popa, M. Giazzon, M. Liley, and L. Ploux, The interaction of cells and bacteria with surfaces structured at the nanometre scale, Acta Biomaterialia 6 (2010) 3824-3846.

21. J. Fiedler, B. Özdemir, J. Bartholomä, A. Plettl, R. E. Brenner, and P. Ziemann, The effect of substrate surface nanotopography on the behavior of multipotnent mesenchymal stromal cells and osteoblasts, Biomaterials 34 (2013) 8851-8859.

22. G. Thomas, N. A. Burnham, T. A. Camesano, and Q. Wen, Measuring the mechanical properties of living cells using atomic force microscopy, Journal of visualized experiments : JoVE (2013) 50497.

23. T. Zhang, Y. Chao, K. Shih, X.-Y. Li, and H. H. P. Fang, Quantification of the lateral detachment force for bacterial cells using atomic force microscope and centrifugation, Ultramicroscopy 111 (2011) 131-139.

24. J. Albuschies and V. Vogel, The role of filopodia in the recognition of nanotopographies, Scientific Reports 3 (2013) 1658.

25. N. Leijnse, B. Oddershede Lene, and M. Bendix Poul, Helical buckling of actin inside filopodia generates traction, Proceedings of the National Academy of Sciences 112 (2015) 136-141.

26. J. Kashef and C. M. Franz, Quantitative methods for analyzing cell–cell adhesion in development, Developmental Biology 401 (2015) 165-174.

27. J. Friedrichs, J. Helenius, and D. J. Muller, Quantifying cellular adhesion to extracellular matrix components by single-cell force spectroscopy, Nature Protocols 5 (2010) 1353-1361.

28. S. M. Deupree and M. H. Schoenfisch, Quantitative Method for Determining the Lateral Strength of Bacterial Adhesion and Application for Characterizing Adhesion Kinetics, Langmuir 24 (2008) 4700-4707.

29. M. Roy, P. H. Reddy, M. Iijima, and H. Sesaki, Mitochondrial division and fusion in metabolism, Current opinion in cell biology 33 (2015) 111-118.

30. E. Bartolák-Suki, J. Imsirovic, Y. Nishibori, R. Krishnan, and B. Suki, Regulation of Mitochondrial Structure and Dynamics by the Cytoskeleton and Mechanical Factors, International Journal of Molecular Sciences 18 (2017).

31. D. Guadarrama Bello, A. Fouillen, A. Badia, and A. Nanci, Nanoporosity Stimulates Cell Spreading and Focal Adhesion Formation in Cells with Mutated Paxillin, ACS Applied Materials & Interfaces (2020).

32. A. J. Valente, L. A. Maddalena, E. L. Robb, F. Moradi, and J. A. Stuart, A simple ImageJ macro tool for analyzing mitochondrial network morphology in mammalian cell culture, Acta Histochemica 119 (2017) 315-326.

33. C. J. Bettinger, R. Langer, and J. T. Borenstein, Engineering Substrate Topography at the Micro- and Nanoscale to Control Cell Function, Angewandte Chemie International Edition 48 (2009) 5406-5415.

34. H. Zheng et al., Hierarchical Micro-Nano Topography Promotes Cell Adhesion and Osteogenic Differentiation via Integrin α2-PI3K-AKT Signaling Axis, Frontiers in Bioengineering and Biotechnology 8 (2020).

35. C. D. Reyes and A. J. García, A centrifugation cell adhesion assay for high-throughput screening of biomaterial surfaces, J Biomed Mater Res A 67 (2003) 328-33.

36. L. Y. Koo, D. J. Irvine, A. M. Mayes, D. A. Lauffenburger, and L. G. Griffith, Co-regulation of cell adhesion by nanoscale RGD organization and mechanical stimulus, Journal of Cell Science 115 (2002) 1423-1433.

37. M. C. Harwig et al., Methods for imaging mammalian mitochondrial morphology: A prospective on MitoGraph, Anal Biochem 552 (2018) 81-99.

38. M. Ranieri et al., Mitochondrial fusion proteins and human diseases, Neurology research international 2013 (2013) 293893-293893.

39. B. Geiger and A. Bershadsky, Exploring the Neighborhood: Adhesion-Coupled Cell Mechanosensors, Cell 110 (2002) 139-142.

40. L. B. Case et al., Molecular mechanism of vinculin activation and nanoscale spatial organization in focal adhesions, Nature Cell Biology 17 (2015) 880-892.

41. M. Nemethova, S. Auinger, and J. V. Small, Building the actin cytoskeleton: filopodia contribute to the construction of contractile bundles in the lamella, The Journal of cell biology 180 (2008) 1233-1244.

42. M. Prass, K. Jacobson, A. Mogilner, and M. Radmacher, Direct measurement of the lamellipodial protrusive force in a migrating cell, Journal of Cell Biology 174 (2006) 767-772.

43. C.-C. Wu, H.-W. Su, C.-C. Lee, M.-J. Tang, and F.-C. Su, Quantitative measurement of changes in adhesion force involving focal adhesion kinase during cell attachment, spread, and migration, Biochemical and Biophysical Research Communications 329 (2005) 256-265.

Chapitre 5 – Discussion générale

La conception des dispositifs médicaux repose sur la capacité des systèmes biologiques à réagir à leurs caractéristiques physico-chimiques, un processus qui a conduit au développement d'une nouvelle génération de biomatériaux. Ces nouveaux biomatériaux sont conçus en suivant des approches visant à manipuler leurs surfaces afin d'améliorer leur capacité d'assimilation dans l'organisme.

La chimie, la géométrie, la topographie et les propriétés mécaniques des biomatériaux modulent les interactions cellules-surface. Le résultat d'un implant est essentiellement déterminé par les événements cellulaires et moléculaires qui se produisent à l'interface biomatériau-tissu. Ces événements, ainsi que ceux qui guident le fonctionnement des cellules dans leur habitat naturel, se produisent à l'échelle nanométrique. Ce principe fondamental, associé aux progrès récents de la nanotechnologie, a réorienté notre attention vers la modification des surfaces à l'échelle nanométrique pour imiter les systèmes biologiques. Comprendre le comportement des cellules à l'interface matériau-tissu de l'hôte est une condition préalable fondamentale pour concevoir des biomatériaux capables de diriger des événements cellulaires vers un résultat biologique souhaité.

Le Ti et ses alliages sont des biomatériaux avantageux, car leur couche d'oxyde superficielle peut facilement être modifiée à l'aide d'approches physico-chimiques relativement simples. Parmi les différentes approches de modification de la surface du Ti, le nanopatterning oxydatif présente des avantages distincts en raison de sa simplicité, du contrôle précis des caractéristiques physico-chimiques de la surface, de son applicabilité à des géométries complexes ainsi que de sa facilité de transfert à la fabrication à grande échelle. Cette approche nous a permis aussi de modifier la topographie d'autres métaux, comme le CrCoMo, et le Ta (75, 76). Plus récemment, nous avons modifié la topographie de l'acier inoxydable pour obtenir une surface qui présente les mêmes caractéristiques topographiques obtenues sur la surface du Ti. Avec une anodisation directe, en utilisant un mélange de H_2SO_4/H_2O_2, nous avons produit une couche mince mésoporeuse d'oxyde cristallin à la surface de l'acier inoxydable, qui présente simultanément un impact sélectif sur l'activité cellulaire et les propriétés antibactériennes (**Annexe 1**). Considérant que la chimie de la surface nanoporeuse obtenue sur l'acier diffère de celle sur le Ti, mais que les

effets sont sensiblement les mêmes, on peut en conclure que la topographie de la surface est un facteur déterminant.

À partir des connaissances acquises au sujet du comportement cellulaire à l'échelle nanométrique sur une surface de Ti, nous discuterons certains points saillants qui démarquent notre travail ainsi que leurs limites.

Premièrement, nous avons montré que les aspects physiques de la nanotopographie des surfaces de Ti prédominent sur l'effet de la cristallinité et de l'hydrophilie. Ceci indique que bien qu'il puisse y avoir une évolution de l'état de surface pendant le stockage standard d'une surface de Ti traité, cela ne devrait pas altérer de manière significative leurs performances, une considération importante pour la fabrication de dispositifs médicaux. Tandis que la surface nanoporeuse influence la formation et la maturation des FAs ainsi que stimule la formation de filopodes avec des nanoprotrusions, quelle que soit sa cristallinité ou sa mouillabilité de surface, la surface amorphe présentait une fréquence plus élevée d'adhésions matures. De plus, les propriétés antibactériennes que la nanotopographie confère au Ti sont maintenues avec les deux phases d'oxyde de Ti, ce qui pourrait indiquer que le mécanisme par lequel les bactéries interagissent avec la surface est en premier lieu biophysique. Étant donné que des paramètres comme la mouillabilité de la surface n'ont pas eu un effet sur les propriétés antibactériennes, il est probable que la topographie elle-même puisse expliquer la faible capacité des bactéries à adhérer à la surface traitée. Cette capacité à interférer avec l'étape initiale de la colonisation bactérienne peut aider à prévenir la cascade subséquente conduisant à la formation de biofilms. La fixation bactérienne est un processus complexe où différents facteurs comme l'interaction entre les propriétés de surface, les facteurs biologiques et les conditions environnementales jouent un rôle essentiel (153). Bien que les travaux aient été réalisés en utilisant la bactérie E. Coli, au lieu d'autres bactéries plus pertinentes dans le contexte buccodentaire ou orthopédique, nous tenons à souligner que cette surface a déjà été testée avec d'autres bactéries telles que le *staphylococcus aureus* (154), et plus récemment (donnés non publiés) avec *P. gingivalis*, où le même effet de la surface a été observé. L'effet antibactérien a également été observé avec le *bacillus subtilis* (annexe) sur des surfaces en acier inoxydable nanostructurées, démontrant le rôle déterminant de la topographie.

Deuxièmement, les données obtenues en utilisant un modèle cellulaire de mutation génétique, démontrent que la nanoporosité, affecte positivement le comportement cellulaire

indépendamment de la présence ou de l'absence de mutations de la paxilline. Ce résultat a été confirmé par l'augmentation de l'expression génétique des différents gènes associés avec la formation de filopodes, avec des marqueurs des FAs et aux différentes intégrines. La formation FAs, que ce soit sur une matrice extracellulaire naturelle ou sur des biomatériaux synthétiques, repose sur l'autoassemblage de complexes moléculaires intrinsèquement structurés à l'échelle nanométrique. La modulation des FAs et la formation des filopodes sont des caractéristiques critiques pour l'intégration d'un biomatériau, cependant les mécanismes impliqués ne sont pas encore précisément définis pour toutes les échelles topographiques. L'influence de la taille, de la géométrie et de l'organisation des caractéristiques des surfaces à l'échelle nanométrique sur l'activité cellulaire est encore un sujet de controverse (155, 156). Différentes études ont montré que la formation des FAs est sensible à l'arrangement spatial et à la présentation des ligands dans les matrices extracellulaires. Comme la tête d'un hétérodimère d'intégrine possède un diamètre d'environ 20 nm (157, 158), une variation à l'échelle nanométrique dans la topographie du substrat peut affecter directement la conformation et le regroupement des intégrines et donc l'organisation des protéines adaptatrices et de signalisation dans les FAs. Différents résultats montrent que les nanomotifs peuvent affecter l'adhésion des cellules en modifiant l'expression des intégrines et en facilitant la taille et la densité des FAs. La structuration à l'échelle nanométrique est, donc susceptible d'avoir un impact significatif sur l'organisation et le type des FAs formées, soit en perturbant leur formation, soit en induisant un recrutement spécifique d'intégrines (79). L'analyse des gènes étudiés pour les cellules avec des mutations, suggère que la nanoporosité régule la formation des FAs par une voie alternative qui relie le regroupement des intégrines à l'activation des membres de la famille des Rho GTPases. L'augmentation de l'expression de Rac 1, un gène qui joue un rôle essentiel dans la promotion de la formation de adhésions naissants et qui est activé par l'adhésion des intégrines à la MEC (110, 159), corrobore notre hypothèse selon laquelle la surface nanostructurée induit un regroupement d'intégrines qui conduit à l'assemblage des FAs. Cela se produit même en l'absence de phosphorylation de la paxilline qui conduit à l'activation des voies de signalisation associées à Rac1. L'utilisation de cette ligné cellulaire épithéliale, moins pertinent en raison de son origine, nous a néanmoins permis d'apporter un éclairage sur les mécanismes qui pourraient expliquer le comportement différentiel de la surface que nous avons observés avec diverses lignés cellulaires, incluant des cellules souches (75), des fibroblastes (160), des macrophages (55) et diverses lignés des cellules ostéogéniques (75, 76).

Finalement, avec des cellules ostéoblastiques, nous avons montré pour la première fois que la topographie de surface peut modifier l'interaction adhésive d'une structure subcellulaire qui est fondamentale dans la détection des caractéristiques physico-chimiques de la surface. Alors que des études de force d'adhésion ont été faites sur d'autres nanostructures, ces études ont porté sur l'ensemble de la force d'adhésion cellulaire et non sur la contribution de compartiments subcellulaires spécifiques à cette force d'adhésion. À partir d'une méthode quantitative par AFM nous avons démontré que les filopodes perçoivent et répondent à la surface de titane nanoporeuse pour développer localement une relation biomécanique plus forte avec le substrat. Le fait que cinq fois plus de force soit nécessaire pour déplacer les filopodes sur la surface Ti-Nano par rapport au Ti-Control indique une adhérence significativement plus élevée. Comme les nanoprotrusions latérales ne se trouvent que sur Ti-Nano, le différentiel d'adhérence observé doit en partie résulter de leur développement. L'association intime des filopodes et de leurs nanoprotrusions avec la surface suggère que le mécanisme peut impliquer des changements dans la conformation et le regroupement des intégrines qui modifient l'organisation dynamique des protéines de signalisation dans les FAs tel que discuté précédemment. Nous avons également analysé distinctement les modifications structurelles et fonctionnelles des cellules lorsqu'elles sont soumises à une force de centrifugation externe. Les changements observés dans le nombre et la distribution des filopodes, dans la taille globale de l'empreinte du réseau mitochondrial et dans la distribution des FAs indiquent que les cellules cultivées sur le Ti-Nano réagissent différemment à une force externe.

Le fait d'avoir utilisé une surface polie comme contrôle, alors qu'une surface micro-rugueuse avec des composants nanotopographiques est une topographie plus cliniquement utilisée peut constituer une limite de notre étude. Cependant, cette surface a été choisie pour éliminer toute caractéristique topographique qui pourrait confondre la contribution de la nanotopographie en créant une topographie multiniveau qui pourrait potentiellement influencer ou masquer ses caractéristiques. Plus précisément, l'un des objectives de notre travail était de déterminer comment la topographie à l'échelle nanométrique elle-même influence directement l'adhésion des filopodes et leurs nanoprotrusions.

La seule façon d'accomplir cet objectif sans avoir une combinaison des facteurs est de comparer les résultats avec une surface sans caractéristiques topographiques. De plus, l'utilisation d'une surface micro-rugueuse pourrait interférer avec l'application de l'AFM en mode contact, qui est nécessaire pour identifier et déplacer une structure fine telle qu'un filopode. En effet, nous avons dû adapter la durée du traitement chimique à 1h30 (161) pour éliminer la formation d'une topographie de second niveau en plus des nanopores et ainsi éliminer la possibilité que la microrugosité contribue aux effets cellulaires étudiés. Toutefois, nous tenons à souligner que les implants utilisés avec une surface nanoporeuse pour nos études *in vivo* avaient initialement une surface microrugueuse avec une géométrie cylindrique et même dans cette circonstance ont montré des avantages significatifs (162, 163).

Chapitre 6 – Conclusions générales

La conception de caractéristiques à l'échelle nanométrique nécessite de mieux comprendre les mécanismes moléculaires impliqués à la formation des adhésions et à l'assemblage du cytosquelette d'actine. Ces événements ne dépendent pas exclusivement des propriétés physico-chimiques de la surface des biomatériaux, mais aussi de la nature multifonctionnelle des composants des tissus et des fluides car le corps est un environnement complexe et dynamique qui doit être pris en considération.

La combinaison des méthodologies utilisées dans ce travail a permis de mettre en place un profil unique de caractérisation biomécanique, structurel et fonctionnel, qui pourrait être transféré pour l'évaluation d'autres surfaces à intérêt médical. Nos résultats ont contribué de manière significative à la connaissance sur le sujet des interactions cellule-substrat, ce qui pourrait permettre d'améliorer le succès des implants de Ti en modifiant leurs propriétés physico-chimiques afin d'améliorer la guérison tissulaire sans l'ajout d'agents biologiques. Il peut y avoir des situations particulières où la fonctionnalisation de la surface avec des biomolécules capables de favoriser l'activité ostéogénique sur les implants en titane serait un avantage.

Alors que des études supplémentaires seront nécessaires pour établir l'universalité de nos découvertes, les informations fournies par nos analyses offrent une voie pour la conception rationnelle et l'évaluation des surfaces d'implants afin de contrôler le comportement des cellules et d'inhiber l'adhésion des cellules bactériennes.

Dans l'ensemble, nos résultats soulèvent la possibilité que les surfaces nanostructurées puissent être utilisées non seulement pour guider/accélérer l'intégration de biomatériaux dans des conditions normales, mais également dans des situations où l'activité cellulaire est compromise. Ces résultats sont particulièrement pertinents pour les prothèses soumises à des charges externes, telles que les implants orthopédiques et dentaires.

Chapitre 7 – Perspectives

Les travaux réalisés au cours de cette thèse ont permis d'approfondir la compréhension de la l'interaction cellulaire avec une surface de Ti modifiée à l'échelle nanométrique et, au même temps, ont soulevé certaines questions qui méritent d'être investiguées.

1. Biomécanique cellulaire avec des cellules vivantes.

Nous considérons qu'une compréhension plus profonde des mécanismes qui expliquent la biomécanique cellulaire avec des cellules vivantes est nécessaire. L'une des limitations de nos études était que les mesures par AFM étaient faites sur des cellules fixées chimiquement. Bien que nous croyions fermement que les différences de force de détachement latéral observées sont significatives car les deux surfaces ont été testées dans les mêmes conditions, la prochaine étape de notre étude consistera à mesurer les forces d'adhésion sur des cellules vivantes. Ce qui entraînera un défi majeur car les filopodes sont des structures dynamiques qui pourraient réagir et changer au cours du processus de mesure de la force. Il est important de comprendre comment la topographie induit différentes forces d'adhésion, ainsi que l'impact que l'adhésion pourrait avoir sur les fonctions de traction et de rétraction des filopodes, car les filopodes jouent un rôle très important dans la détection de la topographie.

Ensemble avec les filopodes, nous avons vu que les nanoprotrusions pourraient avoir un impact sur la force d'attachement cellulaire. En plus, il est connu que les FAs fournissent un lien mécanique entre la MEC et le cytosquelette. Jusqu'à maintenant, nous avons toujours caractérisé les cellules séparément par différentes techniques. Avec la mise au point d'une technique corrélative qui nous permets de regarder la même cellule en utilisant différentes techniques, tel que montré dans la Figure 47, nous serons capables de fixer les cellules après les mesures de force, faire un marquage des FAs par IF et les visualiser aussi par MEB. Ensemble, ces 3 techniques (AFM, IF et MEB) nous permettront d'avoir un profil plus large qui corrèle la force d'adhésion, la quantité et taille des FAs et la distribution des filopodes et leur nanoprotrusions en même temps.
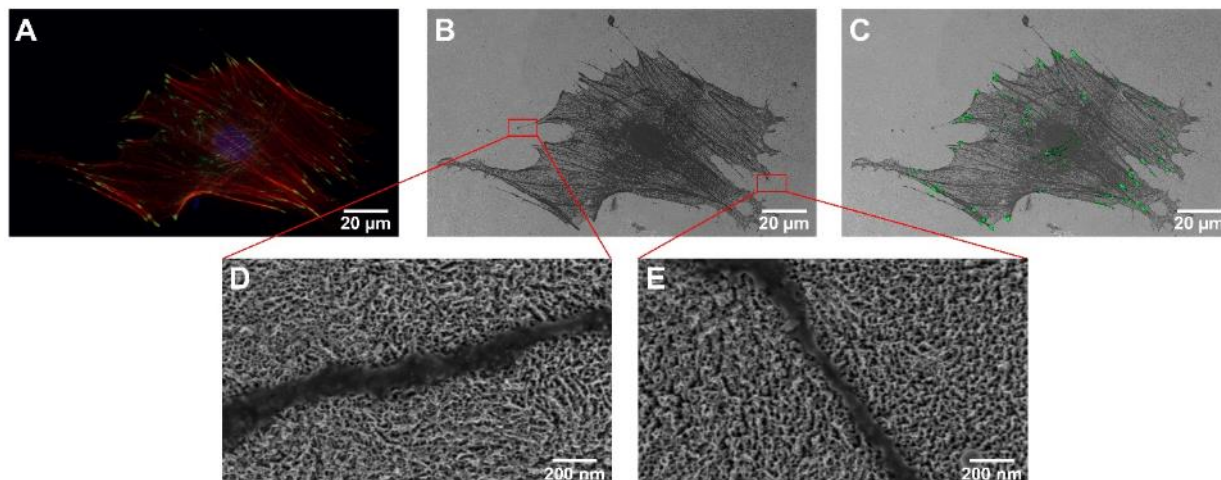
Figure 49. – (A) Micrographie de fluorescence d'une cellule MC3T3-E1 sur une surface nanoporeuse de Ti. Marquage avec du DAPI (bleu) pour le noyau, de la rhodamine/phalloïdine (rouge) pour l'actine et de l'anti-vinculine (vert) pour la vinculine. (B) Micrographie obtenue par MEB. (C) Corrélation entre A et B. (D et E) Micrographie MEB à haute résolution des filopodes.

2. Contribution de la nanotopographie à l'ostéointégration *in vivo* avec des animaux médicalement compromis.

Tel que nous avons discuté précédemment par rapport à la possibilité que les surfaces nanostructurées puissent guider/accélérer l'intégration de biomatériaux dans des situations où l'activité cellulaire est compromise, nous aimerions dans le futur définir la contribution de la nanotopographie à l'ostéointégration *in vivo* avec des modèles animaux d'ostéoporose et/ou modèles de diabète. Il est connu que des maladies telles que l'ostéoporose et le diabète, entre autres, affectent négativement l'ostéointégration (164-166). Récemment, dans une étude avec des animaux en bonne santé, nous avons démontré que des implants de Ti avec nanotopographie peuvent atteindre un niveau élevé de formation osseuse dans des condition de mise en charge et limiter la réponse inflammatoire à la surface de l'implant (163). Cette nouvelle découverte soulève la possibilité que les implants dotés de surfaces nanostructurées puissent mieux supporter des conditions de charge difficiles lors de la cicatrisation osseuse initiale, particulièrement dans le cas des patients médicalement compromis. Les connaissances pouvant découler de ces études seraient très bénéfiques pour un large segment de la population touchée par ces deux maladies.

3. Mécanisme d'interaction des bactéries avec la surface de Ti nanoporeuse.

Nous avons observé que la surface nanostructurée du Ti limite l'adhésion bactérienne. Il existe deux théories qui se retrouvent largement dans la littérature pour décrire le phénomène qui peux se produire lorsque des bactéries interagissent avec une surface nanotopographique: (1) les caractéristiques des surfaces empêchent l'adhésion des bactéries et/ou (2) une fois que les bactéries adhèrent à la surface, elles ne survivent pas à cause d'une rupture ou déformation de la membrane plasmique bactérienne causée par la nanotopographie (120). Des études supplémentaires seront nécessaires pour connaître le mécanisme par lequel les bactéries interagissent avec la surface. Avec l'utilisation des bactéries buccales, plus pertinentes dans le contexte des implants dentaires, nous allons étudier les réponses morphologiques et physiologiques des bactéries aux surfaces nanotopographiques. Pour élucider l'impact de la topographie, sur l'intégrité des bactéries, et déterminer si les nanopores induisent une lyse cellulaire à cause d'une rupture mécanique, des techniques comme le faisceau d'ions focalisé (FIB) seront utilisées pour reconstruire des visualisations 3D détaillées de bactéries adhérées aux surfaces.

Récemment, notre équipe a étudié comment plusieurs bactéries associées aux maladies parodontales pouvaient agir sur la lame basale spécialisée (LBS) qui permet l'accolement des cellules épithéliales de l'épithélium de jonction à la surface minéralisée de la dent (167). La LBS est une matrice extracellulaire constituée de 4 protéines : Amélotine (AMTN), Odontogenic ameloblast-associated (ODAM), secretory calcium-binding phosphoprotein proline-glutamine rich 1 (SCPPPQ1) et la laminine-332 (Lam332), qui interagissent entre elles afin de former un réseau supramoléculaire (168). Ces études ont montré que tous les constituants de la LBS, excepté SCPPPQ1, sont digérés par certaines bactéries périodontopathogènes telles que *Porphyromonas gingivalis* (*P. gingivalis*) (169).

À partir de cette connaissance, nous envisageons étudier l'adsorption de SCPPPQ1 sur les surfaces de Ti pour évaluer l'effet combiné de cette protéine pré adsorbées et la topographie de surface sur l'attachement de *P. gingivalis* et des cellules ostéoblastiques *in vitro*. Pendant ce temps, nous avons cultivé la bactérie *P. gingivalis* directement sur les surfaces Ti-Poli et Ti-Nano et nos résultats préliminaires (Figure 48) montrent qu'il pourrait avoir un effet antibactérien de la topographie face à cette bactérie aussi.
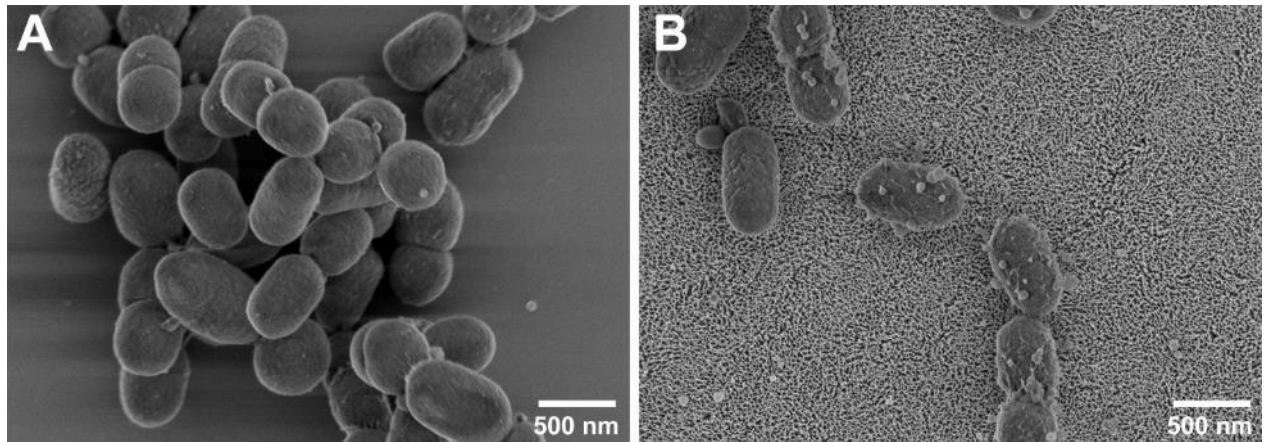
Figure 50. – Micrographies MEB après incubation avec *P. gingivalis* pendant 30 min sur une surface de titane (A) poli et (B) nanostructurée.

4. Séquençage d'ARN

Finalement, nous envisageons l'utilisation du séquençage d'ARN. Dans l'étude *in vivo* qu'on vient de mentionner (163), nos résultats ont montré que la majorité des gènes qui ont été régulés à la hausse ou à la baisse pendant la mise en charge ne sont pas classés. Cela indique qu'un certain nombre d'"acteurs" inattendus pourraient être impliqués dans l'ostéointégration des implants, et ceux-ci peuvent représenter des cibles potentielles pour favoriser la formation osseuse autour des implants. De la même façon, avec la nanoporosité, les gènes liés aux voies de signalisation inflammatoires n'ont pas été différentiellement sollicité (163). Grâce à cette technique, nous pourrons déterminer l'expression relative des gènes sur la surface nanoporeuse, en comparaison à une surface polie afin d'obtenir un profil plus large des changements cellulaires induits par la nanotopographie.

Références bibliographiques

1.   Hudecki A, Kiryczyński G, Łos MJ. Chapter 7 - Biomaterials, Definition, Overview. In: Łos MJ, Hudecki A, Wiecheć E, editors. Stem Cells and Biomaterials for Regenerative Medicine: Academic Press; 2019. p. 85-98.

2.   Todros S, Todesco M, Bagno A. Biomaterials and Their Biomedical Applications: From Replacement to Regeneration. Processes. 2021;9(11).

3.   Sharma A, Sharma G. Biomaterials and their applications. AIP Conference Proceedings. 2018;1953(1):080041.

4.   Prasad K, Bazaka O, Chua M, Rochford M, Fedrick L, Spoor J, et al. Metallic Biomaterials: Current Challenges and Opportunities. Materials (Basel). 2017;10(8):884.

5.   Canada CIfHII. CJRR annual report: Hip and knee replacements in Canada 2021 June 15 [

6.   Grandfield K. Bone, implants, and their interfaces. Physics Today. 2015;68(4):40-5.

7.   van Velzen FJ, Ofec R, Schulten EA, Ten Bruggenkate CM. 10-year survival rate and the incidence of peri-implant disease of 374 titanium dental implants with a SLA surface: a prospective cohort study in 177 fully and partially edentulous patients. Clinical oral implants research. 2015;26(10):1121-8.

8.   Chappuis V, Buser R, Brägger U, Bornstein MM, Salvi GE, Buser D. Long-term outcomes of dental implants with a titanium plasma-sprayed surface: a 20-year prospective case series study in partially edentulous patients. Clinical implant dentistry and related research. 2013;15(6):780-90.

9.   Diz P, Scully C, Sanz M. Dental implants in the medically compromised patient. Journal of dentistry. 2013;41(3):195-206.

10.   Cheng A, Cohen DJ, Kahn A, Clohessy RM, Sahingur K, Newton JB, et al. Laser Sintered Porous Ti–6Al–4V Implants Stimulate Vertical Bone Growth. Annals of Biomedical Engineering. 2017;45(8):2025-35.

11.   Beikler T, Flemmig TF. Implants in the medically compromised patient. Critical reviews in oral biology and medicine : an official publication of the American Association of Oral Biologists. 2003;14(4):305-16.

12.   Unnanuntana A, Rebolledo BJ, Khair MM, DiCarlo EF, Lane JM. Diseases affecting bone quality: beyond osteoporosis. Clinical orthopaedics and related research. 2011;469(8):2194-206.

13.   Shah FA, Nilson B, Brånemark R, Thomsen P, Palmquist A. The bone-implant interface – nanoscale analysis of clinically retrieved dental implants. Nanomedicine: Nanotechnology, Biology and Medicine. 2014;10(8):1729-37.

14.   Boskey AL. Mineralization of Bones and Teeth. Elements. 2007;3(6):385-91.

15.   Boskey AL. Bone composition: relationship to bone fragility and antiosteoporotic drug effects. Bonekey Rep. 2013;2:447-.

16.   Young MF. Bone matrix proteins: their function, regulation, and relationship to osteoporosis. Osteoporosis International. 2003;14(3):35-42.

17.   Zapanta LeGeros R. Apatites in biological systems. Progress in Crystal Growth and Characterization. 1981;4(1):1-45.

18.   Georgiadis M, Müller R, Schneider P. Techniques to assess bone ultrastructure organization: orientation and arrangement of mineralized collagen fibrils. Journal of The Royal Society Interface. 2016;13(119):20160088.

19.   Gonciulea A, de Beur SJ. The dynamic skeleton. Reviews in Endocrine and Metabolic Disorders. 2015;16(2):79-91.

20.   Bianco P, Gehron Robey P. Marrow stromal stem cells. The Journal of clinical investigation. 2000;105(12):1663-8.

21.   Liu X, Chu PK, Ding C. Surface modification of titanium, titanium alloys, and related materials for biomedical applications. Materials Science and Engineering: R: Reports. 2004;47(3):49-121.

22.   Wall I, Donos N, Carlqvist K, Jones F, Brett P. Modified titanium surfaces promote accelerated osteogenic differentiation of mesenchymal stromal cells in vitro. Bone. 2009;45(1):17-26.

23.   de Viteri VS, Fuentes, E. . In: Gegner, J. , editor. Tribology - Fundamentals and Advancements [Internet]. London: IntechOpen; 2013 [cited 2022 Apr 22]. Available from: https://www.intechopen.com/chapters/44858 doi: 10.5772/55860. Titanium and Titanium Alloys as Biomaterials.

24.   Stephen L, editor Titanium Dioxide Versatile Solid Crystalline: An Overview2020.

25.   Dohan Ehrenfest DM, Coelho PG, Kang B-S, Sul Y-T, Albrektsson T. Classification of osseointegrated implant surfaces: materials, chemistry and topography. Trends in Biotechnology. 2010;28(4):198-206.

26. Bocchetta P, Chen L-Y, Tardelli JD, Reis AC, Almeraya-Calderón F, Leo P. Passive Layers and Corrosion Resistance of Biomedical Ti-6Al-4V and β-Ti Alloys. Coatings. 2021;11(5).

27. Kulinets I. 1 - Biomaterials and their applications in medicine. In: Amato SF, Ezzell RM, editors. Regulatory Affairs for Biomaterials and Medical Devices: Woodhead Publishing; 2015. p. 1-10.

28. Ionita D, Prodana M, Caposi M. Modification of Passive Layer on TiNbZrTa Alloy in Simulated Body Fluid (SBF) at Various pH. Key Engineering Materials. 2009;415:17-20.

29. Baino F, Yamaguchi S. The Use of Simulated Body Fluid (SBF) for Assessing Materials Bioactivity in the Context of Tissue Engineering: Review and Challenges. Biomimetics (Basel). 2020;5(4):57.

30. Bryant SR, Zarb GA. Outcomes of implant prosthodontic treatment in older adults. Journal (Canadian Dental Association). 2002;68(2):97-102.

31. Smeets R, Stadlinger B, Schwarz F, Beck-Broichsitter B, Jung O, Precht C, et al. Impact of Dental Implant Surface Modifications on Osseointegration. BioMed Research International. 2016;2016:6285620.

32. Chug A, Shukla S, Mahesh L, Jadwani S. Osseointegration—Molecular events at the bone–implant interface: A review. Journal of Oral and Maxillofacial Surgery, Medicine, and Pathology. 2013;25(1):1-4.

33. Branemark PI. Vital microscopy of bone marrow in rabbit. Scand J Clin Lab Invest. 1959;11 Supp 38:1-82.

34. Brånemark PI, Hansson BO, Adell R, Breine U, Lindström J, Hallén O, et al. Osseointegrated implants in the treatment of the edentulous jaw. Experience from a 10-year period. Scand J Plast Reconstr Surg Suppl. 1977;16:1-132.

35. Brånemark PI. Osseointegration and its experimental background. J Prosthet Dent. 1983;50(3):399-410.

36. Nuss KMR, von Rechenberg B. Biocompatibility issues with modern implants in bone - a review for clinical orthopedics. Open Orthop J. 2008;2:66-78.

37. Florencio-Silva R, Sasso GRdS, Sasso-Cerri E, Simões MJ, Cerri PS. Biology of Bone Tissue: Structure, Function, and Factors That Influence Bone Cells. BioMed research international. 2015;2015:421746-.

38. Anselme K. Osteoblast adhesion on biomaterials. Biomaterials. 2000;21(7):667-81.

39.   Fini M, Giardino R. In vitro and in vivo tests for the biological evaluation of candidate orthopedic materials: Benefits and limits. Journal of applied biomaterials & biomechanics : JABB. 2003;1(3):155-63.

40.   Basoli F, Giannitelli SM, Gori M, Mozetic P, Bonfanti A, Trombetta M, et al. Biomechanical Characterization at the Cell Scale: Present and Prospects. Frontiers in physiology. 2018;9:1449-.

41.   Mirbagheri M, Adibnia V, Hughes BR, Waldman SD, Banquy X, Hwang DK. Advanced cell culture platforms: a growing quest for emulating natural tissues. Materials Horizons. 2019;6(1):45-71.

42.   Grandfield K, Gustafsson S, Palmquist A. Where bone meets implant: the characterization of nano-osseointegration. Nanoscale. 2013;5(10):4302-8.

43.   Ratner BD, Bryant SJ. Biomaterials: Where We Have Been and Where We Are Going. Annual Review of Biomedical Engineering. 2004;6(1):41-75.

44.   Latour RA, editor Biomaterials: Protein-Surface Interactions2005.

45.   Huang J, Yue Y, Zheng C. [Vroman effect of plasma protein adsorption to biomaterials surfaces]. Sheng wu yi xue gong cheng xue za zhi = Journal of biomedical engineering = Shengwu yixue gongchengxue zazhi. 1999;16(3):371-6.

46.   Rodil SE. Modificación superficial de biomateriales metálicos. Revista Latinoamericana de Metalurgia y Materiales. 2009;29:67-83.

47.   Han M, Sethuraman A, Kane RS, Belfort G. Nanometer-Scale Roughness Having Little Effect on the Amount or Structure of Adsorbed Protein. Langmuir. 2003;19(23):9868-72.

48.   Rechendorff K, Hovgaard MB, Foss M, Zhdanov VP, Besenbacher F. Enhancement of Protein Adsorption Induced by Surface Roughness. Langmuir. 2006;22(26):10885-8.

49.   Kulkarni M, Patil-Sen Y, Junkar I, Kulkarni CV, Lorenzetti M, Iglič A. Wettability studies of topologically distinct titanium surfaces. Colloids and Surfaces B: Biointerfaces. 2015;129:47-53.

50.   Gongadze E, Kabaso D, Bauer S, Slivnik T, Schmuki P, van Rienen U, et al. Adhesion of osteoblasts to a nanorough titanium implant surface. Int J Nanomedicine. 2011;6:1801-16.

51.   Kulkarni M, Mazare A, Gongadze E, Perutkova Š, Kralj-Iglič V, Milošev I, et al. Titanium nanostructures for biomedical applications. Nanotechnology. 2015;26(6):062002.

52.   Yun K-D, Yang Y, Lim H-P, Oh G-J, Koh J-T, Bae I-H, et al. Effect of nanotubular-micro-roughened titanium surface on cell response in vitro and osseointegration in vivo. Materials Science and Engineering: C. 2010;30(1):27-33.

53.   Arima Y, Iwata H. Effect of wettability and surface functional groups on protein adsorption and cell adhesion using well-defined mixed self-assembled monolayers. Biomaterials. 2007;28(20):3074-82.

54.   Werner S, Grose R. Regulation of Wound Healing by Growth Factors and Cytokines. Physiological Reviews. 2003;83(3):835-70.

55.   Ariganello MB, Guadarrama Bello D, Rodriguez-Contreras A, Sadeghi S, Isola G, Variola F, et al. Surface nanocavitation of titanium modulates macrophage activity. Int J Nanomedicine. 2018;13:8297-308.

56.   Ribeiro M, Monteiro FJ, Ferraz MP. Infection of orthopedic implants with emphasis on bacterial adhesion process and techniques used in studying bacterial-material interactions. Biomatter. 2012;2(4):176-94.

57.   Bandara CD, Ballerin G, Leppänen M, Tesfamichael T, Ostrikov KK, Whitchurch CB. Resolving Bio–Nano Interactions of E. coli Bacteria–Dragonfly Wing Interface with Helium Ion and 3D-Structured Illumination Microscopy to Understand Bacterial Death on Nanotopography. ACS Biomaterials Science & Engineering. 2020;6(7):3925-32.

58.   Ayukawa Y, Oshiro W, Atsuta I, Furuhashi A, Kondo R, Jinno Y, et al. Long Term Retention of Gingival Sealing around Titanium Implants with CaCl(2) Hydrothermal Treatment: A Rodent Study. J Clin Med. 2019;8(10):1560.

59.   Savić I, Bošnjak A, Beader N, Lovrić Ž, Salihagić A, Gašparac I. Anaerobic Bacteria in Implants and Homologous Teeth 2-14 Years after Implantation. Acta Stomatol Croat. 2018;52(3):193-202.

60.   Godoy-Gallardo M, Wang Z, Shen Y, Manero JM, Gil FJ, Rodriguez D, et al. Antibacterial Coatings on Titanium Surfaces: A Comparison Study Between in Vitro Single-Species and Multispecies Biofilm. ACS Applied Materials & Interfaces. 2015;7(10):5992-6001.

61.   Denardo L, Raffaini G, Ganazzoli F, Chiesa R. 5 - Metal surface oxidation and surface interactions. In: Williams R, editor. Surface Modification of Biomaterials: Woodhead Publishing; 2011. p. 102-42.

62.   Chen W, Shao Y, Li X, Zhao G, Fu J. Nanotopographical Surfaces for Stem Cell Fate Control: Engineering Mechanobiology from the Bottom. Nano today. 2014;9(6):759-84.

63.   Dobbenga S, Fratila-Apachitei LE, Zadpoor AA. Nanopattern-induced osteogenic differentiation of stem cells – A systematic review. Acta Biomaterialia. 2016;46:3-14.

64.   Kapoor N NA, Verma R, Thakur J , Singla A, . A review on surface treatment of titanium implant. IP Ann Prosthodont Restor Dent 2020;6(4):194-200.

65.   Hanawa T. Titanium–Tissue Interface Reaction and Its Control With Surface Treatment. Frontiers in Bioengineering and Biotechnology. 2019;7.

66.   Xue T, Attarilar S, Liu S, Liu J, Song X, Li L, et al. Surface Modification Techniques of Titanium and its Alloys to Functionally Optimize Their Biomedical Properties: Thematic Review. Frontiers in Bioengineering and Biotechnology. 2020;8.

67.   Jaafar A, Hecker C, Árki P, Joseph Y. Sol-Gel Derived Hydroxyapatite Coatings for Titanium Implants: A Review. Bioengineering. 2020;7(4).

68.   Jaafar A, Schimpf C, Mandel M, Hecker C, Rafaja D, Krüger L, et al. Sol–gel derived hydroxyapatite coating on titanium implants: Optimization of sol–gel process and engineering the interface. Journal of Materials Research. 2022.

69.   Dohan Ehrenfest DM, Coelho PG, Kang BS, Sul YT, Albrektsson T. Classification of osseointegrated implant surfaces: materials, chemistry and topography. Trends Biotechnol. 2010;28(4):198-206.

70.   Sun Y, Zhang X, Luo M, Hu W, Zheng L, Huang R, et al. Plasma Spray vs. Electrochemical Deposition: Toward a Better Osteogenic Effect of Hydroxyapatite Coatings on 3D-Printed Titanium Scaffolds. Frontiers in Bioengineering and Biotechnology. 2021;9.

71.   Chen H, Wang C, Yang X, Xiao Z, Zhu X, Zhang K, et al. Construction of surface HA/TiO2 coating on porous titanium scaffolds and its preliminary biological evaluation. Materials Science and Engineering: C. 2017;70:1047-56.

72.   Balza JC, Zujur D, Gil L, Subero R, Dominguez E, Delvasto P, et al. Sandblasting as a surface modification technique on titanium alloys for biomedical applications: abrasive particle behavior. IOP Conference Series: Materials Science and Engineering. 2013;45:012004.

73.   Tęczar P, Majkowska-Marzec B, Bartmański M. The Influence of Laser Alloying of Ti13Nb13Zr on Surface Topography and Properties. Advances in Materials Science. 2019;19(1):44-56.

74.   Variola F, Brunski JB, Orsini G, Tambasco de Oliveira P, Wazen R, Nanci A. Nanoscale surface modifications of medically relevant metals: state-of-the art and perspectives. Nanoscale. 2011;3(2):335-53.

75.   Vetrone F, Variola F, Tambasco de Oliveira P, Zalzal SF, Yi J-H, Sam J, et al. Nanoscale Oxidative Patterning of Metallic Surfaces to Modulate Cell Activity and Fate. Nano Letters. 2009;9(2):659-65.

76.   de Oliveira PT, Nanci A. Nanotexturing of titanium-based surfaces upregulates expression of bone sialoprotein and osteopontin by cultured osteogenic cells. Biomaterials. 2004;25(3):403-13.

77.   Dalby MJ, Riehle MO, Johnstone H, Affrossman S, Curtis AS. Investigating the limits of filopodial sensing: a brief report using SEM to image the interaction between 10 nm high nano-topography and fibroblast filopodia. Cell biology international. 2004;28(3):229-36.

78.   Luo J, Walker M, Xiao Y, Donnelly H, Dalby MJ, Salmeron-Sanchez M. The influence of nanotopography on cell behaviour through interactions with the extracellular matrix – A review. Bioactive Materials. 2022;15:145-59.

79.   Anselme K, Davidson P, Popa AM, Giazzon M, Liley M, Ploux L. The interaction of cells and bacteria with surfaces structured at the nanometre scale. Acta Biomaterialia. 2010;6(10):3824-46.

80.   Lehnert D, Wehrle-Haller B, David C, Weiland U, Ballestrem C, Imhof BA, et al. Cell behaviour on micropatterned substrata: limits of extracellular matrix geometry for spreading and adhesion. Journal of Cell Science. 2004;117(1):41-52.

81.   Wang X, Ha T. Defining Single Molecular Forces Required to Activate Integrin and Notch Signaling. Science. 2013;340(6135):991.

82.   Mattila PK, Lappalainen P. Filopodia: molecular architecture and cellular functions. Nature Reviews Molecular Cell Biology. 2008;9(6):446-54.

83.   Albuschies J, Vogel V. The role of filopodia in the recognition of nanotopographies. Scientific Reports. 2013;3(1):1658.

84.   Bornschlögl T, Romero S, Vestergaard Christian L, Joanny J-F, Van Nhieu Guy T, Bassereau P. Filopodial retraction force is generated by cortical actin dynamics and controlled by reversible tethering at the tip. Proceedings of the National Academy of Sciences. 2013;110(47):18928-33.

85.   Hoffmann B, Schäfer C. Filopodial focal complexes direct adhesion and force generation towards filopodia outgrowth. Cell adhesion & migration. 2010;4(2):190-3.

86.   Yang C, Svitkina T. Filopodia initiation. Cell Adhesion & Migration. 2011;5(5):402-8.

87.   Di Cio S, Gautrot JE. Cell sensing of physical properties at the nanoscale: Mechanisms and control of cell adhesion and phenotype. Acta Biomaterialia. 2016;30:26-48.

88.   Kechagia JZ, Ivaska J, Roca-Cusachs P. Integrins as biomechanical sensors of the microenvironment. Nature Reviews Molecular Cell Biology. 2019;20(8):457-73.

89.   Mitra SK, Hanson DA, Schlaepfer DD. Focal adhesion kinase: in command and control of cell motility. Nat Rev Mol Cell Biol. 2005;6:56.

90.   Cavalcanti-Adam EA, Micoulet A, Blümmel J, Auernheimer J, Kessler H, Spatz JP. Lateral spacing of integrin ligands influences cell spreading and focal adhesion assembly. European Journal of Cell Biology. 2006;85(3):219-24.

91.   Sjöström T, Dalby MJ, Hart A, Tare R, Oreffo ROC, Su B. Fabrication of pillar-like titania nanostructures on titanium and their interactions with human skeletal stem cells. Acta Biomaterialia. 2009;5(5):1433-41.

92.   Pérez-Campo FM, Riancho JA. Epigenetic Mechanisms Regulating Mesenchymal Stem Cell Differentiation. Current genomics. 2015;16(6):368-83.

93.   Das RK, Zouani OF. A review of the effects of the cell environment physicochemical nanoarchitecture on stem cell commitment. Biomaterials. 2014;35(20):5278-93.

94.   Gattazzo F, Urciuolo A, Bonaldo P. Extracellular matrix: a dynamic microenvironment for stem cell niche. Biochimica et biophysica acta. 2014;1840(8):2506-19.

95.   Engler AJ, Sen S, Sweeney HL, Discher DE. Matrix Elasticity Directs Stem Cell Lineage Specification. Cell. 2006;126(4):677-89.

96.   Anselme K, Wakhloo NT, Rougerie P, Pieuchot L. Role of the Nucleus as a Sensor of Cell Environment Topography. Advanced Healthcare Materials. 2018;7(8):1701154.

97.   McBeath R, Pirone DM, Nelson CM, Bhadriraju K, Chen CS. Cell Shape, Cytoskeletal Tension, and RhoA Regulate Stem Cell Lineage Commitment. Developmental Cell. 2004;6(4):483-95.

98.   Bettinger CJ, Langer R, Borenstein JT. Engineering Substrate Topography at the Micro- and Nanoscale to Control Cell Function. Angewandte Chemie International Edition. 2009;48(30):5406-15.

99. McMurray RJ, Gadegaard N, Tsimbouri PM, Burgess KV, McNamara LE, Tare R, et al. Nanoscale surfaces for the long-term maintenance of mesenchymal stem cell phenotype and multipotency. Nature Materials. 2011;10(8):637-44.

100. Tsimbouri PM. Adult Stem Cell Responses to Nanostimuli. Journal of functional biomaterials. 2015;6(3):598-622.

101. Nobes CD, Hall A. Rho, Rac, and Cdc42 GTPases regulate the assembly of multimolecular focal complexes associated with actin stress fibers, lamellipodia, and filopodia. Cell. 1995;81(1):53-62.

102. Hall A. Rho GTPases and the Actin Cytoskeleton. Science. 1998;279(5350):509.

103. Rottner K, Hall A, Small JV. Interplay between Rac and Rho in the control of substrate contact dynamics. Current Biology. 1999;9(12):640-S1.

104. Prowse PDH, Elliott CG, Hutter J, Hamilton DW. Inhibition of Rac and ROCK signalling influence osteoblast adhesion, differentiation and mineralization on titanium topographies. PloS one. 2013;8(3):e58898-e.

105. Dobbenga S, Fratila-Apachitei LE, Zadpoor AA. Nanopattern-induced osteogenic differentiation of stem cells - A systematic review. Acta Biomater. 2016;46:3-14.

106. Özkale B, Sakar MS, Mooney DJ. Active biomaterials for mechanobiology. Biomaterials. 2021;267:120497.

107. Dobner S, Amadi OC, Lee RT. Chapter 14 - Cardiovascular Mechanotransduction. In: Hill JA, Olson EN, editors. Muscle. Boston/Waltham: Academic Press; 2012. p. 173-86.

108. Khalili AA, Ahmad RM. A Review of Cell Adhesion Studies for Biomedical and Biological Applications. International Journal of Molecular Sciences. 2015;16(8).

109. Webb DJ, Donais K, Whitmore LA, Thomas SM, Turner CE, Parsons JT, et al. FAK–Src signalling through paxillin, ERK and MLCK regulates adhesion disassembly. Nat Cell Biol. 2004;6(2):154-61.

110. Wu C. Focal adhesion: a focal point in current cell biology and molecular medicine. Cell adhes Migr. 2007;1(1):13-8.

111. Zouq NK, Keeble JA, Lindsay J, Valentijn AJ, Zhang L, Mills D, et al. FAK engages multiple pathways to maintain survival of fibroblasts and epithelia: differential roles for paxillin and p130Cas. J Cell Sci. 2009;122(Pt 3):357-67.

112.   Janoštiak R, Pataki AC, Brábek J, Rösel D. Mechanosensors in integrin signaling: The emerging role of p130Cas. Eur J Cell Biol. 2014;93(10):445-54.

113.   López-Colomé AM, Lee-Rivera I, Benavides-Hidalgo R, López E. Paxillin: a crossroad in pathological cell migration. Journal of Hematology & Oncology. 2017;10(1):50.

114.   Brown MC, Curtis MS, Turner CE. Paxillin LD motifs may define a new family of protein recognition domains. Nat Struct Mol Biol. 1998;5:677.

115.   Brown MC, Perrotta JA, Turner CE. Identification of LIM3 as the principal determinant of paxillin focal adhesion localization and characterization of a novel motif on paxillin directing vinculin and focal adhesion kinase binding. J Cell Biol. 1996;135(4):1109-23.

116.   Nayal A, Webb DJ, Brown CM, Schaefer EM, Vicente-Manzanares M, Horwitz AR. Paxillin phosphorylation at Ser273 localizes a GIT1-PIX-PAK complex and regulates adhesion and protrusion dynamics. J Cell Biol. 2006;173(4):587-9.

117.   Spriano S, Yamaguchi S, Baino F, Ferraris S. A critical review of multifunctional titanium surfaces: New frontiers for improving osseointegration and host response, avoiding bacteria contamination. Acta Biomaterialia. 2018;79:1-22.

118.   Chouirfa H, Bouloussa H, Migonney V, Falentin-Daudré C. Review of titanium surface modification techniques and coatings for antibacterial applications. Acta Biomaterialia. 2019;83:37-54.

119.   Jenkins J, Ishak MI, Eales M, Gholinia A, Kulkarni S, Keller TF, et al. Resolving physical interactions between bacteria and nanotopographies with focused ion beam scanning electron microscopy. iScience. 2021;24(7):102818.

120.   Linklater DP, Baulin VA, Juodkazis S, Crawford RJ, Stoodley P, Ivanova EP. Mechano-bactericidal actions of nanostructured surfaces. Nature Reviews Microbiology. 2021;19(1):8-22.

121.   Au - Oh M-J, Au - Kuhr F, Au - Byfield F, Au - Levitan I. Micropipette Aspiration of Substrate-attached Cells to Estimate Cell Stiffness. JoVE. 2012(67):e3886.

122.   Giannini M, Primerano C, Berger L, Giannaccini M, Wang Z, Landi E, et al. Nano-topography: Quicksand for cell cycle progression? Nanomed Nanotechnol. 2018;14(8):2656-65.

123.   Ladoux B, Nicolas A. Physically based principles of cell adhesion mechanosensitivity in tissues. Reports on progress in physics Physical Society. 2012;75 11:116601.

124.	Liu J, Wang Y, Goh WI, Goh H, Baird MA, Ruehland S, et al. Talin determines the nanoscale architecture of focal adhesions. Proceedings of the National Academy of Sciences of the United States of America. 2015;112(35):E4864-E73.

125.	Fiedler J, Özdemir B, Bartholomä J, Plettl A, Brenner RE, Ziemann P. The effect of substrate surface nanotopography on the behavior of multipotnent mesenchymal stromal cells and osteoblasts. Biomaterials. 2013;34(35):8851-9.

126.	Ungai-Salánki R, Peter B, Gerecsei T, Orgovan N, Horvath R, Szabó B. A practical review on the measurement tools for cellular adhesion force. Advances in Colloid and Interface Science. 2019;269:309-33.

127.	Parsons JT, Horwitz AR, Schwartz MA. Cell adhesion: integrating cytoskeletal dynamics and cellular tension. Nature Reviews Molecular Cell Biology. 2010;11:633.

128.	Li G, Song Y, Shi M, Du Y, Wang W, Zhang Y. Mechanisms of Cdc42-mediated rat MSC differentiation on micro/nano-textured topography. Acta Biomaterialia. 2017;49:235-46.

129.	Myers JP, Robles E, Ducharme-Smith A, Gomez TM. Focal adhesion kinase modulates Cdc42 activity downstream of positive and negative axon guidance cues. J Cell Sci. 2012;125(12):2918-29.

130.	Schaller MD, Hildebrand JD, Shannon JD, Fox JW, Vines RR, Parsons JT. Autophosphorylation of the focal adhesion kinase, pp125FAK, directs SH2-dependent binding of pp60src. Molecular and cellular biology. 1994;14(3):1680-8.

131.	Dreier B, Gasiorowski JZ, Morgan JT, Nealey PF, Russell P, Murphy CJ. Early responses of vascular endothelial cells to topographic cues. American journal of physiology Cell physiology. 2013;305(3):C290-C8.

132.	Hoon J, Tan M, Koh C-G. The regulation of cellular responses to mechanical cues by Rho GTPases. Cells. 2016;5(2):17.

133.	Zaidel-Bar R, Ballestrem C, Kam Z, Geiger B. Early molecular events in the assembly of matrix adhesions at the leading edge of migrating cells. Journal of cell science. 2003;116(22):4605-13.

134.	Carisey A, Tsang R, Greiner Alexandra M, Nijenhuis N, Heath N, Nazgiewicz A, et al. Vinculin Regulates the Recruitment and Release of Core Focal Adhesion Proteins in a Force-Dependent Manner. Current Biology. 2013;23(4):271-81.

135.   Mendonça G, Mendonça DBS, Aragão FJL, Cooper LF. The combination of micron and nanotopography by H2SO4/H2O2 treatment and its effects on osteoblast-specific gene expression of hMSCs. Journal of Biomedical Materials Research Part A. 2010;94A(1):169-79.

136.   Tambasco de Oliveira P, Nanci A. Nanotexturing of titanium-based surfaces upregulates expression of bone sialoprotein and osteopontin by cultured osteogenic cells. Biomaterials. 2004;25(3):403-13.

137.   de Oliveira PT, Zalzal SF, Beloti MM, Rosa AL, Nanci A. Enhancement of in vitro osteogenesis on titanium by chemically produced nanotopography. Journal of Biomedical Materials Research Part A. 2007;80A(3):554-64.

138.   Zhou DW, García AJ. Measurement systems for cell adhesive forces. Journal of biomechanical engineering. 2015;137(2):020908-.

139.   Kashef J, Franz CM. Quantitative methods for analyzing cell–cell adhesion in development. Developmental Biology. 2015;401(1):165-74.

140.   Chu L, Tempelman LA, Miller C, Hammer DA. Centrifugation assay of IgE-mediated cell adhesion to antigen-coated gels. AIChE Journal. 1994;40(4):692-703.

141.   Binnig G, Quate CF, Gerber C. Atomic Force Microscope. Physical Review Letters. 1986;56(9):930-3.

142.   Addae-Mensah KA, Wikswo JP. Measurement Techniques for Cellular Biomechanics In Vitro. Experimental Biology and Medicine. 2008;233(7):792-809.

143.   Friedrichs J, Helenius J, Muller DJ. Quantifying cellular adhesion to extracellular matrix components by single-cell force spectroscopy. Nature Protocols. 2010;5(7):1353-61.

144.   Hogan B, Babataheri A, Hwang Y, Barakat AI, Husson J. Characterizing cell adhesion by using micropipette aspiration. Biophysical journal. 2015;109(2):209-19.

145.   Nguyen JNT, Harbison AM. Scanning Electron Microscopy Sample Preparation and Imaging. In: Espina V, editor. Molecular Profiling: Methods and Protocols. New York, NY: Springer New York; 2017. p. 71-84.

146.   Fischer ER, Hansen BT, Nair V, Hoyt FH, Dorward DW. Scanning electron microscopy. Curr Protoc Microbiol. 2012;Chapter 2:Unit2B.-B..

147.   Guadarrama Bello D, Moraille P, Boughari S, Badia A, Nanci A. Adhesion response of filopodia to an AFM lateral detachment force and functional changes after centrifugation of cells grown on nanoporous titanium. Materials Today Bio. 2022;14:100250.

148.   Smyth MS, Martin JH. x ray crystallography. Mol Pathol. 2000;53(1):8-14.

149.   Fischer K, Gawel A, Rosen D, Krause M, Abdul Latif A, Griebel J, et al. Low-Temperature Synthesis of Anatase/Rutile/Brookite TiO2 Nanoparticles on a Polymer Membrane for Photocatalysis. Catalysts. 2017;7(7).

150.   Pelaez M, Nolan NT, Pillai SC, Seery MK, Falaras P, Kontos AG, et al. A review on the visible light active titanium dioxide photocatalysts for environmental applications. Applied Catalysis B: Environmental. 2012;125:331-49.

151.   Im K, Mareninov S, Diaz MFP, Yong WH. An Introduction to Performing Immunofluorescence Staining. Methods Mol Biol. 2019;1897:299-311.

152.   Jamur MC, Oliver C. Permeabilization of Cell Membranes. In: Oliver C, Jamur MC, editors. Immunocytochemical Methods and Protocols. Totowa, NJ: Humana Press; 2010. p. 63-6.

153.   Cheng Y, Feng G, Moraru CI. Micro- and Nanotopography Sensitive Bacterial Attachment Mechanisms: A Review. Front Microbiol. 2019;10:191-.

154.   Variola F, Zalzal SF, Leduc A, Barbeau J, Nanci A. Oxidative nanopatterning of titanium generates mesoporous surfaces with antimicrobial properties. Int J Nanomed. 2014;9:2319-25.

155.   Lim JY, Dreiss AD, Zhou Z, Hansen JC, Siedlecki CA, Hengstebeck RW, et al. The regulation of integrin-mediated osteoblast focal adhesion and focal adhesion kinase expression by nanoscale topography. Biomaterials. 2007;28(10):1787-97.

156.   Milner KR, Siedlecki CA. Submicron poly(L-lactic acid) pillars affect fibroblast adhesion and proliferation. Journal of Biomedical Materials Research Part A. 2007;82A(1):80-91.

157.   Zhang Y, Gordon A, Qian W, Chen W. Engineering Nanoscale Stem Cell Niche: Direct Stem Cell Behavior at Cell–Matrix Interface. Advanced Healthcare Materials. 2015;4(13):1900-14.

158.   Kim HS, Kim YJ, Jang JH, Park JW. Surface Engineering of Nanostructured Titanium Implants with Bioactive Ions. Journal of Dental Research. 2016;95(5):558-65.

159.   Geiger B, Bershadsky A. Assembly and mechanosensory function of focal contacts. Curr Opin Cell Biol. 2001;13(5):584-92.

160.   Richert L, Vetrone F, Yi J-H, Zalzal SF, Wuest JD, Rosei F, et al. Surface Nanopatterning to Control Cell Growth. Advanced Materials. 2008;20(8):1488-92.

161. Guadarrama Bello D, Fouillen A, Badia A, Nanci A. A nanoporous titanium surface promotes the maturation of focal adhesions and formation of filopodia with distinctive nanoscale protrusions by osteogenic cells. Acta Biomater. 2017;60:339-49.

162. Tavares MG, Tambasco de Oliveira P, Nanci A, Hawthorne AC, Rosa AL, Xavier SP. Treatment of a commercial, machined surface titanium implant with H2SO4/H2O2 enhances contact osteogenesis. Clin Oral Implants Res. 2007;18(4):452-8.

163. de Barros ELBR, Ponce KJ, Dias AP, Guadarrama Bello D, Brunski JB, Nanci A. Influence of Nanotopography on Early Bone Healing during Controlled Implant Loading. Nanomaterials (Basel). 2020;10(11).

164. Sam L, Chattipakorn S, Khongkhunthian P. Osseointegration of Maxillary Dental Implants in Diabetes Mellitus Patients: A Randomized Clinical Trial Human Histomorphometric Study. Applied Sciences. 2020;10(19):6762.

165. Li C-X, Wang F, Jin Z-L. A four-year prospective study of self-assembling nano-modified dental implants in patients with type 2 diabetes mellitus. Journal of Dental Sciences. 2020;15(3):294-301.

166. Giro G, Chambrone L, Goldstein A, Rodrigues JA, Zenóbio E, Feres M, et al. Impact of osteoporosis in dental implants: A systematic review. World journal of orthopedics. 2015;6(2):311-5.

167. Fouillen A, Grenier D, Barbeau J, Baron C, Moffatt P, Nanci A. Selective bacterial degradation of the extracellular matrix attaching the gingiva to the tooth. European journal of oral sciences. 2019;127(4):313-22.

168. Fouillen A, Dos Santos Neves J, Mary C, Castonguay J-D, Moffatt P, Baron C, et al. Interactions of AMTN, ODAM and SCPPPQ1 proteins of a specialized basal lamina that attaches epithelial cells to tooth mineral. Scientific Reports. 2017;7(1):46683.

169. Mary C, Fouillen A, Moffatt P, Guadarrama Bello D, Wazen RM, Grenier D, et al. Effect of human secretory calcium-binding phosphoprotein proline-glutamine rich 1 protein on Porphyromonas gingivalis and identification of its active portions. Scientific Reports. 2021;11(1):23724.

Annexes

Annexe 1 - Chemical nanocavitation of surfaces to enhance the utility of stainless steel as a medical material

Colloids and Surfaces B: Biointerfaces **2018** *161*:677-687

Alejandra Rodriguez-Contreras [a], Dainelys Guadarrama Bello [a], Sam Flynn [a], Fabio Variola [b], James D. Wuest [c], Antonio Nanci [a, d*]

[a] Laboratory for the Study of Calcified Tissues & Biomaterials, Faculté de Médecine Dentaire, Université de Montréal, Montréal, Québec H3T 1J4 Canada

[b] Department of Mechanical Engineering, University of Ottawa, Ottawa, Ontario K1N 6N5, Canada

[c] Département de Chimie, Université de Montréal, Montréal, Québec H3C 3J7 Canada

[d] Département de Biochimie et Médecine Moléculaire, Université de Montréal, Montréal, Québec H3C 3J7, Canada

Corresponding Author

Antonio Nanci

Faculté de Médecine Dentaire

Université de Montréal

C.P. 6128, succ. Centre-ville

Montréal (Québec) H3C 3J7

E-mail: antonio.nanci@umontreal.ca

Phone: 514 343-5846

Fax: 514 343-2233

Abstract

While stainless steel is a broadly used alloy with interesting mechanical properties, its applications in medicine suffers from inherent biocompatibility limitations. An attractive opportunity to improve its performance is to alter its surface, but this has proven challenging. We now show how high range anodization conditions using H_2SO_4/H_2O_2 as an atypical electrolyte can efficiently nanocavitate the surface of both stainless steel SS304 and SS316 and create a topography with advantageous biomedical characteristics. We describe the structural and chemical features of the resulting surfaces, and propose a nanocorrosion/transpassivation/repassivation mechanism for its creation. Our approach creates a thin mesoporous layer of crystalline oxide that selectively promotes mammalian cell activity and limits bacterial adhesion. The modified surfaces favor the formation and maturation of focal adhesion plaques and environment-sensing filopodia with abundant extra small lateral membrane protrusions, suggesting an increase in membrane fluidity. These protrusions represent a yet undescribed cellular response. Such surfaces promise to facilitate the integration of implantable SS devices, in general. In addition, our strategy simultaneously provides a simple, commercially attractive way to control the adhesion of microorganisms, making nanostructured stainless steel broadly useful in hospital environments, in manufacturing medical devices, as well as offering possibilities for non-medical applications.

Keywords: Stainless steel, Electrochemical anodization, Nanotopography, Cell adhesion, Antibacterial properties

1- Introduction

The widespread use of stainless steel (SS) as a medical material reflects its appealing mechanical properties, resistance to wear, low reactivity, and modest cost. Austenitic 304 and 316 steels (SS304 and SS316) have been used to make a wide range of medical devices, including coronary stents, hip implant stems, spinal disc replacements, and fracture fixations, as well as surgical tools such as needles, scalpels, blades, curettes, forceps, and retractors (1), (2). In all these applications, however, SS behaves as a foreign material that can cause allergic and toxic reactions, particularly after long periods of implantation (2). To deal with this problem and to enhance the utility of SS as a medical material, various surface modifications have been explored, as summarized and referenced in Supplemental (Table 1 and 2). The use of coatings, superficial chemical modifications, and molecular functionalization has revealed inherent limitations, including the instability and inhomogeneity of modified surfaces, which can lead to the eventual failure of implants (3). More recently, nanotechnology has been exploited in attempts to restructure the surface of SS for various applications, but the methods used are typically complex and often yield thick and irregular films (Table 1 and 2 in Supplemental). Very significant advances have been made but a key problem in the field of medical materials remains unsolved: how can the inherently desirable properties of SS as a medical material be enhanced by simple nanoscale modifications of its surface?

Many naturally-occurring surfaces have complex topographies that confer unique properties of biological importance. For example, the superhydrophobic nanostructured surface of lotus leaves repels water, and the nanopillars of cicada wings are extremely effective at breaking down the walls of bacterial cells (4), (5). These examples provide a strong biomimetic rational for controlling biological activity through nanotopography.

Our group introduced a simple oxidative method for nanostructuring the surface of Ti and its alloys by exposure to mixtures of H_2SO_4 and H_2O_2 (6), (7), (8). This generates a thin amorphous layer of TiO_2 on the surface, characterized by an intricate network of nanometric pores (9). The approach has also been used to modify the surfaces of other relevant implantable metals, such as CrCoMo and Ta (10). The physicochemical characteristics of the resulting mesoporous surfaces selectively influence the growth and activity of various cells *in vitro*, including stem cells (11), (12), and osteogenic activity is promoted both *in vitro* (10) and *in vivo* (13). More recently, we further demonstrated that mesoporous surface layers of this type hamper the adhesion and/or retention of bacteria, in addition to affecting the integrity of a yeast variety (14).

160

The strong resistance of SS to chemical attack makes the creation of nanostructured surfaces inherently difficult. Indeed, chemical oxidation with H_2SO_4/H_2O_2 at 25 °C was ineffective with SS, but we discovered that this solution can be used as electrolyte for electrochemical anodization. We report here unique conditions for anodization that produce a thin crystalline mesoporous layer of oxide on the surface of SS304 and SS316. Moreover, we present evidence to establish that this simple modification enhances mammalian cell activity and limits bacterial adhesion.

2- Material and methods

2.1. SS plates

Commercial samples of SS304 and SS316 in the form of plates of dimensions 25 mm × 15 mm × 1.3 mm (CBR Laser, Plessisville, Québec, Canada) were mechanically polished to a mirror finish (PowerPro 5000, Buehler, Lake Bluff, IL, USA) by first using SiC grinding paper, then diamond paste, and finally a non-crystallizing aqueous suspension of colloidal silica (Buehler, Lake Bluff, IL, USA). The polished plates were then cleaned by ultrasonication (Fisher Scientific, Fair Lawn, NJ, USA), first in distilled water (15 min), then in 100% ethanol (15 min), and finally in toluene (15 min). The cleaned plates were dried in air. Before treatment, the plates were scored with a grid consisting of 48 squares (2.5 mm × 3.5 mm) to partition the surface.

2.2. Nanocavitating SS surfaces by anodization

Before further treatment, half of each SS plate (24 grid squares) was covered with nail polish to render the surface inert. The uncoated half of each plate was dipped into an electrolyte prepared by mixing equal volumes of 96% H_2SO_4 and 30% aqueous H_2O_2. The resulting nominal concentrations of H_2SO_4 and H_2O_2 were about 9 M and 5 M, respectively (6). Controlled anodization was carried out in a two-electrode electrochemical cell fitted with a 100 W multi 60 V/5A DC power supply (B&K Precision 9110, Yorba Linda, CA, USA). Pt mesh (25 × 25 mm) was used as the cathode. The current was maintained at 0.5 A (density of 700 A/m²), and the temperature was controlled by packing ice around the electrochemical bath. The initial temperature was 40 °C, and anodization was stopped when the temperature reached 80 °C, which required about 12 min. After quick ultrasonication in distilled water to detach the nail polish, the plates were cleaned ultrasonically, first with 100% ethanol and then with toluene (15 min each). Analyses by field-emission scanning electron microscopy (FE-SEM) and X-ray photoelectron spectroscopy (XPS)

confirmed the absence of any nail polish residues. The region of the plate initially covered by nail polish constituted the control surface. Anodization of SS was also performed in 96% H2SO4, in aqueous H2SO4 (1:1 v:v), and in aqueous 30% H_2O_2 as electrolytes.

2.3. Wettability and contact angle (CA)

Static contact angles, surface energy (SE), and polarity were measured with ultrapure distilled water (Millipore Milli-Q, Merck Millipore Corporation, Billerica, MA, USA) and diiodomethane (Sigma, St. Louis, MO, USA) using the sessile drop method (Contact Angle System OCA 15 Plus, DataPhysics, Filderstadt, Germany). Measurements were made at 25 °C, with a volume of 1.5 μL and a dosing rate of 1 μL/min. Data were analyzed with SCA 20 software (DataPhysics). Surface energies were calculated for the two liquids using the standard method of Owens, Wendt, Rabel, and Kaelble (OWRK).

2.4. Field-emission scanning electron microscopy (FE-SEM)

The topography of SS surfaces and the morphology of cells were examined by FE-SEM, using a JEOL JSM-7400F (JEOL Ltd., Tokyo, Japan) or a Zeiss Gemini SEM 500 instrument (Zeiss GmbH, Oberkochen, Germany) operating at 1.5–2 kV. High-resolution images allowed pore diameters to be measured using Photoshop (Adobe Systems, San Jose, CA, USA). Energy-dispersive spectroscopy (EDS) with a silicon-drift detector (Octane, EDAX Inc., Mahwah, NJ, USA) was used to analyze SS surfaces before and after oxidative treatment. A helium-ion microscope (HIM) (Orion, Carl Zeiss Microscopy, Peabody, MA, USA) operating at 35 kV was used to obtain more detailed images of filopodia.

2.5. High-resolution scanning transmission electron microscopy (HR-STEM)

To extend our characterizations of surfaces, a focused ion beam system (Scios, FEI, Netherlands) was used to cut ultrathin cross sections of treated surfaces for HR-STEM. Structural characterizations of the treated SS surfaces were performed using a double-corrected TEM (Titan Themis 300, FEI, Netherlands) operating at 200 Kv with a high angle annular dark field detector (HAADF). Images and chemical maps were acquired by HR-STEM, using a convergence angle of 29 mrad. Raw data from EDS images (Super-X EDS system, FEI, Netherlands) were processed using Esprit imaging software (Bruker, Billerica, MA, USA) for background subtraction and series peak

deconvolution. Maps were acquired for 15–20 min with count rates about 8 kcps. To measure the thickness of oxide layers, HR-STEM images were analyzed by Photoshop (Adobe Systems).

2.6. Atomic force microscopy (AFM)

AFM images were acquired in air at 21 °C using PeakForce tapping mode on a Dimension Icon microscope (Bruker) performed at a scan rate of 1 Hz using ScanAsyst-Air SiN cantilevers with a nominal spring constant of ≈0.4 N/m and tip radius <10 nm.

2.7. X-Ray photoelectron spectroscopy (XPS)

XPS was used to analyze the chemical composition of surfaces. Spectra were acquired with an XR 50 Mg anode X-ray source operating at 150 W and a PHOIBOS 150 MCD-9 detector (SPECS Surface Nano Analysis GmbH, Germany). High-resolution spectra of Cr 2p, Fe 2p, Ni 2p, and O 1 s were recorded with a pass energy of 25 eV (0.1 eV steps) at a pressure below 7.5×10^{-9} mbar, and the spectra were processed with CasaXPS software Version 2.3.1 (15), (16). Binding energies were referred to the C 1 s signal at 284.8 eV. Two samples were studied with no baseline adjustment for each experimental condition.

2.8. Cellular assays

Mouse calvaria-derived osteoblasts (MC3T3, ATCC® CRL-2593™ American Type Cultural Collection), rat smooth-muscle embryonic cells (SmC, A7r5, ATCC® CRL-1444™, American Type Cultural Collection), and mouse embryonic fibroblasts (NIH3T3, ATCC® CRL-1658™, American Type Cultural Collection) were cultured on SS surfaces in Falcon 6-well plates (Becton-Dickinson, Lincoln Park, NJ) for 1, 3, and 7 days at a cellular density of 20000 cells/well. SS samples were previously washed with 100% ethanol and left under UV overnight. Each well contained a plate with both treated and untreated surfaces. Osteoblasts were grown in alpha minimum essential medium (α-MEM, Gibco® culture medium) with Earle's salts, L-glutamine, ribonucleosides, and deoxyribonucleosides (Invitrogen, Burlington, Ontario, Canada). SmC and fibroblasts were grown in Dulbecco's modified Eagle's medium (DMEM). Both media were supplemented with 10% fetal bovine serum (Invitrogen) and incubated at 37 °C in a humidified atmosphere with 5% CO_2.

2.9. Cell preparation for FE-SEM

Cells on SS plates were fixed with 2.5% aqueous glutaraldehyde (1 h at 4 °C), washed 3 times (5 min each) with 0.1 M phosphate buffer (PB, pH 7.2–7.4), postfixed with a 1% aqueous osmium solution (1 h at 4 °C), and washed 3 times (5 min) with PB. The cells were then dehydrated by exposure to a graded sequence of aqueous ethanol (30–100%) and finally dried in a critical point drier (Leica Microsystems Inc., Richmond Hill, ON, Canada).

2.10. Immunofluorescence microscopy

SS plates with cells were washed with PB and then processed for immunofluorescence labeling. For visualization of actin filaments, vinculin, and nuclei, cells were fixed for 30 min at 4 °C using periodate-lysine-paraformaldehyde (PLP) solution in PB. The cells were then permeabilized by exposure to a 0.5% solution of Triton X-100 in PB (10 min), followed by blocking with 5% skimmed milk in PB (1 h). The first antibody, anti-vinculin (1:200; Monoclonal Anti-Vinculin Clone hVIN-1, Sigma), was used simultaneously with rhodamine-phalloidin (red fluorescence for actin labeling) (1:150, Thermo Fisher). The secondary antibody used was Alexa Fluor 488 (green fluorescence for vinculin labeling) (1:400, Thermo Fisher Scientific, Waltham, MA, USA). Antibodies were diluted in a 0.5% solution of skimmed milk in PB and were incubated in a dark humidified environment for 2 h at 25 °C. Between each incubation step, the samples were washed with PB (3 times for 5 min). A glass cover slip was mounted on the cell-covered surfaces of the plates using a medium containing 4′,6-diamidino-2-phenylindole (DAPI) to make nuclei blue-fluorescent (Molecular Probes, Thermo Fisher Scientific). Samples were then examined under a Zeiss Axio Imager upright fluorescence microscope (Zeiss GmbH). For quantitative cell counting, ten microscope fields under the 10 x objective were selected at random from the four inner squares on untreated and treated surfaces.

To estimate the size of focal adhesions (FA) and their number per surface area, immunofluorescence images from 24 h cultures were captured under 40 x objective. Images were separated into single-channel grayscale using the ImageJ split-channel command. FAs were classified in size ranges and expressed as a percentage of the total measurements. Those with length >5 μm were considered as mature (17).

2.11. Bacterial assays

Escherichia coli and Bacillus subtilis were used as representative gram-negative and gram-positive bacteria, respectively, to evaluate the antibacterial properties of nanotextured SS. Bacteria diluted in lysogeny broth (LB) were used to inoculate cultures with an OD600 of 0.2 (108 CFU/mL). A standard volume of this solution (4 mL) was placed onto sterilized SS samples, which were then incubated at 37 °C for 1 and 4 h. The samples were then washed with PB, fixed with a 2.5% solution of glutaraldehyde in PB for 30 min, washed 3 times with PB, postfixed in a 1% aqueous osmium solution for 30 min, dehydrated in graded aqueous ethanol (30–100%), and dried in a critical point drier (Leica Microsystems Inc.).

2.12. Co-culture of E. coli with MCT3T Osteoblastic cell

E. coli (concentration of 108 bacteria ml^{-1}) suspended in LB medium were deposited on treated and control surfaces and incubated at 37 °C for 2 h. The LB medium was removed, and samples were washed three times with sterile PBS. Then, osteogenic cells (MC3T3) were seeded on bacteria-coated surfaces at a density of 20,000 cells/well under the laminar flow hood. Bacteria and osteoblasts were then placed in an incubator and cultured at 37 °C in a humidified atmosphere with 5% CO_2 for 24 h. Samples were then fixed and processed for SEM as above.

2.13. Statistical analyses

Biological results were expressed as a mean value of standard deviation (SD) for each sample. The t-test was used with a 95% confidence interval to evaluate statistical differences in means between two groups.

3- Results

3.1. Bulk elemental analyses

SS304 and SS316 are composed primarily of Fe, Cr, and Ni. SS316 also contains Mo. Energy-dispersive spectroscopy (EDS) analyses of the two alloys before and after electrochemical treatment did not reveal any major changes in the elemental composition of the bulk (see Table 3 in Supplemental).

3.2. Physical characterization of the surfaces

Field-emission scanning electron microscopy (FE-SEM) images of untreated SS surfaces showed no distinctive topographical features other than polishing marks (Fig. 1a). Anodizing SS in electrolytes consisting of H_2SO_4 or a mixture of H_2SO_4 and water (1:1) textured the surface but not at the nanoscale. The use of aqueous H_2O_2 alone as electrolyte did not change the superficial topography (see Fig. 1 in Supplemental).
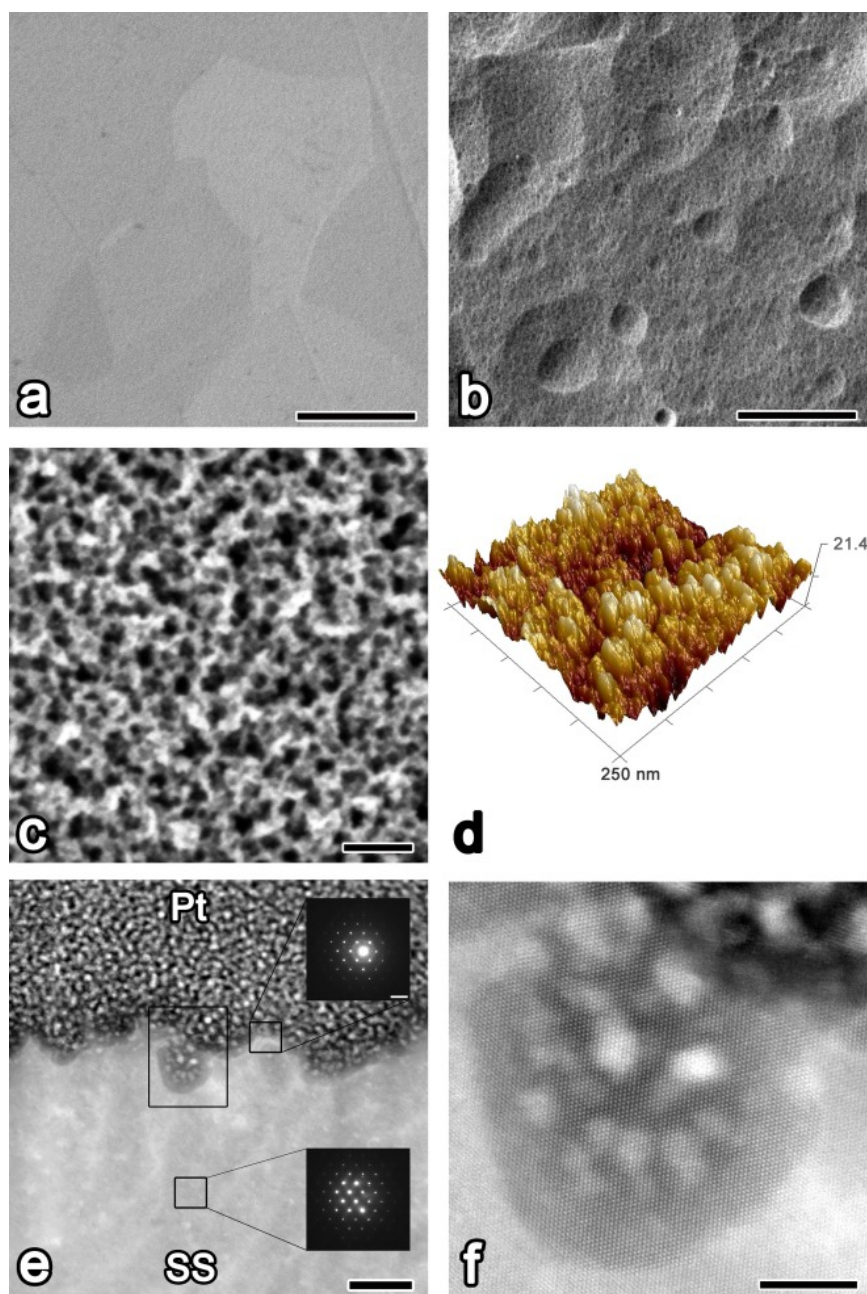

Figure 51. – Fig. 1. Surface characterization of SS304. FE-SEM images of (a) untreated and (b) anodized surfaces (bar = 3 μm). (c) Higher magnification FE-SEM (bar = 20 nm) and (d) AFM images of the mesoporous surface. (e) HR-STEM image of the cross section of an anodized

surface (bar = 20 nm). Insets illustrate the diffraction patterns of the mesoporous surface (upper) and the bulk SS (bottom). (f) Atomic resolution HR-STEM image of the interface between the mesoporous layer and the bulk SS, showing crystalline atomic organization. (For SS316 see Supplemental).

In contrast, when SS304 and SS316 were anodized in a mixture of equal volumes of H_2SO_4 and aqueous H_2O_2, a distinctive surface nanotopography was produced (Fig. 1b–c). The surface layer is mesoporous, with pores about 20 nm in diameter (16.4 ± 4.2 nm for SS304 and 17.6 ± 7.1 nm for SS316). Analysis by atomic force microscopy (AFM) (Fig. 1d) revealed that the roughness of the surface (Ra) increased from 4.5 ± 0.8 nm before electrochemical treatment to 11.5 ± 2.7 nm (SS304) and 9.7 ± 1.3 nm (SS316) after treatment. Analysis of cross-sectional profiles by high-resolution scanning transmission electron microscopy (HR-STEM) showed that the surface layer ranged in thickness from 4.7 to 8.0 nm (Fig. 1e) and was crystalline (Fig. 1f). Electron diffraction patterns of the surface layer and of the underlying bulk material (insets in Fig. 1e) confirmed that both regions are crystalline (data for SS316 in Supplemental, Fig. 2).

3.3. Chemical characterization of nanostructured surfaces

EDS mapping of anodized surface of SS304 revealed the presence of oxygen (Fig. 2a), and X-ray photoelectron spectroscopy (XPS) allowed further characterization of the oxides created by anodization (Fig. 2b). The position of the peaks in the XPS spectra indicated that the surface of nanotextured SS304 contained 58% of Fe as Fe(II) and 33% as Fe(III); 82% of Cr appears as Cr(III) and 14% as Cr(III) hydroxide; and 30% of Ni is found as Ni(II) and 43% as Ni(II) hydroxide. The amount of Fe in the surface layer that exists nominally as Fe(0) is much lower than in the bulk material. Moreover, peaks corresponding to Fe(0) (at 706 eV) and Cr(0) (at 573 eV) are more pronounced on the untreated surface than on the anodized surface (Fig. 2b). Analysis of O also showed an increase of oxides on nanotextured surfaces, especially in the form of hydroxides. Species formed by anodizing the surface of SS304 were also detected in the case of SS316, albeit with a higher decrease in Ni(0) and Fe(0). Mo was not detected on anodized surfaces, but EDS mapping showed that it was present in the bulk material (data for SS316 in Supplemental, Figs. 3).
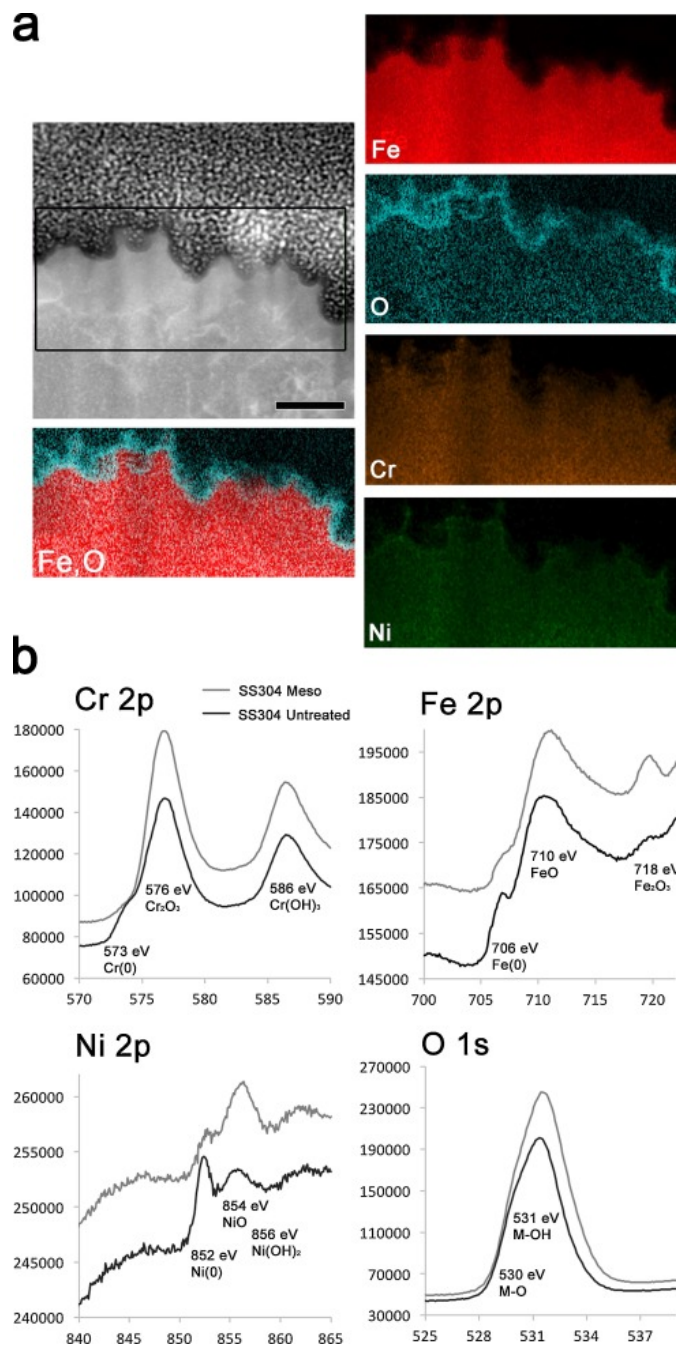
Figure 52. – Fig. 2. Chemical composition of the mesoporous surface of SS304. (a) EDS mapping of elements in a cross section of the surface (bar = 40 nm). (b) Compositional analysis by XPS, showing high-resolution spectra of Cr 2p, Fe 2p, Ni 2p, and O 1 s on the surfaces of anodized (Meso) and untreated samples. In all cases, the x-axis corresponds to peak positions in eV, and the y-axis shows intensity. (For SS316 see Supplemental).

3.4. Hydrophilicity of surfaces

Anodizing SS reduced the contact angles of H_2O by 11% for SS304 and by 17% for SS316, relative to the non-treated surface, with corresponding changes in the SE (Table 1).

SS	CA$_{water}$ (°)	CA$_{DIM}$ (°)	SE (mN/m)	Polarity (mN/m)
304 Untreated	78.2 ± 3.7	43.3 ± 3.5	39.9 ± 2.6	5.5 ± 1.9
304 Mesoporous	69.3 ± 2.1	33.0 ± 1.1	46.5 ± 3.5	8.4 ± 1.2
316 Untreated	77.2 ± 2.4	36.5 ± 2.4	42.9 ± 1.2	5.2 ± 2.1
316 Mesoporous	64.3 ± 3.0	22.4 ± 1.5	51.5 ± 2.5	10.4 ± 1.5

Tableau 2. – Table 1. Contact angles (CA) measured with H_2O and CH_2I_2 (DIM), surface energies (SE), and polarity for SS304 and SS316.

3.5. Cell growth

Cell counts showed that mesoporous SS304 and SS316 both promote the growth of osteogenic and smooth muscle cells (SmC). Significant differences ($p < 0.05$) were observed between the treated and the untreated surfaces (Fig. 3a). Osteoblasts appeared to proliferate 2-fold faster on the mesoporous SS surface at each culture interval examined. A similar pattern was observed for SmC (Fig. 3a). The number of fibroblasts on treated SS was similar to that on controls, with no significant differences after 24 and 72 h of culture; by seven days, however, cell growth showed a tendency to decrease (Fig. 3a) (data for SS316 in Supplemental, Figs. 4).
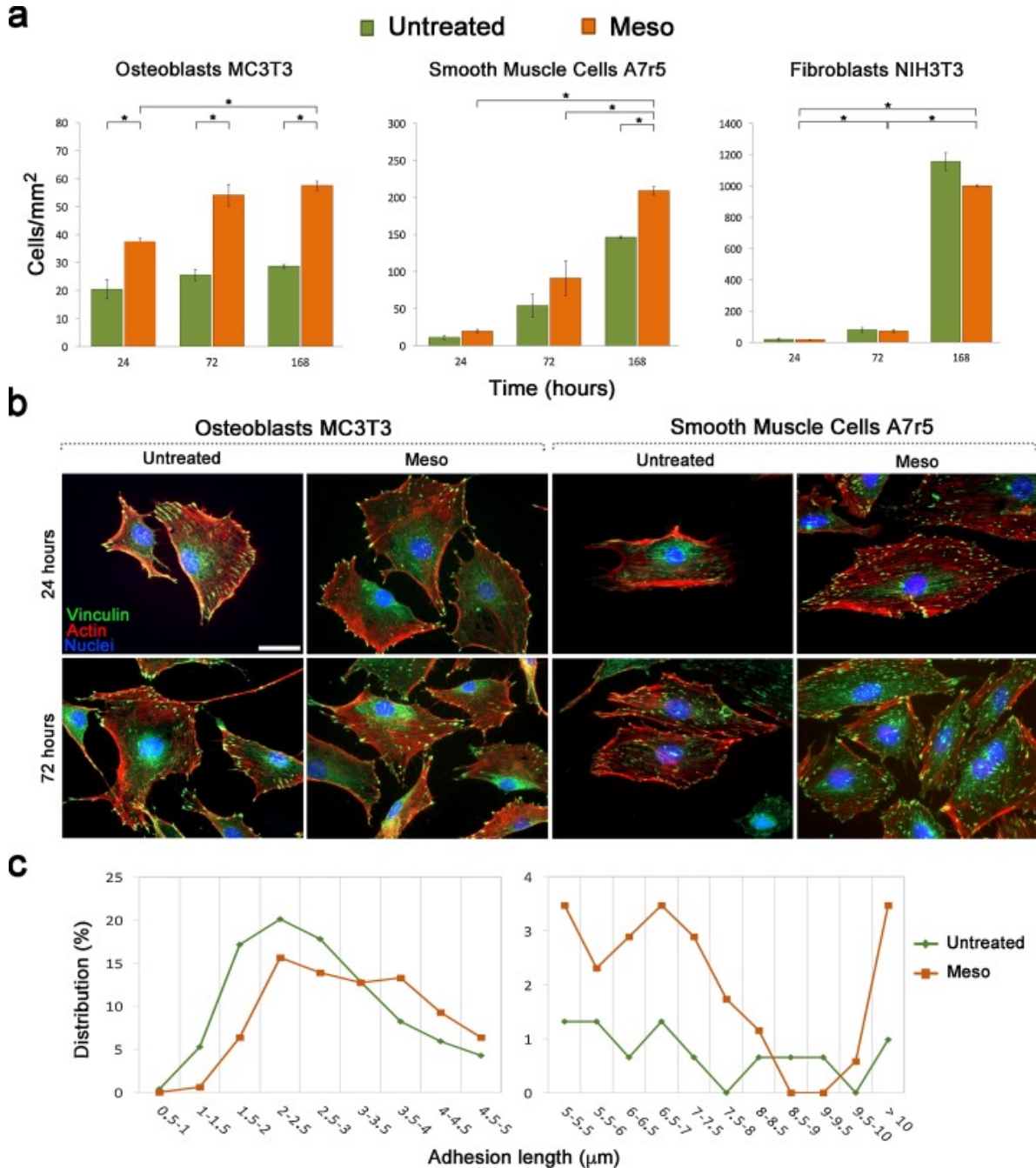
Figure 53. – Fig. 3. Cell attachment, growth, and spreading on SS304. (a) Numbers of osteoblasts, smooth muscle cells, and fibroblasts at 24, 72, and 168 h on untreated (green) and mesoporous (Meso, orange) surfaces. Values showing significant differences ($p < 0.05$) are indicated with an asterisk. (b) Fluorescence micrographs showing vinculin (green) and actin (red) distribution in cells after 24 and 72 h of culture. Nuclei are stained in blue (bar = 20 μm). (c) Quantitative analysis of FA lengths. (For SS316 see Supplemental).

3.6. Cell shape, attachment, and spreading

170

FE-SEM images of osteoblasts and SmC on the mesoporous surfaces of both SS alloys showed more abundant filopodia. These adapted to the nanotopography of the surface by developing extremely small, polymorphous lateral membrane protrusions (Fig. 4a–b). More detailed analyses of interactions of osteogenic cells with anodized surfaces by HR-STEM revealed the very intimate contact of the filopodia with the surface (Fig. 4c–d). Fibroblasts similarly emitted filopodia with lateral membrane protrusions but in much smaller numbers.
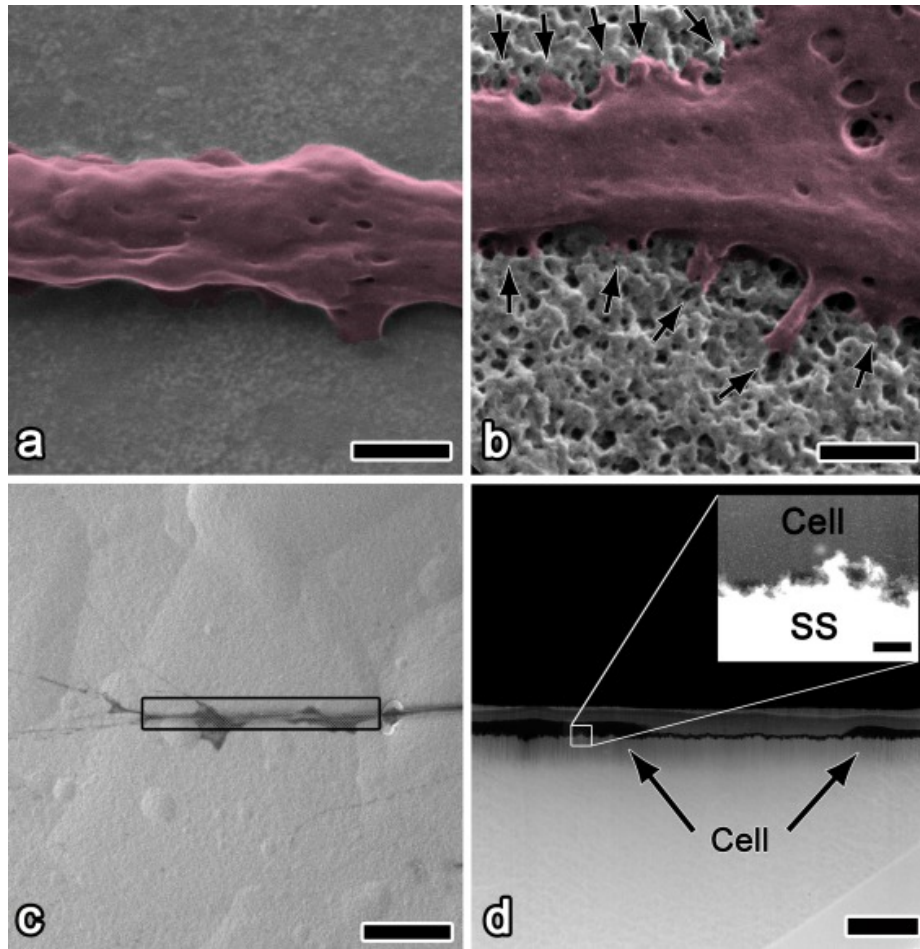
Figure 54. – Fig. 4. Electron microscope images of osteogenic cell filopodia morphology on SS304. HIM images from cells growing on (a) an untreated and (b) mesoporous surfaces (bar = 100 nm). Lateral membrane protrusions (arrows) emerging from a filopodium, here colored in crimson. (c) SEM image of a filopodium on the anodized surface selected for FIB cross-sectioning (bar = 8 μm). (d) TEM image of the section within the rectangle in (c) (bar = 500 nm, inset bar = 40 nm).

Osteoblasts and SmC grown on mesoporous anodized surfaces showed vinculin immunoreactive plaques associated with actin filaments, especially after 72 h of culture (Fig. 3b). In contrast, fibroblasts did not generally show distinct, well-developed actin cytoskeletons and vinculin plaques. There were significant differences in the length (Fig. 3c) and number (0.45 ± 0.03 FA/μm2 on control and 0.61 ± 0.11 FA/μm2 on nanocavitated surfaces) of these complexes and a greater tendency to form mature FA for osteoblastic cells cultured on untreated surfaces compared to mesoporous SS.

3.7. Bacterial assays

Very few E. coli adhered to the nanotextured surface of both SS alloys after 1 h of incubation, and the number remained virtually unchanged after 4 h, showing the absence of significant proliferation; in contrast, the number increased substantially on untreated surfaces (Fig. 5a–b). While in general there was more adhesion with B. subtilis than with E. coli, there were major differences between the number of B. subtilis on treated and untreated surfaces after 1 and 4 h of incubation (Fig. 5a). In neither case was bacterial proliferation exponential (data for SS316 in Supplemental, Figs. 5).
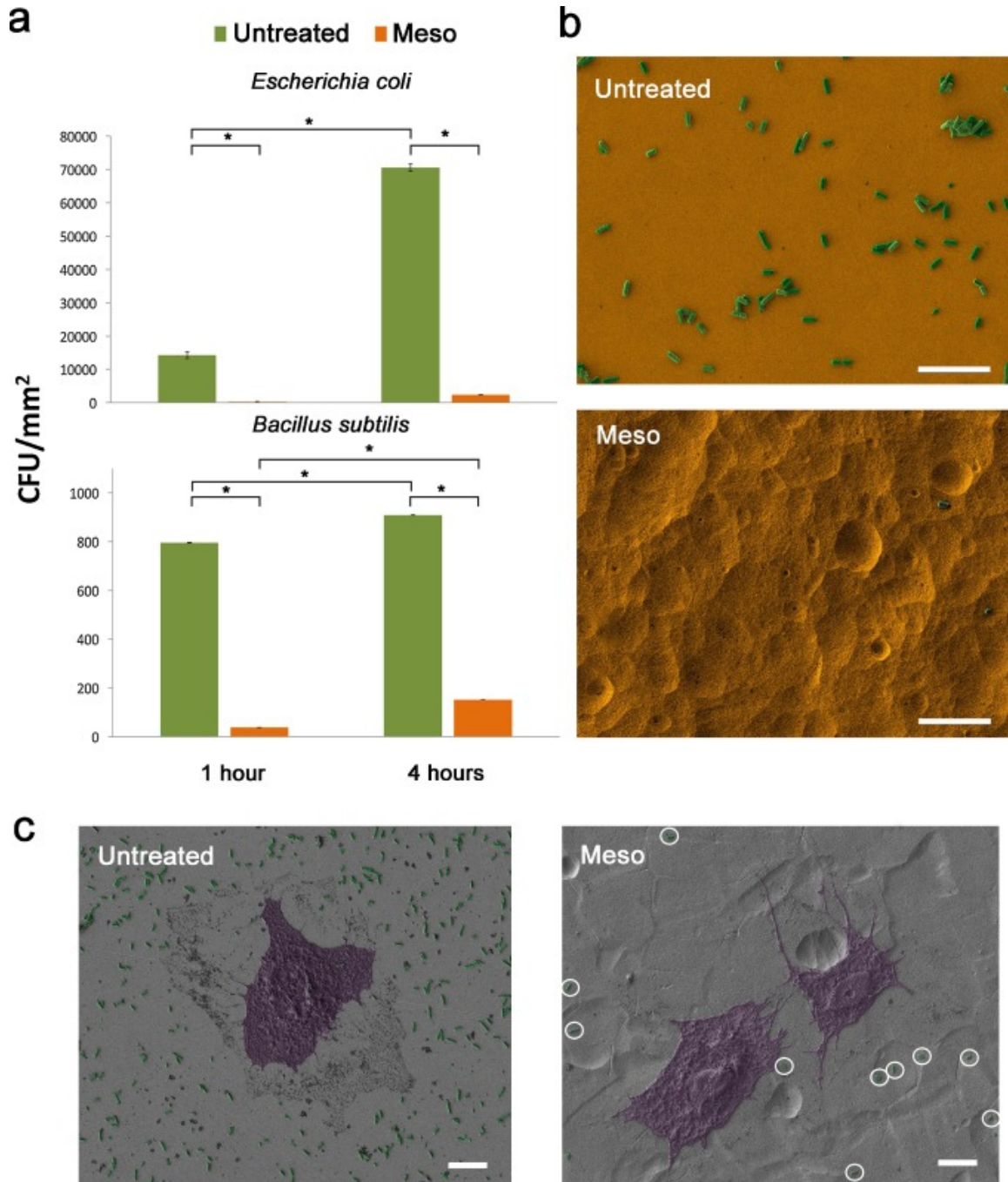
Figure 55. – Fig. 5. Bacterial adhesion and proliferation on SS304. (a) Bacterial counts on untreated and mesoporous (Meso) surfaces. Values showing significant differences (p < 0.05) are indicated with an asterisk. (b) FE-SEM micrographs after incubation with E. coli (colored in green) for 4 h (bar = 10 μm). (For SS316 see Supplemental). (c) Co-culture of E. coli with MCT3T Osteoblastic cells (bar = 10 μm).

3.8. Co-culture of E. coli with HMCT3T osteoblastic cell

Because change on the culture medium in the presence of bacteria, cell growth and structure was not optimal on both SS with and without the nanotopography (Fig. 5c). It is noticeable, however, that osteoblasts still spread better on nanocavitated surfaces in the presence of bacteria compared to the untreated sample. Most importantly, the antibacterial activity observed in cultures with only bacteria alone was still present in the presence of cell (Fig. 5c).

4- Discussion

Engineering the physicochemical characteristics of surfaces on the nanoscale promises to have a major impact in medicine and on the effort to control microbes in hospital settings and other environments. As a result, it is urgently important to develop a deeper understanding of how modified surfaces can be created and how they perform. The surface of SS is difficult to modify by direct chemical etching because the presence of Cr creates a chemically stable oxide layer that resists corrosion in various aqueous environments [18], [19]. We now report a simple process that reproducibly nanostructures the surface of both SS304 and SS316 in ways that have significant biological consequences. The fact that this has not been previously achieved, despite numerous previous studies of SS, highlights the contribution of our work.

4.1. Nanocavitating the surface of SS

H_2O_2 is a potent oxidant, but it cannot by itself penetrate the layer of native oxide that passivates SS. Similarly, concentrated H_2SO_4 is a strong acid, but it is not highly dissociated and does not readily engage in corrosive action [20]. However, the combination of aqueous H_2O_2 and H_2SO_4 leads to extensive dissociation and ionic conductivity, making the mixture suitable as an electrolyte. Recently, the use of a 5:2 mixture of H_2SO_4 and aqueous H_2O_2 as an electrolyte was reported for the electrochemical oxidation of SS304 by Asoh and colleagues [21]. Their conditions used [21] led to the deposition of thick films of insoluble oxide consisting of $FeCr_2O_4$ nanoparticles. Consequently, their work does not provide a way to create very thin surface layers on SS similar to those that we have previously produced on Ti and other tractable metals. To achieve this goal and reveal the biological consequences, we found that we needed to change the composition of the electrolyte and the conditions of anodization in significant ways. We altered the proportion of H_2SO_4 and H_2O_2 in the electrolyte, and we performed the anodization at a higher current density (700 A/m2).

In this way, a distinctive topography defined by the presence of interconnected nanoscale cavities (16.4 ± 4.2 nm) and characteristic roughness (11.5 ± 2.7 nm) could be created on both SS304 and SS316. Furthermore, we confirmed that our method has no effect on the bulk composition of SS and that changes are limited to the surface. The mesoporous surface layer is homogeneous and composed of crystalline metallic oxides and hydroxides. It is rich in oxidized Fe and also includes Cr and Ni as oxides and hydroxides.

We suggest that the characteristic porosity arises from two closely linked phenomena: (I) Nanoscale corrosion leading to local cavitation (due to physicochemical inhomogeneities in the native oxide layer on SS, which facilitates selective dissolution) and (II) transpassivation caused by the application of an electrochemical potential. Transpassivation depletes alloying elements, ultimately making the surface more susceptible to localized chemical attack. In addition, transpassivation causes the accumulation of defects such as vacancies at the metal/film interface, according to the point-defect model (22), (23). The formation of a network of nanocavities (formation of nanoscale space within a solid object or body) may ultimately be linked to the accumulation of defects (such as vacancies) at the metal/film interface (23), (24). The thin native passivating film dissolves, exposing the accumulated vacancies at the metal/film interface, which become points of pit nucleation. The resulting nanocavitated metal surface is exposed to the environment, and a new thin barrier layer of oxide (4.7–8.0 nm in thickness) is created by repassivation.

Physicochemical properties of the surfaces of biomaterials, including wettability and topography, are known to have important effects on cell behavior. Hydrophilic surfaces are considered to favor cellular growth and biocompatibility (25), (26). In the specific case of osteoblasts on Ti, adherence and proliferation appear to depend primarily on the wettability of the surface, and hydrophilic surfaces typically provide better conditions for cellular adhesion than hydrophobic surfaces (25), (26), (27). Our method for modifying the surface of SS is not expected to yield dramatic changes in energy and hydrophilicity compared with untreated controls, which already have oxidized surfaces, but the use of H_2SO_4/H_2O_2 is nevertheless likely to alter the native oxide layer in various ways and to possibly introduce a greater density of hydroxyl groups, thereby increasing the hydrophilicity of the surface to a degree. The enhanced adherence of osteoblasts and SmC that we observe on SS is therefore consistent with current understanding of hydrophilic surfaces.

As observed previously in the case of oxidatively nanopatterned Ti (12), the nanostructured surface of SS does not enhance the attachment and growth of fibroblasts. Other studies have noted

that surfaces with nanoscale topographic features can selectively promote the adhesion of osteoblasts but not fibroblasts (28). Mouse fibroblasts seem to attach better to moderately hydrophilic surfaces (29), especially when the contact angles are in the range 60–80° (30). Because the contact angles of untreated SS (78°) and anodized SS (65°) both fall within the optimal range, the similar response of the two surfaces to fibroblasts is not surprising. However, it is possible that for certain types of cells, the topography of surfaces is more important than their chemistry. In any case, the control of fibroblasts has high clinical relevance because fibrous encapsulation can prevent complete osteointegration of orthopedic and dental implants, leading eventually to their failure (31). For these reasons, materials with high cytoselectivity, such as an ability to selectively enhance the adhesion and subsequent functions of osteoblasts while at the same time interfering with competitive cells such as fibroblasts, promise to have a major impact in the realm of medicine.

4.2. SS with a mesoporous surface stimulates the formation of filopodia

Filopodia are involved in many cellular processes, including adhesion, spreading, and migration (32). During the spreading of cells, filopodia form the initial sites of adhesion. Subsequently, other components of FA complexes (such as talin) are recruited to the sites to form mature FA (17), (32). As previously shown in the case of osteogenic cells on nanotextured Ti (7), the three cell lines studied in the present work likewise develop filopodia with unique nanoscale lateral membrane protrusions. These are particularly abundant on osteoblasts and SmC, and they are likely to make a major contribution to the strength of cell adhesion. These protrusions differ from what has previously been reported as nanopodia (33), (34). They ensure a very intimate adhesion of the filopodia to the mesoporous surface, and they illustrate the fluid nature of their membrane. These lateral protrusions represent a yet undescribed cellular response that can be elicited directly by nanotopography.

Osteoblasts and SmC also exhibited well-developed FA. The higher number of osteoblasts that we have observed on the mesoporous surface of anodized SS correlates with the significant increase in the quantity and size of FA, as well as in their degree of maturity. Larger FA lead to stronger interactions between the cytoskeleton and substrate (35). Fibroblasts, which show no enhanced growth on the nanotextured surfaces of either SS304 or SS316, exhibit virtually no FA. These observations indicate that the unique physicochemical characteristics of SS with a mesoporous surface influence the cellular mechanisms that regulate the formation and maturation of FA.

176

While it is clear that the observed changes on cell activity, focal adhesions, and membrane fluidity are related to the physical characteristics of the mesoporous nanocavitated surface, elucidating the precise mechanism will require additional analyses. For instance, the surface nanotopography can produce cellular deformation summed up to affect the skeleton of the cell. It is also possible that the protein adsorption can be alter on the nanotopography, affcting their orientation and conformation (36), and this could selectively interact with cell to activate signaling pathways.

4.3. Antibacterial properties

Infected implants are difficult to treat, and their removal is frequently required (37). These infections are caused not only by post-operative infections of the wound but also by microorganisms introduced on the surfaces of metallic implants and surgical instruments, due to inadequate sterilization. Because SS has many applications in the field of medicine, discovering a simple way to impart antibacterial properties would have a broad impact. Unfortunately, conventional SS is not inherently antibacterial, but many attempts have been made to modify its properties by altering the surface (Table 1 and 2 in Supplemental) or by adding elements known to be antibacterial, including Ag (38) and Cu (39). Our simple oxidative electrochemical treatment is advantageous because it does not rely on the creation of thick surface layers that can alter the biomechanical characteristics, nor does it rely on changing surface composition. Instead it achieves antibacterial properties by simply altering texture at the very surface to limit both bacterial adhesion and growth.

The antibacterial effect of nanotextured surfaces has been attributed to repulsive forces that are increased in importance by the relatively large surface areas of nanotopographies (40). In general, hydrophobic surfaces are better than hydrophilic ones in accommodating bacterial adhesion, and low surface energies are better than high ones. Since these parameters are only marginally altered on the nanostructured surface of anodized SS, it is likely that topography itself may account for the poor ability of bacteria to adhere to the treated surface. This capacity to interfere with the initial step in bacterial colonization can help prevent the subsequent cascade leading to the formation of biofilms.

5- Conclusions

SS is widely used in hospital settings; for some applications, biocompatibility is essential, for others, antimicrobial capacity is required. Finding a simple way to attain these divergent objectives is clearly a daunting challenge. Indeed, past attempts to simultaneously achieve these two long-sought goals have largely relied on deposition of adlayers and have resulted in limited success. We

have also found a way to nanocavitate both SS304 and SS316 by using a mixture of H_2SO_4/H_2O_2 for direct anodization, an electrolyte not commonly used for this process. Surfaces produced by this method consist of a thin mesoporous layer of crystalline oxide, which simultaneously exhibit a selective impact on cellular activity and antibacterial properties. Notably, the mesoporous surface influences the formation and maturation of FA and elicits the outgrowth of filopodia. The latter emit unique, ultra-small lateral membrane protrusions that suggest an effect on membrane fluidity. Together, these features are likely to have a major impact on the nanoscale cell biomechanics and cell signaling, either directly or through the mediation of protein adsorption. The ability to create such thin mesoporous surface layers on SS now allows technology to shift dramatically away from the inherent limitations of traditional thick adlayers. Because it only alters texture at the very surface, the process of nanocavitation embodies a conceptual advance that promises to be broadly useful in the hospital setting for improved medical devices and to control bacterial growth, but also to facilitate innovative translational applications of SS in other areas of industry.

Appendix A. Supplementary data

Reference	Material	Technique	Electrolyte	Cell or Bacteria Studies	Application	Characterization Methods	Topography Dimension
(Dhawan et al. 2017)	SS304L	Anodization process	Perchloric acid with ethylene-glycol monobutylether – 15 to -5 $^\circ$C	MG63 Osteoblastic cells	Biomedical applications	SEM	Diameter of the porous between 100 and 220 nm
(Asoh, Nakatani, Ono 2016)	SS304	Anodization process	Sulfuric acid 3-7 M -60 $^\circ$C Sulfuric acid 3-7 M and hydrogen peroxide 2 M	N/A	Valve metals	TEM, SEM, FIB, EDS	Thickness of the oxide layer between 20 and 50 nm obtained with sulfuric acid. Thickness between 300 nm and 1 μm obtained with hydrogen peroxide and sulfuric acid.
(Fu et al. 2016)	SS316L	Anodization process	Hydrogen chloride 20 % - 10 h at 20 $^\circ$C	CD34+ KG-1a cells	Biomedical applications	SEM	Pore size of about 400 nm Thickness of about 130 nm
(Rezaei et al. 2016)	SS316	Anodization Process with Cu deposition	Ethyleneglycol with perchloric acid (19:1,v:v) - 15 min at 0-5 $^\circ$C	N/A	Biosensors	FE-SEM, EDS XRD	None dimension was determined

(Rezaei, Havakeshian, and Ensafi 2015)	SS	Anodization Process with Cu deposition	Ethyleneglycol with 5% of perchloric acid 15 min at 0-5 ºC	N/A	Biosensors	FE-SEM, EDS AFM	Depth of the porous around 10 nmPores size between 60 and 70 nm
(Rezaei, Havakeshian, andEnsafi 2014)	SS304	Anodization Process with Cu and Pt deposition	Ethyleneglycol with 5% of perchloric acid - 15 min at 0-5 °C	N/A	Electrochemical devices	SEM AFM	Depth of the porous around 10 nm Pores size around 70 and 100 nm
(Ni et al. 2014)	SS316L	Anodization process	Ethyleneglycol with 5% of perchloric acid	Human dermal fibroblast	Biomedical applications	SEM, AFM, XPS, CA	Pores size between 25 and 60 nm
(Pan et al. 2013)	SS316L	Anodization process	Perchloric acid with ethylene-glycol monobutylether	Fibroblast	Biomedical applications	SEM, AFM	Pores size between 40 and 210 nm
(Kang et al. 2013)	SS316L	Indirect anodization process	Oxalic acid 0.3 M - 2 h at 2 ºC with 1 μm-thick aluminum layer	N/A	Medical devices	SEM	Pore size between 100 and 200 nm Pore size of 10 μm for polished samples
(Kure et al. 2012)	SS304	Anodization process/ annealing	Ethylene glycol 0.1 M with ammonium fluoride 0.1-0.5 M	N/A	Valve metals	SEM, XRD, GDOES, XPS	Thickness of the oxide films from around 4 μm to 50 nm
(Doff et al. 2011)	SS316L	Square wave pulse polarization	Sulphuric acid 5 M - 60 ºC	N/A	Unspecified	SEM, GDOES, XPS, RBS	Thickness of the films between 150 and 200 nm Pores of size up to around 10 nm
(Martin et al. 2009)	SS304L duplex SS	Anodization process	Perchloric acid with ethylene-glycol monobutylether - 15 to -5 °C	N/A	Unspecified	FE-SEMAFM STEM	Distance between pores between 20 and 230 nm Depth of the porous around 70 nm Thickness of the walls of between 30 and 40 nm
(Díaz et al. 2008)	SS316L	Anodization process	Sulfuric acid with Chromium trioxide (2:1) - 80 ºC (constant and alternating current)	Platelet	Biomedical applications	N/A	None surface characterization was performed
(Fujimoto et al. 1999)	SS304	Square wave potential pulse polarization	Sulfuric acid 5 M - 50–80 ºC	N/A	Unspecified	UV-vis light Reflectance spectra	Thickness of the oxide layer around 10 nm

Tableau 3. –   Table 1: References on SS surface texture modification by anodization

Abbreviations:

Scanning electron microscopy (SEM), Transmission electron microscopy (TEM), Focus ion beam (FIB), Energy Dispersive X-ray Spectroscopy (EDS), Field emission scanning electron microscopy (FE-SEM), X-ray Diffraction (XRD), Atomic force microscopy (AFM), X-ray photoelectron spectroscopy (XPS), Contact angle (CA), Glow discharge optical emission

spectroscopy (GDOES), Rutherford backscattering spectrometry (RBS), Scanning transmission electron microscopy (STEM).

Bibliography:

Asoh, Hidetaka, Madoka Nakatani, and Sachiko Ono. 2016. 'Fabrication of thick nanoporous oxide films on stainless steel via DC anodization and subsequent biofunctionalization', Surface and Coatings Technology, 307, Part A: 441-51.

Dhawan, Udesh, Hsu-An Pan, Meng-Je Shie, Ying Hao Chu, Guewha S. Huang, Po-Chun Chen, and Wen Liang Chen. 2017. 'The Spatiotemporal Control of Osteoblast Cell Growth, Behavior, and Function Dictated by Nanostructured Stainless Steel Artificial Microenvironments', Nanoscale Research Letters, 12: 86.

Díaz, M., P. Sevilla, A. M. Galán, G. Escolar, E. Engel, and F. J. Gil. 2008. 'Evaluation of ion release, cytotoxicity, and platelet adhesion of electrochemical anodized 316 L stainless steel cardiovascular stents', Journal of Biomedical Materials Research Part B: Applied Biomaterials, 87B: 555-61.

Doff, J., P. E. Archibong, G. Jones, E. V. Koroleva, P. Skeldon, and G. E. Thompson. 2011. 'Formation and composition of nanoporous films on 316L stainless steel by pulsed polarization', Electrochimica Acta, 56: 3225-37.

Fu, Guowei, Zhanjiang Yu, Yongqiang Chen, Yundai Chen, Feng Tian, and Xiaoda Yang. 2016. 'Direct Adsorption of Anti-CD34 Antibodies on the Nano-Porous Stent Surface to Enhance Endothelialization', Acta Cardiologica Sinica, 32: 273-80.

Fujimoto, Shinji, Shigeki Kawachi, Toshikata Nishio, and Toshio Shibata. 1999. 'Impedance and photoelectrochemical properties of porous oxide film on Type304 stainless steel formed by square wave potential pulse polarisation', Journal of Electroanalytical Chemistry, 473: 265-71.

Kang, M., Y.M. Park, H.C. Yang, Y.H. Seo, and B.H. Kim. 2013. 'Surface Nano-texturing of Stainless Steel for Biocompatibility Enhancement of Implantable Medical Devices ', IFMBE Proceedings, 49: 157-60.

Kure, K., Y. Konno, E. Tsuji, P. Skeldon, G. E. Thompson, and H. Habazaki. 2012. 'Formation of self-organized nanoporous anodic films on Type 304 stainless steel', Electrochemistry Communications, 21: 1-4.

Martin, F., D. Del Frari, J. Cousty, and C. Bataillon. 2009. 'Self-organisation of nanoscaled pores in anodic oxide overlayer on stainless steels', Electrochimica Acta, 54: 3086-91.

Ni, Siyu, Linlin Sun, Batur Ercan, Luting Liu, Katherine Ziemer, and Thomas J. Webster. 2014. 'A mechanism for the enhanced attachment and proliferation of fibroblasts on anodized 316L stainless steel with nano-pit arrays', Journal of Biomedical Materials Research Part B: Applied Biomaterials, 102: 1297-303.

Pan, Hsu-An, Jia-You Liang, Yao-Ching Hung, Chia-Hui Lee, Jin-Chern Chiou, and G. Steven Huang. 2013. 'The spatial and temporal control of cell migration by nanoporous surfaces through the regulation of ERK and integrins in fibroblasts', Biomaterials, 34: 841-53.

Rezaei, Behzad, Elaheh Havakeshian, and Ali A Ensafi. 2015. 'Decoration of nanoporous stainless steel with nanostructured gold via galvanic replacement reaction and its application for electrochemical determination of dopamine', Sensors and Actuators B: Chemical, 213: 484-92.

Rezaei, Behzad, Elaheh Havakeshian, and Ali A. Ensafi. 2014. 'Fabrication of a porous Pd film on nanoporous stainless steel using galvanic replacement as a novel electrocatalyst/electrode design for glycerol oxidation', Electrochimica Acta, 136: 89-96.

Rezaei, Behzad, Leila Shams-Ghahfarokhi, Elaheh Havakeshian, and Ali A. Ensafi. 2016. 'An electrochemical biosensor based on nanoporous stainless steel modified by gold and palladium nanoparticles for simultaneous determination of levodopa and uric acid', Talanta, 158: 42-50.

Reference	Material	Technique	Cell or Bacteria Studies	Application	Characterization Methods	Topography Dimension
(Martínez-Calderon et al. 2016)	SS304	Laser	Stem cells	Biomedical applications	FE-SEM, AFM	Distance between structures around 500 nm Depth of 150 nm
(Yadav et al. 2016)	SS304	Chemical oxidation	N/A	Electrochemical capacitors	FE-SEM, EDS, XPS, AFM, CA	Roughness between 4 and 9 nm

(Kim et al. 2016)	SS	Coating of nanofibrous scaffold of polycaprolactone by electrospinning	Colon cancer cells and bone marrow-derived dendritic cells	Biomedical applications	SEM, porosimeter	Fibers diameter between 400 nm and 2 μm
(Bagherifard et al. 2015)	SS316L	Severe shot peening	Osteoblasts S. aureus S. epidermidis P. aeruginosa E. coli	Biomedical applications	SEM, profilometerAFM, CA	Grain size between 25 nm and 65 μm
(Kheirkhah et al. 2015)	SS316L	Forsterite (Mg$_2$SiO$_4$) coating by sol-gel dip coating technique	N/A	Biomedical applications	SEM, XRD, EDS	Crystallite size of around 40 nm
(Qin et al. 2015)	SS316L	Coating by silver nanoparticles deposition	Stem cells E. coli P. aeruginosa S. aureus S. epidermidis	Biomedical applications	FE-SEM, XPS, CA	Silver particle of about 7 nm
(Shayan et al. 2015)	SS316L	Linear plane-strain machining	Osteoblast	Biomedical applications	SEM, XPS, CA, hardness, profilometer	Roughness of about 20 nm
(Mohan et al. 2015)	SS316	Hydrothermal treatment – NaOH 0.5-10 M, 2-12 h at 150-250 oC,	Endothelial andSmooth musclecells	Biomedical applications	SEM, EDS, XPS, XRD	Roughness between 0.41 and 0.18 nm
(Huang et al. 2015)	SS316L	Coating of TiO$_2$ nanotubes	Platelets	Biomedical applications	SEM, XPS, XRD, CA	Nanotubes diameter of about 55 nm Oxide layer of 900 nm
(Misra et al. 2013)	SS316L	Grain structure (phase-reversion)	Osteoblast	Biomedical applications	SEM, TEM, AFM, CA	Grain size between 300 nm and 22 μm
(Nazneen 2013)	SS316L	Focused ion beam milling	Endothelial cells	Biomedical applications	SEM, AFM	Porous diameter between 65 and 180 nm
(Misra et al. 2011)	204Cu Cr-Mn SS	Grain structure (phase-reversion)	Osteoblast	Biomedical applications	SEM, TEM, AFM, CA	Grain size between 100 nm and 1 μm
(Beckford and Zou 2011)	SS316	Sandblasting	N/A	Electromechanical systems	SEM, CA, profilometer	Asperities with size between 100 and500 nm
(Roguska et al. 2011)	SS316L	Coating of collagen/calcium salt by cathodic deposition	Osteoblast	Biomedical applications	SEM, AFM, AES, FTIR	Average diameter of fibrils between 50 and 500 nm
(Ceylan, Tekinay, and Guler 2011)	SS	Coating of peptide nanofibers	Endothelial cells	Biomedical applications	SEM, TEM, AFM, CA, XPS, FTIR	Coating thickness of about 1.3 μm
(Kang and Lee 2007)	SS316L	Surface functionalization (Protein adsorption)	N/A	Biomedical applications	FE-SEM, AFM, XPS, CA	N/A

(Mahapatro et al. 2006)	SS316L	Surface functionalization (therapeutic drugs attachment)	N/A	Biomedical applications	FTIR, XPS	N/A

Tableau 4. – Table 2: References on SS surface texture modification obtained by methodologies others than anodization

Abbreviations:

Field emission scanning electron microscopy (FE-SEM), Atomic force microscopy (AFM), Energy Dispersive X-ray Spectroscopy (EDS), X-ray photoelectron spectroscopy (XPS), Contact angle (CA), Scanning electron microscopy (SEM), X-ray Diffraction (XRD), Transmission electron microscopy (TEM), Fourier transform Infra-red spectroscopy (FTIR).

Bibliography:

Bagherifard, Sara, Daniel J. Hickey, Alba C. de Luca, Vera N. Malheiro, Athina E. Markaki, Mario Guagliano, and Thomas J. Webster. 2015. 'The influence of nanostructured features on bacterial adhesion and bone cell functions on severely shot peened 316L stainless steel', Biomaterials, 73: 185-97.

Beckford, Samuel, and Min Zou. 2011. 'Micro/nano engineering on stainless steel substrates to produce superhydrophobic surfaces', Thin Solid Films, 520: 1520-24.

Ceylan, Hakan, Ayse B. Tekinay, and Mustafa O. Guler. 2011. 'Selective adhesion and growth of vascular endothelial cells on bioactive peptide nanofiber functionalized stainless steel surface', Biomaterials, 32: 8797-805.

 Huang, Qiaoling, Yun Yang, Ronggang Hu, Changjian Lin, Lan Sun, and Erwin A. Vogler. 2015. 'Reduced platelet adhesion and improved corrosion resistance of superhydrophobic TiO2-nanotube-coated 316L stainless steel', Colloids and Surfaces B: Biointerfaces, 125: 134-41.

Kang, Chan-Koo, and Yoon-Sik Lee. 2007. 'The surface modification of stainless steel and the correlation between the surface properties and protein adsorption', Journal of Materials Science: Materials in Medicine, 18: 1389-98.

Kheirkhah, Mitra, Mohammadhossein Fathi, Hamid Reza Salimijazi, and Mehdi Razavi. 2015. 'Surface modification of stainless steel implants using nanostructured forsterite (Mg2SiO4) coating for biomaterial applications', Surface and Coatings Technology, 276: 580-86.

Kim, Tae-Eon, Chang Gun Kim, Jin Soo Kim, Songwan Jin, Sik Yoon, Hae-Rahn Bae, Jeong-Hwa Kim, Young Hun Jeong, and Jong- Young Kwak. 2016. 'Three-dimensional culture and interaction of cancer cells and dendritic cells in an electrospun nano- submicron hybrid fibrous scaffold', International Journal of Nanomedicine, 11: 823-35.

Mahapatro, Anil, David M. Johnson, Devang N. Patel, Marc D. Feldman, Arturo A. Ayon, and C. Mauli Agrawal. 2006. 'Surface Modification of Functional Self-Assembled Monolayers on 316L Stainless Steel via Lipase Catalysis', Langmuir, 22: 901-05.

Martínez-Calderon, M., M. Manso-Silván, A. Rodríguez, M. Gómez-Aranzadi, J. P. García-Ruiz, S. M. Olaizola, and R. J. Martín- Palma. 2016. 'Surface micro- and nano-texturing of stainless steel by femtosecond laser for the control of cell migration', Scientific reports, 6: 36296.

Misra, R. D. K., C. Nune, T. C. Pesacreta, M. C. Somani, and L. P. Karjalainen. 2013. 'Understanding the impact of grain structure in austenitic stainless steel from a nanograined regime to a coarse-grained regime on osteoblast functions using a novel metal deformation–annealing sequence', Acta Biomaterialia, 9: 6245-58.

Misra, R. Devesh K., Bhupendra Girase, Pavan K. C. Venkata Surya, Mahesh C. Somani, and L. Pentti Karjalainen. 2011. 'Cellular Mechanisms of Enhanced Osteoblasts Functions via Phase-Reversion Induced Nano/Submicron-Grained Structure in a Low-Ni Austenitic Stainless Steel', Advanced Engineering Materials, 13: B483-B92.

Mohan, Chandini C., Anupama Prabhath, Aleena Mary Cherian, Sajini Vadukumpully, Shantikumar V. Nair, Krishnaprasad Chennazhi, and Deepthy Menon. 2015. 'Nanotextured stainless steel for improved corrosion resistance and biological response in coronary stenting', Nanoscale, 7: 832-41.

Nazneen, Feroze; Schmidt, Michael; McLoughlin, Eve; Petkov, Nikolay; Herzog, Gregoire; Arrigan, Damien W. M.; Galvin, Paul. 2013. 'Impact of Surface Nano-textured Stainless Steel Prepared by Focused Ion Beam on Endothelial Cell Growth', Journal of Nanoscience and Nanotechnology, 13: 5283-90.

Qin, Hui, Huiliang Cao, Yaochao Zhao, Guodong Jin, Mengqi Cheng, Jiaxin Wang, Yao Jiang, Zhiquan An, Xianlong Zhang, and Xuanyong Liu. 2015. 'Antimicrobial and Osteogenic Properties of Silver-Ion-Implanted Stainless Steel', ACS Applied Materials & Interfaces, 7: 10785-94.

Roguska, Agata, Sachiko Hiromoto, Akiko Yamamoto, Michał Jerzy Woźniak, Marcin Pisarek, and Małgorzata Lewandowska. 2011. 'Collagen immobilization on 316L stainless steel surface with cathodic deposition of calcium phosphate', Applied Surface Science, 257: 5037-45.

Shayan, Mahdis, Moradi Marzyeh, Shankar Ravi, and Chun Youngjae. 2015. 'Enhanced osteoblast cell growth on the nanograin surface', Proceedings of the 2015 Industrial and Systems Engineering Research Conference: 406-14.

Yadav, A. A., A. C. Lokhande, J. H. Kim, and C. D. Lokhande. 2016. 'Supercapacitive properties of nanoporous oxide layer formed on 304 type stainless steel', Journal of Colloid and Interface Science, 473: 22-27.

SS304	Untreated	Anodized	Theoretical
Si	0.6 ± 0.2	0.5 ± 0.1	<1
Cr	18.3 ± 0.3	17.4 ± 0.3	17.5-20
Mn	1.2 ± 0.0	1.3 ± 0.0	<2
Fe	71.9 ± 0.9	72.4 ± 1.1	rest
Ni	7.9 ± 0.3	8.4 ± 0.4	8-11

SS316	Untreated	Anodized	Theoretical
Mo	2.5 ± 0.6	2.6 ± 0.4	2-3
Cr	16.6 ± 0.2	16.9 ± 0.2	16-18
Mn	1.3 ± 0.2	1.1 ± 0.1	<2%
Fe	69.2 ± 0.9	69.1 ± 0.7	rest
Ni	10.4 ± 0.3	10.3 ± 0.4	10-14

Tableau 5. –   Table 3: EDS elemental analysis of SS304 and SS316 before and after anodization (Atomic %).
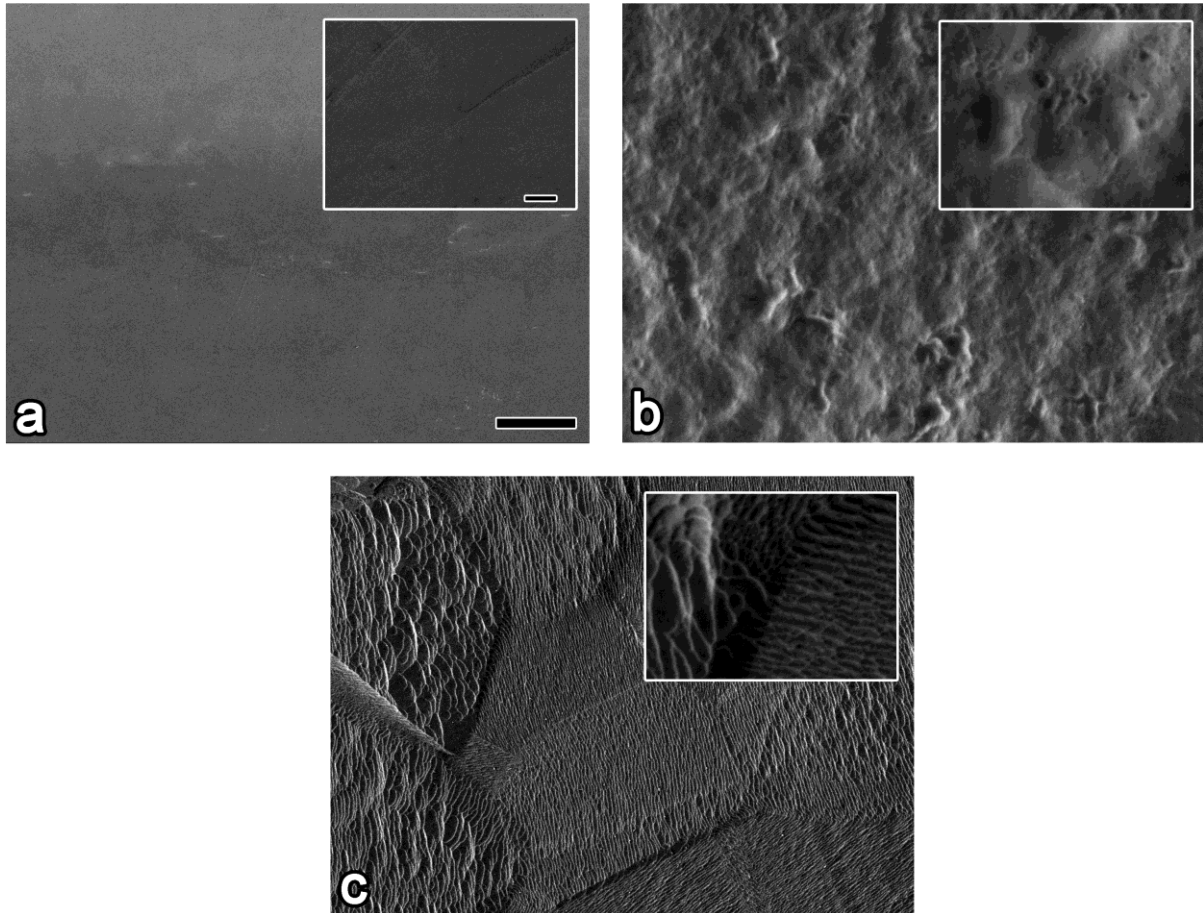
Figure 56. –   Figure 1. FE-SEM images of SS surfaces anodized with different electrolytes: (a) Hydrogen peroxide, (b) sulfuric acid (96%) and (c) a mixture of sulfuric acid (96%) and water (1:1) (bar = 2 µm, inset bar = 100 nm).
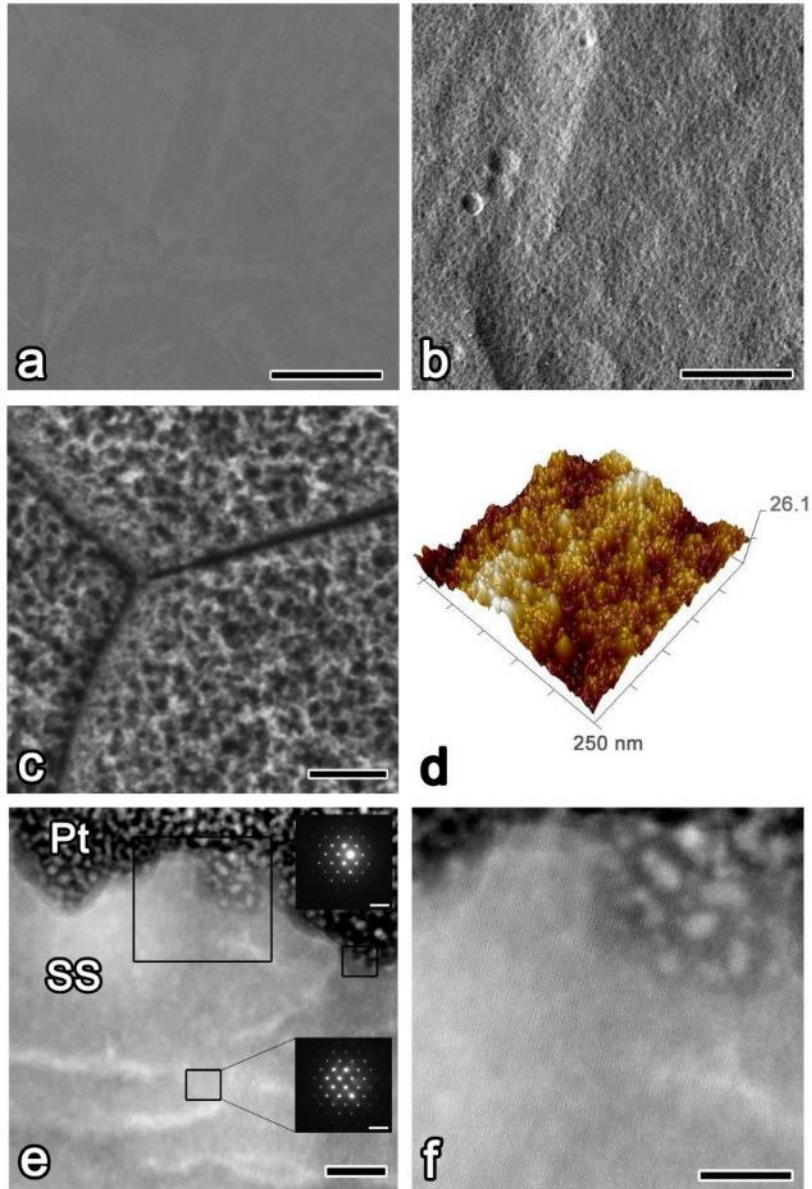
Figure 57. – Figure 2. Surface characterization of SS316. FE-SEM images of (a) untreated and (b) anodized surfaces (bar = 3 μm). (c) Higher magnification FE-SEM (bar = 20 nm) and (d) AFM images of the mesoporous surface. (e) HR-STEM image of the cross section of an anodized surface (bar = 20 nm). Insets illustrate the diffraction patterns of the mesoporous surface (upper) and the bulk SS (bottom). (f) Atomic resolution HR-STEM image of the interface between the mesoporous layer and the bulk SS, showing crystalline atomic organization.
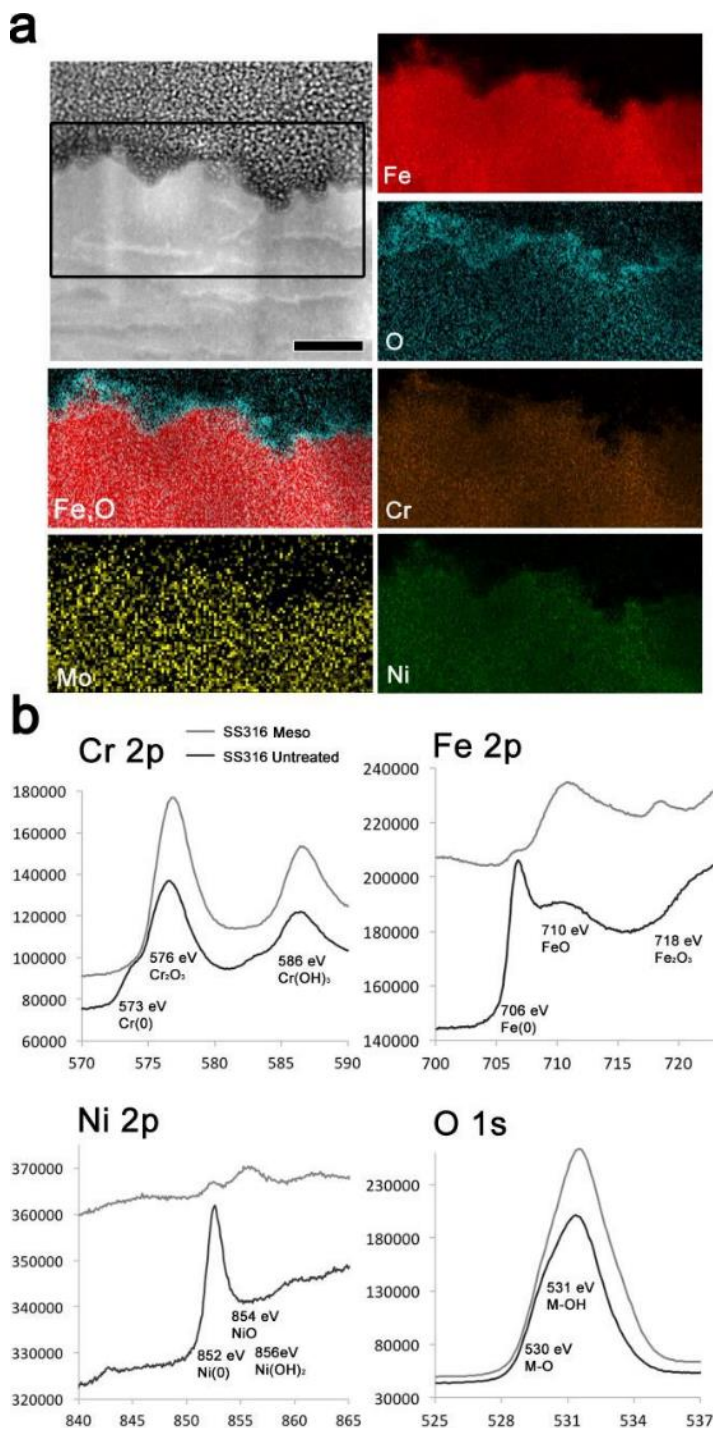
Figure 58. – Figure 3. Chemical composition of the mesoporous surface of SS316. (a) EDS mapping of elements in a cross section of the surface (bar = 40 nm). (b) Compositional analysis by XPS, showing high-resolution spectra of Cr 2p, Fe 2p, Ni 2p, and O 1s on the surfaces of anodized (Meso) and untreated samples. In all cases, the x-axis corresponds to peak positions in eV, and the y-axis shows intensity. (For SS316 see Supplemental).
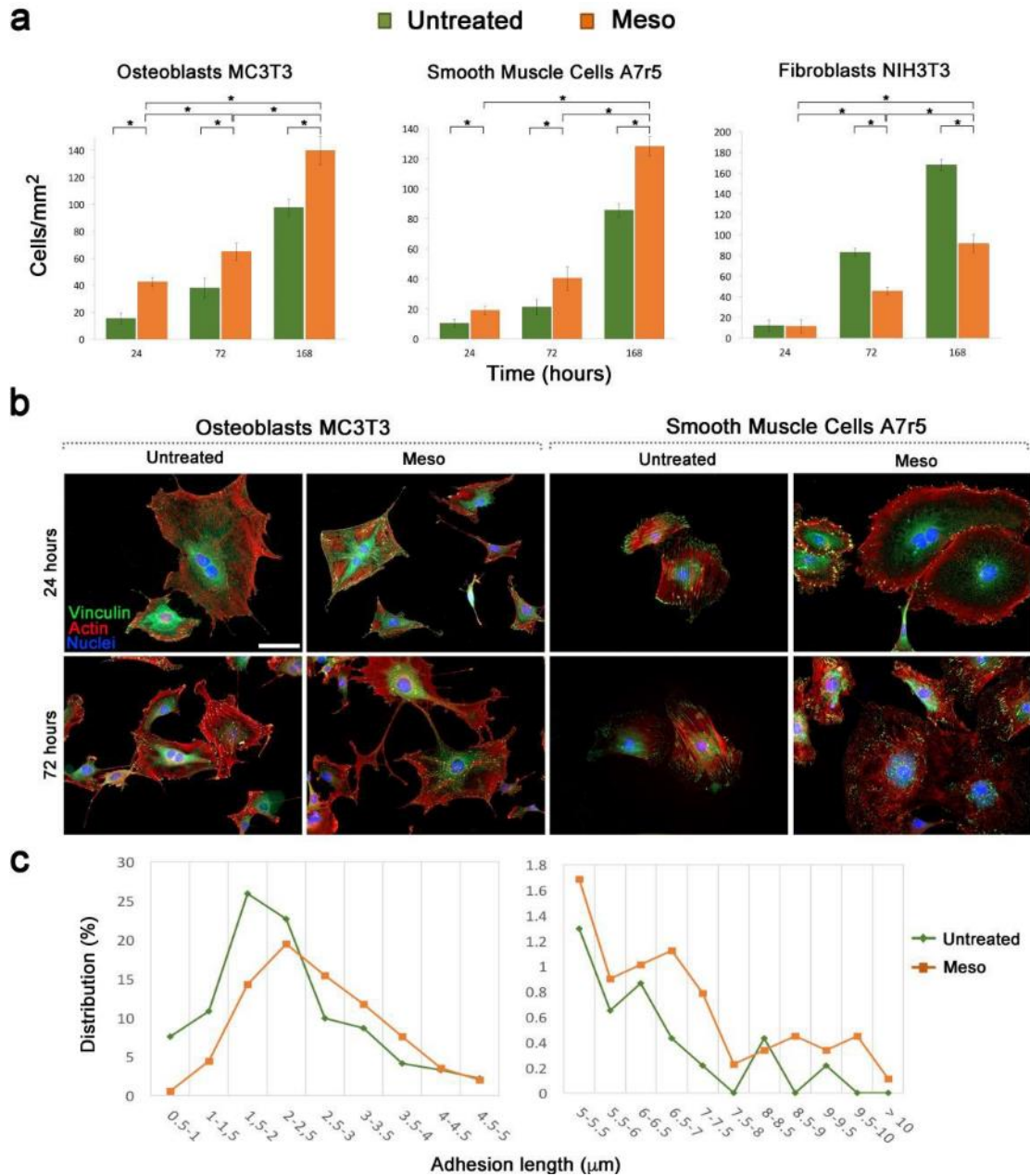
Figure 59. –   Figure 4. Cell attachment, growth and spreading on SS316. (a) Numbers of osteoblasts, smooth muscle cells, and fibroblasts at 24, 72, and 168 h on untreated (green) and mesoporous (Meso, orange) surfaces. Values showing significant differences ($p < 0.05$) are indicated with an asterisk. (b) Fluorescence micrographs showing vinculin (green) and actin (red) distribution in cells 24 and 72 h of culture. Nuclei are stained in blue (bar = 20 µm). (c) Quantitative analysis of FA lengths.
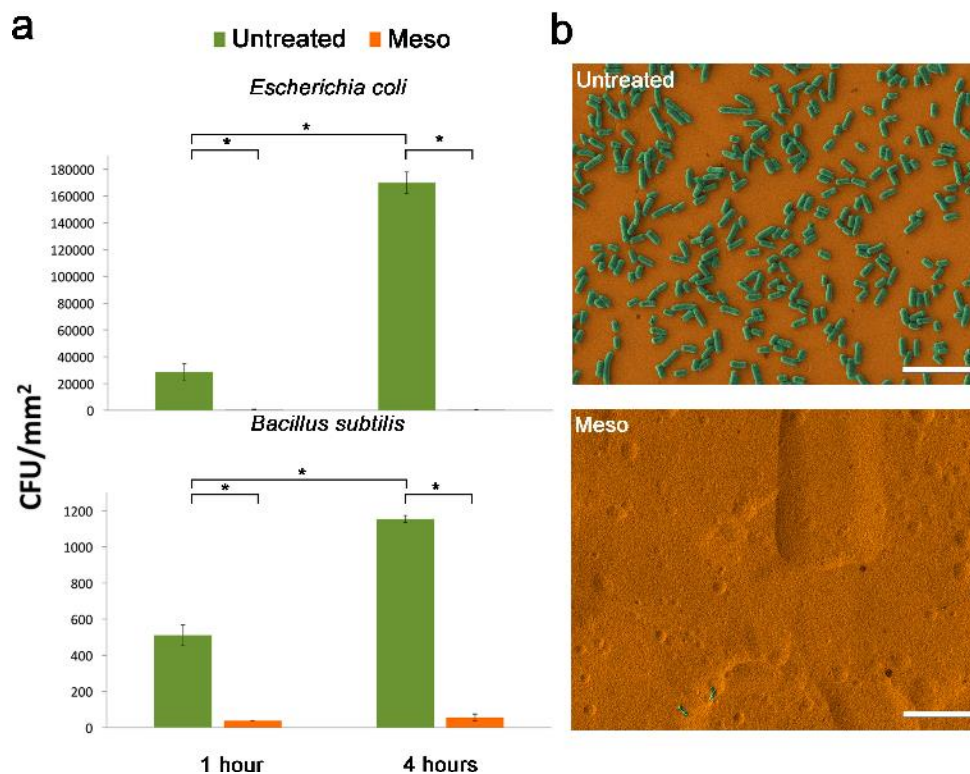
Figure 60. – Figure 5. Bacterial adhesion and proliferation on SS316. (a) Bacterial counts on untreated and mesoporous (Meso) surfaces. Values showing significant differences ($p < 0.05$) are indicated with an asterisk. (b) FE-SEM micrographs after incubation with E. coli (colored in green) for 4 h.

References

1. H. Hermawan, D. Ramda, J.R.P. Djuansjah Metals for Biomedical Applications, Biomedical Engineering From Theory to Applications (2011).

2. G.A.T. Qizhi Chen Metallic implant biomaterials Mater. Sci. Eng. R, 87 (2015), pp. 1-57.

3. B.R. Chrcanovic, T. Albrektsson, A. Wennerberg Reasons for failures of oral implants J. Oral Rehabil., 41 (6) (2014), pp. 443-476.

4. S.H. Nguyen, H.K. Webb, P.J. Mahon, R.J. Crawford, E.P. Ivanova Natural insect and plant micro-/nanostructsured surfaces: an excellent selection of valuable templates with superhydrophobic and self-cleaning properties Molecules, 19 (2014), pp. 13614-13630.

5. C.D. Bandara, S. Singh, I.O. Afara, A. Wolff, T. Tesfamichael, K. Ostrikov, A. Oloyede Bactericidal effects of natural nanotopography of dragonfly wing on escherichia coli ACS Appl. Mater. Interfaces, 9 (8) (2017), pp. 6746-6760.

6. A. Nanci, J.D. Wuest, L. Peru, P. Brunet, V. Sharma, S. Zalzal, M.D. McKee Chemical modification of titanium surfaces for covalent attachment of biological molecules J. Biomed. Mater. Res., 40 (1998), p. 324.

7. P. Tambasco de Oliveira, A. Nanci Nanotexturing of titanium-based surfaces upregulates expression of bone sialoprotein and osteopontin by cultured osteogenic cells Biomaterials, 25 (3) (2004), pp. 403-413.

8. F. Variola, J.-H. Yi, L. Richert, J.D. Wuest, F. Rosei, A. Nanci Tailoring the surface properties of Ti6Al4 V by controlled chemical oxidation Biomaterials, 29 (10) (2008), pp. 1285-1298.

9. J.-H. Yi, C. Bernard, F. Variola, S.F. Zalzal, J.D. Wuest, F. Rosei, A. Nanci Characterization of a bioactive nanotextured surface created by controlled chemical oxidation of titanium Surf. Sci., 600 (19) (2006), pp. 4613-4621.

10. F. Vetrone, F. Variola, P. Tambasco de Oliveira, S.F. Zalzal, J.-H. Yi, J. Sam, K.F. Bombonato-Prado, A. Sarkissian, D.F. Perepichka, J.D. Wuest, F. Rosei, A. Nanci Nanoscale oxidative patterning of metallic surfaces to modulate cell activity and fate Nano Lett., 9 (2) (2009), pp. 659-665.

11. P.T. de Oliveira, S.F. Zalzal, M.M. Beloti, A.L. Rosa, A. Nanci Enhancement of in vitro osteogenesis on titanium by chemically produced nanotopography J. Biomed. Mater. Res. A, 80A (3) (2007), pp. 554-564.

12. L. Richert, F. Vetrone, J.-H. Yi, S.F. Zalzal, J.D. Wuest, F. Rosei, A. Nanci Surface nanopatterning to control cell growth Adv. Mater., 20 (8) (2008), pp. 1488-1492.

13. R.M. Wazen, S. Kuroda, C. Nishio, K. Sellin, J.B. Brunski, A. Nanci Gene expression profiling and histomorphometric analyses of the early bone healing response around nanotextured implants Nanomedicine (London England), 8 (9) (2013), pp. 1385-1395.

14. F. Variola, S.F. Zalzal, A. Leduc, J. Barbeau, A. Nanci Oxidative nanopatterning of titanium generates mesoporous surfaces with antimicrobial properties Int. J. Nanomed., 9 (1) (2014), pp. 2319-2325.

15. B.P. M.C. Biesinger, L.W.M. Payne, A. Lau, R.S.C. Smart Gerson X-ray photoelectron spectroscopic chemical state quantification of mixed nickel metal, oxide and hydroxide systems Surf. Interface Anal., 41 (4) (2009), pp. 324-332.

16. M.C. Biesinger, B.P. Payne, A.P. Grosvenor, L.W.M. Lau, A.R. Gerson, R.S.C. Smart Resolving surface chemical states in XPS analysis of first row transition metals, oxides and hydroxides: Cr, Mn, Fe, Co and Ni Appl. Surf. Sci., 257 (7) (2011), pp. 2717-2730.

17. J.W. Cassidy, J.N. Roberts, C.-A. Smith, M. Robertson, K. White, M.J. Biggs, R.O.C. Oreffo, M.J. Dalby Osteogenic lineage restriction by osteoprogenitors cultured on nanometric grooved surfaces: the role of focal adhesion maturation Acta Biomater., 10 (2) (2014), pp. 651-660.

18. S.J. Kerber, J. Tverberg AES and XPS analysis of the passivation layer on stainless steel can help determine how well it will resist corrosion Adv. Mater. Processes Novembre (2000), pp. 33-36.

19. P.-J. Cunat Alloying elements in stainless steel and other chromium-containing alloys Euro Inox, 2004 (2004), pp. 1-24.

20. F. Variola, A. Lauria, A. Nanci, F. Rosei Influence of treatment conditions on the chemical oxidative activity of H_2SO_4/H_2O_2 mixtures for modulating the topography of titanium Adv. Eng. Mater., 11 (12) (2009), pp. 227-234.

21. M. Asoh Fabrication of thick nanoporous oxide films on stainless steel via DC anodization and subsequent biofunctionalization Surf. Coat. Technol., 307 (Part A) (2016), pp. 441-451.

22. A. Fattah-Alhosseini, N. Attarzadeh The mechanism of transpassive dissolution of AISI 321 stainless steel in sulphuric acid solution Int. J. Electrochem., 2011 (2011), pp. 0-9.

23. A. Fattah-alhosseini, M.H. Alemi, S. Banaei Diffusivity of point defects in the passive film on stainless steel Int. J. Electrochem., 2011 (2011), pp. 1-6.

24. D.D. Macdonald The point defect model for the passive state J. Electrochem. Soc., 139 (12) (1992), pp. 3434-3449.

25. J.I. Rosales-Leal, G. Rodríguez-Valverde, P.J. Ramón-Torregrosa, L. Díaz-Rodríguez, O. García-Martínez, M. Vallecillo-Capilla, C. Ruiz, M.A. Cabrerizo-Vílchez Effect of roughness, wettability and morphology of engineered titanium surfaces on osteoblast-like cell adhesion Coll. Surf. A, 365 (2010), pp. 222-229.

26. G. Zhao, Z. Schwartz, M. Wieland, F. Rupp, J. Geis-Gerstorfer, D.L. Cochran, B.D. Boyan High surface energy enhances cell response to titanium substrate microstructure J. Biomed. Mater. Res. A, 74A (2005), pp. 49-58.

27. L. Feller, Y. Jadwat, R.A.G. Khammissa, R. Meyerov, I. Schechter, J. Lemmer Cellular responses evoked by different surface characteristics of intraosseous titanium implants BioMed Res. Int., 2015 (2015), p. 8.

28. A.J. McManus, R.H. Doremus, R.W. Siegel, R. Bizios Evaluation of cytocompatibility and bending modulus of nanoceramic/polymer composites J. Biomed. Mater. Res. A, 72A (1) (2005), pp. 98-106.

29. K. Webb, V. Hlady, P.A. Tresco Relative importance of surface wettability and charged functional groups on NIH 3T3 fibroblast attachment, spreading, and cytoskeletal organization J. Biomed. Mater. Res., 41 (3) (1998), pp. 422-430.

30. J. Wei, M. Yoshinari, S. Takemoto, M. Hattori, E. Kawada, B. Liu, Y. Oda Adhesion of mouse fibroblasts on hexamethyldisiloxane surfaces with wide range of wettability J. Biomed. Mater. Res. B Appl. Biomater., 81B (1) (2007), pp. 66-75.

31. Z. Chen, T. Klein, R.Z. Murray, R. Crawford, J. Chang, C. Wu, Y. Xiao Osteoimmunomodulation for the development of advanced bone biomaterials Mater. Today, 19 (6) (2016), pp. 304-321.

32. P.K. Mattila, P. Lappalainen Filopodia: molecular architecture and cellular functions Nat. Rev. Mol. Cell Biol., 9 (6) (2008), pp. 446-454.

33. L.E. McNamara, T. Sjöström, K. Seunarine, R.D. Meek, B. Su, M.J. Dalby Investigation of the limits of nanoscale filopodial interactions J. Tissue Eng., 5 (2014), Article 2041731414536177.

34. C.-I. Lin, C.-Y. Lau, D. Li, S.-C. Jaminet Nanopodia –thin, fragile membrane projections with roles in cell movement and intercellular interactions J. Vis. Exp. JoVE (2014), p. 86, 10.3791/51320.

35. A. Diener, B. Nebe, F. Lüthen, P. Becker, U. Beck, H.G. Neumann, J. Rychly Control of focal adhesion dynamics by material surface characteristics Biomaterials, 26 (4) (2005), pp. 383-392.

36. D. Guadarrama Bello, A. Fouillen, A. Badia, A. Nanci A nanoporous titanium surface promotes the maturation of focal adhesions and formation of filopodia with distinctive nanoscale protrusions by osteogenic cells Acta Biomater., 60 (Suppl. C) (2017), pp. 339-349.

37. L.J.A. Heitz-Mayfield Peri-implant diseases: diagnosis and risk indicators J. Clin. Periodontol., 35 (2008), pp. 292-304.

38. Y. Xuan, C. Zhang, N. Fan, Z. Yang Antibacterial property and precipitation behavior of Ag-added 304 austenitic stainless steel Acta Metall. Sin. (English Letters), 27 (3) (2014), pp. 539-545.

39. Y. Yin, X. Zhang, D. Wang, L. Nan Study of antibacterial performance of a type 304 Cu bearing stainless steel against airborne bacteria in real life environments Mater. Technol., 30 (2015), pp. B104-B108.

40. M. Hoevar, M. Jenko, M. Godec, D. Drobne An overview of the influence of stainless-steel surface properties on bacterial adhesion Mater. Technol., 48 (5) (2014), pp. 609-617.